UNIVERSITEIT VAN PRETORIA
UNIVERSITY OF PRETORIA
YUNIBESITHI YA PRETORIA

Influence of particle irradiation on the electrical and defect properties of GaAs

by

Stewart Alexander Goodman

Submitted in partial fulfilment of the requirements for the degree

Philosophiae Doctor

in the

Faculty of Science (Department of Physics)

University of Pretoria

PRETORIA

JULY 1994

Promoter : Professor F.D. Auret
Co-promoter : Professor E. Friedland

© University of Pretoria

UNIVERSITEIT VAN PRETORIA
UNIVERSITY OF PRETORIA
YUNIBESITHI YA PRETORIA

SUMMARY

Influence of particle irradiation on the electrical and defect properties of GaAs

by

Stewart Alexander Goodman

Promoter : Professor F.D. Auret
Co-promoter : Professor E. Friedland

Submitted in partial fulfilment of the requirements for the degree Philosophiae Doctor in the Faculty of Science.

The beginning of the space-age in the 1950s led to interest in the effects of radiation on semiconductors. The systematic investigation of defect centres in semiconductors began in earnest over 30 years ago. In addition to defect identification, information was also obtained on energy-level structures and defect migration properties. When designing electronic systems for operation in a radiation environment, it is imperative to know the effect of radiation on the properties of electronic components and materials comprising these systems.

In some instances, the effects of irradiating electronic materials can be used to obtain desired material properties (mesa isolation, implantation, etc.). However, when electronic devices are exposed to radiation, defects may be introduced into the material. Depending on the application, these defects may have a detrimental effect on the performance of such a device. For this study, the semiconductor gallium arsenide (GaAs) was used and the defects were introduced by electrons, alpha-particles, protons, neutrons and argon

© University of Pretoria

sputtering. These particles were generated using radio-nuclides, a high-energy neutron source, a 2.5 MV Van de Graaff accelerator and a sputter gun.

The influence of particle irradiation on the device properties of Schottky barrier diodes (SBDs) fabricated on GaAs is presented. These device properties were monitored using a variable temperature current-voltage (I-V) and capacitance-voltage (C-V) apparatus. In order to have an understanding of the change in electrical properties of these contacts after irradiation, it is necessary to characterize the radiation-induced defects. Deep level transient spectroscopy (DLTS) was used to characterise the defects in terms of their DLTS "signature", defect concentration, field enhanced emission, and thermodynamic properties.

261 Words

© University of Pretoria

UNIVERSITEIT VAN PRETORIA
UNIVERSITY OF PRETORIA
YUNIBESITHI YA PRETORIA

SAMEVATTING

Invloed van deeltjie bestraling op die elektriese en defek eienskappe van GaAs

deur

Stewart Alexander Goodman

Studieleier : Professor F.D. Auret
Mede-studieleier : Professor E. Friedland

Voorgelê ter gedeeltelike vervulling van die vereistes vir die graad Philosophiae Doctor in die Fakulteit Natuurwetenskappe.

Belangstelling in die effek van straling op halfgeleiermateriale kan teruggevoer word tot die ontstaan van die ruimte-eeu in die 1950s. Wetenskaplike studies in hierdie veld het egter eers dekades later 'n drastiese toename getoon. Addisioneel tot die blote identifikasie van defekte, is daar ook inligting verkry betreffende die energievlak-strukture en die migrasie eienskappe van genoemde defekte. Wanneer elektroniese komponente ontwerp word vir gebruik in gebiede met stralingsgevare, is dit belangrik om te weet wat die invloed van bestraling sal wees op die eienskappe van elektroniese komponente en halfgeleier materiale waaruit hierdie stelsels bestaan.

Onder sekere omstandighede, kan die effek van bestraling op halfgeleier materiale gebruik word om sekere verlangde materiaal-eienskappe te verkry, byvoorbeeld, mesa isolering en implantering. Wanneer elektroniese komponente aan straling blootgestel word, mag sekere defekte in die materiaal geskep word. Afhangende van die toepassing, mag hierdie defekte 'n negatiewe invloed op die werking van hierdie komponent hê. Vir hierdie studie is galliumarsenied (GaAs) as elektroniese materiaal gebruik. Defekte is doelbewus deur

© University of Pretoria

middel van elektrone, alfa-deeltjies, protone, neutrone en argon verstuiwing in hierdie materiaal geïnduseer. Hierdie deeltjies is verkry deur van radio-nukliedes, 'n hoë-energie neutron bron, 'n 2.5 MV Van de Graaff-versneller en 'n verstuiwingskanon gebruik te maak.

Die invloed van deeltjie bestraling op die eienskappe van Schottky-diodes wat op GaAs vervaardig is, word aangebied. Diode eienskappe is deur temperatuur afhanklike stroom-spanning en kapasitansie-spanning tegnieke bepaal. Om die veranderinge in die elektriese eienskappe van hierdie diodes na deeltjie bestraling beter te verstaan, was dit nodig om die stralings-geïnduseerde defekte in die GaAs te karakteriseer. Diepvlakoorgangspektroskopie (DLTS) was gebruik om die defekte in terme van hulle DLTS "handtekening", defek konsentrasie, veld-verhoogde emissie en die termodinamiese eienskappe te karakteriseer.

278 Woorde

© University of Pretoria

UNIVERSITEIT VAN PRETORIA
UNIVERSITY OF PRETORIA
YUNIBESITHI YA PRETORIA

TO MY WIFE CASSI

"To laugh often and much; to win the respect of intelligent people and the affection of children; to earn the appreciation of honest critics and endure the betrayal of false friends; to appreciate beauty, to find the best in others; to leave the world a bit better, whether by a healthy child, a garden patch or a redeemed social condition; to know even one life has breathed easier because you have lived. This is to have succeeded."

Ralph Waldo Emerson

© University of Pretoria

UNIVERSITEIT VAN PRETORIA
UNIVERSITY OF PRETORIA
YUNIBESITHI YA PRETORIA

Acknowledgements

I would like to sincerely thank the following persons for their contribution towards the completion of this study:

My promoter, Professor F.D. Auret for his enthusiasm, guidance and support during this study.

My co-promoter, Professor E. Friedland for his assistance.

Dr. Gerrit Myburg for the vacuum deposition of ohmic and Schottky contacts.

Mr. Michael Hayes for assistance and helpful discussions concerning irradiations in the Van de Graaff accelerator.

Dr. Dan Jones and his staff for performing neutron irradiations at the National Accelerator Centre (NAC).

Mr. Gerrit Pretorious and Mr. Roelf van Weele for their technical assistance during this study.

The Foundation for Research Development for their financial assistance during this study.

Mr Walter Meyer for interesting discussions, especially on the modelling aspects.

Professor A.R. Peaker and Dr. Missous for supplying MBE grown p-type GaAs.

The staff of the Physics department of the University of Pretoria for their willingness to assist.

My wife for her support, patience and encouragement during this study.

My parents for providing me with the initial opportunity to further my education.

© University of Pretoria

UNIVERSITEIT VAN PRETORIA
UNIVERSITY OF PRETORIA
YUNIBESITHI YA PRETORIA

CONTENTS

© University of Pretoria

UNIVERSITEIT VAN PRETORIA
UNIVERSITY OF PRETORIA
YUNIBESITHI YA PRETORIA

© University of Pretoria

UNIVERSITEIT VAN PRETORIA
UNIVERSITY OF PRETORIA
YUNIBESITHI YA PRETORIA

CHAPTER 1

INTRODUCTION

Gallium arsenide is an important material for devices to be used in space applications, owing to the increased speed of carriers in this material and its resistance to radiation damage. Gallium arsenide (GaAs) emerged as an optoelectronic material in the early 1960s and consolidated its position with the development, a decade later, of double heterostructure strip lasers. A more recent development is the first commercial single-mode diode laser with a continuous output power greater than 1 watt. Applications of this device include optical communication between satellites, telecommunication systems and thermal printing systems. High electron mobility transistors (HEMTs) have improved gain and noise performance over an extended frequency range. A further advantage of this device is that it can be incorporated into either monolithic or hybrid microwave and millimeter-wave integrated circuits. GaAs Schottky barrier diodes (SBDs) are becoming more important in space applications; SBDs operating in the terahertz frequency range are used in radio astronomy and remote sensing of the earth's atmosphere.

The radiation environment experienced by earth-orbiting spacecraft is largely a manifestation of the interaction of charged particles with the earth's magnetic field, forming the radiation- or Van Allen belts. Other sources of radiation include solar flares, cosmic rays, low energy plasma, other planets and secondary radiation. Typical particles in space are electrons, protons, alphas, neutrons and, to a lesser extent, heavier nuclei. The beginning of the space age in the 1950s led to interest in the effects of radiation on semiconductors. Thus, in the 1960s, extensive studies on radiation-induced defects were performed. In addition to defect identification, the studies on radiation-induced defects addressed a number of fundamental aspects of defect physics, such as defect migration and lattice relaxation.

© University of Pretoria

It was discovered almost forty years ago that neutron irradiation profoundly affected the electrical characteristics of semiconductors such as germanium and silicon. Present-day interest has been stimulated by such semiconductor applications as solar cell power plants for space stations and satellites, and semiconductor particle and γ-ray detectors. Particle irradiation also plays a significant role in various sectors of semiconductor technology. This irradiation is utilized to controllably modify the properties of electronic materials, such as during device isolation by proton implantation and transmutational doping of semiconductors. It is a widely used processing step because, amongst others, it offers the capability of performing several processing steps in vacuum without exposing the semiconductor surface to atmosphere. Gallium arsenide may be doped with impurities resulting from nuclear reactions based on thermal neutrons, γ-rays and charged particles. It has for instance been shown that nuclear doping of GaAs by α-particle irradiation is possible. However, it is well known that the use of energetic particles may result in unwanted changes in the surface and sub-surface.

Hence, when designing electronic systems for operation in a radiation environment, it is imperative to know the effect of radiation on the properties of electronic components and materials comprising these systems. A knowledge of the influence of radiation damage on the performance of these devices has become an active field of research. The effect of irradiation on an electronic material and the consequent degradation in performance of devices made from such material will depend upon, amongst other factors, the type and fluence of radiation.

To evaluate the influence of radiation-induced defects on materials and devices, and to optimally utilize their beneficial effects in defect engineering, the characteristics of radiation-induced defects in different materials should be known. In the 1970s, a major breakthrough occurred in experimental techniques. In these new techniques, measurements were done on junctions such as rectifying metal-semiconductor interfaces. A variant of these junction experiments was deep level transient spectroscopy (DLTS), which allows one to scan a temperature range and observe individual deep levels as peaks in a continuous spectrum, yielding, amongst other factors, the well-known DLTS

© University of Pretoria

"signature" of the defect. Further information regarding defect migration and the nature of the defect may be obtained from a knowledge of the thermodynamic properties of the defect under consideration.

The technique used for defect characterization in this study, namely DLTS, is presented in section 1 of chapter 2. A general introduction into the theoretical aspects of defect production is considered in the second section of the same chapter. Finally, field-assisted emission and defect annealing are discussed in the last two sections of this chapter.

In chapter 3, the experimental techniques (DLTS, I-V and C-V) and apparatus are discussed, as well as certain theoretical aspects of the experimental techniques.

In chapter 4, the results of this study are presented as publications. Section 4.2 deals with the material characterization prior to irradiation. In section 4.3 the defects intentionally introduced into epi-layers are characterized and the change in electrical properties of the metal-semiconductor system using different incident particles is presented. The relationship between the electric field strength in the space-charge layer and the thermal emission rates from defects is presented in section 4.4. The results obtained from an annealing study where the thermodynamic properties of the intentionally-introduced defects were obtained are presented in section 4.5. The defects introduced by neutron irradiation and argon sputtering are characterized and the results presented in section 4.6. Finally, a summary of defect properties and comparisons is given in section 4.7.

The final chapter gives a review of the conclusions that may be drawn from this study.

© University of Pretoria

UNIVERSITEIT VAN PRETORIA
UNIVERSITY OF PRETORIA
YUNIBESITHI YA PRETORIA

CHAPTER 2

THEORETICAL ASPECTS

2.1 DEEP LEVEL TRANSIENT SPECTROSCOPY

In this study, deep level transient spectroscopy (DLTS) was used to evaluate and characterize the electrically-active defects in unirradiated GaAs as well as those introduced by particle irradiation. This powerful and sensitive technique was developed by Lang [1)] in 1974. In the years following the invention of this capacitance transient thermal scanning technique, it has established itself as one of the most sensitive, rapid and straightforward techniques in the characterization of deep levels. There have been numerous modifications and variations of the original technique, which have further established it as a necessity for any semiconductor crystal growth or electrical characterization laboratory.

There are also other techniques that may provide further information regarding defect properties. One such technique is electron paramagnetic resonance (EPR); this technique will not be discussed in any detail in this study. The detection methods of electron paramagnetic resonance (EPR) were discovered by Zavoisky in 1944. Since then, the frequency range and sensitivity have greatly been improved. EPR has proven to be an extremely powerful tool for the study of point defects in semiconductors and insulators. The reason for this is that the EPR spectrum of a defect contains highly detailed microscopic information about the structure of the defect which often cannot be obtained in any other way. More information is available when other techniques are used in conjunction with EPR; techniques such as applied uniaxial stress, electric fields and

© University of Pretoria

optical illumination. EPR is the resonant absorption of electromagnetic radiation by systems composed of unpaired electrons placed in a magnetic field [2].

In this section, the electrical behaviour of deep levels will be discussed. The analysis of the capacitance transients will be discussed making use of the lock-in amplifier based DLTS system. Finally, the different variations of DLTS will be discussed with emphasis on those utilised in this study.

2.1.1 DLTS FUNDAMENTALS

Before any meaningful description of the principle of the DLTS technique can be presented, a definition of the term *deep levels* has to be given. Deep levels are quantum states which fall within the forbidden bandgap of the semiconductor; these deep levels are much deeper than typical donor levels, which are typically 5 - 6 meV below the free carrier band for GaAs.

The existence of a space-charge layer at a Schottky barrier is a general feature of semiconductors. When a metal is brought into intimate contact with a semiconductor, the valence- and conduction bands of the semiconductor are brought into a definite energy relationship with the Fermi level of the metal. This relationship serves as a boundary condition on the solution of Poisson's equation in the semiconductor [3]. Under the abrupt junction or depletion approximation, it is assumed that it is possible to divide the semiconductor into two regions: the space-charge region (depletion region) directly below the metal, and the bulk of the semiconductor. In the space-charge region, the charge density (ρ) is qN_D. If the width of this space-charge region is W, the charge density on the semiconductor can be written as:

$$\rho(x) = \begin{pmatrix} qN_D & if\ x \le W \\ 0 & if\ x > W \end{pmatrix}. \qquad (2.1.1)$$

© University of Pretoria

For a uniformly-doped n-type region, the one-dimensional Poisson equation may be written as [3]:

$$\frac{-d^2E}{dx^2} = \frac{\rho(x)}{\varepsilon_s}, \tag{2.1.2}$$

where ρ is the charge density, E the electron energy and ε_s the semiconductor dielectric constant.

Using the abrupt junction approximation, the width of the space-charge region (W) can be calculated by using:

$$W = \sqrt{\frac{2\varepsilon_s}{qN_D}\left(V_{bi} - V - \frac{kT}{q}\right)}, \tag{2.1.3}$$

where q is the electron charge, ε_s the semiconductor dielectric constant, N_D the donor concentration and V_{bi} the built-in potential; V is positive for forward bias and negative for reverse bias. The term kT/q arises from the contribution of the majority carrier distribution tail. When the diode is forward-biased, there is a decrease in the total electrostatic potential across the junction, leading to a decrease in the space-charge width (W). When the diode is reverse-biased, there is an increase in the total electrostatic potential across the junction and consequently an increase in the space-charge width (W). The maximum electric field strength (F_m) in the space-charge layer at $x = 0$ may be calculated by integrating eqn 2.1.2:

$$F_m = \frac{2(V_{bi} - V - kT/q)}{W}. \tag{2.1.4}$$

The existence of the space-charge region, and the fact that its width depends upon the applied bias and charge in this region, makes it possible to characterise the material by measuring the junction capacitance. The junction capacitance (C) is analogous to that of a parallel plate capacitor with an area A:

© University of Pretoria

$$C = \frac{\varepsilon_S A}{W}. \tag{2.1.5}$$

Whenever the thermal equilibrium condition of a system is disturbed, processes exist to restore the system to equilibrium. These processes may involve the emission and capture of electrons and holes. A defect whose associated energy level lies in the forbidden gap, exchanges carriers with the conduction- and valence bands through the emission and recombination of electrons and holes. From these electronic transitions between the defect level (E_T) and the bands, the occupancy of the defect level by carriers may be calculated. The emission and recombination rates depend upon the free energy of ionization, the capture cross-section for electrons and holes of the defect level, and the temperature. Therefore, a study of the emission and recombination rates yields valuable information regarding the electrical characteristics of the defect [2)]. Figure 2.1.1 illustrates the way in which holes and electrons may be recombined through traps [4)]. From this figure it can be seen that a deep level can interact with the conduction band and the valence band by the following four processes:

1. Electron capture from the conduction band (E_C).
2. Electron emission to the conduction band (E_C).
3. Hole capture from the valence band (E_V).
4. Hole emission to the valence band (E_V).

For the sake of simplicity, only an electron trap in an n-type semiconductor will be considered here. The processes involved are governed by Fermi-Dirac statistics. The probability that a quantum state will be occupied (f) in thermal equilibrium is given by:

$$f(E_T) = \frac{1}{1 + \exp(E_T - E_F)/kT}, \tag{2.1.6}$$

© University of Pretoria

where E_T is the energy of the deep level, E_F is the Fermi level, k is Boltzmann's constant and the temperature is represented by T. The probability that a state is empty will be represented by ($f_p = 1 - f$). The capture rate will depend upon three factors: the number of empty traps which are capable of capturing an electron ($f_{pt} N_T$), the average probability per unit time ($M_n(E)$) that an electron in the range dE will be captured by an empty trap, and the number of states in the conduction band that are occupied by electrons ($f(E)N(E)dE$). Here N_T is the number of trapping centres per unit volume and $N(E)$ is the density of energy levels in the conduction band in the energy range (dE). The capture rate (dU_c) will thus be represented by the following equation:

$$dU_c = (f_{pt} N_T)(M_n(E))(f(E)N(E)dE), \tag{2.1.7}$$

where the average probability per unit time ($M_n(E)$) that an electron in the range dE be captured by an empty trap (capture constant) is given by:

$$M_n(E) = v_{th}\sigma_n, \tag{2.1.8}$$

with v_{th} being the thermal velocity of an electron and σ_n the capture cross-section of the empty trap for electrons.

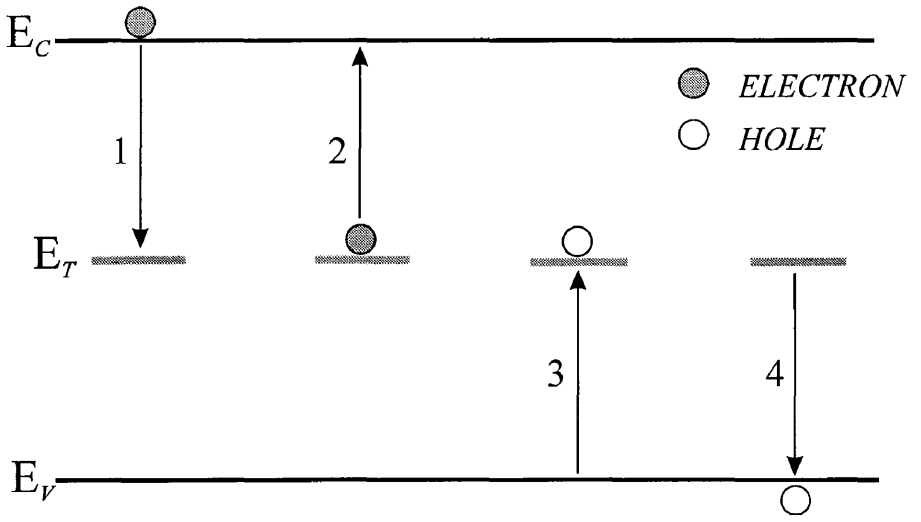

Fig 2.1.1 Emission and capture processes involved by trapping at a deep level E_T.

© University of Pretoria

The same procedure may be applied to calculate the emission rate (dU_e). The equation used for this purpose is:

$$dU_e = (f_t N_T)(N_n(E))(f_p(E)N(E)dE), \tag{2.1.9}$$

where N_n is the emission constant corresponding to the capture constant (M_n). Assuming that the system is in thermal equilibrium, the quasi Fermi level is at the same position as the quasi Fermi level of the traps. The relationship between the capture- and emission constants (M_n and N_n) may be represented in terms of the net capture rate ($dU_{cn} = dU_c - dU_e$):

$$dU_{cn} = [f_{pt} f(E) - (N_n / M_n)(f_t f_p(E)]N_T M_n(E)N(E)dE), \tag{2.1.10}$$

For thermal equilibrium, the quantity in the square brackets must be zero; this leads to the following result [4]:

$$N_n / M_n = \exp[(E_T - E)/kT]. \tag{2.1.11}$$

For the case of non-degenerate statistics, the probability that a state will be empty (f_p) is nearly unity for the states in the conduction band, and consequently the emission constant (N_n) is only a function of the fraction of traps occupied by electrons (f_t) [4]. The emission rate (e_n) of an electron trap in n-type material may be given by: [5]

$$e_n = v_{th}\sigma_n N_c \exp(E_T - E_c)/kT. \tag{2.1.12}$$

In the above derivation, the degeneracy factor (g) has been taken as equal to unity for simplicity.

© University of Pretoria

2.1.2 DLTS "signature"

Before the concept of DLTS "signatures" is discussed, the transient response of a semiconductor junction containing traps will be discussed. This signature refers to the position of the defect in the bandgap (E_T) and the capture cross-section (σ_n). This discussion will be limited to Schottky barrier diodes. As a reverse bias is applied to the metal-semiconductor system, a region depleted of mobile free carriers is created (space-charge region). This space-charge region is characterised by the presence of ionised impurities, usually donors. Deep levels or defects in this space-charge region may be detected either by their effect on the junction current or on the capacitance [6]. The magnitude of the current or capacitance transient corresponding to thermal emission of carriers from the deep level depends upon the defect concentration, emission rate and temperature. The thermal emission rate may also depend upon the electric field strength in the space-charge region. In this study, we monitored the change in capacitance in a Schottky barrier diode, and the capacitance transient is assumed to have the form:

$$C(t) = C(\infty) - \Delta C \exp(-e_n t), \qquad (2.1.13)$$

where $C(t)$ is the capacitance transient at time t, $C(\infty)$ is the quiescent reverse bias capacitance at time $(t) = \infty$ and ΔC is the difference between $C(\infty)$ and the capacitance measured at $(t) = 0$. The capacitance transient due to an electron trap in n-type material, together with the conditions of trap occupation and space-charge layer width, are depicted in figure 2.1.2 [6]. Insert A of this figure depicts the metal-semiconductor junction under reverse bias; under this condition we shall speak of the capacitance as the equilibrium capacitance. As can be seen, the space-charge layer (unshaded region) is depleted of free carriers under this bias condition. Reducing the reverse bias will collapse the space charge region, allowing the capture of majority carriers; this process is illustrated in insert B. Insert C illustrates the increase in the width of the space-charge layer when the reverse bias is re-established. This excess charge in the space-charge region may be transferred to

© University of Pretoria

the conduction band through the emission process as shown in Insert D. From inspection of the capacitance transient in fig 2.1.2, it can be seen that due to the collapse of the space-charge region when the reverse bias is reduced, there is an increase in the junction capacitance. The junction capacitance is reduced when the reverse bias is re-established. This reduction in the capacitance, where the capacitance is much lower than the equilibrium value, is due to the capture of some of the carriers. However, as the trapped carriers are emitted to the conduction band, there is an increase in the capacitance transient. This transient response of the capacitance due to the emission of carriers is the fundamental process from which the trap properties are derived in the DLTS experiment. The characteristic decay time constant (τ) of this transient is related to the emission rate (e_n) by:

$$e_n = 1/\tau \,. \tag{2.1.14}$$

By applying an injection pulse (photo or bias), both majority and minority carriers will be introduced. The relative ratio of concentrations of these carriers may be varied by varying the magnitude of the injection pulse.

One of the aims of performing defect studies is to determine the emission rate (e_n) as a function of temperature (T) since, this enables one to obtain the defect energy (E_T) and capture cross-section (σ_n) using eqn 2.1.12; this may be achieved using DLTS. The DLTS system works on the principle that it sets an emission rate window such that the measurement system only responds when it sees a transient with a rate within this window [1)]. If the emission rate is varied by changing the sample temperature (from eqn 2.1.12), a response peak will be shown at that temperature where the DLTS signal (the concept of DLTS signal is discussed in detail in sect 3.4) has a maximum value within the emission rate window. This rate window may be selected using numerous procedures. For this study, the lock-in amplifier method was utilized. This method will be discussed in more detail in chapter 3.

© University of Pretoria

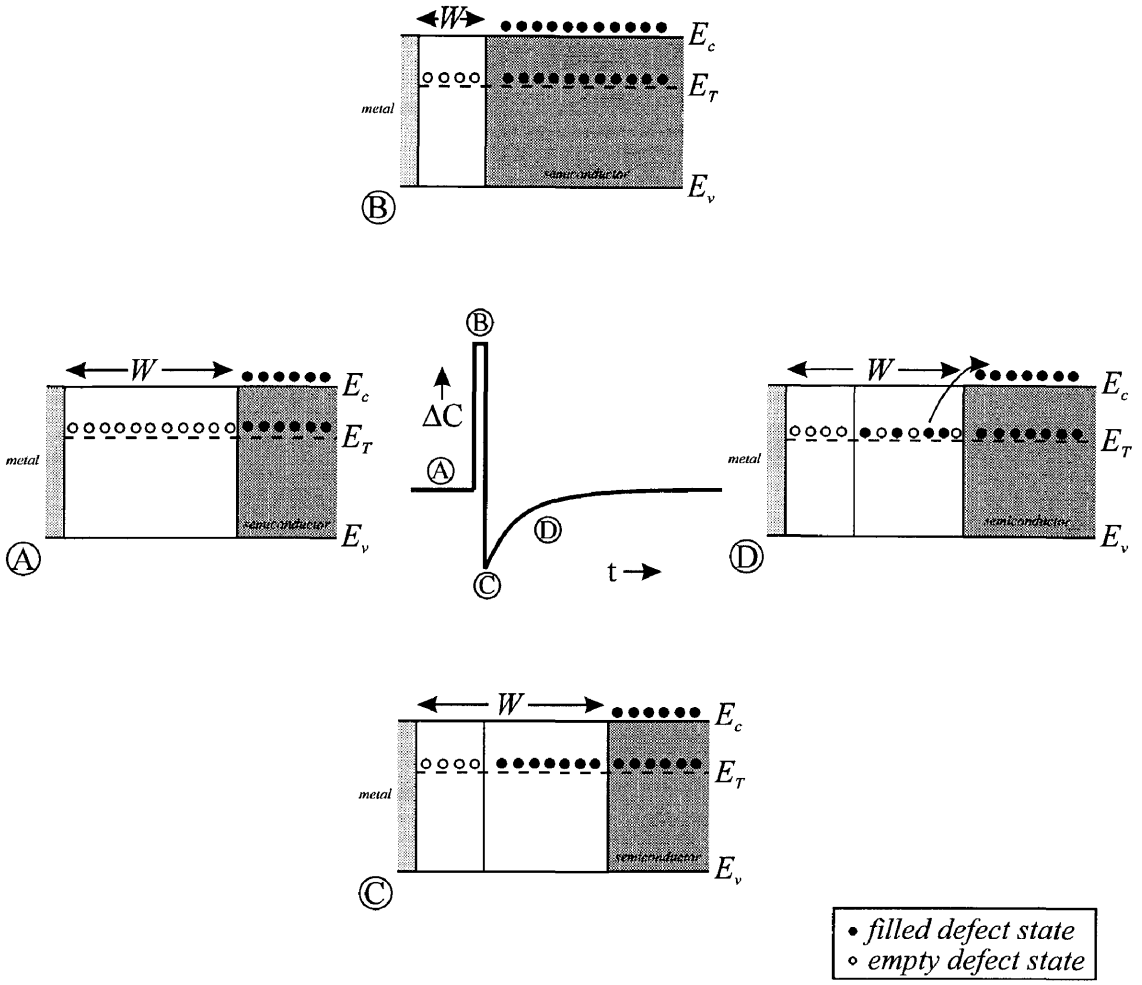

Fig 2.1.2 The capacitance transient due to an electron trap in n-type material, together with the conditions of trap occupation and space-charge layer width.

From DLTS measurements, we obtain the DLTS "signature" of the defect under consideration. This signature refers to the position of the defect in the bandgap (E_T) and the capture cross-section (σ_n). For the majority carriers in n-type material, we shall obtain the position of the electron defect level below the conduction band and the electron capture cross-section, whereas, for p-type material we shall obtain information regarding the position of the hole defect level above the valence band and the hole capture cross-section. Assuming that the emission rate proceeds exponentially, the position of the defect level in the bandgap, often referred to as the activation energy, and the capture cross-section may be determined by constructing an Arrhenius plot of log (e_n) against $1/T$. Although this procedure is very simple and yields valuable information, the temperature

© University of Pretoria

dependence of the capture cross-section has been neglected and this assumption may lead to erroneous DLTS "signatures".

Often it is found that the capture cross-section (σ_n) of a defect is temperature dependent. The procedure used to determine the capture cross-section of a deep level more accurately, using a lock-in amplifier based DLTS system as follows: Monitor the DLTS peak height ($\Delta C(t_p)$) as a function of pulse width (t_p) for different temperatures (T), referred to as variable filling-pulse width measurements [7]. The slope of a graph of $\ln(1 - \Delta C_{max}/\Delta C(t_p))$ versus pulse width (t_p) will yield the capture cross-section (σ_n) at a particular temperature with ΔC_{max} being the maximum peak height. This will be discussed in more detail in sect 2.1.3. The temperature dependence of the capture cross-sections for the defect level *A*, the "oxygen" defect level (*O*) previously believed to be related to oxygen and the electron irradiation-induced defect *E3* in n-type GaAs are depicted in fig 2.1.3 [8,9].

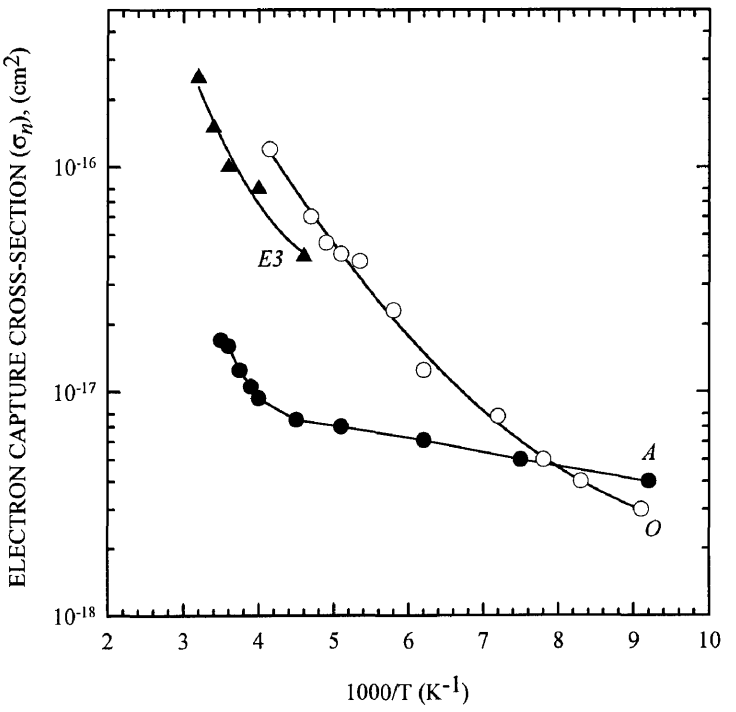

Fig 2.1.3 Electron capture cross-sections for defect levels *E3*, *A* and the "oxygen level" (*O*) as a function of inverse temperature.

© University of Pretoria

A further defect property that is of importance when characterizing defects is the defect concentration (N_T). This allows one to calculate the defect introduction rates after irradiation and to evaluate their effect on devices. One of the simplest methods of obtaining the majority carrier defect concentration (N_T), as proposed by Lang [1], is to monitor the capacitance change ($\Delta C/C$, where $\Delta C \ll C$) using the largest possible majority carrier pulse (all defects in the space-charge region are filled) [1]:

$$N_T = 2(\Delta C/C)(N_D - N_A), \tag{2.1.15}$$

where (N_D - N_A) is the net donor concentration that is often approximated to the donor concentration N_D. A more accurate method is when the space-charge region is profiled inward from W, as the majority pulse amplitude (V) is increased by a small change (δV). The corresponding incremental change in the relative capacitance signal due to the traps being filled by the pulse increment ($\delta(\Delta C/C)$) may be calculated using eqn 2.1.16:

$$\left(\frac{\Delta C}{C}\right) = \left(\frac{\varepsilon_s}{qW^2 N^+}\right)\frac{N_T(x)}{N^+(x)}\delta V, \tag{2.1.16}$$

where q is the carrier charge, W is the space-charge layer thickness at the steady state (between biases), N^+ is the ionized shallow level concentration and ε_s is the dielectric constant. However, this method does not yield accurate defect concentrations and a more accurate procedure has to be followed, as discussed below.

A unique feature of a structure with deep levels is the edge region, in which generation-recombination processes are active in determining the equilibrium occupation of defect states. In this edge region, the deep level is below the Fermi level and, therefore, has at least a 50% probability of being filled with electrons in thermal equilibrium (electron capture rate is much larger than the electron emission rate). Generally, there may not be

© University of Pretoria

sufficient free carriers in this edge region; they can however affect the accurate determination of the defect concentration especially at low bias voltages [6]. Hence, a more accurate method of obtaining the defect concentration is to profile through the space-charge layer, taking into account the influence of carriers in this edge region. Zohta and Watanabe [10] derived a correction formula which extracts the true deep level concentration as a function of distance from the edge of the space-charge region, from experimental DLTS measurements. Their formula was derived by assuming that the capacitance change just after the pulse (ΔC) is small compared to the junction capacitance (C), and that the donor concentration (N_D) and trap concentration (N_T) are slowly varying functions of position:

$$N_T = 2(\Delta C/C)N_D\left[\left(\frac{x-\lambda}{x}\right)^2 - \left(\frac{x_p-\lambda_p}{x}\right)^2\right]^{-1}, \qquad (2.1.17)$$

where λ and λ_p are the edge or transition layer widths before and just after pulsing, respectively, and x and x_p are the space-charge widths before and just after pulsing, respectively. The edge region thickness may be calculated using the following equation:

$$\lambda = \left(\frac{2\varepsilon}{q}\frac{(E_F - E_T)}{N_D}\right)^{1/2}. \qquad (2.1.18)$$

Another method of eliminating the edge region is the double correlation technique (DDLTS) proposed by Lefévre and Schulz [11], which determines deep level concentration profiles using a double-pulse capacitance transient. The advantages of using this DDLTS technique are that, as opposed to DLTS measurements where the electric field strength varies from a minimum at the edge of the space-charge region to a maximum at the interface, this technique examines a small region of known electric field strength. The edge region contribution in this method is eliminated, hence, the transient obtained is

© University of Pretoria

solely dependant upon the thermal emission rate and, finally, there is a reduction of the measurement noise. A schematic diagram illustrating the pulse shape, capacitance signal and the profiled region in the space-charge layer, as used in the DDLTS technique in this study, is presented in fig 2.1.4. In the modified DDLTS technique used in this study, two pulses of different height (V_p and $V_p + \delta V_p$) are used to fill trap levels in the space-charge layer to different depths below the SBD. Subtraction of the capacitance signals caused by the two pulses yields a signal from a narrow region in the space-charge layer. The width of this narrow region is dependent upon the difference in pulse heights.

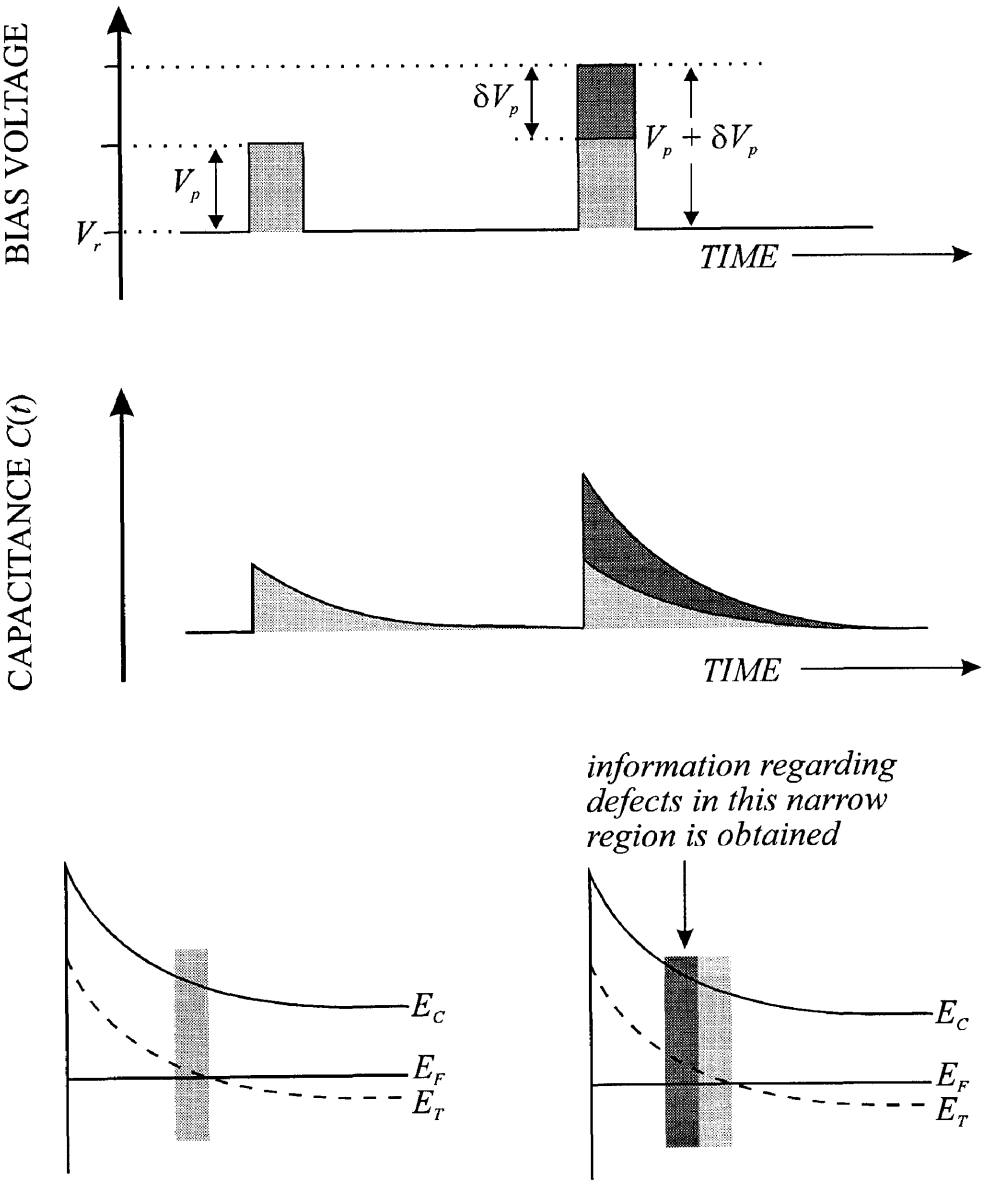

Fig 2.1.4 Schematic diagram of the pulse shape, capacitance signal and the narrow region in the space-charge region from which information is obtained.

© University of Pretoria

2.1.3 CAPTURE CROSS-SECTION TEMPERATURE DEPENDENCE

Thusfar, the DLTS "signature" has been obtained with the assumption that the capture cross-section has exhibited no electric field or temperature dependence. In this section, the temperature dependence of the capture cross-section will be discussed. In some cases where eqn 2.1.12 has been used directly to calculate the capture cross-section, the results have been erroneous. Lang et al [8] reported on the temperature dependence of impurity levels in n-GaAs; they found that some of the capture cross-sections exhibited a strong exponential increase with temperature. Non-radiative multiphonon emission (MPE) was thought to be the mechanism for this temperature dependence; this mechanism is described in sect 2.3.

Only two capture mechanisms appear to be able to explain how non-radiative capture with the associated large energy dissipation can take place: the Auger effect and multiphonon emission (MPE) [9]. A third mechanism, namely, cascade capture into the shallow coulombic excited states of an attractively-charged centre also exists. However, it cannot explain non-radiative capture into deep levels. In this mechanism, the electron loses energy in cascade capture by dropping through a series of closely spaced levels, emitting one phonon during each transition. As deep levels normally only have a single deep level within the bandgap, this model cannot be used to explain the temperature dependence of the capture cross-section. As has been shown by Henry and Lang [9], MPE explains the non-radiative recombination of numerous deep levels in GaAs and GaP. For this discussion, we will concentrate on the MPE mechanism for majority carriers.

The theory of non-radiative transitions by MPE was first developed by Huang and Rhys [12]. Non-radiative capture occurs because the energy of a deep level depends upon the positions of the atoms comprising the defect and those surrounding the defect. The interaction between the electron and these neighbouring atoms is depicted in fig 2.1.5.

© University of Pretoria

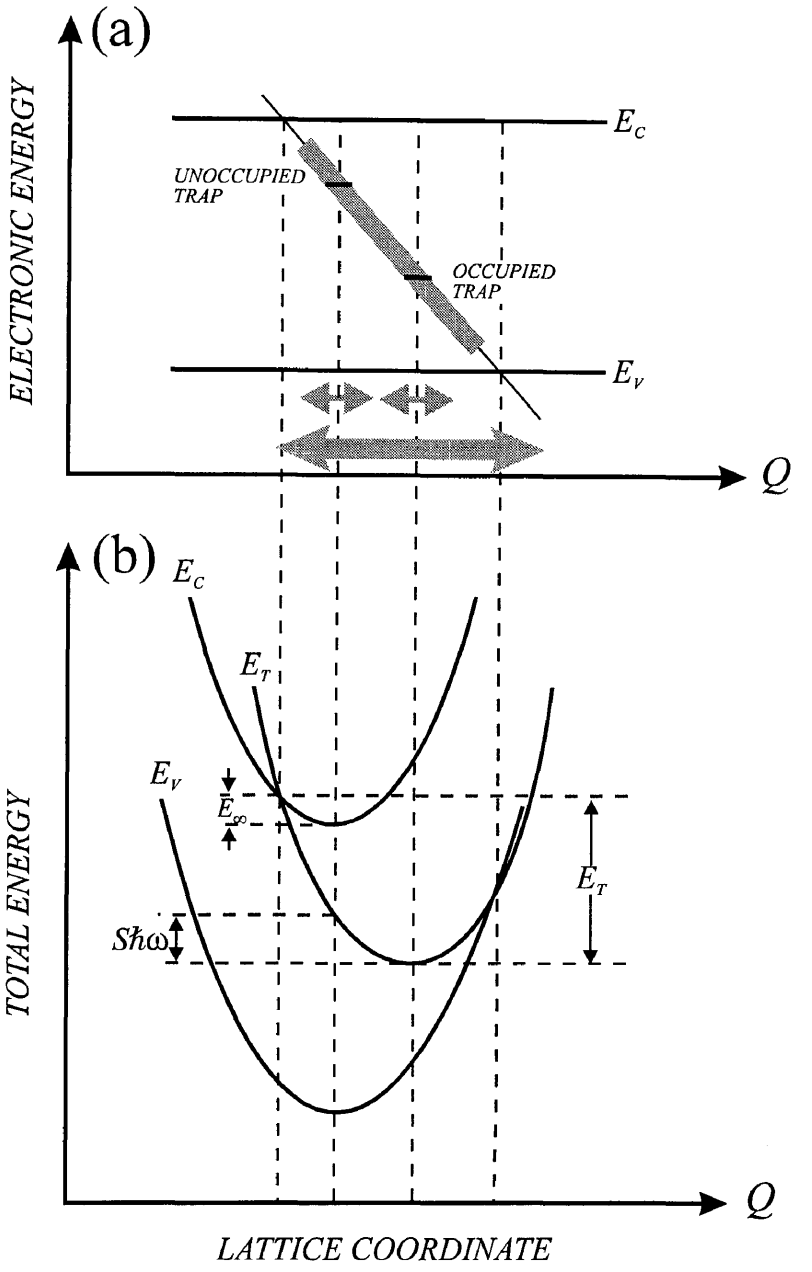

Fig 2.1.5 Diagram illustrating how non-radiative capture of an electron takes place. (a) The equilibrium positions of the lattice co-ordinate and the energy level, before and after capture, are indicated by dashed lines. The thermal vibrations, before and after are represented by the shorter arrows. The large arrow represents the amplitude of lattice vibration about the new equilibrium position, immediately after capture.

(b) The configuration co-ordinate diagram where the total (electronic + elastic) energy versus the one dimensional lattice co-ordinate (Q) is represented.

© University of Pretoria

Considering the non-radiative capture illustrated in fig 2.1.5 (a), it can be seen that in this example, prior to the deep level capturing an electron, the level is in the upper half of the bandgap. For large enough vibrations, the level can cross into the conduction band (E_C) and capture an electron. After this capture, the defect relaxes and the equilibrium position of the level is now lower in the bandgap. After electron capture, there will be a vigorous lattice vibration until it dampens down to the thermal vibration of the lattice; during this dampening the energy is emitted as lattice phonons. Capture by this process is called non-radiative capture by MPE [9].

The most obvious complication when obtaining an accurate position of the deep level in the bandgap is the temperature (T) dependence of the pre-factor in eqn 2.1.12. The T^2 dependence of the average thermal velocity ($\langle v_{th} \rangle$) and the effective density of states in the conduction band (N_C) is taken into account when plotting an Arrhenius plot (log e_n/T^2 versus $1/T$). The third variable in this prefactor may be expressed as:

$$\sigma_n = \sigma_\infty \exp(-E_\infty / kT), \tag{2.1.19}$$

where σ_∞ is the capture cross-section extrapolated to $T = \infty$, and E_∞ is the capture activation energy (thermal barrier for capture), which can be viewed as the energy barrier that a carrier has to overcome to be trapped on the defect site. The temperature dependence of the capture cross-section is discussed in more detail in sect 2.1.2. The temperature dependence of this factor may be determined by plotting $\ln(\sigma_n)$ versus $1/T$, the slope being the thermal barrier for capture (E_∞) and the capture cross-section extrapolated to $T = \infty$ (σ_∞) is the y-intercept. If the deep level exhibits a temperature-dependent capture cross-section, then the corrected activation energy (E_o, position in the bandgap) may be calculated using the following expression:

$$E_o = E_T - E_\infty, \tag{2.1.20}$$

© University of Pretoria

where the symbols have their usual meaning. The study of the temperature dependence of the capture cross-section provides interesting information regarding the configuration co-ordinate diagram and, as previously discussed, the thermal barrier for capture (E_∞), which allows the determination of the positions of the two minima, i.e. the quantity $S\hbar\omega$ as illustrated in fig 2.1.5.

© University of Pretoria

REFERENCES

1) D.V. Lang: J. Appl. Phys. 45 (1974) 3014.

2) J.C. Bourgoin and M. Lannoo: Point Defects in Semiconductors II (Springer-Verlag, Berlin 1983) p. 247.

3) S.M. Sze: Physics of Semiconductor Devices (John Wiley & Sons New York 1981) p. 248.

4) W. Shockley and W.T. Read: Phys. Rev. 87 (1952) 835.

5) G.L. Miller, D.V. Lang and L.C. Kimerling: Ann. Rev. Mater. Sci. (1977) 377.

6) D.V. Lang: Thermally Stimulated Relaxation in Solids (Springer-Verlag, Germany 1979, Ed. P. Brãunlich) p. 95.

7) D.V. Lang: J. Appl. Phys. 45 (1974) 3014.

8) D.V. Lang and R.A. Logan: J. Electr. Mater. 4 (1975) 1053.

9) C.H. Henry and D.V. Lang: Phys. Rev. B 15 (1977) 989.

10) Y. Zhota and M. Watanabe: J. Appl. Phys. 53 (1982) 1809.

11) H. Lefévre and M. Schulz: Appl. Phys. 12 (1977) 45.

12) K. Huang and A. Rhys: Proc. R. Soc. A 204 (1950) 406.

© University of Pretoria

2.2 DEFECT CREATION IN SEMICONDUCTORS

On July 9, 1962, high above the South Pacific Ocean, an event took place which changed the politics of the cold war and the course of radiation-effects physics. The U.S. experimental high-altitude nuclear device, *Starfish*, was detonated on that date. The nuclear contamination resulting from this detonation caused failure in the communication satellite, *Telstar 1* [1)]. Such radiation vulnerability was considered as a possible means to destroy military space systems. Since then, radiation effects in electronic systems using semiconductor devices have become of increasing interest. Electronic systems that need to operate in space, near nuclear reactors, isotopic nuclear sources or accelerators, and after exposure to a nuclear detonation must be designed to tolerate the effects of nuclear irradiation. The manifestations of radiation effects may range from permanent displacement damage in semiconductors to short-term currents produced by pulsed ionizing radiation, but may also include time-dependent displacement effects (short-term annealing). The first work using semiconductors as convenient structures to explore the nature of radiation effects originated in the late 1940s [2)]. This section deals with defects introduced by the interaction of energetic particles with the lattice of a semiconductor.

2.2.1 DEFECT STRUCTURES

Even in the absence of radiation, a crystal cannot exist at finite temperatures in a state of perfection. The vibrations of the lattice constitute one form of imperfection. These may be represented as a statistical distribution, of thermal energy amongst the atoms of the crystal. In any such distribution there is always a finite probability of sufficient energy being concentrated, by local fluctuations, onto a group of atoms to form a defect in the crystal lattice. The energy that an ion loses in a series of collisions while moving through an atomic array of a solid must be dissipated to the atoms of the solid in some manner. This energy may increase the kinetic and potential energies of the atoms in the solid, or may excite or ionize the atomic electrons of the lattice. The proportion of energy partitioned to each process will depend upon the details of each ion-atom encounter [3)]. In

© University of Pretoria

this study, we will mainly deal with point defects. A point defect in a crystal is an entity that causes an interruption in the lattice periodicity [4]. This occurs during the following circumstances:

1. An atom is removed from its regular lattice site; the defect is a vacancy.
2. An atom is in a site different from a regular lattice site; the defect is an interstitial; this defect can be a self-interstitial or an impurity-interstitial.
3. An impurity occupies a substitutional site.

When energetic radiation strikes a crystalline solid, defects are produced in the following manner:

1. An incident particle collides with a lattice atom and transfers energy to the recoil atom.
2. If sufficient energy is transferred, a vacancy is formed and the recoil atom collides with other atoms in the lattice, which can in turn be displaced if the energy transfer is sufficient.
3. The recoil atoms will eventually come to rest, usually in interstitial positions but some may come to rest in vacancy sites. These defects normally form clusters when the recoil energy is much larger than the threshold energy (E_D) for that particular crystal and orientation.
4. The ability of the defect to migrate through the crystal is determined by the thermal energy of the crystal and its charge state.
5. These mobile defects may be annihilated by recombining with a vacancy or an interstitial or by moving to the surface.

2.2.1a VACANCIES

Each atom is bound to its equilibrium lattice position by the forces of interaction with its neighbours. In the event of a collision, it can receive enough kinetic energy to overcome

© University of Pretoria

these binding forces and be ejected from its equilibrium position, creating a vacancy in the atomic array, and displacing an extra lattice atom to some distance from this vacancy. A vacant lattice site is considered as the simplest of all defects [5]. Figure 2.2.1 (a) depicts a vacancy defect in a diamond lattice. As is illustrated, four bonds are broken in order to create the vacancy. The distortion of the lattice depends upon the charge state of the vacancy [6]. The split-vacancy is depicted in fig 2.2.1 (b), where a lattice atom adjacent to the vacancy is moved to a position halfway between lattice sites (this configuration is also known as the saddle-point configuration for vacancy migration in the diamond lattice).

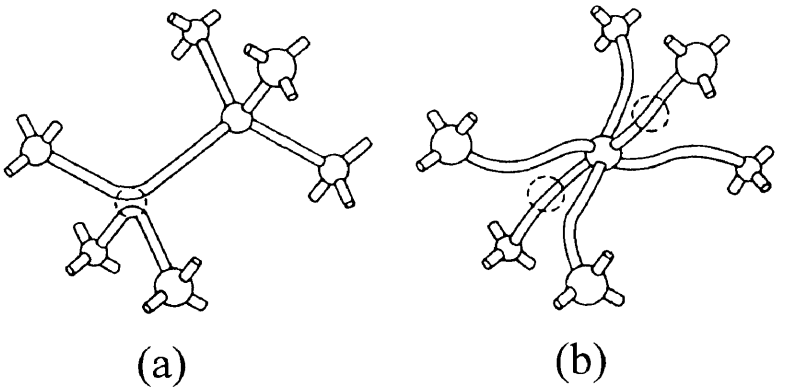

Fig 2.2.1 Configuration of the vacancy in a diamond lattice (a). The saddle-point configuration is illustrated in (b).

The di-vacancy is formed by the removal of two neighbouring atoms. The di-vacancy in the diamond lattice has the configuration shown in fig 2.2.2. (b). Migration of the di-vacancy presumably involves a saddle-point configuration such as illustrated in fig 2.2.2 (a) [7].

© University of Pretoria

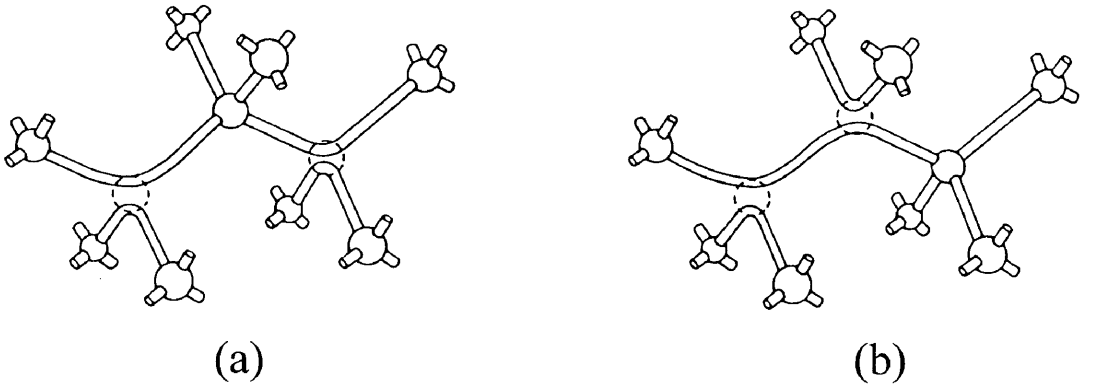

Fig 2.2.2 Configuration of the saddle-point di-vacancy in a diamond lattice (b). The di-vacancy configuration is illustrated in (a).

The formation of vacancy defects may be described as follows:

In any solid at a finite temperature (T), the lattice atoms are in continuous vibration about their equilibrium positions. The amplitude of these vibrations will increase with increasing temperature and may be sufficiently large for an atom to leave its equilibrium position, thus creating a vacancy. The energy of formation (E_f) of each vacancy is the energy required to take an atom to the crystal surface from the interior (E_H), minus the lattice energy per atom (E_L). A Schottky defect may be defined as a vacancy that is formed when an atom moves to the crystal surface or to some other surface within the body of the crystal [8]. Assuming that there are n Schottky defects, the internal energy of the crystal will change by an amount:

$$nE_f = n(E_H - E_L). \tag{2.2.1}$$

In creating a vacancy, the energy of the solid will be increased. The total internal energy of the disordered crystal (E) is:

$$E = E_P + nE_f, \tag{2.2.2}$$

© University of Pretoria

where E_P refers to the internal energy of the perfect lattice. The frequency of success (ν_f) of a vacancy being formed is determined by Maxwell Boltzmann statistics for occupancy of a given energy level, at a defined temperature (T) [3]:

$$\nu_f = \nu_{fo} \exp\left(\frac{-E_f}{kT}\right), \tag{2.2.3}$$

where k is Boltzmann's constant. The factor ν_{fo} is related to the thermal entropy changes through the changes in the vibrational frequencies due to the formation of the defect. The probability of annihilation of vacancy defects depends upon their ability to move through the solid and encounter excess atoms. This migration process needs to be energetically activated. The energy required (E_m) for such a migration process at a particular temperature (T) is related to the Boltzmann probability function (ν_m) [3] :

$$\nu_m = \nu_{mo} \exp\left(\frac{-E_m}{kT}\right). \tag{2.2.4}$$

The factor ν_{mo} is related to the thermal entropy changes through the changes in the vibrational frequencies due to the migration of the defect. In many materials, the process of diffusion or atomic transport is determined by the generation and migration of vacancies. The rate of vacancy formation and migration is given by the product of equations 2.2.3 and 2.2.4 [3,8]:

$$\nu = \nu_o \exp\left(\frac{E_f + E_m}{kT}\right). \tag{2.2.5}$$

The factor ν_o is defined as the lattice oscillation frequency. This vacancy diffusion mechanism is important in the diffusion of substitutional impurities in solids. The probability that an atom may jump into the next site depends upon the vacancy

© University of Pretoria

concentration and upon the probability that it may acquire sufficient energy to make the jump. The activation energy for self-diffusion (E_{SD}) is calculated from:

$$E_{SD} = E_f + E_m. \tag{2.2.6}$$

2.2.1b INTERSTITIALS

There is much less information regarding the interstitial than the vacancy in semiconductor materials. The three most probable types are the dumbbell, the bond-centered and the Crowdion interstitials [5]. The Crowdion configuration requires considerably more formation energy than the other two configurations. The energy of the crystal is raised by such a process [9] and the lattice surrounding the interstitial defect will become strained. The bond-centered interstitial configuration is depicted in fig 2.2.3. In this configuration, the interstitial atom sits at the centre of the bond. Figure 2.3.4 illustrates some split interstitial configurations. A possible distortion of this substitutional configuration leads to the split interstitial configuration. In this configuration, the interstitial atom and one of its neighbours are displaced in such a way that they form a dumbbell, centered on the original substitutional site of this neighbour. This split interstitial can have various orientations depending upon the orientation of this dumbbell.

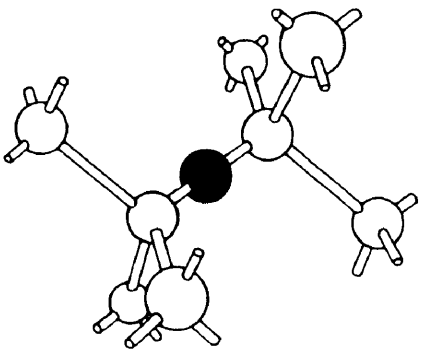

Fig 2.2.3 The bond-centered interstitial configuration in the diamond lattice.

© University of Pretoria

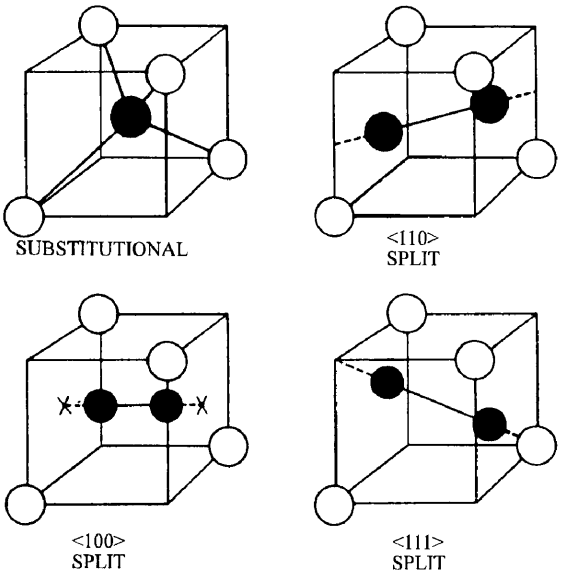

Fig 2.2.4 Various orientations of the split interstitial configuration in the diamond lattice.

The formation energy for the interstitial is higher than the corresponding energy for a vacancy. Since the formation probability exhibits a similar statistical temperature process as the vacancy (eqn 2.2.3), the thermally-activated equilibrium concentration of interstitials will be many orders of magnitude lower than the vacancy concentration. Due to the large lattice strain caused by the introduction of an interstitial, the motion of such a defect relieves this strain and, hence, generally occurs more readily than a vacancy. In radiation damage, interstitials and vacancies are produced in equal numbers and in many cases the interstitial is associated with a nearby vacancy, the two having been formed in the same collision event. It is often useful to think of this interstitial-vacancy pair, or Frenkel pair, as a single defect. The lattice strain associated with a vacancy and an interstitial is such that if they are separated by a short distance, they will relax together spontaneously to relieve the strain. A mechanism related to interstitial diffusion is the intersticialcy mechanism. In this process, an interstitial atom moves into a lattice site by displacing the atom on that site into an adjacent interstitial site.

© University of Pretoria

2.2.1c IMPURITIES

Impurities can play a dominant role in radiation damage experiments. These impurities can locate themselves in many different ways in the host lattice. If such an atom occupies a lattice site, it is known as a substitutional impurity, or if in isolation on a non-normal lattice site, an interstitial impurity. Substitutional impurities may be acceptors, donors or amphoteric impurities. Impurities which exhibit this amphoteric behaviour may behave as donors or acceptors.

2.2.1d COMPLEX DEFECTS

When a simple defect moves through the crystal lattice, it can interact with other intrinsic, as well as extrinsic, point defects, giving rise to a more complex defect. High energy collisions can result in extensively-damaged regions, called spikes. These spike-type damaged regions are observed in semiconductors and the evidence at present seems to indicate that they are due to displacements [7]. The structure of such spikes is not well established but we must recognise that there are a wide variety of possibilities. The spike structure may consist solely of distinct point defects and their aggregates, or of a variant of three other structures: an amorphous structure, dislocation structure, or that of another phase of the material.

The recoiling energetic atom, often referred to as the primary knock-on atom (PKA), can have a number of energetic progeny which can also cause displacement damage. Seeger [10] discussed the nature of the damage process as follows: the high energy recoil atoms move into the lattice, ending up as interstitials and leaving vacancies behind. The vacancies are created primarily along the trail of the higher energy recoil atoms, particularly the primary knock-on atom, with the consequence that there is a zone which is depleted of atoms, surrounded by a shell enriched in interstitial atoms. This

© University of Pretoria

displacement damage depends upon the incident energy, sample temperature and the presence of other defects in the material [7]. Figure 2.2.5 illustrates the formation of a displacement spike where a region depleted of atoms is surrounded by interstitials.

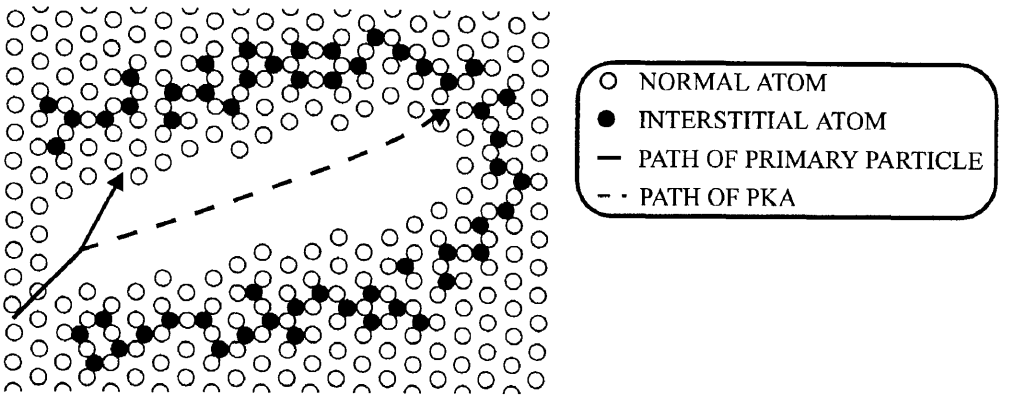

Fig 2.2.5 Schematic representation of interstitials around a multiple vacancy during production of a displacement spike.

When a high energy particle interacts with a crystal, a great deal of energy is deposited in a localized volume. This increase in energy can result in an increase in lattice temperature, which decays by thermal conduction. Such a region of localised temperature is known as a thermal spike. Thermal spikes are important in that they may contribute to diffusion processes in the material.

2.2.2 ASPECTS RELATED TO THE THEORY OF DISPLACEMENT OF ATOMS IN SOLIDS

In this section, we discuss the basic aspects related to the interaction of particles with semiconductors. We are particularly concerned with those interactions that can create damage in the semiconductor. The manner in which an incident particle interacts with an

© University of Pretoria

atom depends upon the properties of the particle such as its mass, electrical charge and kinetic energy [2]. It also depends upon the mass and charge of the target material. During the collisions, energy will be exchanged between the moving particle and the initially stationary lattice atoms. The energy loss causes the particles to slow down and eventually come to rest in the lattice, with the gain in energy in the lattice resulting in the creation of defects or disorder in the lattice. In order to understand and predict the particle penetration and lattice disorder, a good understanding of the collision dynamics is required.

In a collision between a moving particle and a stationary atom, we are confronted with the situation where there are forces of attraction between nuclei and electrons, and forces of repulsion between nuclei, and forces of repulsion between electrons. The total interatomic force is the sum of the various interparticulate forces. There are basically two types of collisions, the first being where the total energy of the system is conserved and there is an exchange of energy between the moving incident particle and the spatial potential energy. Such a collision event is termed an elastic collision, and as the trajectory of the incident particle is changed, scattering is said to have taken place. The second type is when electron excitation or even ionization occurs. Subsequent decay of the excited electrons will lead to photon emission or even further electron emission. As a portion of the incident energy is absorbed during these excitation processes, there is a change in the internal energy of the lattice, and the collision process is an inelastic one.

Before the collision mechanism is explained, the incident particles should be classified. In radiation damage, there are three important classes of incident ions [5]. The first is the energetic particle such as the proton, electron, and deuteron or alpha-particle. These particles usually have an incident energy greater than 1.0 MeV. The second is the highly energetic heavy ion that emanates from nuclear fission and is referred to as the fission fragment, with an energy greater than 100 MeV. The third category is the heavy ions with an incident energy less than 1 MeV. In this study, we shall deal mainly with the first category, namely, the energetic particle.

© University of Pretoria

Firstly, we shall consider the laboratory co-ordinate system (LCS), where the target atom is considered to be at rest. Figure 2.2.6 illustrates the relationship between the particle velocities and scattering angles in this co-ordinate system. An incident particle of mass m_a moving at a velocity V_a collides with a stationary atom of mass M_A. The resulting interaction yields an emerging projectile of mass m_b at an angle θ_b from the incident projectile direction, and a residual target atom of mass M_B moving at a velocity V_B at an angle θ_B from the incident projectile direction. In an elastic collision a=b and A=B.

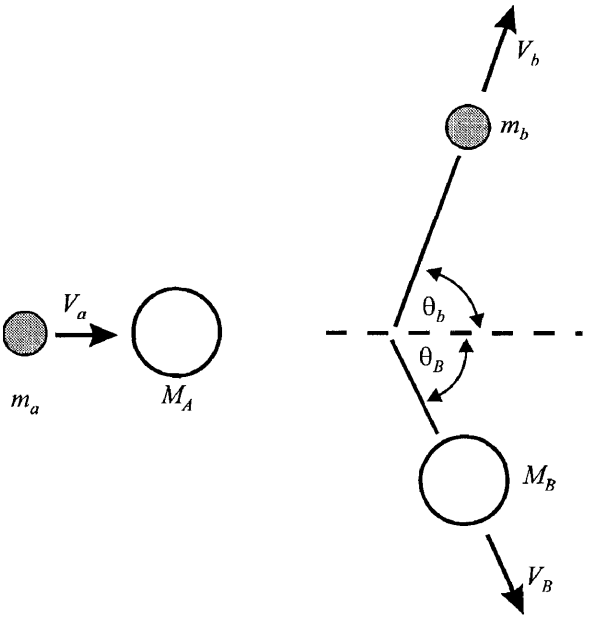

Fig 2.2.6 The relationship between particle velocities and scattering angles in the laboratory co-ordinate system.

From inspection of fig 2.2.6, it can be seen that the struck atom moves at an angle θ_B to the initial direction of particle motion. If, before the collision the incident particle velocity is V_a and after collision its velocity is V_b, and it is moving at an angle θ_b to its initial direction of motion, while the struck atom receives a velocity increment from 0 to V_B, then the energy and momentum conservation may be written as:

© University of Pretoria

$$½m_a V_a^2 = E_0 = E_1 + E_2, \tag{2.2.7}$$

where

$$E_1 = ½M_b V_b^2 \quad and \quad E_2 = ½M_B V_B^2. \tag{2.2.8}$$

When describing an interaction, the interaction rate (the number of interactions per unit time) is important. This rate is estimated from the probability that one incident particle per cm^2 will interact with one nucleus. This probability depends upon the target's effective range of interaction and is expressed as the interaction cross-section (σ, cm^2/target atom). A variation of this interaction cross-section, termed the differential cross-section ($d\sigma/d\Omega$), is often useful as it provides a definition of the interaction cross-section per unit energy transferred or per unit solid angle ($d\Omega$) as a function of scattering angle. In order to describe this interaction cross-section more efficiently, the distance of closest approach of the incident particle to the target nucleus, more commonly known as the impact parameter (p), [11] is required. If we extend the above collision description to include a uniform parallel flux of incident particles extending to infinity, perpendicular to the direction of motion, incident upon the stationary atom, then only those particles with impact parameter $p \leq 2R_o$ (target atom radius) can collide with the atom. When using the classical approximation, an area $\pi(2R_o)^2$ defines a total collision cross-section for collisions.

It is usually simpler and more convenient to describe the dynamics of the interactions using a co-ordinate system in which the total momentum is zero. This system is called the center-of-mass co-ordinate system (CMCS). In this co-ordinate system the particle motions are considered, where the centre of mass of the system is at rest. The relationship between the particle velocities and scattering angles using the CMCS is illustrated in fig 2.2.7.

© University of Pretoria

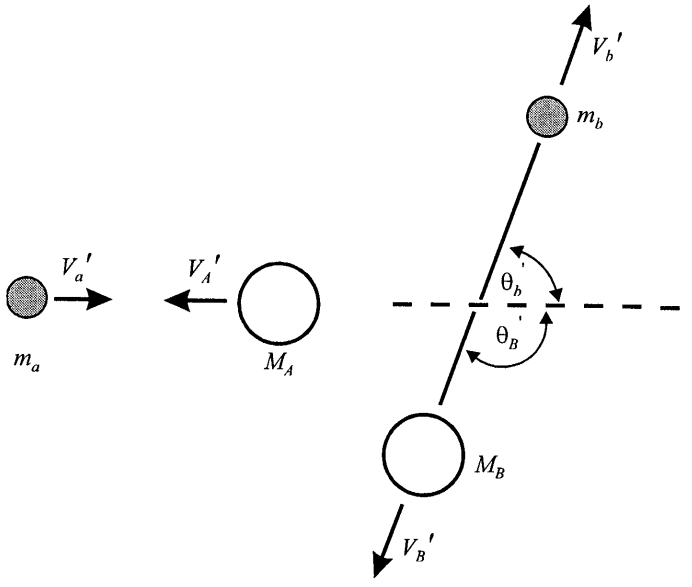

Fig 2.2.7 The relationship between particle velocities and scattering angles in the center-of-mass co-ordinate system.

Of great importance when investigating the displacement of atoms in solids by irradiation, is an estimate of the energy required to displace an atom from a normal site in the crystal lattice. In the case of semiconductors, the simplest model for the displacement of an atom by electron irradiation requires an unscreened coulombic collision between an electron and a nucleus. The recoiling nucleus must have enough kinetic energy to break all its lattice bonds and overcome the potential barrier encountered due to its neighbours. The minimum electron energy necessary to cause displacements into a nearby interstitial position from a head-on collision (impact parameter $p = 0$) is called the threshold energy (E_D), [12] or sometimes the Wigner energy [13]. The ease of displacement of an atom from the influence of its neighbours will depend upon the direction in which it moves relative to these neighbours after the collision. Therefore, the threshold energy exhibits a directional dependence and, hence, it does not have a unique value but will vary from a certain minimum value for a particular orientation to a maximum value where displacement is assured in any direction [3]. The primary knock-on atom (PKA) may also displace further atoms from their lattice sites if it is able to transfer an energy larger or

© University of Pretoria

equal to the threshold energy for that particular displacement. The value of E_D may be estimated using the argument proposed by Seitz [14], who made use of the isotropic square well potential to describe the binding of an atom to its substitutional site. He proposed that the threshold energy for a lattice atom, moving slowly (allowing the lattice to relax) through a path of least resistance, is approximately twice the sublimation energy. However, in reality the atom does not follow the path of least resistance and as it receives a sharp blow, the lattice is not allowed to relax as it passes through the lattice, hence, a more accurate approximation is about 4 to 5 times the sublimation energy ($E_D = 25$ eV). As stated previously, the threshold energy can vary with orientation and the PKA can cause displacement damage. A more appropriate model was thus required to fit experimental data. The details of these models will not be discussed in this work.

The energy dependence for displacements in GaAs has been discussed for more than 25 years, but the magnitude of this energy is still controversial. The value of E_D has been reported to vary from 25 [14] to 9 - 10 eV [15]. A procedure proposed by Lehmann and Bräunig [16] makes use of an isothermal DLTS technique to determine the displacement energy for two different orientations of GaAs. A threshold energy of 15.5 eV was obtained on <100> GaAs, whereas, 9 eV was obtained for the <111> orientation.

In a compound semiconductor, the threshold energy can exhibit an orientation dependence [17]. This anisotropy can be of considerable use in determining the nature of radiation-induced defects in GaAs. From inspection of the zinc-blende structure of GaAs in fig 2.2.8, it can be seen that the displacement of an As atom for irradiation in the [111] Ga direction is difficult because a nearest neighbour Ga atom is in the forward beam direction. However, it will be easier to displace a Ga atom due to the opening in the lattice behind it. This anisotropic defect introduction led these workers to conclude that the main defects after electron irradiation originate in the As sub-lattice. By comparing their results to theoretical predictions, they concluded that the threshold energy for the [111] As orientation is 9 eV, whereas, for the [111] Ga direction the value is between 7 and 11 eV [17].

© University of Pretoria

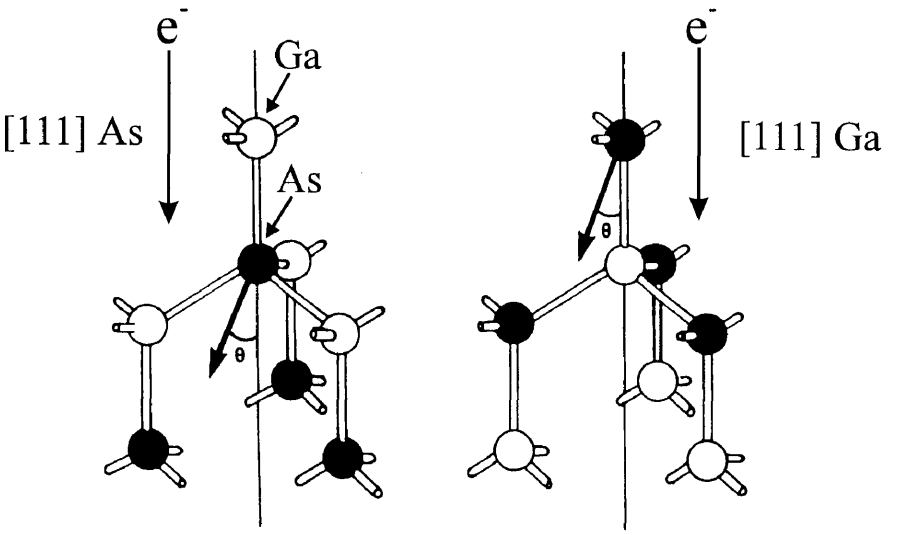

Fig 2.2.8 Schematic diagram illustrating As displacement along two different directions, with the As recoil angle being denoted by θ [17].

Particles that travel through the crystal lattice along their path x are slowed down due to the transfer of their energy to the lattice. The rate of energy loss $(-dE/dx)$ can be written in terms of the stopping powers (S_n) [3]:

$$-\frac{dE}{dx} = N_e(S_n(E) + S_e(E)), \tag{2.2.9}$$

where N_e is the number of target atoms per unit volume and $S_n(E)$ and $S_e(E)$ are the nuclear and electronic stopping powers, respectively. The stopping power is also referred to as the stopping cross-section, and is calculated from:

$$S_n = \int T d\sigma, \tag{2.2.10}$$

© University of Pretoria

where $d\sigma$ is the differential cross-section for energy transfer T. The range of the incident ion ($R(E)$) is obtained directly from the stopping power:

$$R(E) = \int_0^E \frac{dE}{(-dE/dx)}, \tag{2.2.11}$$

where E is the incident energy. Numerical calculations have been performed by Lindhard, Scharff and Schiøtt [18] to describe the collisions in terms of the universal nuclear and electronic stopping powers, making use of a Thomas-Fermi statistical model.

© University of Pretoria

REFERENCES

1) T.P. Ma and P.V. Dressendorfer: Ionizing Radiation Effects in MOS Devices and Circuits (John Wiley & Sons, USA) 1989 p. 47.

2) V.A.J. van Lint, T.M. Flanagan, R.E. Leadon, J.A. Naber and V.C. Rogers: Mechanisms of Radiation Effects in Electronic Materials: (John Wiley & Sons, Canada) 1980 p. 1.

3) G. Carter and W.A. Grant: Ion Implantation of Semiconductors (The Pitman Press, Bath, Great Britian 1976) p. 109.

4) J.C. Bourgoin and M. Lannoo: Point Defects in Semiconductors I (Springer-Verlag, Berlin 1981) p. 1.

5) M.W. Thompson: Defects and Radiation Damage in Metals (Cambridge University Printing House 1969) p. 11

6) J.C. Bourgoin and M. Lannoo: Point Defects in Semiconductors I (Springer-Verlag, Berlin 1981) p. 3.

7) J.H. Crawford and L.M. Slifkin: Point Defects in Solids (Plenum Press, New York 1975) p. 8.

8) B. Henderson: Defects in Crystalline Solids (University Press, Belfast 1972) p. 11.

9) B.T. Kelly: Irradiation Damage to Solids (Pergamon Press, UK 1966) p. 72.

10) A. Seeger: Handbuch der Physik (Springer Verlag, Berlin 1955) Vol. VII, Part 1.

11) H. Haken and H.C. Wolf: Atomic and Quantum Physics (Springer-Verlag, Berlin Heidelberg 1984) p. 39.

12) J.A. Grimshaw and P.C. Banbury: Proc. Phys. Soc. 84 (1964) 151.

13) J.J. Loferski and P. Rappaport: J. Appl. Phys. 30 (1959) 1296.

14) F. Seitz: Disc. Faraday Soc. 5 (1949) 271.

15) D. Pons, P.M. Mooney and J.C. Bourgoin: J. Appl. Phys. 51 (1980) 2038.

16) B. Lehmann and D. Bräunig: J. Appl. Phys. 73 (1993) 2781.

17) D. Pons and J.C. Bourgoin: Phys. Rev. Lett. 47 (1981) 1293.

© University of Pretoria

18) J. Lindhard, M. Scharff and H.E. Schiøtt: Matt. Fys. Medd. Kgl Danske Videnskab Selskab 33 (1963).

© University of Pretoria

2.3 ELECTRIC FIELD EFFECT

Deep levels in semiconductors are often studied by experimental methods based on the thermal emission of electrons or holes by the traps in the space-charge region. It is often assumed that the electric field affecting the defect is negligible. However, there is strong evidence that in some cases the emission rate does depend upon the applied bias and doping. The electric field dependence of the thermal emission of trapped carriers at deep level centres in semiconductors may adversely affect the accurate determination of defect concentration [1,2], as saturation of the defect peak amplitudes may occur depending on the effect of the electric field on the emission of electrons from the defect. According to Pons and Makram-Ebeid, [2] the DLTS [3] signal of a defect that saturates quickly with an increase in filling pulse amplitude has an emission rate that depends strongly on the electric field strength in the space-charge region. The presence of an electric field in the space-charge region may also adversely influence the accurate determination of the DLTS "signature" (position in the band-gap (E_T) and capture cross-section (σ_n)) [3]. It is well established that the thermal emission probability from deep levels is influenced by the local electric field within the space-charge region of a semiconductor junction. Due to the spatial variation of this electric field, substantial deviations from the simple exponential capacitance transients have frequently been observed. The field-dependent emission rate contains information about the potential well structure around defects, that might provide valuable insight into the nature of the defect. There are several mechanisms that may be responsible for the enhanced thermal emission of a trapped carrier from a defect level. Below, those mechanisms most frequently presented in literature are discussed.

2.3.1 POOLE-FRENKEL MECHANISM

The first and probably the most well known, emission enhancement mechanism is the Poole-Frenkel mechanism [4]. This mechanism enhances the emission rate of a defect by lowering the defect potential. Emission enhancement due to this mechanism is predominantly for shallow levels. At “low” electric field strengths, the Poole-Frenkel

© University of Pretoria

effect is the dominant enhancement mechanism, however, at higher field strengths other mechanisms may dominate. The Poole-Frenkel mechanism cannot account for the strong field enhancement observed for deeper lying levels. The Poole-Frenkel effect leads to a decrease (ΔE_i) of the ionisation energy (E_i), so that the more general expression for the thermal emission rate (e_n) represented by eqn 2.3.1,

$$e_n = e_n^{\infty} \exp\left(\frac{-E_i}{kT}\right), \tag{2.3.1}$$

is modified by the Poole-Frenkel potential lowering (ΔE_i), and the new emission rate ($e_n^{'}$) is represented by [5] eqn 2.3.2:

$$e_n^{'} = e_n^{\infty} \exp\left(\frac{\Delta E_i - E_i}{kT}\right), \tag{2.3.2}$$

where e_n^{∞} is a property of the defect under consideration. It is assumed that it is not modified by the electric field and, hence, in this model, the capture-cross section is field independent. The decrease (ΔE_i) depends upon the shape of the defect potential [6]. When the defect potential is an ideal Dirac well, the potential well is lowered to a lesser extent [5]. For a coulombic well [5], ΔE_i is represented by the following eqn:

$$\Delta E_i = \sqrt{\frac{qF}{\pi\varepsilon}}, \tag{2.3.3}$$

where ε is the dielectric constant of the material, F the electric field strength in the space-charge region and q the electron charge. The Poole-Frenkel effect is temperature independent and does not require a critical electrical field strength as do other enhancement mechanisms, such as tunnelling.

© University of Pretoria

When a defect lies in a region where there is an electric field (F), the electron experiences the defect potential plus the pertubative potential ($-qFz$), where z is the electron co-ordinate along the field. The potential barrier lowering of a long range potential defect results in an enhancement of the emission rate from the defect site. This barrier lowering, or Poole-Frenkel effect, is schematically represented in fig 2.3.1. Zhu et al [7] calculated the Poole-Frenkel lowering for a three-dimensional Gaussian potential for a defect in InGaP. For short range potential defects, the effect of the electric field on the potential lowering cannot be fully explained only by the Poole-Frenkel effect.

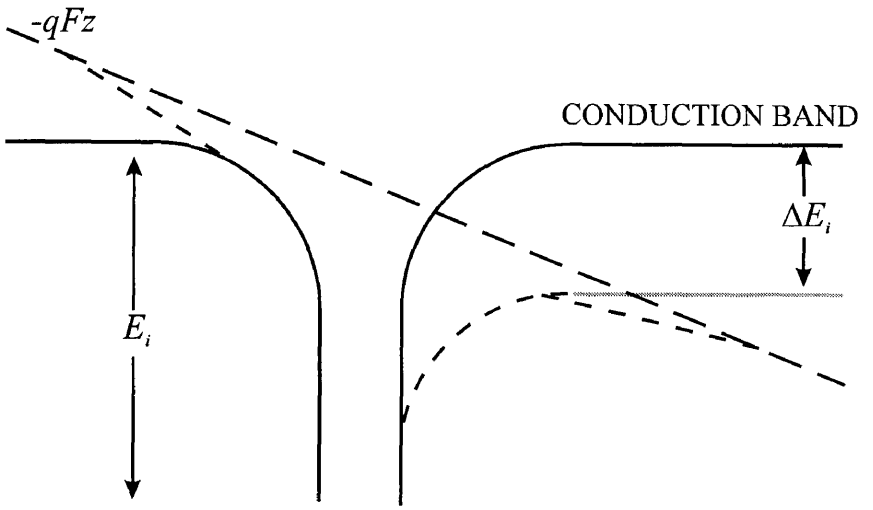

Fig 2.3.1 Schematic representation of the potential barrier lowering (Poole-Frenkel effect).

2.3.2 TUNNELLING MECHANISMS

The electric field can also allow electron emission from a defect site by tunnelling from the defect site to the conduction band. As explained in the following paragraph, this mechanism favours the deeper-lying defects. It is generally accepted that a tunnelling mechanism is responsible for the enhancement of the emission rate in material where

© University of Pretoria

there is a strong field present in the space-charge region. Two possible tunnelling mechanisms are "pure" tunnelling and phonon-assisted tunnelling, with the "pure" tunnelling mechanism being predominant in the high field regions (> 8.0 x 10^7 $V.m^{-1}$) [5].

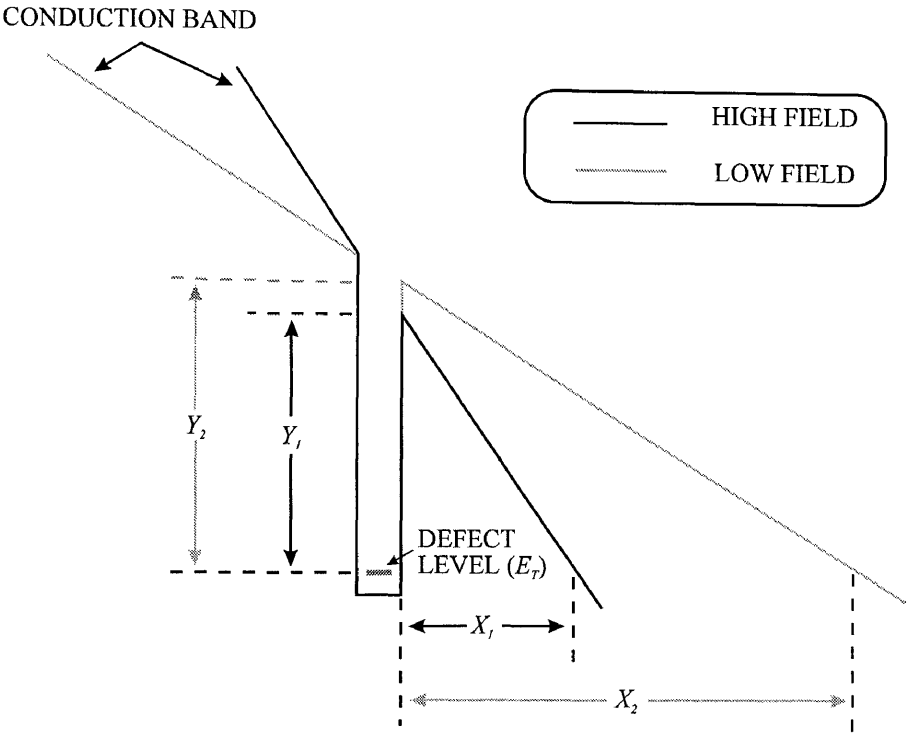

Fig 2.3.2 Schematic representation of a defect potential under two different field strengths ("pure" tunnelling).

Figure 2.3.2 illustrates how a defect potential is perturbed under the influence of an electric field. Firstly, we consider the low field case: the probability of an electron tunnelling from the defect site (E_T) to the conduction band (a distance X_2) is lower than the electron being emitted over the potential barrier (Y_2). Whereas, in the case of the high field condition where the potential barrier is lowered even further than for the low field case, the probability of the trapped electron tunnelling through a distance X_1 is higher than being emitted over the barrier Y_1.

The phonon-assisted tunnelling mechanism is very sensitive to the interaction of the deep levels with the vibronic modes of the lattice, resulting in a coupling mechanism between

© University of Pretoria

the deep levels and the lattice phonon modes [2]. Because of this coupling, the trapped electron can occupy a set of stationary quasi-levels separated by $\hbar\omega$, with $\hbar\omega$ being the phonon energy. Elastic tunnelling can then occur from any of these quasi-deep levels to the conduction band.

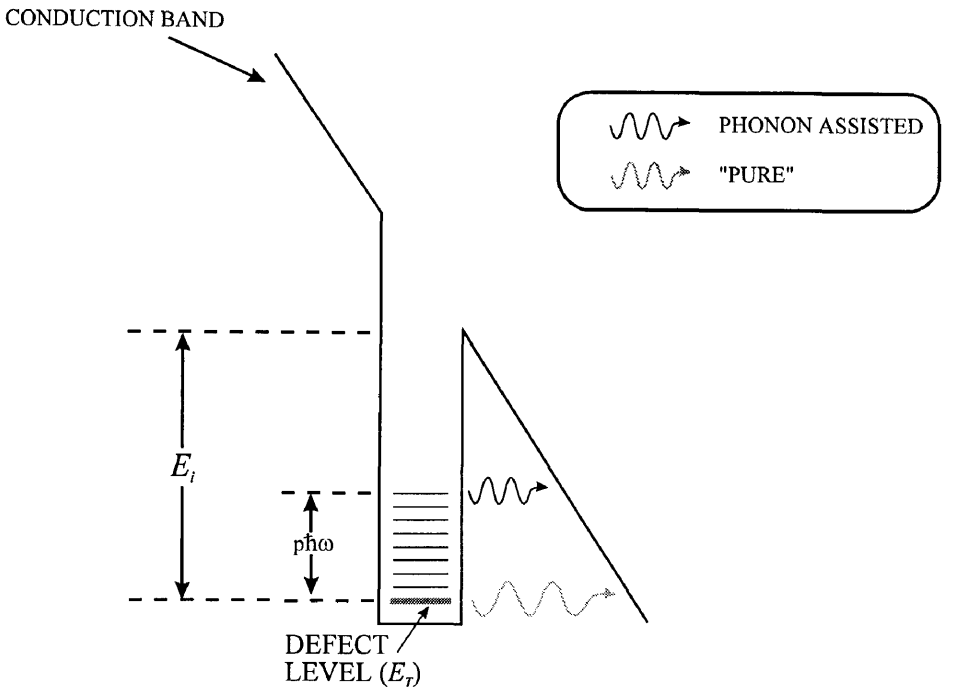

Fig 2.3.3 Energy diagram in the presence of an electric field; also illustrated is the quasi-levels associated with an occupied trapping site.

In fig 2.3.3, the perturbation of the defect potential due to the presence of an electric field in the space-charge region is illustrated. The formation of the quasi-levels due to the coupling between the lattice phonon modes and the defect level is also illustrated. The probability of "pure" tunnelling being the emission enhancement mechanism, where the trapped carrier tunnels from the ground defect state (E_T), is lower than the probability of the enhancement mechanism being phonon-assisted tunnelling, where the trapped carrier tunnels from one of the quasi-levels to the conduction band.

© University of Pretoria

The effect of electron-lattice coupling is effectively visualised in terms of the configuration co-ordinate (C.C.) diagram such as in fig 2.3.4, assuming a coupling of the defect with one lattice co-ordinate Q [2)]. Both the electronic- and the lattice energies are shown as functions of the normalized lattice displacement Q.

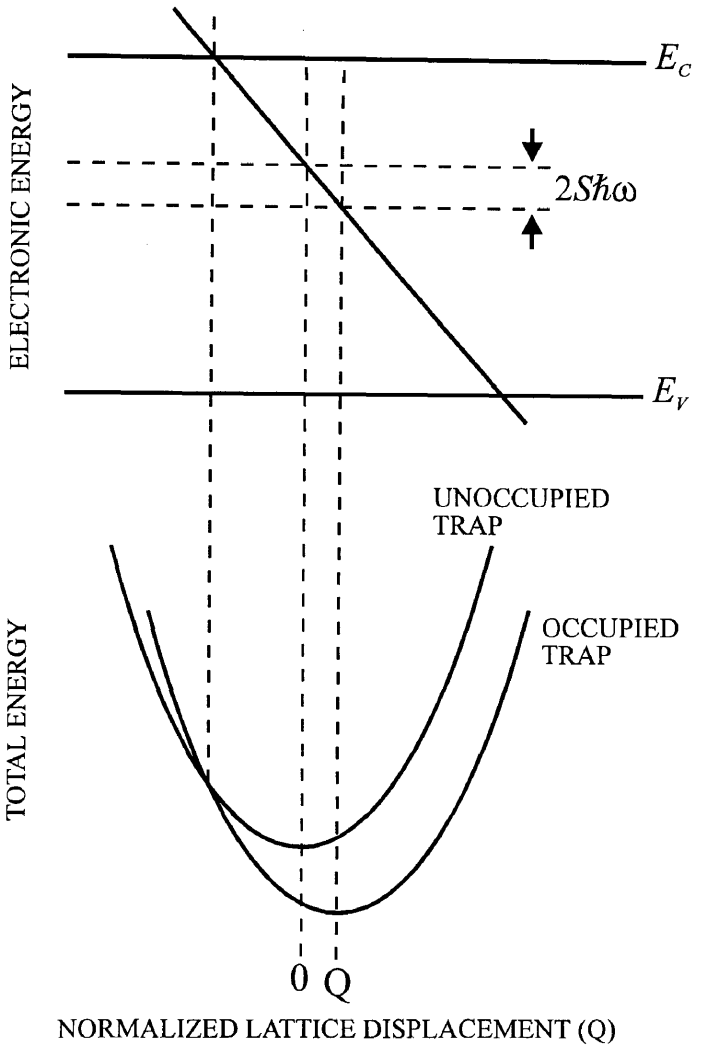

Fig 2.3.4 Configuration co-ordinate diagram showing the electronic level and the total energy (sum of elastic and electronic energy) of the defect as a function of the normalized lattice displacement.

According to the Franck-Condon principle, the energy of a localised state in the bandgap depends on whether the state is occupied or not [8)]. If the localised state is occupied by an electron, an additional polarisation of the lattice may take place and the defect finds a new equilibrium position in the lattice. This electron-lattice coupling exhibits a strong

© University of Pretoria

dependence on temperature, increasing as the temperature increases. It results in rapid broadening of the optical emission (absorption) spectrum with temperature, corresponding to all the possible transitions between the vibrational states of the system [9].

The difference in electronic energy between the unoccupied and the occupied level is shown to be twice the Frank-Condon shift ($S\hbar\omega$) [2]; the stronger the coupling, the larger the coupling constant S. The possibility of strong coupling to the lattice of a deeply-bound localised state increases the probability of a multiphonon capture mechanism [8]. When making use of the DLTS technique to study carrier capture and emission, the deep levels are in the space-charge region and, hence, subject to rather substantial electric fields. The study of the capture cross-section (σ_n) as a function of temperature has shown that electron-phonon interaction often plays an important role on the properties of defects [10]. When the capture cross-section exhibits a strong temperature-dependence, one must correct the observed activation energy for emission to obtain the "true energy" depth of the level. The true energy depth (E_o) is calculated by subtracting the activation energy for carrier capture (E_∞) from the activation energy measured from thermal emission experiments for carrier emission (E_T). The quantity E_∞ can be viewed in the multiphonon emission capture process as the energy barrier that a carrier has to overcome to be trapped on a defect site. In fig 2.3.5, the configuration co-ordinate diagram illustrating the activation energy for carrier capture and the Frank-Condon shift for an electron defect is depicted.

© University of Pretoria

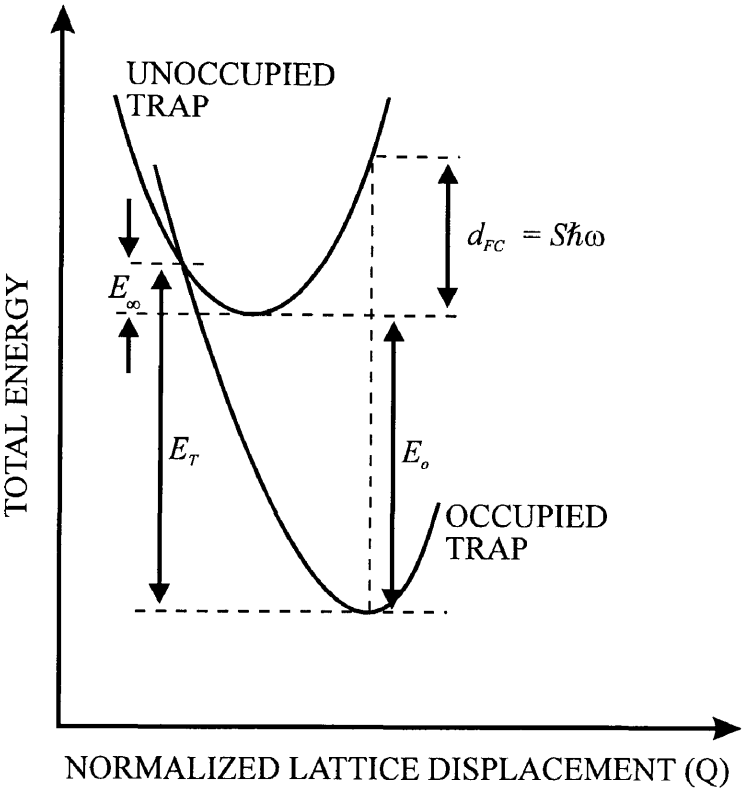

Fig 2.3.5 Configuration co-ordinate diagram illustrating the activation energy for carrier capture and the Frank-Condon shift.

The two quantities, E_∞ and d_{FC}, define the configuration co-ordinate diagram for this defect, illustrating the effect of electron-phonon interaction [11]. In this diagram, the thermal activation depth is represented by the symbol E_o. A knowledge of two of the above-described three quantities (E_∞, d_{FC} and E_o) is sufficient to define the configuration co-ordinate diagram when the parameter k of the vibrational energy term is known [10].

The phonon-assisted tunnelling mechanism is illustrated in fig 2.3.6. Also shown in this figure is the probability of occupation (Π_p) of a particular quasi-level, from which the trapped carrier will tunnel to the conduction band.

© University of Pretoria

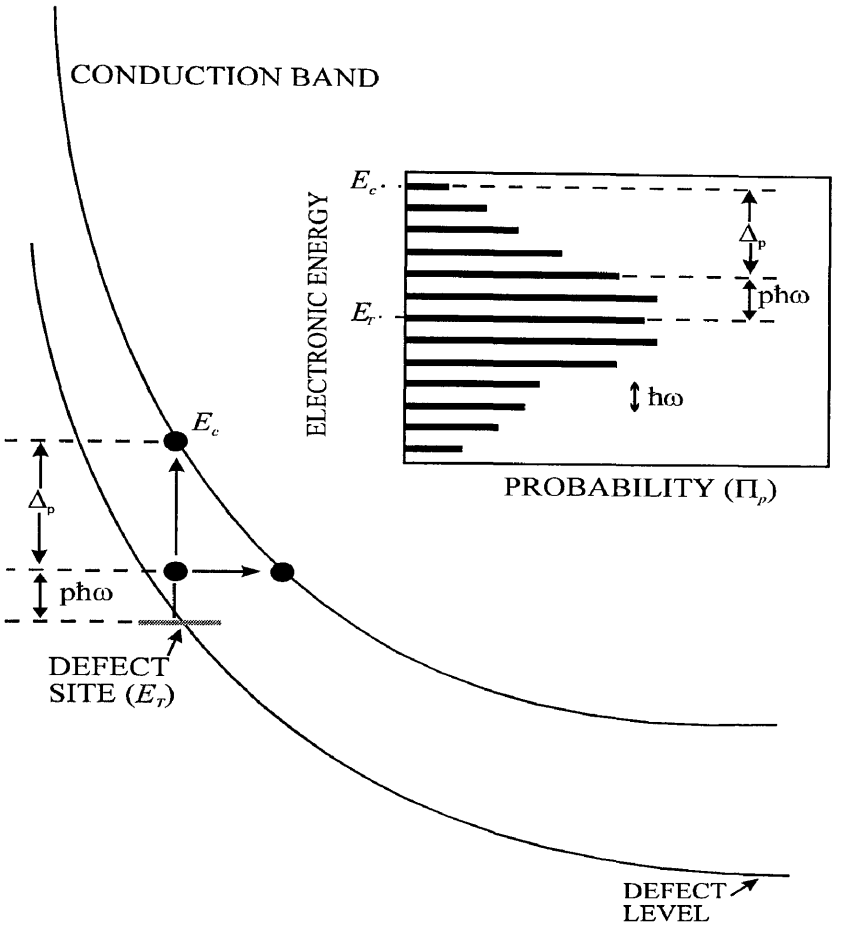

Fig 2.3.6 Energy diagram illustrating the profile of the conduction band edge of a n-type semiconductor near the metal, the probability of occupation (Π_p) of each quasi-level of energy (E_c - Δ_p).

The coupling constant, or Huang-Rhys factor (S) [12], is represented by the following equation [13] where the phonon energy is $\hbar\omega$:

$$S = \frac{\Delta E}{\hbar\omega}, \tag{2.3.4}$$

where ΔE refers to the change in energy due to lattice relaxation. When the trap (E_T) is occupied, the trapped electron can be emitted from any one of the quasi-levels (E_c - Δ_p).

© University of Pretoria

The probability for this process is the product of three factors: the probability of finding the trapped electron at the quasi-level (Π_p), the tunnel emission probability ($\Gamma(\Delta_p)$) and the Fermi-Dirac probability of finding an empty conduction band state. The field emission rate due to phonon assisted tunnelling emission, as derived by Pons and Makram-Ebeid [2], is given in eqn 2.3.5:

$$e_f = \sum_p \Pi_p . \Gamma(\Delta_p).(1 - f_{1,p}). \tag{2.3.5}$$

The $(1 - f_{1,p})$ factor in the above equation is the Fermi-Dirac probability of finding an empty conduction band state. The tunnelling emission probability for an electron at a quasi level $\Gamma(\Delta)$, as found by Korol [14], for an electron trapped in a delta function potential well can be written as:

$$\Gamma(\Delta) = \gamma \frac{\Delta}{qK} \exp^{-K}, \tag{2.3.6}$$

where Δ is the energy position of the deep level below the conduction band and K is the WKB approximation of the wave function across the potential barrier separating the trapping site from the free conduction band states [2]. The factor γ depends on the exact form of the short range potential, and assuming a uniform field (F) and a triangular barrier, K is calculated using [2]:

$$\mathrm{K} = \frac{4}{3} \frac{\sqrt{2m^*}}{\hbar F} \Delta^{3/2}. \tag{2.3.7}$$

The electric field strength in the space-charge region is represented by the symbol F and the electron effective mass by m^*. The probability (Π_p) of finding the trapped electron at a given quasi-level ($E_C - \Delta_p$, where $p = 0, \pm1, \pm2, \ldots$) may be calculated from [2]:

$$\Pi_p = \left(1 - \exp^{-\hbar\omega/\mathrm{kT}}\right) \sum_{n=0}^{+\infty} \exp^{-n\hbar\omega/kT} J_p^2\left(2\sqrt{\mathrm{S}\left(n + \frac{1}{2}\right)}\right), \tag{2.3.8}$$

© University of Pretoria

where J_p is a Bessel function of the first kind and n the integer number of phonons. This model is based on the assumption that the phonons have a single well-defined angular frequency (ω). Figure 2.3.7 [5] illustrates the field strength regimes in which the different enhancement mechanisms are dominant. In this graph, the ratio of the thermal emission rate with and without an electric field versus field strength is presented. This particular graph is for an electron defect at 300 K, situated 0.8 eV below the conduction band. One can clearly see that the "pure" tunnelling mechanism is dominant in the 2 - 9 x 10^8 V.m^{-1} region, whereas the Poole-Frenkel and the phonon-assisted mechanisms are more dominant in the 1 x 10^6 - 5 x 10^7 V.m^{-1} range.

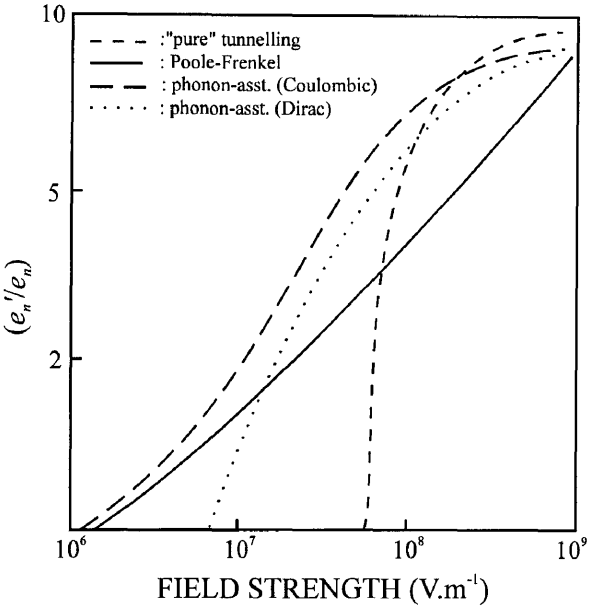

Fig 2.3.7 The ratio of the thermal emission rate with or without electric field versus electric field strength for the different enhancement mechanisms.

To conclude, when performing routine DLTS measurements there are two areas where erroneous conclusions can be made. Firstly, incorrect DLTS "signatures" may be calculated as a result of DLTS peak shift and peak broadening due to enhanced carrier emission from the defect under consideration. Secondly, a peak broadening may also indicate the presence of a second defect positioned very close to the original defect under investigation, and may not always be conclusive evidence that a single defect is

© University of Pretoria

experiencing enhanced emission. When the emission rate of a well-defined single defect is enhanced by one of the mechanisms described above, the DLTS peak may appear broadened towards the low temperature side of the DLTS scan or the peak position of the DLTS peak may move as a function of field strength. To confirm this emission rate field dependence, the bias conditions (field strength) should be changed, and if the peak shape or position varies with field strength, the emission rate is field dependent. To determine which mechanism or mechanisms are responsible for this enhancement, modelling of the experimental data has to be performed.

As stated previously, a broad peak that shifts with field strength may in fact be two defects positioned very close to each other. To investigate this possibility, DLTS spectra have to be recorded using the DDLTS [15] technique, where the field strength in a narrow region is known.

© University of Pretoria

REFERENCES

1) H. Lefevre and M. Schulz: J. Appl. Phys. 12 (1977) 45.

2) D. Pons and S. Makram-Ebeid: J. Phys. (Paris) 40 (1979) 1161.

3) D.V. Lang: J. Appl. Phys. 45 (1974) 3014.

4) J. Frenkel: Phys. Rev. 54 (1938) 657.

5) G. Vincent, A. Chantre and D. Bois: J. Appl. Phys. 50 (1979) 5484.

6) M. Zazoui, S.L. Feng and J.C. Bourgoin: Semicond. Sci. Technol. 6 (1991) 973-978

7) O.S. Zhu, K. Hiramatsu, N. Sawaki, I. Akasaki and X.N. Liu: J. Appl. Phys. 73 (1993) 771.

8) M. Jaros: Deep Levels in Semiconductors (Adam Hilger Ltd. Techno House, Redcliffe Way, Bristol BS1 6NX 1982 p. 19.

9) J.C. Bourgoin and M. Lannoo: Point Defects in Semiconductors II (Springer-Verlag, Berlin 1983) p. 91.

10) C.H. Henry, D.V. Lang: Phys. Rev. B 15 (1977) 989.

11) J.C. Bourgoin, H.J. von Bardeleben and D. Stievenard: J. Appl. Phys. 64 (1988) R65.

12) K. Huang and A. Rhys: Proc. Roy. Soc. London, Ser. A 204 (1950) 406.

13) S. Makram-Ebeid: Appl. Phys. Lett. 37 (1980) 464.

14) E.N. Korol: Sov. Phys. Solid State 19 (1977) 1327.

15) H. Lefévre and M. Schulz: Appl. Phys. 12 (1977) 45.

© University of Pretoria

2.4 DEFECT ANNEALING

A knowledge of the thermodynamic and electronic characteristics of radiation-induced defects in semiconductors may be useful in the identification of these intentionally-introduced defects. The effect of radiation on an electronic material and the consequent degradation in performance of devices made from such material will depend upon, amongst other factors, the type and fluence of radiation. The increased carrier mobility (speed) and radiation hardness of GaAs has prompted an increase in the use of this semiconductor for applications in space and other radiation environments [1,2]. When defects have been intentionally introduced (during particle irradiation) in a solid, it is possible, under certain circumstances, to reduce the defect concentration or even completely remove these intentionally-introduced defects by annealing the material at the correct temperature for a specific period. As early as 1962, the annealing of n-type GaAs irradiated with electrons at room temperature was investigated [3]. In 1970, Thommen [4] investigated the recovery of low temperature electron radiation-induced damage in n-GaAs, identifying 3 major irreversible recovery stages (stages I, II and III). In this section, the annealing kinetics and parameters associated with defect annealing in semiconductors will be discussed.

2.4.1 ANNEALING KINETICS

If a solid contains a defect concentration in excess of the thermal equilibrium level, these defects will, if conditions allow, react to reduce the free energy of the solid [5]. Under the correct conditions, the thermodynamic driving forces reduce the concentration of defects to the equilibrium concentration characteristic of the material [6]. An excess of defects disappears due to one of the following processes:

1. The defects migrate to sinks (surfaces, grain boundaries, etc.) or they recombine with their counterparts (vacancy-interstitial pair).
2. They form complex defects by association with themselves or impurities; these complexes then dissociate.

© University of Pretoria

The technique used in this work to study defect annealing is deep level transient spectroscopy (DLTS) [7]. However, as Aukerman and Graft [3] have illustrated, the effect of defect annealing can be observed by monitoring the carrier concentration and conductivity. The electrical resistivity and Hall coefficient have also been monitored to study the effect of annealing on defect properties [4]. Immobile space-charge depth profiling has also been used to obtain more information on the thermal annealing-induced changes [8]. One of the most important contributions to defect annealing in GaAs was the discovery of three recovery stages by Thommen [4]. In his work, Thommen irradiated undoped n-GaAs with electrons having incident energies between 0.46 and 1.30 MeV at 5 and 77 K. From this work, he concluded that there are three major irreversible recovery stages centered near 235 K (stage 1), 280 K (stage II) and 520 K (stage III).

A knowledge of the electronic and thermal properties of defects is important in understanding the operation of devices in an environment where the device may be subjected to radiation. The rate (number of defects that dissociate per unit time) at which these defects dissociate and the order of the annealing reaction may provide more detailed information about the nature of radiation-induced defects in GaAs. Consider N defects which migrate to sinks: assuming both the defects and the sinks are randomly distributed, the decrease in the number of defects (dN) per unit time (dt) may be written as [6]:

$$\frac{dN}{dt} = -KN^{\alpha}, \qquad (2.4.1)$$

with α being the order of the annealing reaction and K the rate constant which is proportional to the diffusion coefficient of the defect under consideration. For the purpose of this study, only the difference between first and second order reactions will be discussed.

Interstitials (I) and vacancies (V) are created by particle irradiation; these defects are randomly distributed in pairs. The representation of a pair distribution is presented in fig 2.4.1 [6].

© University of Pretoria

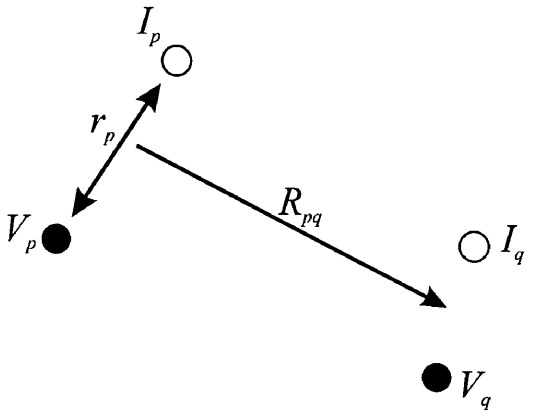

Fig 2.4.1 Representation of a vacancy-interstitial pair distribution.

The recombination occurs through the diffusion of one element of the pair. The order of the annealing reaction reflects the distribution in distance of the pairs ($g(r_p)$), i.e. the number of vacancy-interstitial pairs which are separated by a distance r_p. The reaction order may also be characterised by the correlation factor (γ), which is defined by making use of fig 2.4.1 as the ratio of the distance R_{pq} between two pairs (p and q) to the distance r_p between two elements of one pair:

$$\gamma = \frac{R_{pq}}{r_p}. \tag{2.4.2}$$

When the correlation factor is large, the vacancy-interstitial pairs are termed close pairs and the kinetics are governed by first-order kinetics and the activation energy governing the annealing reaction is the barrier separating the pair. However, when the correlation factor is small ($\gamma \approx 1$), the defects are randomly distributed and the annealing kinetics are governed by the diffusion coefficient, resulting in a second order reaction. In the case of a second order reaction, eqn 2.4.1 becomes: if N_I and N_V are the concentrations of I and V, respectively, we have:

$$\frac{dN_I}{dt} = \frac{dN_V}{dt} = -KN_I N_V. \tag{2.4.3}$$

© University of Pretoria

Since

$$N_I = N_V, \tag{2.4.4}$$

eqn 2.4.3 will reduce to:

$$\frac{dN_I}{dt} = -KN_I^2. \tag{2.4.5}$$

Clearly, eqn 2.4.5 represents a second order process. As has been illustrated, to realistically analyze thermal annealing experiments, the order (α) of the process must be determined. An increase in the order of the reaction increases the range of temperatures over which a single process occurs. This phenomena is illustrated in fig 2.4.2 [5].

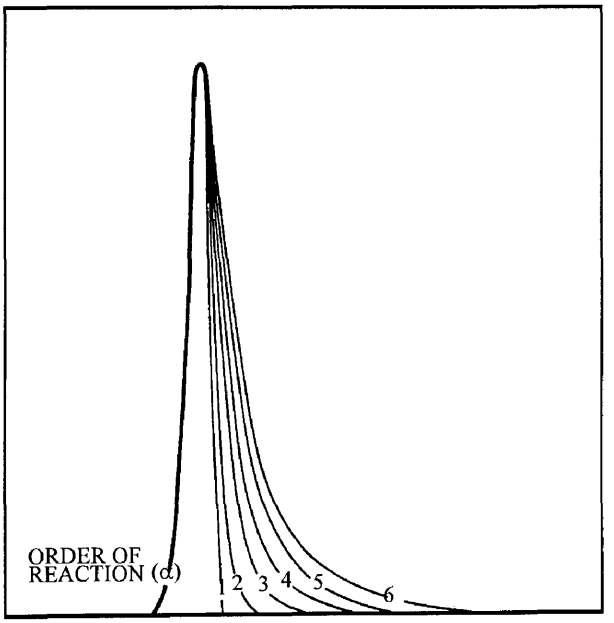

Fig 2.4.2 Effect of increasing order of reaction on property changes in annealing.

It is assumed that a defect requires a certain energy in order to undergo some reaction which modifies its contribution to the measured property change. This energy is defined as the activation energy, or migration enthalpy (ΔH). The fraction of defects possessing

© University of Pretoria

this energy (ΔH) is given by a Boltzmann factor (exp(-$\Delta H/kT$)). This activation energy may be calculated in various ways: the first, and probably the most simple, method to be discussed is where the variation in defect concentration (dN) is monitored as a function of time (dt) for two different temperatures (T_1 and T_2). The annealing rate ($A_1 = dN/dt$) is recorded at a constant temperature (T_1) [6]:

$$A_1 = \nu \exp\left(-\frac{\Delta H}{kT_1}\right). \tag{2.4.6}$$

The value of ν depends upon the change in entropy (ΔS) associated with the defect migration process and the number of jumps (N_j) before the defect is annihilated, with the lattice frequency represented by ν_o:

$$\nu = \frac{\nu_o}{N_j}\exp\left(\frac{\Delta S}{k}\right). \tag{2.4.7}$$

At a given time (t_o), the temperature is abruptly changed to T_2 so that the annealing rate now becomes:

$$A_2 = \nu \exp\left(-\frac{\Delta H}{kT_2}\right). \tag{2.4.8}$$

Equations 2.4.6 and 2.4.8 can now be rewritten as:

$$\left[\frac{A_1}{A_2}\right]_{t=t_o} = \exp\left[\frac{-\Delta H}{kT_1} + \frac{-\Delta H}{kT_2}\right]. \tag{2.4.9}$$

Plotting graphs of change in defect concentration (dN) versus increase in time (dt) for both temperatures (T_1 and T_2), allows one to obtain the slopes labelled α_1 and α_2, respectively. Equation 2.4.9 can now be rewritten as:

© University of Pretoria

$$\ln\left[\frac{\alpha_1}{\alpha_2}\right]=\frac{-\Delta H}{k}\left[\frac{1}{T_1}+\frac{1}{T_2}\right]. \qquad (2.4.10)$$

Finally, the activation energy (ΔH) can be obtained, with the advantage that no knowledge of the nature of the annealing kinetics was required [6]:

$$\Delta H = k\frac{T_1 T_2}{T_1 - T_2}\ln\left[\frac{\alpha_1}{\alpha_2}\right]. \qquad (2.4.11)$$

A second more complete and accurate method is to plot a graph of change in defect concentration (ΔN) versus time (t) for a specific temperature (T); the slope of this graph ($d\Delta N/dt$), being the annealing rate (A) for that specific defect at that specific temperature. This procedure is repeated for different temperatures. To calculate the activation energy (ΔH) for a first order reaction for this particular defect, the slope of a graph of $\ln(A)$ versus $1/T$ is determined, using eqn 2.4.6. As stated previously, the value of ν depends upon, amongst other factors, the number of jumps (N_j) before the defect is annihilated. A factor (ν) which is very small (10^2 s^{-1}) is indicative of long-range diffusion, whereas, a larger factor (10^{12} s^{-1}) implies the annihilation of close defects [9].

2.4.2 PARTICLE-IRRADIATION INDUCED DEFECTS IN GaAs

Stage I and stage II, as shown by Thommen, exhibit first-order annealing kinetics. However, defects that anneal in stage III may not be described by simple first-order annealing kinetics. The first two stages typically account for only about 10-20% of the carrier removal after 1 MeV electron irradiation [10]. Auckerman and Graft [3] found that the annealing stage around 500 K, namely, stage III, in n-GaAs can consist of two first-order substages (λ_1 and λ_2). Annealing experiments have shown that electron defects E7 and E9 are ascribed to stage I [11], while all the other electron traps (E1 - E6) anneal in stage III [12], with approximately the same migration enthalpy. In n-GaAs it has been

© University of Pretoria

UNIVERSITEIT VAN PRETORIA
UNIVERSITY OF PRETORIA
YUNIBESITHI YA PRETORIA

observed that after stage III annealing, three further defects (P1, P2 and P3) are detected by DLTS. It is believed that P1 originates due to the annealing of the primary defects (E1 - E6), whereas P2 and P3 are directly created by irradiation, but prior to annealing they are masked by the presence of E4 and E5 [11]. Figure 2.4.3 illustrates the isochronal (10 minute) annealing behaviour of traps E2 - E5 and P1 - P3 in VPE-grown material [9]. It has been speculated that defect P1 is the same defect as EL5, which is a native defect in VPE-grown layers [9].

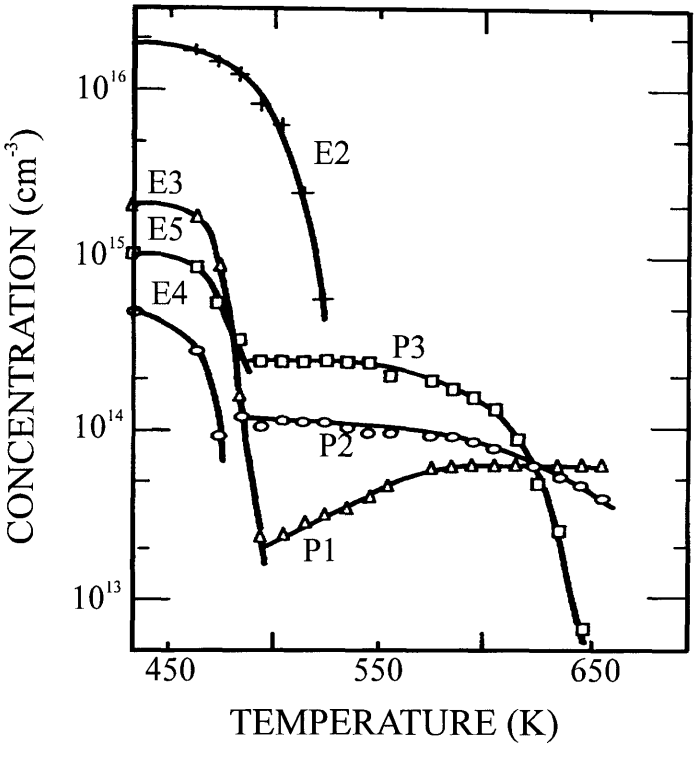

Fig 2.4.3 Isochronal annealing behaviour of traps E2 - E5 and P1 - P3 introduced by electron-irradiation in VPE material [13].

In p-type GaAs, the annealing of hole defects is more complex than the situation for electron defects in n-type GaAs [9]. Hole defects H0 - H5 are observed after electron irradiation; defects H0 and H1 have the same annealing behaviour (stage III) as that of the electron traps detected in n-type GaAs, which are related to the arsenic vacancy-interstitial pair. The hole defect labelled H2 is more complex than the other hole defects

© University of Pretoria

in that its annealing kinetics exhibit two components which are not fully understood. Defects H3 and H4 anneal with first order kinetics with a very small factor ($\nu \approx 10^2$ s^{-1}), indicating a long-range diffusion [9].

Pons et al [14] have shown that only the electron radiation-induced electron trap E2 exhibits two distinct first-order kinetics. Farmer and Look [15] have speculated that the first-order substage λ_1 is nearly independent of sample growth conditions and doping levels, whereas, the second substage λ_2 exhibits a dependence on the free carrier concentration of the sample. Aukerman and Graft [3] have shown that ν of the λ_2 sub-stage depends upon the donor concentration, which they attributed to a Fermi level dependence of the annealing rate. The annealing rate of the first fraction (λ_1) is slower than the remaining fraction [16] and is shown to be the same as the annealing rate of E3 and E5 [11].

Positron lifetime measurements have also been utilised to study the annealing kinetics of radiation-induced defects in GaAs. Sen Gupta et al [17] made use of the positron annihilation technique to study the recovery of defects in n-type GaAs after α-particle irradiation at 300 K; their conclusion from this isochronal annealing study was that the defects revealed a smooth recovery at temperatures greater than 400 K. Hautojärvi et al [18] revealed, using positron lifetime measurements, that gallium vacancies (V_{Ga}) exist after 3 MeV electron irradiation and that they recover between 200 - 350 K.

When looking at the annealing behaviour of more heavily irradiated GaAs or of particle damage where clusters of defects are important, it can be seen that with an increase in particle fluence and incident particle mass, there is an increase in anneal temperature and the anneal stages are broader. It has been proposed that, unlike the point defects which anneal out in stage III (500 K), defect clusters break up at approximately 680 K [10].

© University of Pretoria

2.4.3 ENHANCEMENT OF DEFECT MIGRATION

The possibility that the energy of nonradiative electron-hole recombination might enhance the motion of a defect has been suggested by Corbett and Bourgoin [19]. Lang and Kimerling [20] were the first to observe this effect using DLTS in GaAs, when studying the annealing of defects in a GaAs p-n junction. Recombination-enhanced annealing was first observed for the electron defect E3 in n-type GaAs [20]. This study revealed that the enhanced annealing rate was proportional to the electron-hole recombination rate and could not be explained by changes in the charge state of the defect as was originally reported by Aukerman and Graft [3]. However, it was later demonstrated by Pons [21] that a charge state effect is operative in stage III, and that the annealing kinetics of the electron defects are related to the position of the Fermi level. Mamontov and Peshev [22] investigated the annealing of defects introduced after room temperature irradiation; they concluded that the annealing of E3 was field-dependent. Defect-enhanced annealing due to the charge state of the defect or through carrier recombination has been extensively studied [21,23,24]. Recombination-enhanced annealing was observed for electron defects E1 and E2 [25]. The one electron trap that does not seem to exhibit an annealing rate that is dependent upon current injection is E4 [11]. Thus, it is clear that there are mechanisms available which will promote defect migration.

The charge state of a defect corresponds to the number of carriers which remain localized on the site of the defect, in addition to the electrons that the defect possesses in its neutral state. The concentration of a defect in a given charge state is determined by the position of the Fermi level, which depends upon the temperature, the doping impurity concentration and the concentration of other deep levels [6]. Defect migration can be altered by one of the following three mechanisms [6]:

© University of Pretoria

1. *ELECTROSTRICTION MECHANISM*

The presence of electrons and holes in the conduction- and valence bands reduces the bonding energy and increases the anti-bonding energy. Consequently, it modifies the migration and formation enthalpies. Electron-hole recombination results in a change in the energy of the lattice, the dilation per electron-hole pair is such that this mechanism is negligible.

2. *IONIZATION-ENHANCED MIGRATION*

The migration enthalpy is changed due to the Fermi level position, in other words, due to a change in the fraction of the defect population, which is in a given charge state. Consider a defect in a state A positioned at a level E_T with a charge state q; in this charge state the Fermi level is above the defect level. This defect may also be in a state B with a charge state Q when the Fermi level is below the defect level. The change in charge from q to Q induces a corresponding change in the migration enthalpy ($\Delta H_A \rightarrow \Delta H_B$) and, consequently, in the jump probability. This modification of the migration enthalpy due to the charge state of a defect is illustrated in fig 2.4.4.

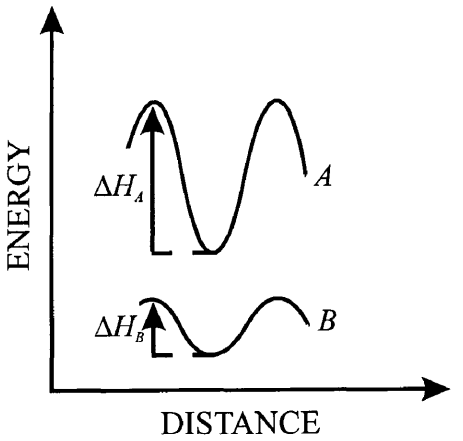

Fig 2.4.4 Schematic representation of the migration enthalpy versus atomic distance for the ionization-enhanced migration mechanism.

© University of Pretoria

3. ATHERMAL-ENHANCED MIGRATION

This migration mechanism is said to be athermal because the migration does not require thermal energy. The energy necessary to induce the migration is provided by the electronic carrier. The average state of a particular defect is a temporal average obtained by a continual succession of electronic transitions between the defect state and the bands (conduction and valence). The rate of transition between this state and the bands or the change in charge state is given by the capture and generation rates of electrons and holes. Such changes in the charge state can lead to athermal defect migration.

The athermal defect migration mechanism may be described by using fig 2.4.5. Consider a defect in a charge state *A*; it is in an equilibrium position (1). When the charge state of the defect changes to state *B*, the defect is now in a new saddle-point position (2) and relaxes to a position (3) in charge state *B*. When the defect reverts back to its original charge state, it relaxes from position (4) to position (5). The defect has thus migrated from position (1) to position (5).

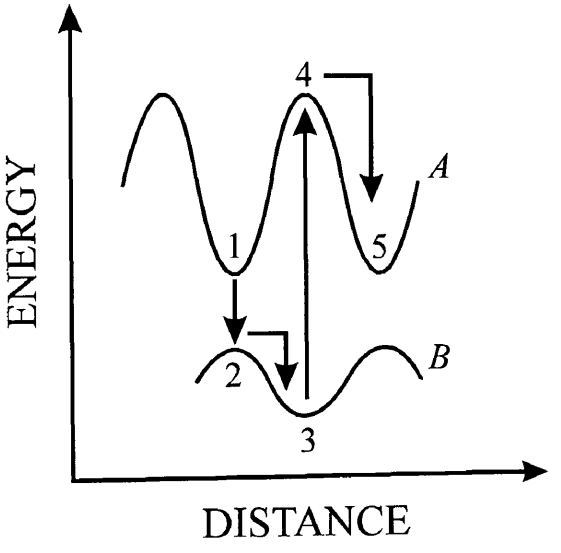

Fig 2.4.5 Schematic representation of the athermal-enhanced migration mechanism.

© University of Pretoria

REFERENCES

1) A.F. Galashan and S.W. Bland: J. Appl. Phys. 67 (1990) 173.
2) A.R. Knudson, A.B. Cambell, W.J. Stapor, P. Shapiro and G. P. Mueller: IEEE Trans. Nucl. Sci. NS-32 (1985) 4388.
3) L.W. Aukerman and D.D. Graft: Phys. Rev. 127 (1962) 1576.
4) K. Thommen: Radiat. Effects. 2 (1970) 201.
5) B.T. Kelly: Irradiation Damage to Solids (Pergamon Press, UK 1966) p. 179.
6) J.C. Bourgoin and M. Lannoo: Point Defects in Semiconductors II (Springer-Verlag, Berlin 1983) p. 247.
7) D.V. Lang: J. Appl. Phys. 45 (1974) 3014.
8) A.A. Rezazadeh and D.W. Palmer: J. Phys. C: Solid State Phys. 18 (1985) 43.
9) D. Stievenard, X. Boddaert and J.C. Bourgoin: Phys. Rev. B 34 (1986) 4048.
10) D.V. Lang: Inst. Phys. Conf. Ser. 31 (1977) 70.
11) D. Pons and J.C. Bourgoin: J. Phys. C: Solid State Phys. 18 (1985) 3839.
12) D.V. Lang, R.A. Logan and L.C. Kimerling: Phys. Rev. B 15 (1977) 4874.
13) D. Pons, A. Mircea, A. Mitonneau and G.M. Martin: Inst. Phys. Ser. 46 (1979) 352.
14) D. Pons, A. Mircea and J. Bourgoin: J. Appl. Phys. 51 (1980) 4150.
15) J.W. Farmer and D.C. Look: Phys. Rev. B 21 (1980) 3389.
16) D. Stievenard, X. Boddaert, J.C. Bourgoin and H.J. von Bardeleben: Phys. Rev. B. 41 (1990) 5271.
17) A. Sen Gupta, S.V. Naidu and P. Sen: Appl. Phys. A 40 (1986) 95.
18) P. Hautojärvi, P. Moser, M. Stucky, C. Corbel and F. Plazaola: Appl. Phys. Lett. 48 (1986) 809.
19) J.H. Crawford and L.M. Slifkin: Point Defects in Solids (Plenum Press, New York 1975) p. 296.
20) D.V. Lang and L.C. Kimerling: Phys. Rev. Lett. 33 (1974) 489.
21) D. Pons: Inst. Phys. Conf. Ser. 59 (1981) 269.
22) A.P. Mamontov and V.V. Peshev: Sov. Phys. Semicond. 18 (1984) 624.
23) D. Stievenard and J.C. Bourgoin: Phys. Rev. B 33 (1986) 8410.

© University of Pretoria

24) D.V. Lang and L.C. Kimerling: Phys. Rev. Lett. 35 (1975) 22.

25) D.V. Lang, L.C. Kimerling and S.Y. Leung: J. Appl. Phys. 47 (1976) 3587.

© University of Pretoria

UNIVERSITEIT VAN PRETORIA
UNIVERSITY OF PRETORIA
YUNIBESITHI YA PRETORIA

CHAPTER 3

EXPERIMENTAL TECHNIQUES

3.1 INTRODUCTION

In this chapter, the techniques and apparatus utilised in this study will be described. Deep level transient spectroscopy (DLTS), current-voltage (I-V) and capacitance-voltage (C-V) measurements were performed on unirradiated and irradiated samples. Current-voltage measurements yield important information regarding the electrical quality of the metal-semiconductor contact. The parameters of interest obtained from these measurements are the series resistance (R_S), the Schottky barrier height (ϕ_b) and the reverse leakage current measured at -1.0 V ($I_{-1.0\,V}$).

It is usually assumed in DLTS experiments that the sample impedance is purely capacitive [1], however, in the case of measurements on resistive samples, one should also consider the effect of sample resistance [2,3]. It is shown in sect 4.3 that particle irradiation increases the series resistance; depending upon the magnitude of this resistance, the DLTS peak magnitude may be reduced or the peak may appear inverted [2]. Ignoring this effect can result in erroneous conclusions about the trap density and the nature of the trap. It must also be remembered that both the sample capacitance and series resistance depend on temperature. The influence of the series resistance on DLTS measurements is expressed in terms of the quality factor (Q):

$$Q = R_S C_S \omega, \tag{3.1}$$

© University of Pretoria

where C_S is the diode capacitance and ω the measuring frequency. The quantitative discrepancies associated with an increase in series resistance are clearly illustrated when looking at the electron defect E3. When $Q < 1$ there is a 10 - 15% discrepancy in DLTS peak magnitude, which increases up to 50% when $Q = 3$ ($R_S = 980\ \Omega$) [2].

The Schottky barrier height (ϕ_b) may play a role in DLTS measurements for defects positioned near midgap [4]. Using the well-known EL2 defect, it has been found that for barrier heights between 0.62 and 0.83 eV, the DLTS signal decreases with decreasing barrier height. Furthermore, the DLTS signal saturates for barrier heights higher than 0.83 eV and disappears when barrier heights are below 0.62 eV. It has been shown that these results can be interpreted in terms of the variation of the quasi-Fermi level due to the barrier height change [4]. Care must be taken when performing DLTS measurements on particle irradiated material, as depending upon the barrier height, these defects may not be detected.

Generally, the effect of reverse bias leakage current in the space-charge layer is ignored when performing DLTS measurements. However, Chen et al [5] have found that for the case of a broad density of states, leakage current can have a dramatic effect on the DLTS spectra. This effect arises from the competition between thermal emission and capture of carriers to change the trap occupancy.

I-V measurement allows one to determine the device properties, as well as the suitability of such a device to yield accurate DLTS results. C-V measurements are used to monitor the change in carrier density after particle-irradiation. This technique is also important in determining accurate defect concentrations, by determining the free carrier density at temperatures at which the defects are observed.

© University of Pretoria

The procedure followed in investigating the change in electrical characteristics and defect introduction after a sample has been exposed to particle radiation is as follows:

⇒ Fabricate ohmic contacts and Schottky barrier diodes (SBDs) on the material to be characterized.

⇒ Perform current-voltage (I-V) and capacitance-voltage (C-V) measurements on the unirradiated material.

⇒ Perform control DLTS measurements to establish the presence of any defects in the as-grown unirradiated material.

⇒ Irradiate the sample using high energy particle sources, i.e. radionuclides or a Van de Graaff accelerator.

⇒ Measure the change in electrical characteristics by I-V and C-V measurements.

⇒ Characterize the defects introduced by irradiation, using the DLTS technique.

⇒ Study the annealing kinetics of the radiation-induced defects, using an annealing furnace with an ultra-high purity argon flow.

The techniques and apparatus used for this study will be described in the above order.

3.2 OHMIC CONTACT AND SBD FABRICATION

Cleanliness is crucial to achieving high yields and reproducible processes in the production of any semiconductor device [6]. In order to obtain ohmic contacts with a contact resistance typically as low as 10^{-6} $\Omega.cm^2$ and high quality SBDs with a low leakage current when reverse biased, the semiconductor surface before metallization should be atomically as clean as possible and stoichiometrically perfect [7].

Before metallization the following cleaning procedure was followed:

- Degrease the sample in boiling trichloroethylene (TCE) for approximately 10 minutes.
- Remove the TCE by boiling in isopropanol for approximately 2 minutes.

© University of Pretoria

- Rinse three times in deionized water (18 MΩ.cm).
- Dry the sample in a stream of filtered nitrogen gas.

The remaining oxide layer was removed as follows:

- Etch with HCl : H_2O in the ratio 1 : 1 for 2 to 5 minutes.
- Rinse twice in deionized water.
- Dry the sample in a stream of filtered nitrogen gas.

Ohmic contacts were resistively evaporated onto the substrate side of the n^+ substrates. The ohmic contact consisted of 100 Å Nickel, 2500 Å of gold-germanium (88 : 12), followed by a 2500 Å thick gold capping layer. These contacts were then annealed for two minutes at 450 ^{o}C in an ultra-high purity argon atmosphere.

To aid the cleaning procedure prior to SBD fabrication, a thin top-layer of the sample was removed by wet chemical etching. There are numerous etchants available that are suitable for this function. In this study, the samples were etched with $H_2O : H_2O_2 : NH_3(aq)$ in the ratio 150 : 1 : 3 for approximately 30 to 60 seconds, depending upon the doping concentration, active layer thickness and temperature. This etchant has an etch rate at 25^{o}C of about 3000 Å.min^{-1}. After etching, the sample was rinsed three times in deionized water and the oxide layer was removed as described above. The samples were inserted by a fast introduction system into a turbomolecular pumped ultra-high vacuum system in which the pressure recovered to the 10^{-8} mbar range within minutes. Circular SBDs were then fabricated onto the GaAs through a metal contact mask, either by electron beam evaporation or resistive evaporation depending on which metal was used.

3.3 I-V AND C-V MEASUREMENTS

Prior to irradiation, the current-voltage (I-V) and capacitance-voltage (C-V) characteristics of the metal-semiconductor system were measured. The formation of a

© University of Pretoria

Schottky and an ohmic contact will be briefly discussed using the work-function model where it is assumed that there are no interface states. The formation of a rectifying- or Schottky barrier diode (SBD) on an n-type semiconductor is illustrated in fig 3.3.1. When a metal is brought into close contact with the surface of a semiconductor, electrons will flow from the semiconductor to the metal due to the difference in their Fermi level positions (E_F). This electron transfer will take place until the Fermi levels coincide. As a result of this charge transfer, an electric field is established with the semiconductor being depleted of carriers, forming the space-charge region (positively charged) of width W and with the surface of the metal being negatively charged. The parabolic potential barrier that has formed is known as the Schottky barrier (ϕ_b) , with the magnitude of this barrier in the absence of interface states being given by the difference in the metal work function (ϕ_m) and the electron affinity (χ) of the semiconductor. The built-in voltage of the semiconductor is represented by V_i.

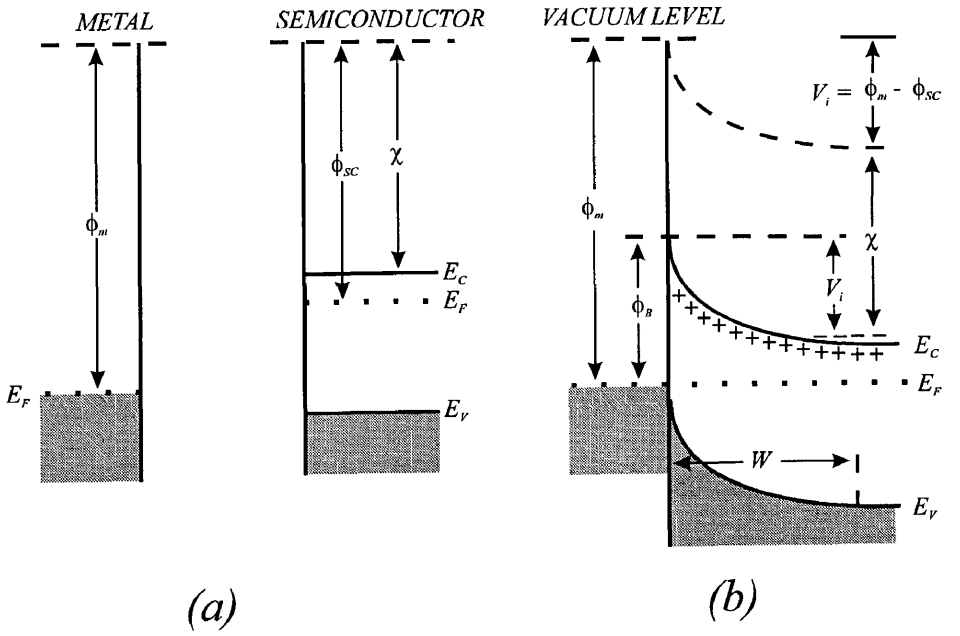

Fig 3.3.1 The energy band diagrams of a metal n-type semiconductor with $\phi_m > \phi_{SC}$. *(a)* Metal and semiconductor isolated from each other. *(b)* At thermal equilibrium after contact is made.

© University of Pretoria

When the work function of the semiconductor (ϕ_{SC}) is larger than that of the metal (ϕ_m), the electrons from the semiconductor will not encounter a barrier and an ohmic contact is formed.

In order to facilitate accurate defect concentration determinations, C-V measurements were performed in the temperature range 15 - 300 K. As discussed in the introduction of this chapter, the characteristics of interest in the I-V measurements are the reverse leakage current measured at 1.0 volt ($I_{-1.0\,V}$), the series resistance (R_S) of the metal-semiconductor system, and the barrier height (ϕ_b). The equation used in the I-V measurements according to thermionic emission theory is:

$$I = I_o \exp(qV / nkT), \tag{3.2}$$

where I is the current density (current (I) / unit area), n the ideality factor (introduced to accommodate non-ideal behaviour) and I_o the saturation current density which is given by:

$$I_o = A^{**} T^2 \exp(-q\phi_b / kT), \tag{3.3}$$

with ϕ_b being the effective barrier height (image-force lowering taken into account), A^{**} the Richardson constant and T the temperature of the metal-semiconductor junction.

Deviations from ideality may occur and these deviations are due to: the generation and recombination of carriers, the tunnelling of carriers, and the series resistance effect. In fig 3.3.2, the forward and reverse I-V characteristics of an ideal SBD and a practical or not so ideal SBD are illustrated. In this figure, the processes responsible for deviation from ideality are depicted. The different processes are: the generation-recombination region (a), the thermionic emission current region (b), the series resistance effect (c) and the reverse leakage current due to generation-recombination (d) [8].

© University of Pretoria

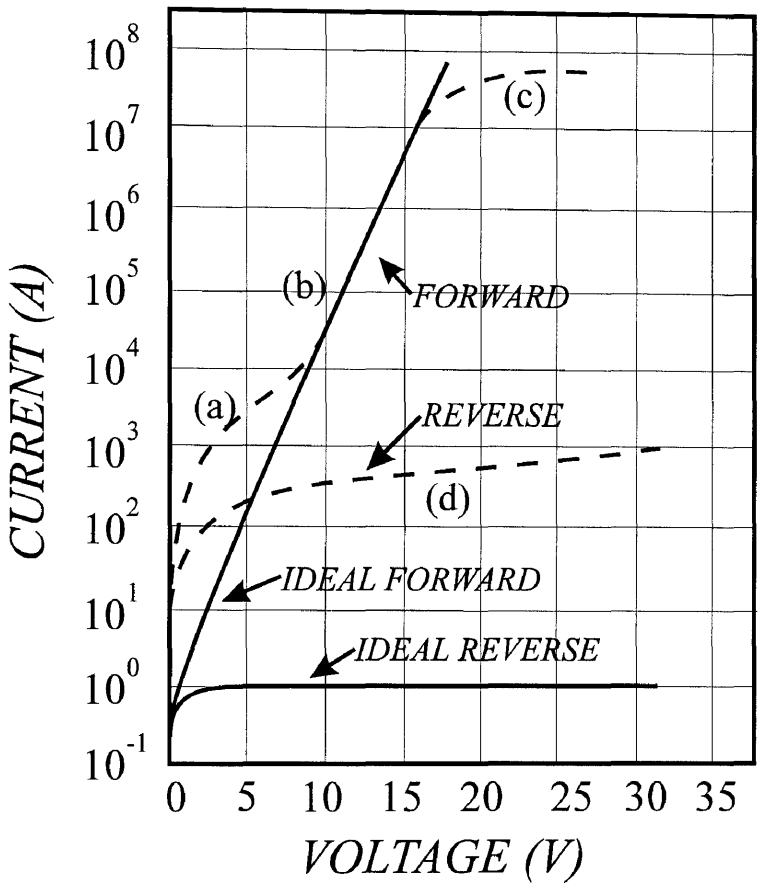

Fig 3.3.2 Current-voltage characteristics of an ideal and a practical (non-ideal) Schottky barrier diode.

Donoval et al [9] proposed a model which determines the barrier height of rectifying metal-semiconductor contacts, avoiding the use of the so called ideality factor (n). This model was modified by accounting for the effect of image force lowering; using this model, the series resistance (R_S) and the recombination current factor (I_g) can be calculated. The equation used in this modelling procedure is:

$$I = I_o \left\{\exp\left[q\left(V - IR_S\right)/ kT\right] - 1\right\} + I_g \left\{\exp\left[q\left(V - IR_S\right)/ 2kT\right] - 1\right\} + \left(V - IR_S\right)/ R_{SH} \quad (3.4)$$

where R_{SH} is the leakage resistance. The experimental set-up used to measure the I-V and C-V properties of the metal-semiconductor system is depicted in fig 3.3.3.

© University of Pretoria

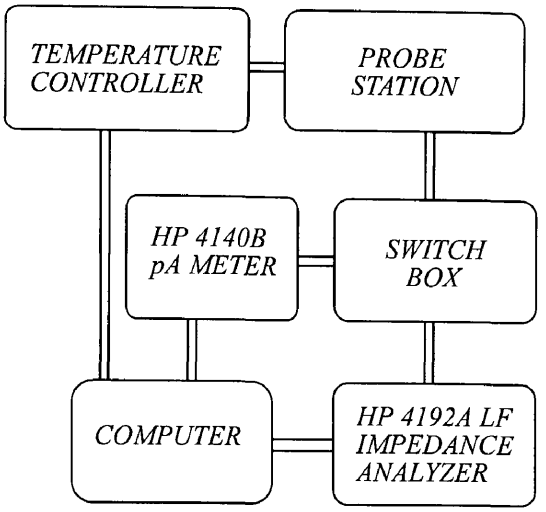

Fig 3.3.3 Block diagram of I-V and C-V measurement apparatus.

3.4 DLTS MEASUREMENTS

As discussed in sect 2.1.2, the DLTS system works on the principle that it sets an emission rate window such that the system responds maximally when it sees a transient with a rate within this window. The rate window in this study was selected using a lock-in amplifier-based DLTS system. When deep levels emit their carriers by way of thermal emission to the conduction band in the case of n-type material, there is a relaxation of the capacitance [10]. This emission takes place with a characteristic time constant (τ), which depends on the temperature and the defect properties. The signal information of importance in DLTS measurements is the time-dependent change in the value of the capacitance of the metal semiconductor junction. The emission rate ($e_n = 1/\tau$) is calculated from the following equation:

$$e_n = \nu_{th}\sigma_n N_c \exp(E_T - E_C) / kT. \qquad (3.5)$$

In the above equation, ν_{th} is the thermal velocity, σ_n the capture cross-section, N_c the effective density of states in the conduction band, E_T the trap position, E_C the conduction band edge, k the Boltzmann constant and T the sample temperature. The rate window was

© University of Pretoria

originally implemented by a dual-gate signal averager, also known as a double boxcar [7]; the procedure by which this rate window produces a DLTS peak is illustrated in fig 3.4.1.

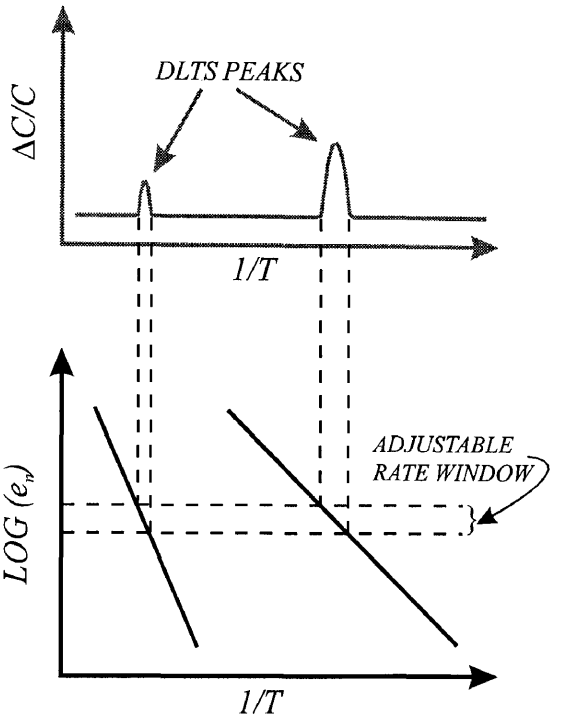

Fig 3.4.1 A diagram indicating how a rate window produces a DLTS peak in its output response [10].

In this method, the transient amplitude is monitored at two times, t_1 and t_2, after the trailing edge of the applied pulse. The DLTS signal is then the difference between the transient amplitude at these two times, with a maximum signal being monitored when the emission rate is equal to the transient time constant (τ_{max}). The transient time constant giving rise to the maximum output may be calculated using the following equation:

$$\tau_{max} = \frac{t_1 - t_2}{\ln(t_1/t_2)}, \tag{3.6}$$

with the signal to noise ratio being proportional to the square root of the gate width $(t_1 - t_2)$ [11].

© University of Pretoria

An alternate method of implementing the rate window is a lock-in amplifier [10]. Apart from this type of system allowing a fairly straightforward analysis of the DLTS spectra, it allows the recording of the in-phase (I) and the quadrature (Q) signals during a single scan [12]. An important advantage of this facility, where different mixing functions (sine and cosine for in-phase and quadrature, respectively) are used, is that features of a compound DLTS signal that do not show up in the in-phase spectrum may show up in the quadrature spectrum, and vice versa. In this method, the rate window is set by the choice of lock-in operating frequency. The LIA system discards all other Fourier components except the fundamental Fourier component of the capacitance transient signal using sine and cosine weighting (multiplier) functions. One disadvantage of using the LIA-based DLTS system is that the large spike-like signal from the capacitance meter corresponding to the filling pulse introduces excess noise. To eliminate this spike, a sample and hold circuit [10] is used which gates off these contributions, yielding a partially exponential capacitance transient. This limits the frequency range over which DLTS measurements may be acquired and also introduces noise. Using the transient time constants (τ_{max}) recorded at different LIA frequencies, the emission rates (e_n) can be calculated at various temperatures (T). Substitution in eqn 3.5 allows the construction of an Arrhenius plot of T^2 / e_n versus $1000/T$ which yields the DLTS "signature" (E_T, σ_n).

Figure 3.4.2 [13] illustrates the filling pulse (V_P) of width t_p, exponential capacitance transient and the weighting functions (sine and cosine) of the dual-phase lock-in-amplifier. In this study, the “bias-pulse reference mode” was used for the phase settings. In this mode, the lock-in zero crossing is set at the end of the filling pulse [14]. As discussed previously, a portion of the capacitance transient is gated off to prevent excess noise, with the gate-off width being $t_p + t_d$. The LIA output for the in-phase response (a_1) to this partially exponential waveform (i.e. its first Fourier component), is the integral of the product of the LIA weighting function ($w(t)$, this function = $\sin 2\pi t/t_o$ for the in-phase signal) and the LIA input signal $f(t)$ (i.e. the solid line in fig 3.4.2 (b)).

© University of Pretoria

$$a_1 = C \int_{t_d}^{t_o+t_d} f(t)\sin\frac{2\pi t}{t_o}dt. \tag{3.7}$$

The output for the quadrature response (b_1) is represented in eqn 3.8:

$$b_1 = C \int_{t_d}^{t_o+t_d} f(t)\cos\frac{2\pi t}{t_o}dt. \tag{3.8}$$

The transient time constant giving rise to the maximum output for the in-phase signal ($\tau_{max,I}$) and the quadrature signal ($\tau_{max,Q}$) may be calculated from the following equation [15]:

$$\tau_{max,I} = 2.696\tau_{max,Q} = 0.4243 / f. \tag{3.9}$$

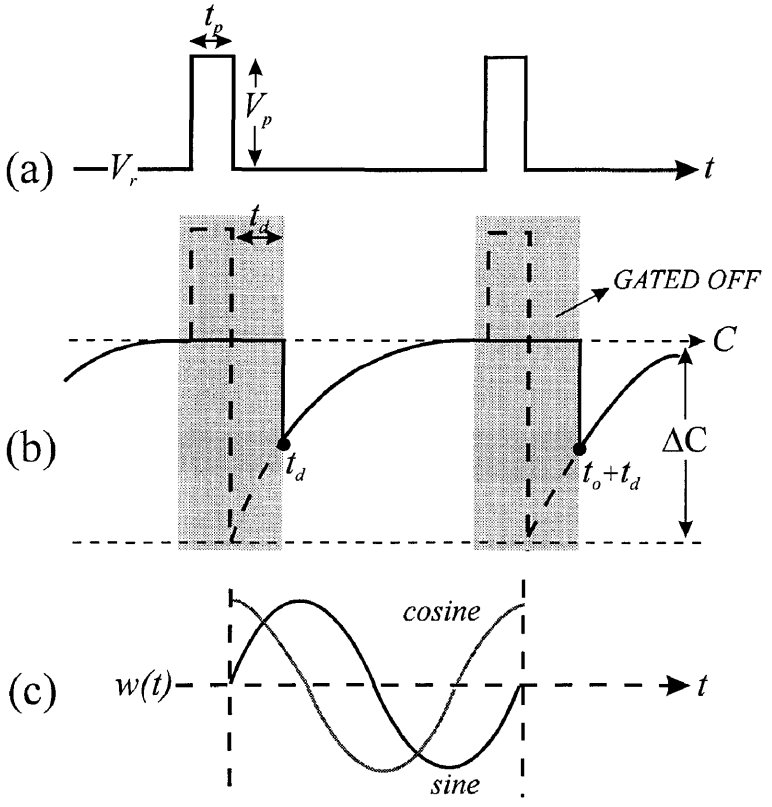

Fig 3.4.2 Phase settings and gate-off effect in the "bias-pulse phase reference" mode. (a) Filling pulse of width t_p. (b) Modified exponential capacitance transient. (c) Sine and cosine weighting functions.

© University of Pretoria

The layout of the DLTS system used in this study is illustrated in fig 3.4.3, with the basic components being shaded.

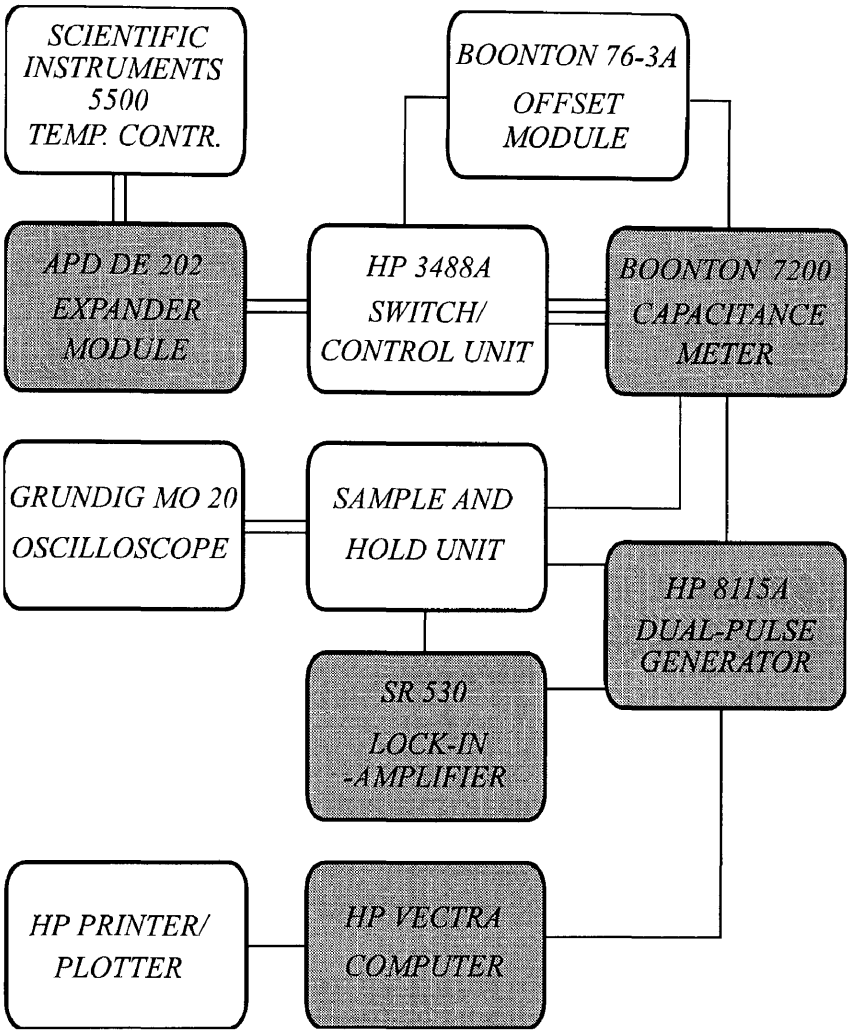

Fig 3.4.3 Block diagram of LIA-based DLTS system, with the important components being shaded.

The expander module allowed DLTS scans to be recorded between 15 K and 375 K. The sample holder was modified [15] to ensure that sample temperature was measured as accurately as possible, especially when performing low-temperature DLTS measurements and when the scan rate is high, allowing the sample to be in thermal equilibrium with the cold finger.

© University of Pretoria

3.5 VAN DE GRAAFF ACCELERATOR

An AN-2500 positive ion accelerator was used to accelerate protons and alpha-particles. This accelerator is a Van de Graaff belt-type electrostatic generator which can develop accelerating voltages up to 2.5 MV. The accelerating voltage is obtained by removing electrons from the high voltage terminal, using the positively-charged belt and transporting them to ground with the charging screen. The high voltage terminal is thus positively charged, and this charge is removed as a column current flowing through a set of resistors. This column current generates a uniform voltage gradient along the accelerator tube, which accelerates positive ions to energies up to 2.5 MeV. The simplified experimental set-up of the Van de Graaff accelerator is depicted in fig 3.5.1. Gas introduced into the ion source is ionized (RF energy); the resulting plasma is magnetically concentrated at the exit canal and expelled into the acceleration path when a potential is applied. Further accelerations are caused by the voltage gradient in the evacuated column.

To ensure energy selection of the selected ion type of positive ions that strike the target, the ion beam is deflected by an analyzing magnet. The beams of positively-charged ions then pass through the slits that stabilise the accelerating voltage and are collimated before they reach the target. Secondary electrons are suppressed by application of a voltage to an insulated ring in front of the target holder. Using this accelerator, alpha-particles and protons were generated and used to irradiate both n- and p-type GaAs.

© University of Pretoria

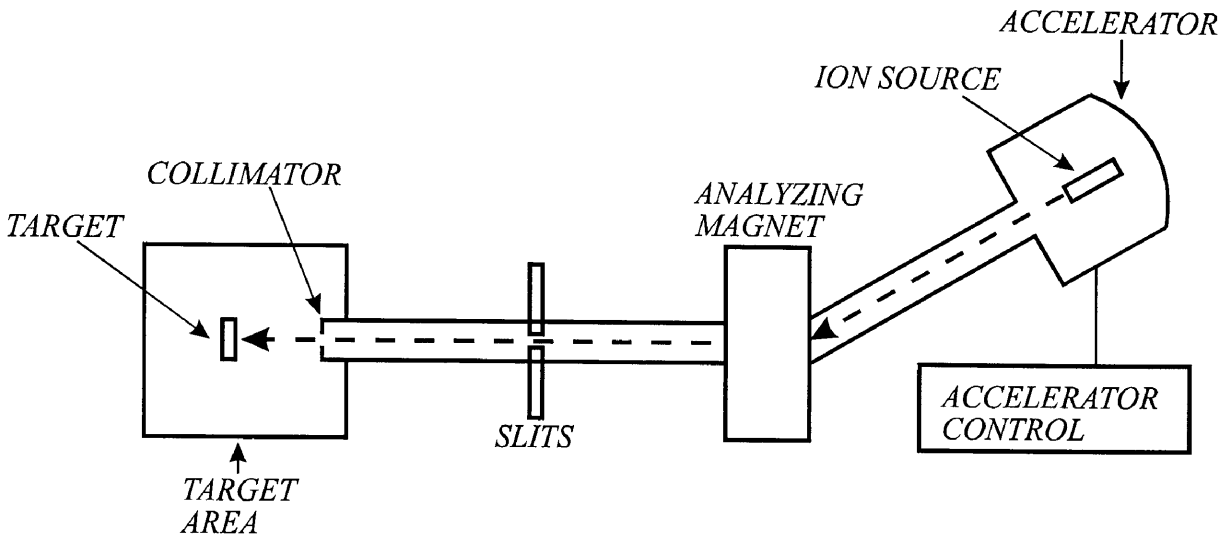

Fig 3.5.1 Experimental set-up of the AN-2500 positive ion accelerator.

3.6 RADIONUCLIDE SOURCES

In this study, two radionuclide sources were utilised: americium-241 (^{241}Am) and a disc-shaped strontium-90 (^{90}Sr) source. The advantage of radionuclides is that they are small enough to fit into a cryostat, thereby allowing low temperature irradiations.

3.6.1 AMERICIUM-241 (^{241}Am)

Two alpha-particle radionuclide sources were used in this study. A 12.5 mm wide strip of americium foil was used as the first alpha-particle source; this radionuclide had an activity of 192 μCi.cm^{-2} and a half-life of 432 years. The second source, which was disc-shaped, had an activity of 0.53 μCi.cm^{-2}. During the decay of ^{241}Am to ^{237}Np, 85.2% of the alpha-particles are emitted with a sharply defined energy of 5.484 MeV, while 12.5% have an

© University of Pretoria

energy of 5.442 MeV, and 1.6% have an energy of 5.387. The particle energies and transition probabilities for the ^{241}Am radionuclide are as follows [16]:

ENERGY (MeV)	*TRANSITION PROBABILITY (%)*
5.387	*1.6*
5.442	*12.5*
5.484	*85.2*
5.511	*0.20*
5.543	*0.34*
OTHER	*LOW*

A typical alpha spectrum for ^{241}Am is illustrated in fig 3.6.1. It was assumed that the alpha source was monoenergetic.

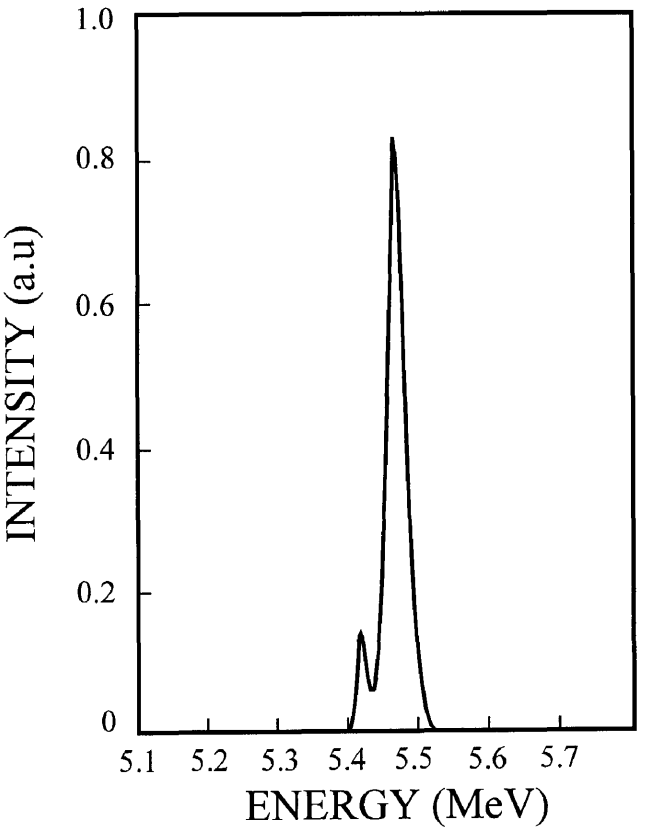

Fig 3.6.1 Energy distribution of alpha-particles emitted by ^{241}Am.

© University of Pretoria

3.6.2 STRONTIUM-90 (^{90}Sr)

The strontium source used was disc-shaped, with a diameter of 8.4 mm and an activity of 36 mCi.cm^{-2}. The ^{90}Sr radionuclide with a half-life of 28.5 years decays firstly to yttrium, with a half-life of 64.1 hours, via the emission of a 0.5 MeV electron. The yttrium in turn decays by the emission of a 2.27 MeV electron to Zirconium, which is the stable isotope [17]. This results in a continuous energy distribution as is illustrated in fig 3.6.2. For completeness, we have shown, using a solid line, the total contribution (Sr + Y) of both decays; the line is displaced in the positive y-direction for clarity. It should be noted that most electrons from this source have energies above the so-called threshold energy for producing point defects by elastic collisions (i.e. 220 keV for GaAs).

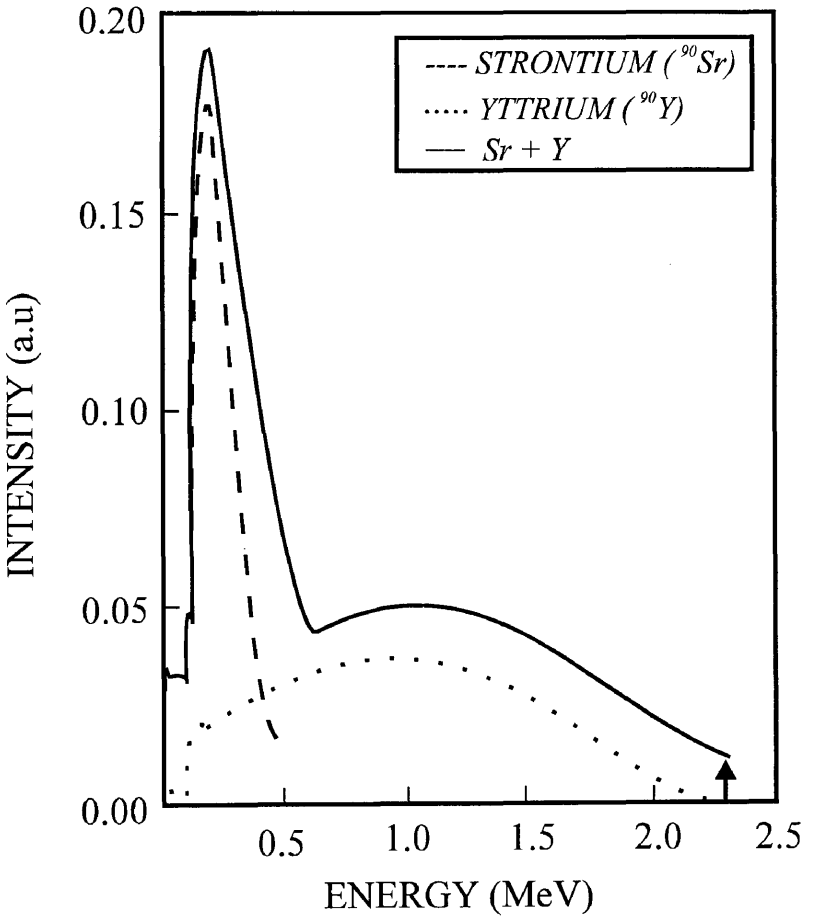

Fig 3.6.2 Energy distribution of electrons emitted by ^{90}Sr and ^{90}Y radionuclides.

© University of Pretoria

3.7 ANNEALING APPARATUS

All defect annealing experiments were carried out in a Lindberg "hevi-duty" furnace (200 - 1200°C), in an ultra-high purity argon atmosphere at an approximate flow rate of 3 litres.min^{-1}. A thermocouple was placed inside the sample holder just beneath the sample. Figure 3.7.1 illustrates the annealing furnace used in this study.

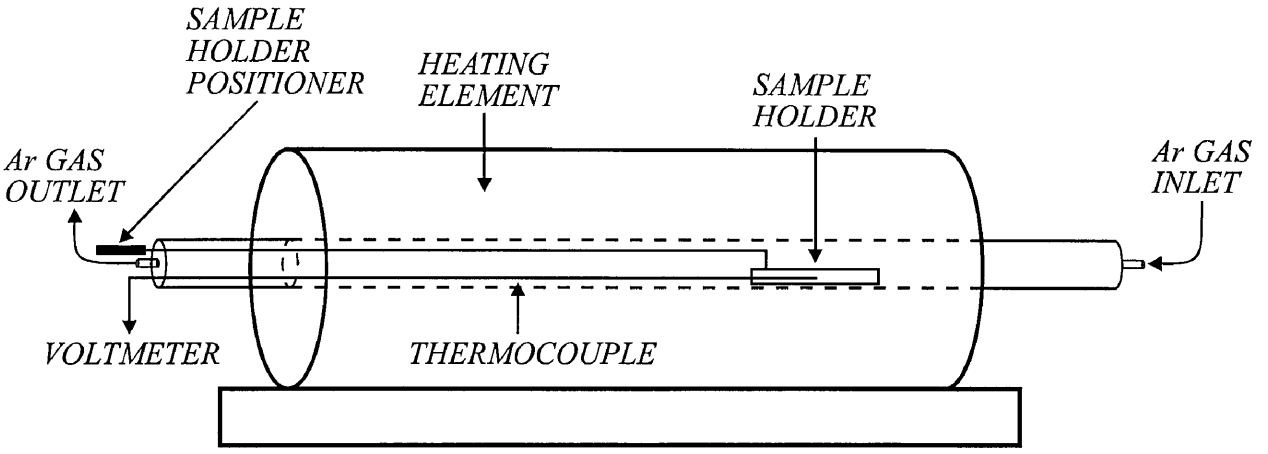

Fig 3.7.1 Experimental set-up of the annealing furnace.

© University of Pretoria

REFERENCES

1) D.V. Lang: J. Appl. Phys. 45 (1974) 3023.

2) A. Broniatowski, A. Blosse, P.C. Srivastava and J.C. Bourgoin: J. Appl. Phys. 54 (1983) 2907.

3) E.V. Astrova, A.A. Lebedev and A.A. Lebedev: Sov. Phys. Semicond. 19 (1985) 850.

4) Q.Y. Ma, T. Schmidt, X.Wu, H.L Evans and E.S. Yang: J. Appl. Phys. 64 (1988) 2469.

5) M.C. Chen, D.V. lang, W.C. Dautremont-Smith, A.M. Sergent and J.P. Harbison: Appl. Phys. Lett. 44 (1984) 790.

6) R.E. Williams: Gallium Arsenide Processing Techniques (Artech House 1984) p. 85.

7) F.D. Auret, W.O Barnard, G. Myburg and L.J. Bredell: S. Afr. J. Sci. 87 (1991) 127.

8) S.M. Sze: Physics of Semiconductor Devices (John Wilety & Sons 1981) p.91.

9) D. Donoval, J. De Sousa Pires, P.A. Tove and R. Harman: Solid State Electronics 32 (1989) 11.

10) G.L. Miller, D.V. Lang and L.C. Kimerling: Ann. Rev. Mater. Sci. (1977) 377.

11) D.V. Lang: Thermally Stimulated Relaxation in Solids (Springer-Verlag, Germany 1979, Ed. P. Brãunlich) p. 111.

12) F.D. Auret and M. Nel: J. Appl. Phys. 63 (1988) 973.

13) F.D. Auret: Rev. Sci. Instrum. 57 (1986) 1597.

14) D.S. Day, M.Y. Tsai, B.G. Streetman and D.V. Lang: J. Appl. Phys. 50(1979) 5093.

15) G. Myburg, W.E. Meyer and F.D. Auret: Rev. Sci. Instrum. 63 (1992) 2101.

16) HI041, Issue 1: Amersham Safety Regulations 11.

17) F.D. Auret, S.A. Goodman, G. Myburg and W.E. Meyer: Appl. Phys. A. 56 (1993) 547.

© University of Pretoria

CHAPTER 4

RESULTS

4.1 INTRODUCTION

The results of this study will be presented as publications which have been published in recognised international journals. The results will be presented as follows: firstly, the results obtained from an initial study where the material was characterised before any radiation-induced damage was introduced shall be presented (sect 4.2). The second part of the study entails a detailed electrical- and defect characterization of n- and p-type GaAs after irradiation (sect 4.3). The influence of an electric field in the space-charge region of a semiconductor on the emission of carriers from electrically-active deep levels in the bandgap is discussed in sect 4.4. To determine the conditions under which radiation-induced defects can be removed from GaAs, an annealing study was conducted for defects introduced at room temperature (300 K) and at 15 K (sect 4.5). The effect of argon sputtering and neutron irradiation is presented in sect 4.6. Finally, the defect properties are summarised in sect 4.7.

4.2 MATERIAL CHARACTERIZATION

Before a meaningful and accurate study can be conducted to characterize the defects introduced intentionally by a radionuclide or an accelerator, a knowledge of the defects present in the material prior to exposure is necessary. In this study, epitaxial material grown using metalorganic vapour phase epitaxy (MOVPE) and molecular beam epitaxy (MBE) was used. Many of the investigations were carried out using silicon-doped ($1.2 \pm 0.4 \times 10^{16}$ cm^{-3}) n-type GaAs grown by MOVPE. After performing DLTS

© University of Pretoria

measurements on this material at temperatures between 15 K and 375 K, it was seen that the only electrically-active defect present was the well-known EL2 defect.

In the case of unintentionally-doped n-GaAs, there was an additional electron defect present. It was also illustrated from this DLTS investigation of unintentionally-doped material grown on two different substrates (semi-insulating and n^+), that the choice of substrate material may be important when studying process-induced defects. When a semi-insulating substrate is used, only an electron defect is detected in the unintentionally-doped n-type epitaxial layer. However, when a silicon-doped n^+ substrate is used, three hole traps are also detected. One of these hole defects is due to copper contamination, whereas, the origin of the remaining two hole defects has not yet been clarified. It does seem that these hole traps are responsible for a reduction in the carrier concentration of the epitaxial layer grown on the n^+ substrate.

When investigating process-induced defects in MBE-grown p-GaAs, it is imperative that the as-grown material be defect free. It has been shown that, numerous hole defects in the as-grown material make accurate defect identification and characterization of particle irradiated material very difficult.

PUBLICATIONS:

(1) S.A. Goodman, F.D. Auret and G. Myburg, "Hole defects in low free-carrier density GaAs grown by low-pressure metalorganic vapour phase epitaxy", Semicond. Sci. Tech. **7** (1992) 1241.

(2) F.D. Auret, S.A. Goodman and G. Myburg, "DLTS Detection of Hole Traps in MBE Grown p-GaAs Using Schottky Barrier Diodes", J. Electron. Mater. **21** (1992) 1127.

© University of Pretoria

UNIVERSITEIT VAN PRETORIA
UNIVERSITY OF PRETORIA
YUNIBESITHI YA PRETORIA

Semicond. Sci. Technol. 7 (1992) 1241–1244. Printed in the UK

Hole defects in low free-carrier density GaAs grown by low-pressure metalorganic vapour phase epitaxy

S A Goodman, F D Auret and G Myburg

Physics Department, University of Pretoria, Pretoria 0002, Republic of South Africa

Received 24 January 1992, in final form 1 May 1992, accepted for publication 26 May 1992

Abstract. Unintentionally doped epitaxial GaAs grown by low-pressure metalorganic vapour phase epitaxy has been characterized using both conventional electrical deep-level transient spectroscopy (DLTS) [1] and optical DLTS (ODLTS) [2]. From this study it is shown that the choice of substrate material is important when characterizing material to be used for process-induced defect characterization. Material grown on silicon-doped n^+ (10^{18} cm^{-3}) GaAs substrate material has an electron defect, a copper defect [3] and two hole traps that have not yet been reported. The three hole traps, presumably introduced by the n^+ substrate, compensate the material, causing a reduction in the carrier concentration from 2×10^{14} cm^{-3} when the epitaxial layer is grown on semi-insulating (SI) substrate material to 4×10^{13} cm^{-3} when grown on n^+ (10^{18} cm^{-3}) substrate material.

1. Introduction

The growth of ultra-high purity semiconductor layers is of great importance for semiconductor technology as well as for the characterization of process-induced defects. Ideally these layers should be defect free in terms of both electron and hole defects, or in the worst case contain defects in concentrations of no higher than 10^{12} cm^{-3} [4]. If this is not so, the intentionally introduced contaminants and process-induced defects will adversely influence the performance of devices fabricated on this material. Alternatively if process-induced imperfections are being studied, then they may easily be confused with those present in the as-grown epitaxial layers. Feng *et al* [5], have recently reported the presence of electron traps in ultra-low free-carrier concentration GaAs grown by low-pressure metalorganic vapour phase epitaxy (MOVPE) that slightly compensate the epitaxial layer. However, it should be noted that an ultra-low free-carrier concentration may also be the result of compensating hole traps. The purpose of this paper is to present data on two hole traps and previously labelled traps which may 'mask' process-induced defects. These traps may also be responsible for compensation of unintentionally doped GaAs epitaxial layers grown on n^+ GaAs substrates, resulting in ultra-low free-carrier concentrations (4×10^{13} cm^{-3}).

Deep-level transient spectroscopy (DLTS) is presently regarded as one of the most sensitive and popular methods to characterize electrically active defects in semiconductors. In order to obtain a defect activation energy, E_t, and capture cross section, σ_t, by DLTS, the capacitance or current transients caused by periodically relaxing the reverse bias across a rectifying junction, have to be analysed as a function of temperature. In this paper the simple method termed IQ-DLTS [6] will be used to characterize defects in which E_t and σ_t are determined from the defects in-phase (I) and quadrature (Q) DLTS spectra, which are simultaneously recorded during a single temperature scan using a two-phase lock-in amplifier with a sine wave mixing function. An important advantage of IQ-DLTS over conventional lock-in-amplifier (LIA)-DLTS, where only the I signal is usually recorded, is that the Q spectrum may show up features of a compound DLTS peak not clearly visible on the I spectrum [6]. The reason for this is that different mixing functions are used (sine and cosine for I and Q respectively) to analyse the signal.

To minimize resistance effects, and thus to allow the detection of minority carriers without optical excitation, the substrate material chosen had a high carrier concentration (n^+, 10^{18} cm^{-3}). This high carrier concentration allows the fabrication of the Schottky contact pad on the epitaxial layer and the ohmic contact on the reverse side of the n^+ substrate. However, from this study it has been observed that using an n^+ substrate may introduce hole traps in the epitaxial material, which could inhibit the detection of process-induced defects.

0268-1242/92/101241+04 $07.50 © 1992 IOP Publishing Ltd

© University of Pretoria

UNIVERSITEIT VAN PRETORIA
UNIVERSITY OF PRETORIA
YUNIBESITHI YA PRETORIA

2. Experimental procedure

Eight micron thick undoped epitaxial layers, were simultaneously grown by MOVPE on a silicon-doped n^+ (10^{18} cm^{-3}) substrate and on a semi-insulating GaAs substrate both having (100) orientations. The resistivity of the semi-insulating substrate was larger than 10^7 Ω cm. After the appropriate cleaning procedure, Ni-Au/Ge-Au ohmic contacts [7] were formed on the n^+ and n^- sides of the n^--n^+ and n^--SI structures respectively. Schottky barrier diodes (SBDs) were formed on the n^- epilayers by electron beam evaporation of 20 nanometre thick platinum (Pt) contacts. A shield was used to prevent any primary stray electrons striking and possibly damaging the sample [8].

The ideality factor for both structures was equal to or less than 1.04. Capacitative DLTS measurements were made in the temperature range 15–300 K, on the SBDs using a LIA based system, comprising a Stanford Research SR530 LIA, a modified Boonton 72BD capacitance meter [9] and an Air Products cryostat with temperature controller. All DLTS spectra were obtained by performing a double temperature scan up and down in temperature under the same pulse conditions) and obtaining the average so as to limit any errors due to sample temperature discrepancies. In the past the use of forward bias injection pulses for SBDs has mostly been avoided because they may also show the presence of surface states which are sometimes confused with, or prevent, the detection of deep levels. However, if the detection of minority carrier defects is to be carried out without optical excitation it is necessary to apply this method [10].

3. Results

The activation energy (E_t) and the capture cross section (σ_t) of the deep traps were calculated using the conventional assumption that capture cross section (σ_t) is independent of temperature, and the emission rate, e, of carriers by a trap varies with temperature according to the following equation [11]:

$$e = \gamma T^2 \sigma_t \exp(-\Delta E_t / kT)$$

where γ is a constant equal to 1.62×10^{21} and 2.21×10^{20} cm^{-2} s^{-2} K^{-2} for a hole trap and an electron trap in GaAs respectively. These values are similar to those used by Mitonneau *et al* [3, 12]. Thus, in this paper a spin degeneracy factor (g) of 1 is used in all applicable calculations.

Upon initial investigation of the DLTS spectra for both types of substrate there appeared only to be one electron trap (E1) in addition to the well-known EL2 trap. However, upon varying the pulse conditions (pulse width and frequency) and using an electrical minority injection pulse, it was found that the undoped layer grown on the n^+ substrate also contained the copper trap (H2) [3, 13] and two hole traps, labelled H0 and H1. The DLTS spectrum for the layer grown on the n^+ substrate is illustrated by curve (*a*) in figure 1. The pulse conditions

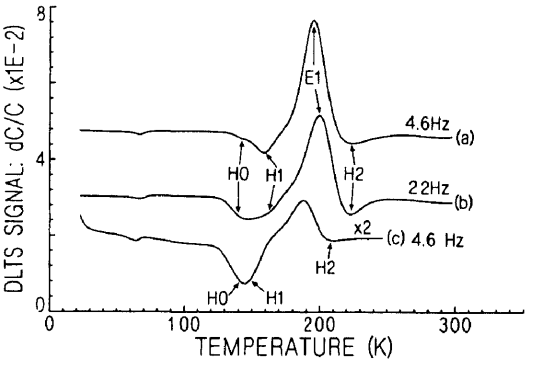

Figure 1. DLTS spectra of the majority and the minority carrier traps detected in the n^+–n^- structure. Curve (*a*) is the Q spectrum obtained at a LIA frequency of 4.6 Hz, under conditions to accentuate hole trap H1. The quiescent bias was 1.0 V and the filling pulse 1.9 V. Curve (*b*) is an I spectrum recorded at a LIA frequency of 22 Hz, using the same bias conditions as curve (*a*); hole trap H0 is accentuated. Curve (*c*) is the majority and the minority carrier I spectrum obtained by ODLTS using a HeNe laser, at a LIA frequency of 4.6 Hz. The quiescent bias was 1.0 V and the filling pulse was 0.5 V.

chosen for the DLTS spectra in figure 1 are not selected to maximize the peaks but to allow the best possible separation of the traps. Under optimum biasing conditions the hole-trap peaks are at least an order of magnitude larger. To confirm the presence of these three hole traps the ODLTS technique [2], using a HeNe laser, was applied to the same sample, resulting in a similar spectrum, illustrated in curve (*c*) of figure 1. These three hole traps were not detected in the layer grown on the SI substrate, indicating that the hole traps originate in the n^+ substrate, as both layers were grown simultaneously under the same growth conditions.

Because the two hole traps H0 and H1 are almost superimposed on each other, it was necessary to select the correct pulse conditions and to analyse both the I and the Q DLTS spectra which are simultaneously recorded during a single temperature scan, to allow reasonable separation of these two traps. Curve (*a*) in figure 1, is the Q spectrum recorded under conditions which accentuate hole trap H1, whereas trap H0 is accentuated under different conditions in the I spectrum represented by curve (*b*) of figure 1. It was also important to eliminate the effect of the electron trap on the peak position of the three hole traps. This was achieved by performing DLTS measurements with no minority-carrier forward injection, and subtracting this spectrum containing only the electron trap from the spectrum obtained under injection conditions. The signatures of the three hole traps and the electron trap are determined from the Arrhenius graph (plot of T^2/e against $1000/T$) represented in figure 2, and the data are presented in table 1. Whereas it can safely be assumed that trap H2 is due to the presence of copper [3, 13], the exact nature of the remaining two hole traps has not yet been established.

© University of Pretoria

UNIVERSITEIT VAN PRETORIA
UNIVERSITY OF PRETORIA
YUNIBESITHI YA PRETORIA

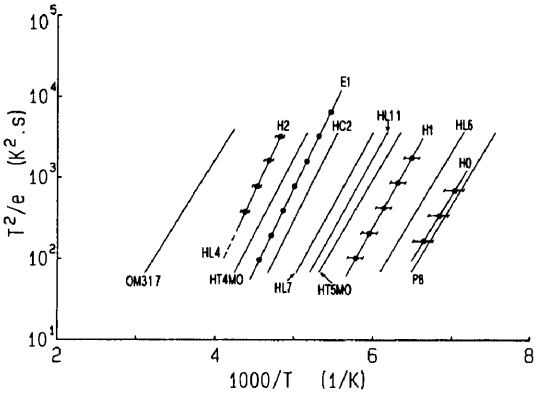

Figure 2. Activation energy plots of both electron and hole defects observed in the epitaxial layer grown on the n^+ substrate and signatures of defects. The lines joined by filled circles with the 2 K error bars represent the experimental data points from this study (H0, H1, H2 and E1). All other traps presented on this graph were obtained from the literature.

To clarify whether traps H0 and H1 were new traps their signatures were compared to traps detected by other authors. In comparing trap signatures care must be taken to ensure which degeneracy factor was used in the calculation of the trap characteristics. Authors seldom specify this factor, so it is very often difficult to accurately compare signatures with confidence. A summary of this comparison is depicted in table 1. The first comparison was made with the traps detected by Wang *et al* [11]. These workers analysed material with a free-carrier concentration ranging from 5×10^{16} to 1×10^{18} cm^{-3}. However, a comparison between traps detected in this material in the presence of the high electric field resulting from the high doping densities [14] and those detected in our low-doped material cannot be expected to be accurate. For example they detected a trap which they labelled HMC, which exhibited a strong electrical field dependence, and whose energy varied from 0.19 eV to 0.39 eV depending upon the free-carrier concentration of the material. Moreover, they attribute the presence of this trap to either the source gases or the growth ambient. As both of our samples were grown simultaneously under the same growth conditions it is highly improbable that H0 and H1 have the same origin as HMC.

Mitonneau *et al* [3] have performed extensive studies on hole traps in low-doped (1×10^{14}) GaAs. They detected three traps with similar signatures to H0 and H1: their defect labels are HL6, HL7 and HL11. In their calculations these workers, as in this work, used a spin-degeneracy factor (g) of one. HL6 according to the authors is possibly due to an impurity, trap HL7 may be related to a native defect in molecular beam epitaxially grown material and HL11 may be related to a native defect in melt-grown material. However, upon examination of the Arrhenius graph it is clear that they are most likely not the same as H0 and H1 detected in the present study. Even a 2 K temperature error as illustrated by the error bars in figure 2, does not result in traps H0 and H1 lining up with the traps detected by Mitonneau *et al* [3].

Partin *et al* [15] performed DLTS studies on both Ni- and Zn-diffused n-GaAs. They worked with free-carrier concentrations in the range of 5×10^{17} cm^{-3}, and no mention of which spin degeneracy factor used is made. So here again it is difficult to make accurate comparisons. They reported a defect with an activation energy of 0.39 eV and capture cross section of 1.3×10^{-14} cm^{-2}, and stated that this trap was due to nickel substitution on a gallium site. Again from figure 2, it can be seen that this

Table 1. DLTS defect characteristics of the electron and hole defects observed in the n^-–n^+ structure. (*a*) Defects found in this study. (*b*) Some deep levels observed in GaAs reported in the literature.

Defect label	E_t (eV)	σ_t (cm^2)	T_{peak}† (K)	I.D.	Ref.
		(*a*)			
H2	0.42	3×10^{-15}	214	Cu	
E1	0.40	9×10^{-14}	195	—	
H1	0.35	8×10^{-14}	158	—	
H0	0.32	2×10^{-13}	142	—	
		(*b*)			
HL6	0.32	5.6×10^{-14}		—	[3]
HL7	0.35	6.4×10^{-15}		—	[3]
HL11	0.35	1.3×10^{-14}		—	[3]
HL4	0.42	3.0×10^{-15}		Cu	[3]
HMC	0.17–0.39	1.2×10^{-18} to 2.7×10^{-20}		—	[11]
HC2	0.39	1.3×10^{-14}		Ni	[14]
HT5MO	0.33	6.0×10^{-15}		Native	[13]
HT4MO	0.37	7.1×10^{-16}		Cu	[13]
P8‡	0.32	2.5×10^{-13}		—	[15]
OM317	0.31	6.5×10^{-19}		—	[16]
OM329	0.35	4.9×10^{-20}		Fe	[16]

†At a LIA frequency of 4.6 Hz, i.e. a decay time constant of 92 ms.
‡Detected in SI material.

© University of Pretoria

UNIVERSITEIT VAN PRETORIA
UNIVERSITY OF PRETORIA
YUNIBESITHI YA PRETORIA

defect is not likely to be one of the 'new' traps reported in this paper.

A comparison between defects H0 and H1 detected in this study and defects detected by other authors in SI material may be more accurate due to the similar electric fields in these two types of material. Young *et al* [16] performed optical current transient spectroscopy (OCTS) on SI GaAs. A trap labelled P8 with a signature almost identical to H0 was detected using this method. It is strange that trap H0 detected in our study was detected on the low-doped epitaxial layer grown on the n^+ substrate and not on the layer grown on the SI substrate as would be expected. Other authors [17] have reported hole traps with almost similar trap signatures and their results are presented in table 1 and figure 2. From this literature survey it appears as if traps H0 and H1 have not yet been reported for any epitaxially grown GaAs material.

To investigate whether these hole traps had any influence on the free-carrier concentration, capacitance–voltage (CV) measurements were performed on both samples. The free-carrier concentration ($N_D - N_A$) of the epitaxial layer grown on the SI substrate had a free-carrier concentration of 2×10^{14} cm^{-3}, whereas the epitaxial layer grown simultaneously on the n^+ substrate had an even lower free-carrier concentration of 4×10^{13} cm^{-3}. This reduction in the carrier concentration is possibly due to compensation caused by the presence of hole traps (H0, H1 and H2) in the layer grown on the n^+ substrate.

4. Conclusion

In summary, the introduction of two new hole traps in MOVPE grown GaAs on n^+ substrates has been reported. When attempting to identify these traps in terms of defects already reported, it became evident that this should be done with extreme caution. To reduce the effect of the internal electric field, which may result in field-assisted thermal emission of carriers by the traps [11], low-doped material should be used when comparing trap signatures. It may further be concluded that in this study the semi-insulating GaAs substrate is a more suitable substrate than the silicon (Si)-doped n^+ substrate for growing high-quality epitaxial layers by MOVPE, intended for DLTS and ODLTS studies of process-induced defects. The hole traps are responsible for the lowering of the free-carrier concentration in the epitaxial layer grown on the n^+ substrate. Therefore both electron [5] and hole defects may be responsible for compensation in low-doped GaAs grown by MOVPE. The two new hole traps as well as the copper trap and the electron trap detected in the epitaxial layer grown on the n^+ substrate may also 'mask' process-induced defects. If n^+ substrates are preferred, they should be carefully selected, as this study has shown that defects can easily be introduced into the epilayer during growth.

References

[1] Lang D V 1974 *J. Appl. Phys.* **45** 3014
[2] Mitonneau A, Martin G M and Mircea A 1977 *Gallium Arsenide and Related Compounds* (*Inst. Phys. Conf. Ser. 33a*)
[3] Mitonneau A, Martin G M and Mircea A 1977 *Electron. Lett.* **13** 666
[4] Auret F D, Nel M and Leitch A W R 1988 *J. Cryst. Growth* **89** 308
[5] Feng S L, Bourgoin J C and Razegh M 1991 *Semicond. Sci. Technol.* **6** 229
[6] Auret F D and Nel M 1988 *J. Appl. Phys.* **63** 973
[7] Barnard W O and Myburg G 1991 *S. Afr. J. Sci.* **87** 143
[8] Auret F D, Myburg G, Bredell L J, Barnard W O and Kunert H W 1992 *Mater. Sci. Forum* **83–87** 1499
[9] Chappel T I and Ransom C M 1984 *Rev. Sci. Instrum.* **55** 200
[10] Auret F D and Nel M 1987 *J. Appl. Phys.* **61** 2546
[11] Wang P J, Kuech T F, Tischler M A, Mooney P, Scilla G and Cardone F (1988) *J. Appl. Phys.* **64** 4975
[12] Mitonneau A, Martin G M and Mircea A 1977 *Electron. Lett.* **13** 191
[13] Zhu H, Adachi Y and Ikoma T 1981 *J. Cryst. Growth* **55** 154
[14] Frenkel J 1938 *Phys. Rev.* **54** 647
[15] Partin D L, Chen J W, Milnes A G and Vassamillet L F 1979 *J. Appl. Phys.* **50** 6845
[16] Young L, Tang W C, Dindo S and Lowe K S 1986 *J. Electrochem. Soc.* **133** 609
[17] Bhattacharya P K, Ku J W, Owen S J T, Aebi V, Cooper C B and Moon R L 1980 *Appl. Phys. Lett.* **36** 304

© University of Pretoria

UNIVERSITEIT VAN PRETORIA
UNIVERSITY OF PRETORIA
YUNIBESITHI YA PRETORIA

Journal of Electronic Materials, Vol. 21, No. 12, 1992

DLTS Detection of Hole Traps in MBE Grown *p*-GaAs Using Schottky Barrier Diodes

F. DANIE AURET, S. A. GOODMAN and G. MYBURG

Physics Department, University of Pretoria, Pretoria 0002, South Africa

The presence of hole traps has been studied by deep level transient spectroscopy (DLTS) characterization of low carrier density *p*-type GaAs grown by MBE on p^+-GaAs substrates using Al and Co Schottky contacts. The results obtained indicate the presence of several hole traps with energy levels of between 0.06 and 0.65 eV above the valence band in concentrations up to $2 \times 10^{12}/cm^3$. Some of these defects, *e.g.* Cu, are ascribed to system-, source- or substrate-related impurities, but the origin of several other defects is unknown.

Key words: Defects, impurities, MBE GaAs, deep level transient spectroscopy

1. INTRODUCTION

The successful operation of small dimension semiconductor devices, such as quantum well lasers and detectors, requires exact dimensional control, as well as careful defect- and impurity engineering, during the growth and subsequent processing of the semiconductor structures. Molecular beam epitaxy (MBE), which allows single atomic layer control of epitaxially grown structures, has been successfully employed for such applications. Despite its successes MBE is nevertheless, like all other crystal growth methods, prone to the introduction of defects due to impurities originating in the growth system, source materials or substrates.[1,2,3] In a recent survey, Peaker *et al.*[4] reported that numerous electron and hole traps have been observed in MBE grown GaAs. Because of the influence of defects on the device performance, defect detection and identification are of the utmost importance. In the case of electrically active defects with energy levels in the bandgap, this can effectively be achieved by deep level transient spectroscopy (DLTS),[5] which is capable of detecting defects in concentrations of as low as $10^{10}/cm^3$ in the depletion region of a rectifying device.

Most research regarding defects in MBE grown GaAs has been performed using *n*-type material and the device most frequently used for DLTS in this case was the Schottky barrier diode (SBD). In MBE grown *n*-GaAs various electron traps labeled M1–M8, have been observed.[1,2] The most commonly observed defects are M1, M3, M4 whose origin has been identified as the As source. Other defects (M5–M8) are believed to be structural defects.[3] It is possible to eliminate most of these defects or reduce their concentrations to the low $10^{11}/cm^3$ range by using ultra-pure source materials[3] and by growing in the so-called 'transition region' with growth conditions between Ga—stabilized and As—stabilized.[6] The hole traps reported for MBE grown *n*-GaAs seem to be mostly due to metallic contaminants and were detected either by using p^+-*n* junctions or by employing optical DLTS (ODLTS).

(Received June 29, 1992)

Much less information is available about defects in MBE grown *p*-type GaAs. In this case n^+-*p* junctions were mostly used[7] and only in Ref. 3 were SBDs used. For *p*-GaAs grown by MBE some traps detected by DLTS were identified as, while others were speculated to be, impurity related.[3,7,8]

In this paper we report DLTS results obtained utilizing Al and Co SBDs on *p*-type GaAs which was grown by MBE on p^+-GaAs substrates. The results presented here indicate, apart from the commonly observed metallic impurities, the presence of some hitherto unreported hole traps in MBE grown *p*-GaAs.

2. EXPERIMENTAL PROCEDURE

A four micron thick Be doped ($4 \times 10^{14}/cm^3$) epitaxial *p*-GaAs layer was grown at 600° C by MBE[9] on a Zn doped ($1 \times 10^{18}/cm^3$) GaAs substrate. Au/Zn ohmic contacts were deposited on the backside of the substrate. Either 200 nm thick Al or 25 nm thick Co Schottky contacts were deposited on the MBE grown *p*-layer after chemical etching.[10] The circular Schottky contacts, 0.73 mm in diameter, were defined using a metal contact mask.

Capacitance—voltage measurements on the SBDs thus formed yielded barrier heights of 0.75 eV and 0.63 eV for Al and Co, respectively, and a carrier concentration of $4 \times 10^{14}/cm^3$ for the epitaxial layer. When taking into account the effect of leakage current on the detectability of defects,[11] the barrier properties of Al and Co SBDs were sufficient to facilitate DLTS detection of defects in the temperature regions below 350 K and 300 K, respectively. DLTS measurements were performed in a lock-in amplifier (SR 530) based system[12] utilizing a closed cycle Air Products cryostat to facilitate temperature cycling between 12 and 400 K. A Boonton 7200 capacitance meter and a EG&G model 181 current sensitive pre-amplifier were employed for capacitance and current DLTS measurements, respectively.

0361-5235/1992/1401-1127$5.00©92 TMS

© University of Pretoria

UNIVERSITEIT VAN PRETORIA
UNIVERSITY OF PRETORIA
YUNIBESITHI YA PRETORIA

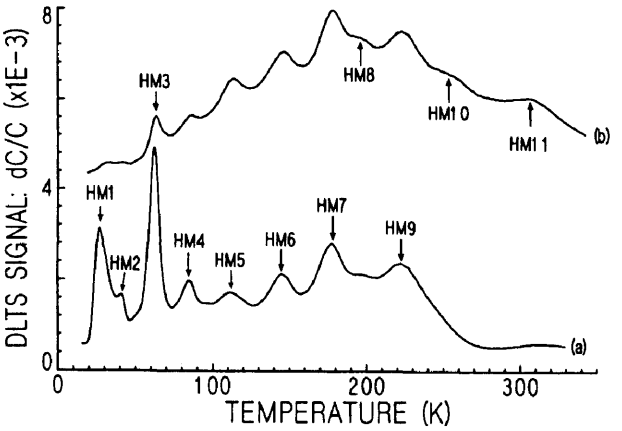

Fig. 1 — Capacitance DLTS scans of MBE grown *p*-GaAs using Co (curve (a)) and Al (curve (b)) SBDs. For curves (a) and (b) the reverse bias, V_r, filling pulse amplitude, V_p, and frequency, f, were 0.5 V, 0.8 V and 46 Hz, respectively.

3. RESULTS

Curves (a) and (b) in Fig. 1 show typical spectra obtained using Co and Al SBDs, respectively. From the applied bias it follows that these spectra represent the first 2–3 μm below the surface. From these spectra it is clear that there are numerous hole traps, indicated as HM1–HM11, in the *p*-epilayer. In the nomenclature used here, "H" indicates hole traps and "M" indicates that the defects were detected in MBE grown GaAs. Although the overall shapes of the spectra in curves (a) and (b) are different, they nevertheless exhibit the same peaks at the same temperature positions. This leads to two conclusions. First, these peaks are characteristic of deep level defects having discrete energy levels, and are not introduced by interface states at the metal—GaAs interface. Second, since the same defect peaks were observed using two different Schottky metals, we conclude that the defects are characteristic of defects introduced during the MBE process and not during Schottky metallization. Further, some peaks, *e.g.* the HM10 and HM11, are better defined on curves recorded using the Al than the Co SBDs. This may be either because the Co SBDs become leaky above room temperature, in which case the leakage current inhibits the DLTS detection of defects,[11] or because the defects are not uniformly distributed across the wafer (the Co and Al SBDs were fabricated on pieces that were about 1 cm apart on the wafer). We attribute the different shape of the baselines of the two spectra (humped for the Al SBDs as opposed to more or less flat for Co SBDs) to interface states which may be different for Al and Co SBDs. This is, amongst others, because their chemical nature, and hence their reaction with the GaAs at the interface are different. Interface states usually exhibit a continuous energy distribution in the GaAs bandgap that could lead to a broad humped baseline,[18] as observed in curves (a) and (b) of Fig. 1.

DLTS scans recorded at various bias and pulse conditions indicated that the concentrations of the defects in the MBE epilayer are all more or less constant. If the defect concentration, N_t, is estimated from the simplified relation[5]

$$N_t = 2(\Delta C/C)N_a \qquad (1)$$

where $\Delta C/C$ and N_a are the DLTS signal and free carrier concentration, respectively, then we may draw two conclusions from curves (a) and (b) in Fig. 1. First, the HM3 concentration is the highest of all defects and is roughly about $1.5–2 \times 10^{12}/\text{cm}^3$ in the Co SBDs. Second, the concentrations of some defects, *e.g.* the HM1 and HM3, are different in Al and Co SBDs. Since the Al and Co SBDs were fabricated on different parts of the wafer, this suggests that the defects are not uniformly distributed across the wafer.

The DLTS 'signatures' of these defects were determined from conventional Arrhenius plots of T^2/e_p vs $1000/T$ (where e_p is the emission rate at a temperature T). The activation energy, E_t, and apparent capture cross section, σ_{pa}, summarized in Table I were calculated from[13]

$$e_p = \gamma_p T^2 \sigma_{pa} \exp(-E_t/kT). \qquad (2)$$

The constant γ_p amounts to $1.62 \times 10^{21}\ \text{cm}^{-2}\text{s}^{-1}\text{K}^{-2}$ for GaAs if a degeneracy of $g = 1$ is used for simplicity. For the purpose of convenient illustration only, the DLTS Arrhenius plots are presented in a modified form in Fig. 2. Here the normal $1000/T$ scale is replaced by $log(1000/T)$ which has the effect of spreading out the 'signatures' more evenly. This representation is especially useful when comparing 'signatures' of defects observed in the entire temperature region from 15 to 400 K. In the discussion that follows it should be borne in mind that when two or more peaks occur in close proximity of each other, their resultant peak positions may be different from their true positions which are measured if only one peak would be present. The fact that so many defect peaks are present so close to each other in Fig. 1 may therefore lead to inaccuracies in the determination of their characteristics, especially when the peaks are not well resolved as for example the HM1–HM2 and HM8–HM11 defect peak combinations.

When constructing the 'signature' of the HM1 using capacitance DLTS data, the conventional Arrhenius plot was not a straight line. Because the HM1 peak seemed to be broader than normal at some frequencies, it was thought that the non-linear 'signature' was the result of emission of two defects with such E_t and σ_{pa} values that their peaks coincide exactly at some, but not at all temperatures. To overcome this problem, current DLTS measurements using a 40 ns wide filling pulse at frequencies of between 1200 and 12000 Hz were made. This apparently eliminated the defect with the smallest capture cross section and resulted in a straight line Arrhenius plot.

To aid the identification of the defects detected in

© University of Pretoria

UNIVERSITEIT VAN PRETORIA
UNIVERSITY OF PRETORIA
YUNIBESITHI YA PRETORIA

Table I. DLTS defect 'signatures' of hole traps in MBE grown *p*-GaAs

	Defects Detected in This Study			
Label	E_t (eV)	σ_p (cm^2)	$T^{(a)}_{peak}$ (K)	Similar Defects[(b)]
HM1	0.058	2.6×10^{-13}	22	? Ge: (0.07, . . .), Li: (0.05, . . .)[17]
HM2	0.070	8.1×10^{-15}	42	? Ge: (0.07, . . .)[17]
HM3	0.136	1.5×10^{-12}	62	Cu: (0.13, 5–20 $\times 10^{-14}$)[1,14]
HM4	0.168	6.8×10^{-14}	86	
HM5	0.235	1.6×10^{-13}	113	? peak at 120 K[3]
HM6	0.332	1.0×10^{-12}	146	? Zn: (0.27, 1×10^{-14})[13]
HM7	0.406	6.0×10^{-13}	179	
HM8	—	—	. . .	
HM9	0.457	2.9×10^{-14}	223	Cu: (0.42, 3–5 $\times 10^{-15}$)[1,13,14]
HM10	—	—	255	
HM11	0.652	3.0×10^{-14}	309	? HL9: (0.69, 10^{-13})[13], Fe: (0.53, 10^{-15})[15]

(a) At a lock-in amplifier frequency of 46 Hz, *i.e.* a decay time constant of 9.23 ms.
(b) Values listed in brackets in this column are (E_t, σ_{pa}) values as listed in the reference next to them. Question marks indicate that there is an uncertainty as to the identification of the defect measured in our study and that listed as 'similar defects'.

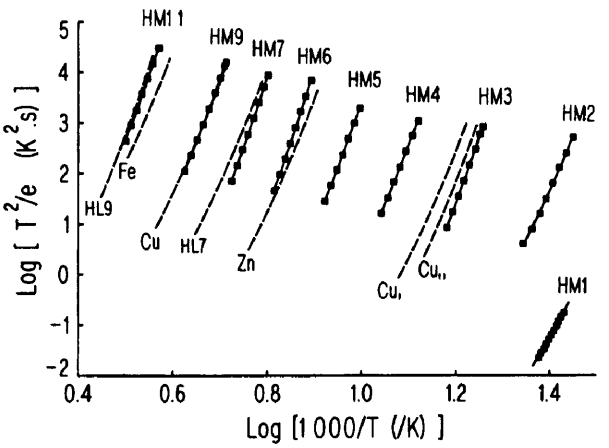

Fig. 2 — Defect 'signatures' on a modified Arrhenius representation which were constructed using DLTS data for the temperatures where the in-phase signal of the lock-in amplifier was a maximum. The squares represent the data from this study. For defects HM2–HM11 the capacitance signal was analyzed, while current DLTS data was used to construct the 'signature' of the HM1. The broken lines were taken from the following references: Cu (Refs. 4, 14), Zn (Ref. 13), Fe (Ref. 15), HL7 and HL9 (Ref. 13).

this study, their 'signatures' are compared to those of some other defects (broken lines in Fig. 2) which have been observed in GaAs. First consider the most common metallic impurities, namely Cu, Fe, Cr and Zn, observed as hole traps in GaAs by DLTS measurements.[4] Where possible, the data taken from the literature was for low carrier density GaAs so as to avoid field assisted lowering of the activation energy and therefore to make a more meaningful comparison with our results which are for lightly doped GaAs. From Fig. 2 it is evident that the 'signature' of the HM9 appears to be very close to that of the frequently reported Cu defect at an energy of 0.42–0.45 eV above the valence band.[4,13,14] We speculate that the slightly higher activation energy (0.46 eV) measured here is due to the closeness of peaks of other defects in the same temperature region. Further, the HM3 has a signature very similar to the low temperature Cu related defect at 0.13–0.15 eV above the valence band.[4,14] For the purpose of illustration, the 'signatures' of Cu with $E_t = 0.13$ eV, but with two differently reported capture cross sections, namely 2×10^{-13} cm^2 (Ref. 14, Cu_{II} in Fig. 2) and 5×10^{-14} cm^2 (Ref. 4, Cu_I in Fig. 2), are shown. Cu is frequently found as a trace contaminant in most source materials as well as in substrates used for epitaxial growth. We therefore assign the HM3 and HM9 to the two copper related defects often encountered in GaAs.

Next consider possible Zn contamination. In the case of Zn there does not seem to be many references to measurements made on low carrier density GaAs. In the extensive study of Wang *et al.*,[16] GaAs with carrier densities of above 2×10^{17}/cm^3 was used to study Zn related levels. In their case, however, the field assisted emission caused variations of more than a factor of two in the measured activation energies. Therefore the activation energies of 0.13–0.29 eV above the valence band that they reported for Zn do not seem suitable for this comparison. On the other hand, the 'signature' cited by Mitonneau[13] was obtained for roughly the same carrier density GaAs as used by us and in Fig. 2 it appears in the same temperature region of the HM6. The misalignment of the two 'signatures' in question is representative of a 5–7 K temperature difference in the emission rate as determined by the two groups. As already pointed out, the closeness of the defect peaks in this study may be a contributing factor to the poor agreement between these two 'signatures'. If all this is taken into account, then we speculate the HM6 may be Zn related.

The other very common impurity in GaAs is Fe[13,15] and its 'signature' is in the same temperature region as that of the HM11. However, it does not coincide well enough to allow a positive identification. It should be noted from Fig. 1 that this peak is not well resolved and that in order to compile its 'sig-

© University of Pretoria

UNIVERSITEIT VAN PRETORIA
UNIVERSITY OF PRETORIA
YUNIBESITHI YA PRETORIA

nature', it had to be measured at temperatures of as high as 320 K. This is in a temperature region in which leakage currents in the SBDs already become non-negligible, and consequently there is a possibility that this may have affected the accuracy of the emission rate determination. We therefore emphasize the presence of the HM11 rather than its unique identification.

Next we compare defects that do not exhibit 'signatures' similar to those of the common metallic impurities. Although the HM11 'signature' is in the same temperature range as that of Fe, it coincides almost exactly with that of the HL9,[13] which is believed to be a characteristic native defect in VPE grown GaAs, but of which the exact nature is however not known. Because of the lack of information on hole traps in p-GaAs, it is not clear whether the HM11 (or HL9) is not perhaps characteristic of MBE GaAs as well. Further, the HM7 observed in our study has a 'signature' in the same region as the HL7 which has been reported before[13] for MBE grown GaAs. The difference in activation energies (0.41 eV in this study vs 0.35 eV in Ref. 13), however, prevents a unique defect identification.

Apart from the defects which have similar 'signatures' to those reported in the literature, we have also detected some defects, HM1, HM2, HM4 and HM5, which have not been reported before in low carrier density *p*-GaAs. Only one example of a spectrum containing a hole trap in *p*-type MBE grown GaAs has been published, but no defect characteristics were given.[3] However, from the rate window and temperature given, the activation energy can be estimated as about 0.2 eV above the valence band, thus resembling the HM4 or HM5 detected in our study. Because the 0.2 eV defect of Ref. 3 was observed only in samples grown using double refined 6N grade As and not in samples grown using 7N grade As, it is reasonable to assume that this defect is introduced as an impurity from the 6N grade As.

Of further significance here are the HM1 and HM2 peaks observed below 50 K. They are in the temperature region in which the DLTS peaks resulting from typical accepter dopants in GaAs are to be expected. Shallow dopant impurities that lead to the formation of *p*-type GaAs are primarily C, Be, Mg, Zn, Cd and Ge, located between 0.025 eV (carbon) and 0.07 eV (germanium) above the valence band.[17] Beryllium, the dopant present in the system during growth of the crystal studied here introduces a level at E_v + 0.028 eV. Of the defects measured in our study, the energy of the HM2 calculated from its 'signature' was 0.07 eV which corresponds closely to that of Ge. Further, as mentioned above, capacitance DLTS measurements indicated that the HM1 may actually be the superposition of two close lying peaks. The energy of 0.058 eV calculated for the HM1 using current DLTS does not correspond closely to any of the well known dopant contaminants, but has an energy which is roughly halfway between that of Ge (0.07 eV) and Li (0.05 eV).[17] Due to the lack of data in the literature regarding especially shallow hole traps in p-GaAs, *e.g.* with levels closer than 0.13 (Cu) from the valence band, the results presented here cannot be fruitfully compared with those of other authors.

4. CONCLUSIONS

Up to now there has been little information available pertaining to the electrical characteristics of hole traps in *p*-GaAs layers grown on p^+-GaAs substrates. The only significant contribution in this area was for OMVPE grown *p*-type layers[16] which had carrier densities of above $10^{17}/cm^3$. For such carrier densities it is known that electric field effects have a major influence on defect properties. The results presented in the present study employing SBDs on lowly doped ($4 \times 10^{14}/cm^3$) *p*-type layers grown by MBE on p^+-GaAs substrates are therefore unique.

The DLTS results presented here for the MBE grown *p*-GaAs epilayers indicate that several hole defects with energy levels in the bottom half of the bandgap were introduced into the epilayer during crystal growth. Although the exact origin of most of the defects detected in this study are not known, several of these defects have characteristics which are in close agreement with those of common metallic impurities, such as Cu and Fe in GaAs. Several shallow levels, one of which closely resembles Ge, were also detected. Because so little is known about native hole defects in p-type GaAs, it is not possible to conclude whether the unidentified defects detected here are native defects or perhaps other less known contaminants.

However, because MBE has been utilized to grow defect free GaAs, the most probable cause of these defects are contaminated source material from which the GaAs is grown[3] or substrates containing fast diffusing impurities.[14] Since the concentrations of impurities detected here are of the order of $10^{12}/cm^3$, they may easily be introduced via source materials with a specification of 'seven nines' or better. On the other hand, fast diffusing impurities can also enter the epitaxial layer from the substrate during the growth process. This has been demonstrated in a study where defects in *n*-GaAs grown by OMVPE on n^+—and semi-insulating GaAs substrates from different suppliers were compared.[14] Therefore, the results presented here emphasize that if GaAs with a very low deep level defect concentration has to be grown by MBE, then, as is the case of all other growth methods, the cleanliness of the growth system and purity of growth constituents (substrates and sources) are of the utmost importance.

In summary, the DLTS results obtained in this study after fabricating SBDs on MBE grown p-p^+ GaAs structures, illustrate that several hole traps were introduced during MBE crystal growth. This study also stressed the necessity of conducting studies directed towards identifying the specific sources of defect or impurity introduction, as well as identifying the hitherto unknown defect levels observed in this study.

© University of Pretoria

UNIVERSITEIT VAN PRETORIA
UNIVERSITY OF PRETORIA
YUNIBESITHI YA PRETORIA

ACKNOWLEDGMENTS

The financial assistance of the South African Foundation for Research and Development is gratefully acknowledged.

REFERENCES

1. D. V. Lang, A. Y. Cho, A. C. Gossard, M. Ilegems and W. Wiegmann, J. Appl. Phys. *47*, 2558 (1976).
2. P. Blood and J. J. Harris, J. Appl. Phys. *56*, 993 (1984).
3. N. Chand, A. M. Sergent, J. P. van der Ziel and D. V. Lang, J. Vac. Sci. Technol. *B7*, 399 (1989).
4. A. R. Peaker and B. Hamilton, "Landolt-Bornstein: Numerical Data and Functional Relationships in Science and Technology," ed. O. Madelung (Springer-Verlag, New York), New Series: Group III, Vol. *22*, 1988.
5. D. V. Lang, J. Appl. Phys. *45*, 3023 (1974).
6. H.-D. Xu, T. G. Andersson and J. M. Weston, J. Appl. Phys. *62*, 2136 (1987).
7. P. K. Bhattacharya, H. L. Buhlmann and M. Ilegems, J. Appl. Phys. *53*, 6391 (1982).
8. R. A. Stall, C. E. C. Wood, P. D. Kirchner and L. F. Eastman, Electron. Lett. *16*, 171 (1980).
9. Quantum Epitaxial Designs, Inc., 115 Research Drive, Bethlehem, PA 18015, USA.
10. G. Myburg and F. D. Auret, Appl. Phys. Lett. *60*, 604 (1992).
11. Q. Y. Ma, M. T. Schmidt, X. Wu, H. L. Evans and E. S. Yang, J. Appl. Phys. *64*, 2469 (1988).
12. F. D. Auret and M. Nel, J. Appl. Phys. *63*, 973 (1988).
13. A Mitonneau, G. M. Martin and A. Mircea, Electron. Lett. *13*, 666 (1977).
14. F. D. Auret, M. Nel and A. W. R. Leitch, J. Electron. Mater. *17*, 111 (1987).
15. M. Kleverman, P. Omling, L-A. Ledebo and H. G. Grimmeiss, J. Appl. Phys. *54*, 814 (1983).
16. P. J. Wang, T. F. Kuech, M. A. Tischler, P. Mooney, G. Scilla and F. Cardone, J. Appl. Phys. *64*, 4975 (1988).
17. S. M. Sze, "Physics of Semiconductor Devices", 2nd Ed., John Wiley and Sons, 1981, p 21.
18. H. Zhang, Y. Aoyagi, S. Iwai and S. Namba, Appl. Phys. Lett. *50*, 341 (1987).

© University of Pretoria

4.3 MATERIAL IRRADIATION

This part of the study contains results pertaining to the defects intentionally introduced in the epi-layer, as well as the change in electrical properties of the metal-semiconductor system using alpha-particles, protons and electrons. The alpha-particle irradiation was performed using either a radionuclide source (^{241}Am) or a Van de Graaff accelerator. The electron irradiation was performed using a ^{90}Sr radionuclide, and the Van de Graaff accelerator was used for the proton beam irradiation.

After alpha-particle irradiation of n-type GaAs, 5 major electron defects were detected (Eα1, Eα2, Eα3, Eα4 and Eα5). It has been shown that Eα1 and Eα2 are the same defects as E1 and E2 (Eβ1 and Eβ2) detected after electron irradiation, believed to be two different charge states of the isolated arsenic vacancy. Electron defect Eα4 is believed to be the same defect as E3 (Eβ4, initially labelled Eβ3). Similar results were obtained for proton-irradiated n-type GaAs. The influence of alpha and proton irradiation on the I-V and C-V properties of metal-semiconductor systems was investigated. In both cases a linear change in the reverse leakage current, measured at -1.0 volt, was observed as a function of incident particle fluence. The carrier removal rate was also calculated as a function of incident particle fluence for both particle types.

When irradiating p-type GaAs with alpha-particles, 5 hole defects were introduced (Hα1 - Hα5). Upon comparing these defects to those detected in p-type GaAs after electron irradiation, it was found that Hα1 and Hα5 correspond to H0 and H1. The defect concentration profiles for these two defects were constant in the region profiled (0.15 - 0.35 μm). However, the concentration of defect Hα4 decreased sharply away from the interface; we speculate that this defect is a more complex type defect that forms between radiation-induced point defects and an impurity or a structural defect, whose concentration depends strongly upon the electric field in the space-charge region.

© University of Pretoria

CHAPTER 5

CONCLUSIONS

5.1 INTRODUCTION

There have been numerous papers published on defect characterization after electron irradiation of n-type GaAs, and to a lesser degree in p-type GaAs. In this study, the electrical and defect characteristics of n-type GaAs after alpha-particle, proton and neutron irradiation and argon sputtering have been determined. The electrical and defect characteristics have also been determined for alpha-particle irradiated p-type GaAs. These defect properties are then compared to the defect properties of electron irradiated material which are better understood. The dependence of the emission rate on the strength of the electrical field in the space-charge region of the major electron traps in electron irradiated n-type GaAs is described. The annealing kinetics of defects detected after alpha-particle irradiation at 300 K and 15 K are also compared to similar defects in electron irradiated material. The damage caused by neutron irradiation and argon sputtering is discussed and compared to damage caused by other particles. Finally, a short summary and proposed future studies are presented.

5.2 MATERIAL CHARACTERIZATION

When using the optical DLTS (ODLTS) and DLTS techniques to study process-induced defects, the choice of substrate material is very important. It has been concluded that semi-insulating GaAs is a more suitable substrate than silicon-doped n^+ substrate material for growing high quality epitaxial layers by MOVPE, intended for DLTS and ODLTS studies of process-induced defects. Three hole traps that may 'mask' process-induced defects are introduced into the epilayer during MOVPE growth, when using a silicon-doped n^+ substrate. However, the quality of the ohmic contacts fabricated on the epitaxial

© University of Pretoria

layer is not as high as those fabricated on the n^+ substrate. Also, the processing of these ohmic contacts on the epitaxial layer is more complicated than those fabricated on the n^+ substrates.

To be able to study process-induced defects in p-type material, it is necessary to use defect-free p-GaAs. The MBE growth technique which is capable of growing high purity epitaxial structures with atomic layer control of epilayer thickness is often used for such applications. It has been found that lowly-doped p-type GaAs layers grown on p^+-GaAs substrates using this technique may contain several hole defects positioned in the bottom half of the bandgap. The most probable cause of these defects are contaminated source material or substrates containing fast diffusing impurities.

5.3 MATERIAL IRRADIATION

From a knowledge of the DLTS "signatures", the defects detected after α-particle irradiation (Eα1, Eα2, Eα4 and Eα5), after proton- irradiation (Ep1, Ep2, Ep4 and Ep5) and after neutron-irradiation (En1, En2, En4 and En5) are shown to be similar to those detected after electron-irradiation (E1, E2, E3 and E5). Eα1 and Eα2 are speculated to be different charge states of the same defect, although, their introduction rates are not the same. It would appear that their emission rates are dependent upon the magnitude of the electric field in the space-charge region. Alpha-particles, protons, neutrons and, to a lesser degree, electrons introduce an electron trap observed at approximately 180 K at a LIA frequency of 46 Hz. The concentration of this defect depends upon the bias conditions and temperature during the DLTS analysis. After neutron irradiation, a defect labelled En5 is detected, whose emission rate exhibits a strong field dependence, and there are indications that it has a band-like energy distribution that results in a broad DLTS peak.

Alpha-particle, proton and neutron irradiation cause degradation of the I-V characteristics of the metal-semiconductor system and a recombination-generation current is present

© University of Pretoria

after irradiation, whose magnitude depends upon the incident particle type and fluence. The change in the reverse leakage current after irradiation depends linearly upon the incident fluence (α-particles and protons). From modelling results, it has been observed that with an increase in α-particle fluence there is a corresponding increase in the series resistance. This increase is not due to degradation of the ohmic or Schottky contact but is due to carrier removal as a result of defects being introduced into the bandgap. The series resistance increases from 1.6 Ω for unirradiated material to 8.5 Ω for 5.4 MeV alpha-particle irradiated n-type GaAs doped with silicon to 1.2×10^{16} cm^{-3} (fluence = 6.2×10^{11} cm^{-2}).

The minimum fluence achievable when using the Van de Graaff accelerator was 1.4×10^{11} cm^{-2}, whereas a fluence as low as 2×10^{4} cm^{-2} was obtained for the ^{241}Am radionuclide source with an activity of 0.53 μCi.cm^{-2}.

5.4 ELECTRIC FIELD EFFECT

An enhancement of the emission rate of electron-irradiation-induced defects in the presence of an electric field in n-type GaAs with carrier concentrations ranging from 1×10^{14} to 1.2×10^{16} cm^{-3}, has been observed. Defect E1 exhibits a fairly strong field dependence. However, this dependence cannot be explained by either the phonon-assisted tunnelling mechanism or the Poole-Frenkel potential lowering. The enhancement may be due to carrier hopping for this defect. On the other hand, the field dependence for defects E2 and E3 is well described by the phonon-assisted tunnelling mechanism; the Huang-Rhys factor being 4.5 ± 0.5 for E2 and 7.5 ± 0.5 for defect E3.

5.5 DEFECT ANNEALING

When irradiating n-GaAs at 15 K, two new defects (Eα7 and Eα9) other than those detected after 300 K irradiation are detected. Eα7 and Eα9 anneal out with first-order kinetics at 245 K and 225 K, respectively. The annealing rate of Eα7 corresponds to an

© University of Pretoria

activation energy of 0.86 eV with a factor (ν) of 1.0 x 10^{15} s^{-1}; and the removal of Eα9 has an activation energy of 0.88 eV and a factor (ν) of 1.7 x 10^{17} s^{-1}. These large factors (ν) may be attributed to a large lattice relaxation during the annealing process. It was concluded that these defects may be complex or di-vacancy type defects related to the Ga-sublattice.

It is speculated that Eα8 transforms into the vacancy-interstitial pair, Eα1 and Eα2, after a 453 K anneal for 15 minutes. A new defect, labelled Pα0, detected at a peak temperature of 102 K at 46 Hz, with DLTS signature (0.152 eV and 1.7 x 10^{-15} cm^{-2}) was first detected after the sample had been annealed at 473 K for 105 minutes. The concentration of this defect increases as the anneal cycle progresses. Defects Eα1 and Eα2 exhibit the same annealing kinetics, thus confirming the theory that they are indeed two charge states of the same defect. From the annealing kinetics and DLTS "signatures", defects Pα1 and Pα2 detected after the removal of Eα4 and Eα5 are speculated to be the same as those observed after annealing of electron-irradiated material (P1 and P2). The emission rate of Pα0 exhibits a fairly strong field dependence, whereas, Pα1 exhibits a weak field dependence. The defect Eα3 exhibits primarily first-order kinetics and anneals out at 460 K.

5.6 DAMAGE CAUSED BY NEUTRON IRRADIATION AND ARGON SPUTTERING

Sputter etching with argon ions before SBD metallization introduces discrete level defects as well as continuous level defects in the bandgap of GaAs. Some of the sputter-induced defects will have a point defect nature, with the others being "cluster-like" or complex defects. Argon sputtering of n-GaAs may reduce the barrier height, causing those defects positioned near midgap not to empty out completely while under reverse quiescent bias. This phenomena may result in an erroneous estimate of defect concentration.

© University of Pretoria

It was found that the barrier height of gold SBDs changed non-monotonically with sputter voltage (0.5 - 5.0 kV), and this could be correlated with the combined effect of sputter-induced defects with discrete and continuous energy levels in the GaAs bandgap.

5.7 SUMMARY AND FUTURE STUDIES

In summary, this study has shown that when irradiating n- and p-type GaAs with heavier particles than electrons, new as well as similar defects are introduced. These defects have been shown to influence the current-voltage characteristics of SBDs, especially the series resistance and the reverse leakage current, two important parameters for the device engineer. By annealing the metal-semiconductor system, defect removal occurs and the current-voltage characteristics recover to a certain degree. This recovery process may be used to possibly repair devices that have been exposed to radiation to such an extent that their performance has been detrimentally influenced.

Future studies should entail a detailed investigation of the microscopic nature of the radiation-induced defects using techniques other than pure DLTS. A correlation between the structural damage and the deterioration of the electrical properties of the metal-semiconductor system after irradiation may yield useful information. An investigation of the electrical and defect properties of SBDs fabricated on GaAs, irradiated with particles such as carbon or beryllium (typical elements used for doping), may promote a better understanding of the activation of implanted semi-insulating material used for device fabrication.

© University of Pretoria

© University of Pretoria

4.6 DAMAGE CAUSED BY NEUTRON IRRADIATION AND ARGON SPUTTERING

Although the main thrust of my Ph.D. was to investigate the effects and defects introduced by alpha-particles, protons and electrons, results are also presented which allow a comparison between those defects introduced by the above-mentioned types of radiation and those detected after neutron irradiation and argon sputtering.

PUBLICATIONS:

(14) F.D. Auret, S.A. Goodman, G. Myburg and W.E Meyer, "Electrical characteristics of Ar-ion sputtered induced defects in epitaxially grown n-GaAs", J. Vac. Sci. & Technol. B **10** (1992) 2366.

(15) F.D. Auret, S.A. Goodman, G. Myburg, W.O. Barnard and D.T.L. Jones, "Electrical characterization of neutron irradiation induced defects in undoped epitaxially grown n-GaAs", J. Appl. Phys. **74** (1993) 4339.

(16) F.D. Auret, A. Wilson, S.A. Goodman, G. Myburg and W.E. Meyer, "Electrical characteristics of neutron irradiation induced defects in n-GaAs", Nucl. Instrum. & Methods B, **90** (1994) 387.

(17) F.D. Auret, G. Myburg, S.A. Goodman, L.J. Bredell and W.O. Barnard, "Effect of sputter voltage on the electrical characteristics of argon ion sputtered n-type GaAs", Nucl. Instrum. & Methods B, **67** (1992) 410.

(18) F.D. Auret, S.A. Goodman, A. Wilson and G. Myburg, "Neutron irradiation induced defects in low free carrier concentration epitaxially grown n-GaAs", accepted for publ. in Jpn. J. Appl. Phys. **33**, 5 (1994) 2633

© University of Pretoria

UNIVERSITEIT VAN PRETORIA
UNIVERSITY OF PRETORIA
YUNIBESITHI YA PRETORIA

Electrical characteristics of Ar-ion sputter induced defects in epitaxially grown *n*-GaAs

F. D. Auret, S. A. Goodman, G. Myburg, and W. E. Meyer
Physics Department, University of Pretoria, Pretoria, 0002 Republic of South Africa

(Received 19 December 1991; accepted 4 August 1992)

Epitaxially grown *n*-type GaAs was sputtered by bombarding it with Ar ions at energies of between 0.5 and 5 keV at a dose of 10^{13} ions/cm^2. The fabrication of Au Schottky barrier contacts followed directly after the sputtering. The electrical characteristics of the the sputter induced defects were studied using deep-level transient spectroscopy (DLTS). Several defects with discrete defect levels ranging from 0.05–0.70 eV below the conduction band, as well as defects with continuously distributed energies in the conduction band, were introduced during sputtering. Concentration depth profiling revealed that whereas some defects are located very close to the interface, others were detected several microns below the interface. The depth of some of these deep lying defects increased with sputter voltage. A possible explanation of the reduction in EL2 DLTS signal previously observed after sputtering is shown to be the sputter induced barrier height lowering.

I. INTRODUCTION

The processing of semiconductor surfaces with energetic particles is a widely used processing step in the semiconductor technology because, among others, it offers the capability of performing several processing steps in vacuum without exposing the semiconductor surface to the atmosphere. It is, however, well-known that the use of energetic particles may result in unwanted changes in the surface and subsurface substrate properties, e.g., structural disorder[1] or nonstoichiometry in the case of compound semiconductors.[1,2] Several studies have shown that the surface and subsurface disorder in semiconductors introduce defects with discrete as well as continuous energy levels in the semiconductor band gap. When these defects are present in high enough concentrations at and close to the surface, they can cause, among others, significant changes in the electrical properties of Schottky barrier diodes (SBDs) fabricated on ion damaged surfaces.[3–5] For example, Schottky barrier diodes fabricated on sputtered surfaces of *n*-type semiconductors exhibit a lower barrier height than those on unsputtered surfaces. For SBDs on sputtered *p*-type semiconductor surfaces the opposite is true.

Based on experimental observations,[6] it has generally been accepted that the concentration, $N_t(x)$, of sputter induced defects at a distance x below the surface can be approximated by

$$N_t(x)=N_{ts}\exp(-x/L), \tag{1}$$

where N_{ts} is the defect concentration at the surface and L is the characteristic length. Using this equation, values of L up to 3 μm have been reported for GaAs etched using 2 keV Ar ions.[7] This is much deeper than the approximate value of 90 Å predicted by the Lindhard–Scharff–Schiott (LSS) theory for the penetration of 2 keV Ar ions into GaAs. A possible explanation for this apparent contradiction may be found in the observation of Dubonos[7] that some sputter induced defects in GaAs are mobile, even at room temperature. A recent investigation by Vaseashta *et al.*[8] confirmed that defects introduced during 1–4 keV Ar sputtering were "located much deeper than predicted by the LSS theory."

Accurate and reproducible defect engineering requires a fundamental understanding of the electrical properties and physical nature of sputter induced defects, which have not yet been uniquely established. One way of gaining insight into the nature of these defects is to compare their properties to those of the primary defects introduced during high-energy electron irradiation, which have been thoroughly studied and identified. Based on such comparisons, it was found that some of the sputter induced defects are similar to electron irradiation induced defects.[7] Several factors, however impede accurate and universal sputter induced defect comparison and identification. Most studies pertaining to Ar sputter induced defects in GaAs were conducted at temperatures above 80 K. Consequently defects with energy levels in the band gap close to the band edges, such as the $E1$–$E2$ combination in electron and proton irradiated GaAs,[9] which have been identified as arsenic-vacancy related defects, could not be detected. Furthermore, because most these studies were carried out on GaAs substrates with different free carrier and imperfection concentrations, often grown by different methods, a comparison of sputter induced defects reported by different authors is often not meaningful.

The aim of this study was to gain a better understanding of Ar sputter induced defects by studying their dependence on sputter voltage and comparing their properties *in the same type of substrate* to those of defects introduced during electron irradiation, of which the structure has been identified. Special attention was paid to the depth distribution of defects created at different sputter voltages as well as the previously reported sputter induced annihilation of the EL2 defect or desensitisation of its deep-level transient spectroscopy (DLTS) signal. This was accomplished by employing conventional capacitance–voltage (C–V) and DLTS[10] measurements.

 0734-211X/92/062366-05$01.00 ©1992 American Vacuum Society

© University of Pretoria

UNIVERSITEIT VAN PRETORIA
UNIVERSITY OF PRETORIA
YUNIBESITHI YA PRETORIA

II. EXPERIMENTAL PROCEDURE

Undoped (100) oriented n-type GaAs epilayers with a free carrier concentration of $3–4\times10^{14}/cm^3$, grown by metalorganic vapor phase epitaxy (MOVPE) on n^+ substrates [$10^{18}/cm^3$ doped with Si, liquid encapsulated Czochralski (LEC) grown], were used to investigate Ar ion sputter induced defects. After wet chemical etching, Au/AuGe/Ni ohmic contacts were fabricated on the n^+ backsides of the wafers. Before sputter etching and subsequent SBD metallization, the samples were once again etched utilizing the same chemical cleaning procedure as before ohmic contact fabrication. This comprised of degreasing in TCE, rinsing in isopropanol, rinsing in water, etching in $NH_4OH:H_2O_2:H_2O$ (3:1:120, 1 min), rinsing in H_2O, oxide stripping in $HCl:H_2O$ (1:1, 2 min), followed by a final rinse in H_2O. Immediately thereafter the samples were inserted into a vacuum system which was evacuated to a pressure of 10^{-8} mbar, whereafter Ar was let into the system to a pressure of 3×10^{-5} mbar. The samples were sputtered by accelerating Ar ions perpendicularly onto their surfaces by an ion gun at voltages of 0.5, 1, 2, 3, and 5 kV, at a dose of $10^{13}/cm^2$. Immediately after sputter etching, without breaking vacuum, Au contacts, 0.73 mm in diameter and 1000 Å thick, were deposited by resistive evaporation on the sputtered surfaces through a metal contact mask. For control purposes, diodes were fabricated identically to those described above, except that the GaAs was not Ar sputtered prior to SBD metallization.

The sputter induced defects in GaAs were characterized by DLTS[10] using a two-phase lock-in amplifier based system[11] between 12 and 375 K. The concentration distribution of the sputter induced defects were calculated by combining the relations[12]

$$\lambda=[2\epsilon(E_t-E_f)/qN_d]^{1/2}, \tag{2}$$

$$x_f=[2\epsilon(V_{bi}-V_f)/qN_d]^{1/2}-\lambda, \tag{3}$$

$$N_t(x)=2(\Delta C/C)N_d/[(1-x_f/x_r)(1+x_f/x_r-2\lambda/x_r)], \tag{4}$$

and

$$x=(x_f+x_r)/2. \tag{5}$$

Here V_{bi} is the built-in voltage of the SBD, V_f and V_r are the voltages across the diode during the filling pulse and quiescent bias, respectively, and the expression for x_r is similar to that of x_f except that V_f is replaced by V_r. Physically, x_f and x_r are the distances from the interface to where the Fermi level intersects the defect level during the filling and reverse biases. The other symbols have their conventional meanings.

III. RESULTS AND DISCUSSION

A. Discrete and continuous level defects

DLTS spectra for SBDs fabricated on unsputtered (control) as well Ar sputtered GaAs are presented in Fig. 1 for surfaces sputtered with 0.5–2 keV Ar ions. The main deep level defect in the control samples [curve (a)] was the EL2,

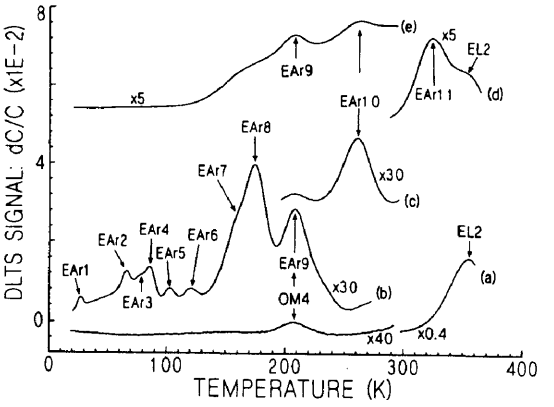

FIG. 1. DLTS spectra of control SBDs [curve (a)], as well as SBDs on GaAs surfaces sputtered with 10^{13} Ar/cm^2 at 0.5 kV [curve (b)] and 2 kV [curves (c)–(e)]. The sections of curves (a) and (d) above 300 K were recorded at a lock-in amplifier frequency of 4.6 Hz and and all other curves at 46 Hz. The quiescent reverse bias V_r for curves (a), (b), (c), and (e) was 2 V, while for curve (d) it was 5 V. The filling pulse amplitudes for curves (a)–(e) were 2.8, 2.8, 1.5, 5.2, and 2.4 V, respectively.

characteristic of all MOVPE grown GaAs, in a concentration of about $1.5–2\times10^{14}/cm^3$. In addition, control samples also contained a defect, the OM4,[13] in a concentration of about $2–3\times10^{11}/cm^3$. The electrical characteristics of the OM4 resemble those of the sputter induced EAr9 defect (which will be discussed). From curves (b)–(e) it can be seen that discrete level defects (DLDs) as well as continuous level defects (CLDs) are present in the sputtered GaAs. The DLDs give rise to DLTS peaks that remain fixed in temperature upon changing the filling pulse amplitude whereas the CLDs result in a skewing of the baseline as in curve (e).[14]

From curve (b) in Fig. 1 it is evident that numerous DLDs, EAr1–EAr9, are present in the 0.5 keV sputtered sample. In order to observe and maximize the DLTS signals of low temperature defects, such as the EAr1, a filling pulse in excess of flatband voltage had to be applied.[15] This pulse requirement stems from the fact that these defects are only present very close to the interface, well within the zero-bias depletion region. Moreover, in the presence of a high density of interface states at an interfacial layer the Fermi level does not remain flat right up to the interface upon applying a forward bias. Therefore, even biasing the SBD to flatband does not guarantee that all the near-surface defects will be filled during the forward bias pulse. The only way in which the DLTS signals of these near-surface low-temperature defects could be maximized was to a apply a bias which was a few tenths of a volt in excess of flatband bias.[4] Fewer different DLDs are present in substrates exposed to Ar ions at higher voltages [curves (c)–(e)] but these samples contain the EAr10 and EAr11 defects. In samples sputtered at 5 keV, for example, the EAr9, EAr10, and EAr11 are the only dominant DLDs.

The defect "signatures" (energies and capture cross sections) calculated from the conventional DLTS Arrhenius plots are graphically presented in a modified form in Fig. 2

© University of Pretoria

UNIVERSITEIT VAN PRETORIA
UNIVERSITY OF PRETORIA
YUNIBESITHI YA PRETORIA

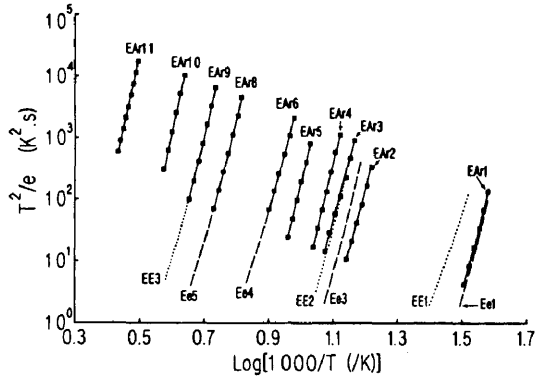

FIG. 2. Modified Arrhenius plots for Ar sputter induced defects in *n*-GaAs. Squares represent the data from this study. Dotted and dashed lines are for defects introduced in the same substrate type (Ref. 16) during 5 MeV and 2 keV electron irradiation, respectively.

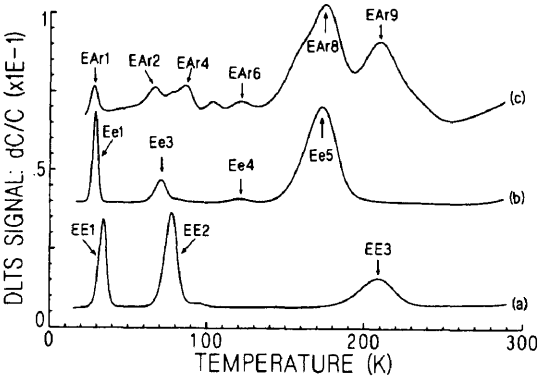

FIG. 3. Comparison of DLTS spectra of defects introduced in organometallic vapor phase epitaxially grown GaAs during high-energy electron irradiation [curve (a): 3.3×10^{11} electrons/cm^2, 2 MeV], low-energy electron irradiation [curve (b): 10^{17} electrons/cm^2, 2 keV], and Ar ion sputtering [curve (c): 10^{13} Ar^+/cm^2, 0.5 kV]. All spectra were recorded at a quiescent reverse bias of 2 V, a filling pulse voltage of 2.8 V and a lock-in amplifier frequency of 46 Hz.

and are summarized in Table I. In a conventional DLTS Arrhenius plot (T^2e versus $1000/T$, where e refers to the emission rate at a temperature T) the signatures of defects with energy levels far from the band edges "group" closer together towards the low $1000/T$ side of the plot. This makes a visual comparison of defects via their signatures difficult if defects with a wide energy range are depicted on the same figure. The modified Arrhenius plot in Fig. 2, which uses $\log(1000/T)$ as the abscissa, spreads the signatures more evenly across the graph, facilitating a more accurate comparison. It should be noted, however, that the energy and apparent capture cross-section values listed in Table I were determined from a conventional Arrhenius plot and that the modified plot is only used for visual comparison.

The CLDs, which reside close to the interface have a continuous energy distribution in the band gap which results in a skewing of the DLTS spectrum baseline.[4] This is clearly illustrated by curve (e) in Fig. 1. These defects could be detected only in the sputtered samples, and not in control samples, upon applying a forward bias filling pulse and their contribution to the DLTS spectrum increased with increasing forward bias V_f. The concentration of the CLDs increased as the sputter voltage was increased from 0.5 to 5 kV, as has been discussed elsewhere.[4] These facts indicate that the CLDs are caused by sputtering and are not characteristic of the metal interface alone.

B. Comparison with electron irradiation induced defects

In the modified Arrhenius plots of Fig. 2, the signatures of the sputter induced defects are compared with those of defects introduced in the same substrate type during 2 keV and 5 MeV electron irradiation.[16] The spectra for these three cases are depicted in Fig. 3, curves (a)–(c), respectively. From these comparisons it is evident that the EAr1, EAr6, and EAr8 sputter induced defects have similar signatures as the Ee1, Ee4, and Ee5, respectively, introduced during low-energy electron irradiation. The EAr3 and

TABLE I. DLTS defect signatures of Ar ion sputter induced defects in *n*-GaAs.

	Defects of this study			Similar defects	
Label	E_t eV	σ_t (cm^2)	T^a_{peak} (K)	Electron Irradiation	Argon ion sputtering
EAr1	0.050	1E-13	30	Ee1 (Ref. 16)	
EAr2	0.107	1E-14	68		DL1 (Ref. 7)
EAr3	0.125	8E-15	79	EE2 (Refs. 16 and 17)	DL2? (Ref. 7)
EAr4	0.16	1E-13	86		DL2? (Ref. 7)
EAr5	0.19	8E-14	103		
EAr6	0.18	1E-15	122	Ee4 (Ref. 16)	
EAr7	...	...	164		
EAr8	0.30	8E-15	175	Ee5 (Ref. 16)	DL3 (Ref. 7)
EAr9	0.40	4E-14	209	EE3 (Refs. 16 and 17)	*L*-2 (Ref. 17), also OM4 (Ref. 13) in control diodes
EAr10	0.52	7E-14	260		*L*-3 (Ref. 17)
EAr11	0.70	3E-14	327[b]		DL5 (Ref. 7), *L*-1 (Ref. 17)

[a]At a lock-in amplifier frequency of 46 Hz, i.e., a decay time constant of 9.23 ms.
[b]At a lock-in amplifier frequency of 4.6 Hz, i.e., a decay time constant of 92 ms.

© University of Pretoria

UNIVERSITEIT VAN PRETORIA
UNIVERSITY OF PRETORIA
YUNIBESITHI YA PRETORIA

EAr9, on the other hand, resemble the signatures of the EE2 and EE3, respectively, introduced during high-energy electron irradiation of the same substrate type. The EE2 defect in turn is the same as the E2 defect which has been identified as one of the two charge states of the V_{As}–As_i defect pair.[9] These comparisons indicate that sputtering involves, among others, the formation of point defects. The sputter induced defects of which the signatures do not correspond to those of the primary irradiation induced defects may be defect complexes or extended defects.

Dubonos *et al.*[7] also compared the defects they detected after Ar sputtering to those introduced during electron irradiation and found three Ar sputter induced defects with similar properties to electron irradiation induced defects. From their Arrhenius plots it seems, within experimental error, as if these defects are the same as some of the defects reported in this study, as indicated in Table I. Similar defects have also been reported by Yuba *et al.*[17] after ion beam etching of GaAs. The authors of Refs. 7 and 17, however, only performed DLTS measurements down to about liquid nitrogen temperature and 120 K, respectively, and consequently defects such as the EAr1 could not be observed.

C. Depth distribution

Concentration profiles for the EAr9, EAr10, and EAr11 defects in substrates sputtered at 1 and 5 keV were constructed using the relations in Eqs. (2)–(5) and are depicted in Fig. 4. These curves show several significant trends. The EAr9 concentration for both sputter voltages decrease exponentially away from the interface according to Eq. (1) with $L=0.27$ μm. Note that beyond 1.5 μm, its concentration is approximately constant and equal to the distribution of the OM4 in the unsputtered control samples. In the first 1.5 μm below the interface the shape of the distribution profile of the EAr8 was similar to that of the EAr9 ($L=0.27$ μm) but its concentration is lower. The concentration profile of the EAr10 follows a different pattern. For all sputter voltages above 0.5 kV its concentration did not follow Eq. (1), but instead displayed a Gaussian-like distribution which peaks at 1.0 and 1.5 μm for sputter voltages of 1 and 5 kV, respectively. The reason for this peculiar distribution is not quite clear. The EAr11 seems to be constant throughout at least the first three microns below the junction. It should be borne in mind that the EAr11 was profiled at a lock-in amplifier frequency of 4.6 Hz which yielded a DLTS peak at 330 K. Therefore, during profiling the temperature of the sample was ramped up and down to 350 K about twenty times at a rate of 5 K/min. This elevated temperature may be the cause for the deep distribution of the EAr11. Concentration profiling of the EAr1–EAr7 defects indicated that they were located closer to the interface than the EAr9. However, due to the low carrier concentration of the GaAs used here, it was not possible to quantitatively calculate their depth distribution.

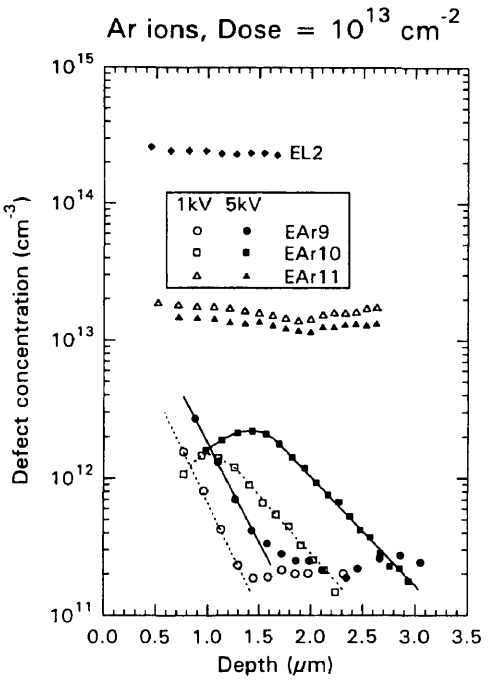

FIG. 4. DLTS concentration profiles [calculated with the aid of Eqs. (2)–(4) in the text] of the EAr9, EAr10, and EAr11 defects in GaAs sputtered with 10^{13} Ar^+/cm^2 Ar ions at 1 and 5 kV, respectively. The concentration profile of the EL2 in an unsputtered sample is also included.

D. EL2 detection

It was reported[8,18] that the EL2 defect peak disappeared in the subsurface region after Ar sputtering. An attempt was therefore made to evaluate the exact depth distribution in of the EL2 in the material sputtered at various voltages. Initial exploratory DLTS scans recorded at a reverse bias of 5 V and filling pulse amplitude of 5.2 V (yielding information regarding all the DLDs in the first 3.5 μm) showed that the EL2 could only be clearly detected in control samples and samples sputtered at 0.5 kV. In all samples sputtered at higher voltages, the EL2 peak only appeared as a slight shoulder to the high-temperature side of the EAr11. Depth profiling employing the fixed-bias varying-pulse method to estimate the postsputter distribution of the EL2 indicated that the EL2 concentration seemed to be much reduced, but constant, throughout the region profiled (first 3 μm below the interface).

This apparent reduction in the EL2 concentration in the first 3 μm below the interface, however, is most likely an artifact, as will be explained below. Ma *et al.*[19] clearly showed that the EL2 cannot be detected if the barrier height is below 0.63 eV and that it can fully be detected only if the barrier height is above 0.85 eV. For a barrier height of 0.66 eV, its concentration *seems to be* reduced by 90%. To apply this to our experiments, first consider the GaAs sample sputtered at 0.5 keV. For this sputter condition the barrier height is 0.74 eV, implying that the EL2 should be detectable if it is present, and should exhibit an

© University of Pretoria

UNIVERSITEIT VAN PRETORIA
UNIVERSITY OF PRETORIA
YUNIBESITHI YA PRETORIA

TABLE II. C–V barrier heights (at elevated temperatures) of Au SBDs on Ar ion sputtered n-GaAs.

	C–V barrier height (eV)	
Sputter voltage (kV)	330 K	350 K
Unsputtered	0.92	0.91
0.5	0.75	0.75
1.0	0.67	0.66
5.0	0.67	0.66

apparent concentration of about 30%–40% of its value in the control sample. DLTS depth profiling using Eqs. (2)–(5) yielded a constant EL2 concentration of apparently about $6–7\times10^{13}/cm^3$. If this value is corrected according to the numbers above, an EL2 concentration of about $1.5–2\times10^{14}/cm^3$ is obtained for the control sample, which is approximately equal to that reported for the control sample in Sec. III A. Next consider GaAs sputtered at higher voltages. For GaAs sputtered at 1 kV and above the barrier heights were all equal to or below 0.67 eV (Table II). From the results of Ma *et al.*, it can thus be predicted that the EL2 should either not be detectable, or at most about 5% of it should be observable. This explains the low EL2 peak in curve (c) of Fig. 1 for the EL2 in GaAs sputtered at 2 kV. If the EL2 concentration of this sample is corrected according to the arguments above, an EL2 concentration of $1–2\times10^{14}/cm^3$ for an unsputtered sample is again obtained. From the discussion above it should be clear that *the sputter voltage dependent reduction of the barrier height is a likely reason why the EL2 concentration seems to be reduced by sputtering.*

IV. CONCLUSIONS

Sputter etching GaAs with Ar ions before SBD metallization introduces DLDs as well as CLDs in the GaAs band gap. Of these DLDs only four or five have been observed before. Five of the DLDs have DLTS signatures similar to the defects formed during above threshold electron irradiation at 5 MeV or subthreshold electron irradiation at 2 keV. This indicates that some of the sputter induced defects will have a point defect nature. The other defects are probably extended defects or defect complexes.

The apparent removal of the EL2 by sputtering was shown to possibly be an artifact caused by the sputter induced barrier height lowering. As soon as the barrier height is reduced to the levels usually caused by sputtering, then the EL2 level does not empty out during the quiescent reverse bias and consequently cannot be detected. Therefore, when using SBD contacts to characterise sputtered structures, it should be borne in mind that defect levels at and near midgap may not be detectable due to a reduction in barrier height.

DLDs have different depth distributions below the surface. While some are very close to the surface (<1 μm), the concentration of others are constant within the first 4 μm. This indicates that the different defects have different diffusion mobilities and are consequently physically different. The high mobility of the EAr11 defect at $E_c-0.70$ eV causing it to move deep into the GaAs poses a threat if accurate shallow defect engineering is to be attempted. Its origin and reason for its extremely rapid diffusion should be further investigated.

ACKNOWLEDGMENT

The financial assistance of the South African Foundation for Research and Development is gratefully acknowledged.

[1] I. L. Singer, J. S. Murday, and J. Comas, J. Vac. Sci. Technol. **18**, 161 (1981).
[2] I. Konomi, A. Kawano, and Y. Kido, Surf. Sci. **207**, 427 (1989).
[3] I. L. Singer, J. S. Murday, and L. R. Cooper, Surf. Sci. **108**, 7 (1981).
[4] F. D. Auret, G. Myburg, S. A. Goodman, L. J. Bredell, and W. O. Barnard, Nucl. Instrum. Methods B **67**, 410 (1992)
[5] S. J. Fonash, S. Ashok and R. Singh, Appl. Phys. Lett. **39**, 423 (1981).
[6] F. H. Mullins and A. Brunnschweiler, Solid-State Electron. **19**, 47 (1976).
[7] S. V. Dubonos and S. V. Koveshnikov, Phys. Status Solidi A **120**, 77 (1990).
[8] A. Vaseashta and L. C. Burton, Nucl. Instrum. Methods B **59**, 1023 (1991).
[9] D. Pons and J. C. Bourgoin, J. Phys. C **18**, 3839 (1985).
[10] D. V. Lang, J. Appl. Phys. **45**, 3014 (1974).
[11] F. D. Auret and M. Nel, J. Appl. Phys. **63**, 973 (1988).
[12] Y. Zohta and M. O. Watanabe, J. Appl. Phys. **53**, 1809 (1982).
[13] G. Myburg and F. D. Auret, J. Appl. Phys. **71**, 6172 (1992)
[14] L. J. Bredell, F. D. Auret, and G. Myburg, Appl. Surf. Sci. **50**, 466 (1991).
[15] F. D. Auret and M. Nel, Meas. Sci. Technol. **2**, 623 (1991).
[16] F. D. Auret, L. J. Bredell, G. Myburg, and W. O. Barnard, Jpn. J. Appl. Phys. **30**, 83 (1991).
[17] Y. Yuba, T. Ishida, K. Gamo, and S. Namba, J. Vac. Sci. Technol. B **6**, 253 (1988).
[18] E. D. Cole, S. Sen, and L. C. Burton, J. Electron. Mater. **18**, 527 (1989).
[19] Q. Y. Ma, M. T. Schmidt, X, Wu, H. L. Evans, and E. S. Yang, J. Appl. Phys. **64**, 2469 (1988).

© University of Pretoria

UNIVERSITEIT VAN PRETORIA
UNIVERSITY OF PRETORIA
YUNIBESITHI YA PRETORIA

Electrical characterization of neutron irradiation induced defects in undoped epitaxially grown *n*-GaAs

F. D. Auret, S. A. Goodman, G. Myburg, and W. O. Barnard
Physics Department, University of Pretoria, Pretoria 0002, South Africa

D. T. L. Jones
National Accelerator Centre, P. O. Box 72, Faure 7131, South Africa

(Received 22 February 1993; accepted for publication 7 June 1993)

Undoped *n*-GaAs, grown by organometallic vapor phase epitaxy, was irradiated with neutrons from a clinical *p*(66)/Be(40) source for a range of fluences. Deep level transient spectroscopy (DLTS), employing Pd Schottky barrier diodes, indicated that four electron traps, *En*1, *En*2, *En*4, and *En*5, with energy levels at 0.04, 0.14, 0.36, and 0.66 eV, respectively, below the conduction band were created during neutron radiation. Their introduction rates varied from 1 cm^{-1} for the *En*1 to 11 cm^{-1} for the *En*5. It was found that the *En*1, *En*2, and *En*4 defects have DLTS "signatures" similar to the *E*1, *E*2, and *E*3 point defects introduced during high energy electron irradiation, indicating their point defect nature. The *En*5 has a very large capture cross section, its emission rate exhibits a strong electric field dependence, and there are indications that it has a band-like energy distribution, that results in a broad DLTS peak. We speculate that this trap is related to the presence of extended defects in the neutron irradiated GaAs.

I. INTRODUCTION

When designing electronic devices for operation in a radiation environment, it is essential to know the effect of the radiation on their characteristics. Radiation induced changes in the properties of semiconductors, for example resistivity, can have a pronounced influence on the characteristics of devices fabricated on them. This has been demonstrated for proton and neutron irradiation of metal-semiconductor field-effect transistors (MESFETs)[1] and neutron radiation of heterojunction bipolar transistors (HBTs).[2] Radiation induced defects can also cause generation—recombination currents in Schottky barrier diodes (SBDs), that lead to inferior rectification properties.[3] The degree to which the material properties and device characteristics are altered depends, among other things, on the radiation hardness of the material as well as on the concentration and electronic properties of the radiation induced defects. There are generally different particle types in radiation environments. In order to evaluate the effect of a radiation environment on the functioning of a device, it is, therefore, essential to know the introduction rates and electronic properties of the defects introduced by each particle type in electronic materials.

Radiation induced defects in semiconductors have been extensively studied during the last few decades. Most of these studies concentrated on electron irradiation, which introduces mainly simple point defects. In comparison, defects introduced by heavier particles, which are more efficient than electrons in creating extended defects, have received much less attention. This lack of information is particularly noticeable for neutron damage in GaAs, despite the fact that high speed GaAs devices are frequently used in space applications where neutron irradiation can be severe.

Although the change in carrier concentration of neutron irradiated GaAs has been documented,[4] little is known about the electrical properties of the defects introduced during irradiation. Photoluminescence has, among others, been used to investigate the annealing behavior of Ga and As antisite defects created during neutron-transmutation doping of semi-insulating GaAs.[5] Deep level transient spectroscopy (DLTS)[6] is usually used to determine the electrical properties (energy level in the band gap and capture cross section, also referred to as the DLTS "signature") of defects in semiconductors. Using this technique, Martin *et al.*[7] observed that fast neutron irradiation of GaAs mainly produces two deep electron traps in the band gap of *n*-GaAs. One of these, referred to as the U-band, was reported to have a wide energy distribution. However, because the substrates used were doped to 10^{17} cm^{-3}, it should be realized that the properties of the neutron defects thus observed were strongly perturbed due to the high electric field. Farmer *et al.*[8] reported that after neutron irradiation of GaAs the DLTS spectrum was dominated by a broad peak, and they also observed two other peaks which could not be resolved. Mamontov *et al.*[9] compared the efficiency of accumulation of defects created by neutron- and alpha-irradiation of GaAs, and also in doped material. To date, however, no accurate description of the nature and electronic properties of neutron induced defects in GaAs exists. Such information can, in part, be obtained if the low field (undistorted) electronic properties of neutron induced defects are compared to those of irradiation induced defects caused by other particles. These have been studied in great detail, for example, electrons.

In this communication we report the electrical properties, as determined by DLTS measurements, of defects created during irradiation of GaAs by neutrons from a clinical source. In order to minimize the effect of the electric field on the emission properties of the defects, GaAs with a low free carrier concentration was used.

 0021-8979/93/74(7)/4339/4/$6.00 © 1993 American Institute of Physics

© University of Pretoria

UNIVERSITEIT VAN PRETORIA
UNIVERSITY OF PRETORIA
YUNIBESITHI YA PRETORIA

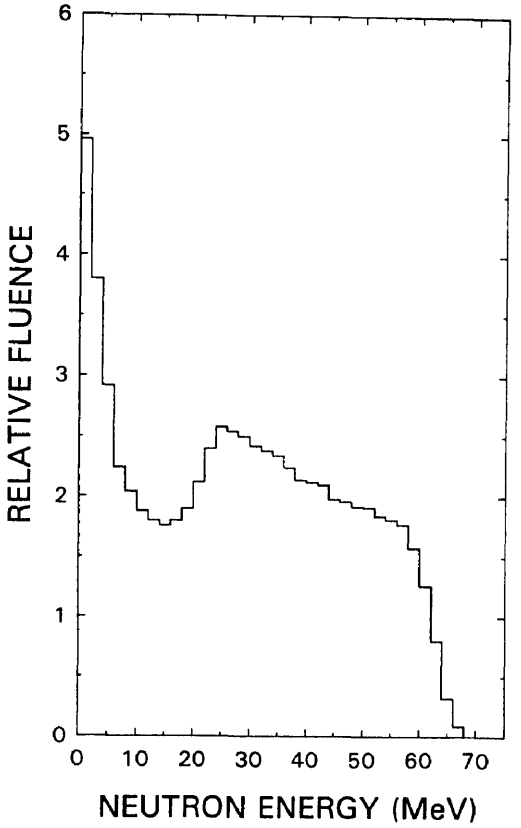

FIG. 1. Neutron fluence, in arbitrary units, of the $p(66)/\mathrm{Be}(40)$ clinical source as a function of neutron energy.

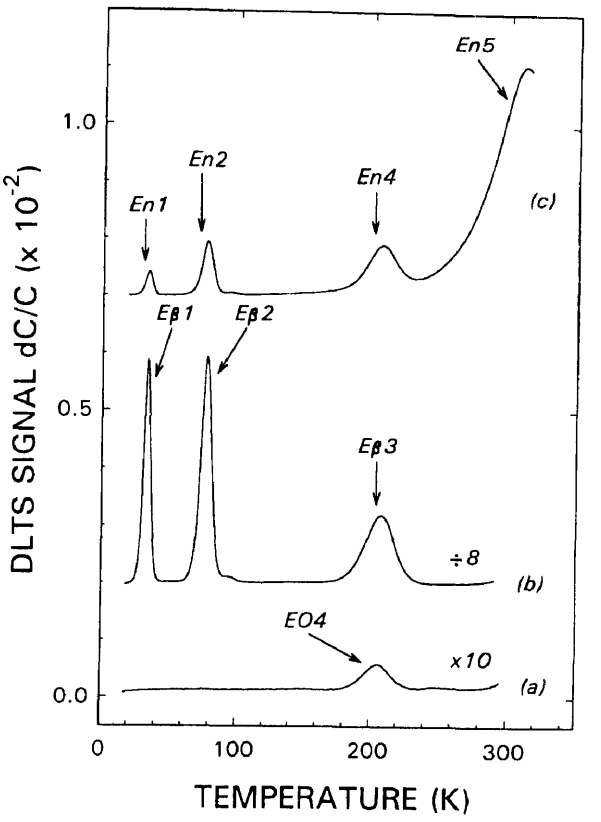

FIG. 2. DLTS spectra of OMVPE grown n-GaAs with $N_d-N_a=4\times10^{14}$ cm^{-3}. Curve (a): unirradiated; curve (b): irradiated with high energy electrons from a Sr radio-nuclide; curve (c): irradiated with neutrons at a fluence of 8.6×10^{12} cm^{-2} from a clinical $p(66)/\mathrm{Be}(40)$ source. All spectra were recorded at a lock-in frequency of 46 Hz, a quiescent reverse bias of 2 V and a filling pulse amplitude of 2.4 V.

II. EXPERIMENTAL PROCEDURE

Undoped n-type GaAs, grown by organometallic vapor phase epitaxy (OMVPE) on 10^{18} cm^{-3} Si-doped bulk grown GaAs substrates, was used for this experiment. After forming Ni/AuGe/Au ohmic contacts on the doped side of the sample, Pd SBDs that are 200 nm thick and 0.75 mm in diameter, were resistively deposited on its epitaxial side. The barrier height of the SBDs was determined by current-voltage (I-V) measurements as 0.90 ± 0.01 eV, and capacitance-voltage (C-V) measurements yielded a value of $N_d-N_a=(4.0\pm0.2)\times10^{14}$ cm^{-3} for the free carrier concentration. Control DLTS spectra were recorded from the unirradiated GaAs SBDs using a lock-in amplifier based system.[10] Thereafter, the GaAs was irradiated through the SBDs with neutrons from a $p(66)/\mathrm{Be}(40)$ clinical source[11] at a fluence rate of 3.3×10^{8} cm^{-2} s^{-1} at fluences of 8.6×10^{10}, 8.6×10^{11}, and 8.6×10^{12} cm^{-2}, hereafter referred to as fluences A, B, and C, respectively. In this source, 66 MeV protons from a cyclotron collide with a Be target, losing 40 MeV in the process, and yield neutrons the energy spectrum of which is depicted in Fig. 1. C-V measurements after irradiation showed that for fluence C the carrier reduction was about 8%. Neither of the other two fluences had any observable influence on the carrier concentration.

III. RESULTS AND DISCUSSION

A DLTS investigation of the unirradiated (control) sample indicated that it contained two electron traps commonly observed in OMVPE grown GaAs,[12] namely, the $EO4$ and $EL2$ in concentrations of $8\text{–}10\times10^{11}$ and $1\text{–}2\times10^{14}$ cm^{-3}, respectively. Because the $EL2$ (with a peak at 390 K at a lock-in amplifier frequency of 46 Hz) is present in such a high concentration and thus dominates the DLTS spectrum above 300 K, we only show spectra up to about 300 K. Curve (c) of Fig. 2 is the spectrum of GaAs irradiated with 8.6×10^{11} cm^{-2} neutrons (fluence B), and it shows that the neutron irradiation introduced the $En1$, $En2$, $En4$, and $En5$ defects. It should be borne in mind that the presence of the $EL2$ prohibits the possible detection of any other irradiation induced defects with peaks about 300 K. The DLTS signatures (energy level E_t in band gap and apparent capture cross section σ_{na}) of these defects were determined from conventional DLTS Arrhenius plots of log (e_n/T^2) vs $1000/T$ using

$$e_n=\gamma_n T^2\sigma_{na}\exp(-E_t/kT). \quad (1)$$

Here e_n is the electron emission rate from the defect site at a temperature T, k is Boltzmann's constant, and γ_n is a

© University of Pretoria

UNIVERSITEIT VAN PRETORIA
UNIVERSITY OF PRETORIA
YUNIBESITHI YA PRETORIA

TABLE I. Comparison between the characteristics of neutron and electron irradiation induced electron traps defects in OMVPE grown *n*-GaAs as detected by DLTS.

Neutron irradiation defects					Electron irradiation induced defects					
	E_t[a]	σ_{na}[b]	η[c] $\times 10^{-15}$	T_p[c]		E_t[a]	σ_{na}[b]	η[c] $\times 10^{-15}$	T_p[d]	
Label	(eV)	(cm^2)	(cm^{-1})	(K)	Label	(eV)	(cm^2)	(cm^{-1})	(K)	Ref.
*En*1	0.041	0.6	1.0	34	*E*1	0.045	2.2	1.5	33	13
					*Eβ*1	0.041	0.5	2.0	34	19
*En*2	0.141	120	2.6	77	*E*2	0.140	120	1.5	75	13
					*Eβ*2	0.139	93	2.0	77	19
*En*4	0.360	3.7	2.8	208	*E*3	0.300	6.2[e]	0.4	167	13
					*Eβ*3	0.378	16	0.7	208	19
*En*5	0.660	600	11.0	305	U-band	···	···	···	<250	7

[a]Effective activation energy, measured below the conduction band.
[b]Apparent majority carrier capture cross section, determined from the Arrhenius plot.
[c]Introduction rate, calculated from η=(defect concentration)/fluence.
[d]DLTS peak temperature, measured at a lock-in amplifier frequency of 46 Hz, that is at a decay time constant of 9.23 ms.
[e]Calculated from the E_t and σ_{na} values given in Ref. 13. The values for *E*3 were obtained in 10^{16} cm^{-3} doped GaAs and may, therefore, be affected by field assisted emission.

constant equal to 2.21×10^{20} cm^{-2} s^{-2} K^{-2} for an electron trap if, for simplicity, the degeneracy is taken as one.

The defect properties calculated from Eq. (1) are summarized in Table I. The most prominent of these defects is the *En*5 with a broad DLTS peak at about 305 K. Its energy level and apparent capture cross section are 0.66 eV and 6×10^{-13} cm^2, respectively, and its emission rate shows a strong dependence on the applied quiescent bias. The large capture cross section and electric field dependence of the *En*5 may be an indication that it is a trap that interacts with electrons while in a double positively charged state. Even for a trap with a field dependent emission rate, its low temperature "tail" extends to exceptionally low temperatures. This may be indicative that it has a band-like energy distribution in the band gap or that emission from the *En*5 does not only occur by thermal emission. The properties mentioned here are often associated with extended defects. The energy level of the *En*1, *En*2, and *En*4 defects were determined as 0.04, 0.14, and 0.36 eV below the conduction band.

To gain some insight as to the nature of the neutron irradiation induced defects, we have compared their properties to those of defects introduced during high energy electron irradiation (of which the nature is known).[13–15] Curve (b) in Fig. 2 was recorded after irradiating a section of the same GaAs wafer (one used for the neutron irradiation) with high energy electrons from a Sr radio-nuclide.[15] It is clear from the DLTS peaks in curves (b) and (c) in Fig. 2, as well as from the signatures in Table I, that the properties of the *En*1, *En*2, and *En*4 neutron induced defects are the same as those of the *Eβ*1, *Eβ*2, and *Eβ*3 defects introduced by electron irradiation from the Sr radio-nuclide,[15] which have, in turn, been shown to be identical to the *E*1, *E*2, and *E*3 defects created by electron irradiation in an accelerator.[13,14] The *E*1–*E*3 defects have well-established signatures and a point defect nature. It has been proposed that the *E*1 and *E*2 are two different charge states, (−/0) and (0/+) of the isolated arsenic vacancy V_{As} in GaAs,[16] while the *E*3 is speculated to be related to close arsenic vacancy-interstitial pairs $V_{As}-As_I$.[13] The correspondence between the DLTS signatures of the neutron and electron irradiation induced defects found here indicates that the *En*1, *En*2, and *En*4 have a point defect nature. Note that because both the electron and neutron irradiations were performed on the same wafer, the uncertainty in the defect identification that is often caused when defects in materials with different doping densities are compared, is eliminated.

The main difference between defects created by neutron and those by electron irradiation is the presence of the *En*5 in neutron irradiated GaAs. Because different mechanisms operate during the interaction of neutrons and electrons with crystal atoms, neutron irradiation can introduce large clusters of defects.[17] It has been speculated previously that the dangling bonds present in extended defects can result in a band of energies in the band gap instead of a discrete level.[18] This, together with the band-like energy distribution and large capture cross section of the *En*5, leads us to believe that it is related to extended defects. The results obtained here, therefore, indicate that in neutron irradiated GaAs extended defects or defect complexes seem to be present in much higher concentrations than point defects. The *En*5 is probably the same defect, as reported by Martin *et al.*,[7] to dominate the DLTS spectrum of neutron irradiated GaAs. However, because of the large doping density (10^{17} cm^{-3}) used in their case, a comparison of defect signatures is not meaningful.

Finally, we determined the introduction rates of *En*1–*En*5 by using fixed-bias variably pulsed DLTS depth profiling in conjunction with the approach of Zohta *et al.*[19] It was found that the concentrations of all neutron induced defects were constant in the first 2 μm below the SBD interface, i.e., the approximate distance probed by a 4 V reverse bias. The concentrations thus calculated were used to calculate the introduction rate η from:

$$\eta = (\text{defect concentration})/(\text{radiation fluence}). \quad (2)$$

© University of Pretoria

UNIVERSITEIT VAN PRETORIA
UNIVERSITY OF PRETORIA
YUNIBESITHI YA PRETORIA

The η values for defects created during fluence A were calculated after numerically subtracting the control spectra form the spectra obtained after irradiation. The average values of the introduction rates calculated for all three fluences agreed to within 10% and are tabulated in Table I. They show that the *En*5 is introduced at a rate of 11 cm^{-1}, whereas the *En*1, *En*2, and *En*4 are created at much lower rates. For comparison, the introduction rates of defects produced during irradiation with high energy electrons are also included.

IV. CONCLUSION

In summary, we have irradiated low free carrier concentration *n*-type GaAs with high energy neutrons from a clinical source and determined the properties of the radiation induced electron traps *En*1, *En*2, and *En*4, and *En*5. The dominant defect, *En*5, has an energy level at E_c–0.66 eV and a very large capture cross section. Its emission rate strongly depends on the applied electric field, and there are indications that its energy level in the band gap is not discrete. We speculate that this defect level is related to extended defects. After comparing the properties of the neutron induced defects with those of the electron irradiation induced defects, *E*1–*E*3,[13] it was concluded that the *En*1, *En*2, and *En*4 have a point defect nature.

ACKNOWLEDGMENT

The financial assistance of the Foundation for Research Development is gratefully acknowledged.

[1] A. F. Galashan and S. W. Bland, J. Appl. Phys. **67**, 173 (1990).
[2] J. J. Liou, Phys. Status Solidi **119**, 337 (1990).
[3] S. A. Goodman, F. D. Auret, M. Hayes, G. Myburg, and W. E. Meyer, South African, J. Phys. **16** (1993).
[4] J. G. Williams, J. U. Patel, A. M. Ougouag, and S.-Y. Yang, J. Appl. Phys. **70**, 4931 (1991).
[5] K. Kuriyama, K. Yokoyama, and K. Tomizawa, J. Appl. Phys. **70**, 7315 (1991).
[6] D. V. Lang, J. Appl. Phys. **45**, 3014 (1974).
[7] G. M. Martin, E. Esteve, P. Langlade, and S. Makram-Ebeid, J. Appl. Phys. **56**, 2655 (1984).
[8] J. W. Farmer and J. M. Meese, J. Nucl. Mater. **108&109**, 700 (1982).
[9] A. P. Mamontov and V. V. Peshev, Sov. Phys. Semicond. **18**, 624 (1984).
[10] F. D. Auret and M. Nel, J. Appl. Phys. **63**, 973 (1988).
[11] D. T. L. Jones, F. D. Brooks, J. E. Symons, M. R. Nchodu, M. S. Allie, T. J. Fulcher, A. Buffler, and M. J. Oliver, Med. Phys. **19**, 1588 (1992).
[12] F. D. Auret, G. Myburg, H. W. Kunert, and W. O. Barnard, J. Vac. Sci. Technol. B **10**, 591 (1992).
[13] D. Pons and J. C. Bourgoin, J. Phys. C **18**, 3839 (1985).
[14] F. D. Auret, L. J. Bredell, G. Myburg, and W. O. Barnard, Jpn. J. Appl. Phys. **30**, 80 (1991).
[15] F. D. Auret, S. A. Goodman, G. Myburg, and W. E. Meyer, Appl. Phys. A **54**, 547 (1993).
[16] B. Ziebro, J. W. Hemsky, and D. C. Look, J. Appl. Phys. **72**, 78 (1992).
[17] T. Kawakubo, Annual Report Res. Reactor Inst. Kyoto University **23**, 97 (1990).
[18] L. C. Kimerling and J. R. Patel, Appl. Phys. Lett. **34**, 73 (1979).
[19] Y. Zohta and M. O. Watanabe, J. Appl. Phys. **53**, 1809 (1982).

© University of Pretoria

UNIVERSITEIT VAN PRETORIA
UNIVERSITY OF PRETORIA
YUNIBESITHI YA PRETORIA

Nuclear Instruments and Methods in Physics Research B 90 (1994) 387–391
North-Holland

NIM B
Beam Interactions with Materials & Atoms

Electrical characteristics of neutron irradiation induced defects in n-GaAs

F.D. Auret *, A. Wilson, S.A. Goodman, G. Myburg and W.E. Meyer
Physics Department, University of Pretoria, Pretoria 0002, South Africa

Palladium Schottky barrier diodes (SBDs) on epitaxially grown n-GaAs were irradiated with neutrons from a reactor and a p(66)/Be (40) clinical source. From current–voltage (I–V) and capacitance–voltage (C–V) measurements it was found that neutron irradiation caused generation–recombination currents and resulted in a reduction in the free carrier concentrations of the epitaxial layers. A linear relation was found between the irradiation fluence, the free carrier removal and the reverse leakage current of neutron irradiated SBDs. Deep level transient spectroscopy (DLTS) indicated that five electron traps, En1–En5, were introduced during neutron irradiation. These defects are shown to be responsible for the degradation of neutron irradiated SBDs.

1. Introduction

When designing electronic devices for operation in a radiation environment, it is essential to know the effect of radiation on their characteristics. To achieve this, it is necessary to know the type, energy and quantity of particles present in the radiation environment, as well as the *introduction rates and electronic properties of the defects introduced by each particle type* in electronic materials. Radiation induced defects in semiconductors have been extensively studied during the last few decades, mostly for electron irradiation, which introduces primarily simple point defects. In comparison, defects introduced by heavier particles, which are more efficient than electrons in creating extended defects, have received much less attention. This lack of information is particularly noticeable for neutron damage in GaAs, despite the fact that high speed GaAs devices are frequently used in space applications where neutron irradiation can be severe [1].

Although the change in carrier concentration of neutron irradiated GaAs has been documented [2], little is known about the electrical properties of the defects introduced during irradiation. Deep level transient spectroscopy (DLTS) [3] is usually used to determine the electrical properties (energy level in the band gap and capture cross section, also referred to the DLTS "signature") of defects in semiconductors. Using this technique, a detailed study has recently been made of the defects produced in lightly doped n-GaAs by high energy neutron irradiation [4]. Little is known, however, regarding the effect of thermal neutrons on semiconductor materials and devices fabricated on them.

In this paper we report and compare the electrical properties of defects created in n-GaAs during irradiation with neutrons in a reactor and from a clinical p(66)/Be(40) source. Furthermore, we investigate the influence of these defects on the characteristics of Pd/n-GaAs Schottky barrier diodes (SBDs).

2. Experimental procedure

Si doped (10^{16} cm^{-3}) and undoped n-type GaAs, grown by organo-metallic vapor phase epitaxy (OMVPE) on n$^+$-GaAs substrates (doped to 10^{18} cm^{-3} with Si), were used for this experiment. After fabrication of Ni/AuGe/Au ohmic contacts on the n$^+$-backsides of the samples, Pd SBDs, 200 nm thick and 0.75 mm in diameter, were resistively deposited on their epitaxial sides. Control DLTS spectra were recorded in the 15–375 K range for the unirradiated GaAs SBDs using a two-phase lock-in amplifier based system [5]. Thereafter, some SBDs were irradiated by neutrons from a reactor and others by neutrons from a clinical p(66)/Be(40) clinical source [6]. The fluence densities in the reactor and clinical source were 4.6×10^{13} and 3.3×10^{8} n cm^{-2}s^{-1}, respectively. In the reactor irradiations were performed at fluences of 1×10^{14}–5×10^{16} n cm^{-2}, while in the clinical source the fluence range was 8.6×10^{10}–8.6×10^{12} n cm^{-2}. An important difference between the two sources is that the clinical

* Corresponding author, tel. +27 12 4202684, fax +27 12 3424143, e-mail fauret@scinet.up.ac.za.

0168-583X/94/$07.00 © 1994 – Elsevier Science B.V. All rights reserved
SSDI 0168-583X(93)E0669-8

© University of Pretoria

UNIVERSITEIT VAN PRETORIA
UNIVERSITY OF PRETORIA
YUNIBESITHI YA PRETORIA

source yields neutrons of which the energies are, within a factor of 10, equally distributed in the 1–66 MeV energy range. In contrast, about one third of the neutrons from the reactor had thermal energies, one third were epithermal and one third had energies above 1 MeV.

The effects of neutron irradiation on the characteristics of SBDs were quantified by using current–voltage (I–V) and capacitance–voltage (C–V) measurements. The DLTS "signatures" (energy level E_t in band gap and apparent capture cross section σ_{na}) of neutron irradiation induced defects were determined from conventional DLTS Arrhenius plots of $\log(e_n/T^2)$ versus $1000/T$, using

$$e_n = \gamma_n T^2 \sigma_{na} \exp(-E_t/kT). \quad (1)$$

Here e_n is the electron emission rate from the defect site at a temperature T, k is Boltzmann's constant and the γ_n is a constant equal to 2.21×10^{20} cm^{-2}s^{-2}K^{-2} for an electron trap, if for simplicity the degeneracy is taken as one.

3. Results and discussion

3.1. Control (unirradiated) samples

The barrier properties of the Pd SBDs and free carrier concentrations of the epilayers on which they were fabricated were determined by room temperature (295 K) I–V and C–V measurements. Unirradiated SBDs had barrier heights and ideality factors of 0.90 ± 0.01 eV and 1.02, respectively, with free carrier concentrations, $N_d - N_a$, of $(4.0 \pm 0.05) \times 10^{14}$ and $(1.3 \pm 0.2) \times 10^{16}$ cm^{-3} for the undoped and doped GaAs, respectively. DLTS spectra recorded using unirradiated SBDs (curves (a) in Figs. 2 and 3) showed that the EL2 [7], which is present in all OMVPE grown GaAs, is the dominant deep level defect in unirradiated GaAs. The EL2 concentrations as determined from DLTS profiling indicated that it is approximately $1–2 \times 10^{14}$ cm^{-3} in the undoped and doped GaAs used for this study. From Figs. 2 and 3 it is clear that the EL2 peak prohibits the detection of any defects in low concentrations above about 320 K and consequently we conclude that the OMVPE GaAs used here is suitable for studying radiation induced defects with concentrations of as low as 10^{12} cm^{-3}, but only at temperatures below 320 K.

3.2. I–V and C–V measurements on irradiated samples

Room temperature I–V and C–V measurements showed that the characteristics of SBDs irradiated in the clinical source remained unchanged, whereas the characteristics of SBDs irradiated in the reactor underwent major changes. We ascribe this, firstly, to the fact that the fluences in the clinical source were much lower than those in the reactor and, secondly, to the large concentration of thermal neutrons in the reactor which can create large clusters of defects [8].

I–V measurements indicated that neutron irradiation in the reactor induced additional forward and reverse currents, commonly referred to as recombination and generation currents, respectively. It is shown in Fig. 1 (curve (a)) that the log of the increase in reverse current (at 1 V reverse bias) increases linearly with the log of the neutron fluence, indicating that the number of recombination centers increases with increasing neutron fluence. Curve (b) in Fig. 1 shows that the carrier removal increases in a similar fashion with neutron fluence, indicating that the number of trapping sites is directly proportional to the number of incident neutrons. While an increase in reverse leakage current results in poorer signal-to-noise ratios of detectors, a reduction in the free carrier concentration is one of the causes of failure in irradiated MESFETs [9].

3.3. DLTS analysis of neutron irradiation induced defects in n-GaAs

The DLTS spectra in Figs. 2 and 3 show the effect of neutron irradiation on undoped and doped n-GaAs, respectively. Curve (b) in Fig. 2 was recorded after irradiating SBDs on undoped GaAs with neutrons from

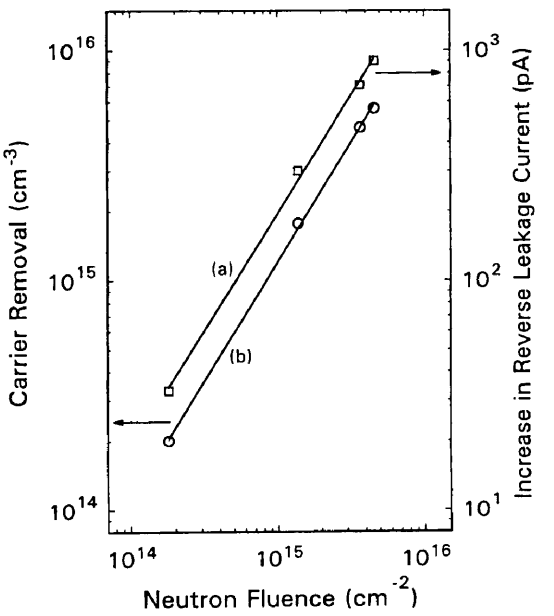

Fig. 1. Increase in reverse leakage current at a reverse bias of 1 V (curve (a)), and free carrier removal (curve (b)) for Pd SBDs on 1.3×10^{16} cm^{-3} doped n-GaAs as a function of neutron fluence for devices irradiated in a reactor.

© University of Pretoria

UNIVERSITEIT VAN PRETORIA
UNIVERSITY OF PRETORIA
YUNIBESITHI YA PRETORIA

the p(66)/Be(40) source at a fluence of 8.6×10^{12} cm^{-2} and shows that the defects En1, En2, En4 and En5 were introduced by neutron irradiation. The most pronounced peak in both these spectra is the peak labeled En5 which is skewed towards the low temperature side. Curve (c) in Fig. 2 shows that irradiation in the reactor also introduced the En4 and En5 defects, but the En2 is present in a much lower relative concentrations. This result is due to the much higher neutron dose in the reactor (1.2×10^{14} cm^{-2}) which introduced large numbers of traps which can be filled more effectively than traps such as the En1 and En2 with energy levels close to the conduction band.

In Fig. 3 we compare the DLTS spectra of 10^{16} cm^{-3} doped GaAs which were irradiated in the two neutron sources. The main features of the DLTS spectra are again the En1–En5 peaks. The En1 and En2 are now observed in GaAs irradiated in both sources but it should be noted that all the defect peaks, especially the En5 peaks, are broader in doped than in undoped GaAs due to field assisted emission [10]. Moreover, the En5 peak is much broader in reactor irradiated GaAs than in GaAs irradiated in the clinical source. A defect in neutron irradiated GaAs with a similar broad DLTS peak, named the "U-band" has also previously been documented [11].

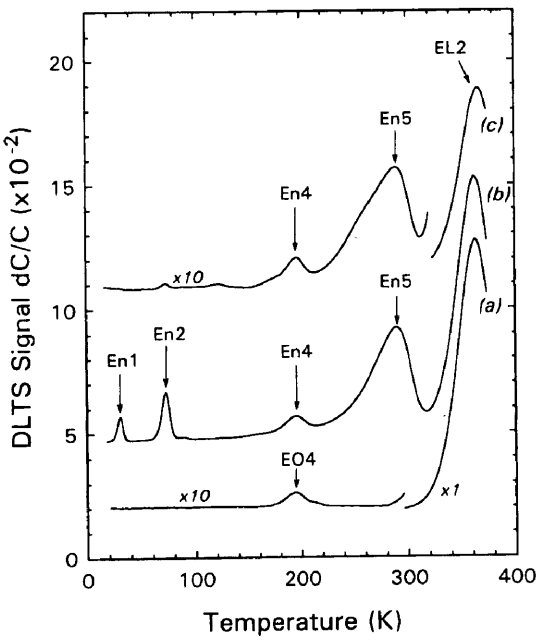

Fig. 2. DLTS spectra of undoped OMVPE grown n-GaAs with $N_d - N_a = 4.0\times10^{14}$ cm^{-3}. curve (a): unirradiated; curve (b): irradiated with high energy neutrons from a p(66)/Be(40) source at a fluence of 8.6×10^{12} cm^{-2}; curve (c): irradiated with neutrons at a fluence of 1.2×10^{14} cm^{-2} in a reactor. All spectra were recorded at a lock-in frequency of 10 Hz, a quiescent reverse bias of 3 V and a filling pulse amplitude and width of 3.4 V and 0.2 ms, respectively.

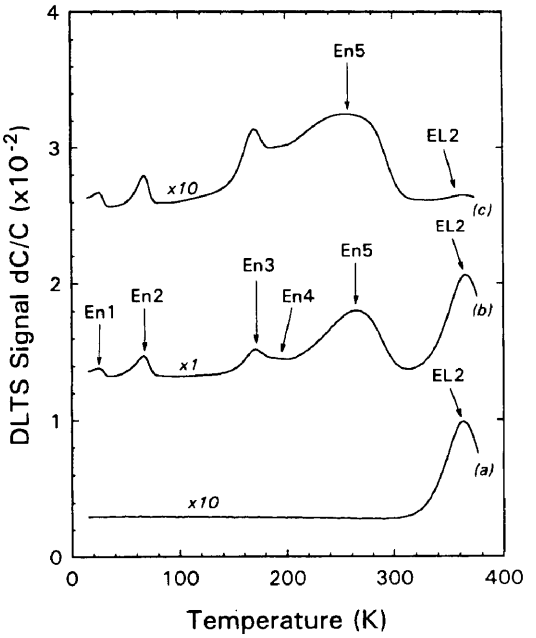

Fig. 3. DLTS spectra of OMVPE grown n-GaAs doped with Si to level of $N_d - N_a = 1.3\times10^{16}$ cm^{-3}. curve (a): unirradiated; curve (b): irradiated with high energy neutrons from a p(66)/Be(40) source at a fluence of 8.6×10^{12} cm^{-2}; curve (c): irradiated with neutrons from a reactor at a fluence of 1.4×10^{15} cm^{-2}. All spectra were recorded at a lock-in frequency of 10 Hz, a quiescent reverse bias of 1 V and a filling pulse amplitude and width of 1.6 V and 0.2 ms, respectively.

The defect properties calculated from conventional DLTS Arrhenius plots using Eq. (1) are summarized in Table 1, where they are compared to the properties of high energy electron irradiation induced defects in GaAs. In order to minimize the effect of field assisted emission, the "signatures" tabulated were determined in material with a carrier density of 4×10^{14} cm^{-3}. From Table 1 it can be seen that the properties (DLTS "signatures") of the neutron irradiation induced defects En1, En2 and En4 are very similar to those of the electron irradiation induced defects [11–13] E1, E2 and E3, respectively. The E1–E3 defects have well established "signatures" and a point defect nature. It has been proposed that E1 and E2 are two different charge states, $(-/0)$ and $(0/+)$ of the isolated arsenic vacancy, V_{As}, in GaAs, while the E3 is speculated to be related to close arsenic vacancy–interstitial pairs, V_{As}–As_I [13,14]. The correspondence between the DLTS "signatures" of the neutron and electron irradiation induced defects therefore strongly suggests that the defects En1, En2 and En4 also have a point defect nature.

The energy level and apparent capture cross section of the En5 in the undoped GaAs irradiated in the clinical source are 0.73 eV and 6×10^{-12} cm^{-2}, re-

© University of Pretoria

UNIVERSITEIT VAN PRETORIA
UNIVERSITY OF PRETORIA
YUNIBESITHI YA PRETORIA

spectively. These values were found to be strongly dependent on the electric field. This is illustrated by the broadness of the defect peak in doped GaAs. The large capture cross section and electric field dependence of the En5 emission rate may be an indication that it interacts with electrons while being in a multiple positively charged state. Furthermore, the low temperature "tail" of the En5 extends to exceptionally low temperatures, even when its strong field dependent emission is taken into account. This most likely indicates that it has a band-like energy distribution in the band gap. The properties mentioned here are often associated with extended defects. Because different mechanisms operate during the interaction of neutrons and electrons with crystal atoms, neutron irradiation can introduce large clusters of defects [15]. It has been speculated before that the dangling bonds present in extended defects can result in a band of energies in the band gap instead of a discrete level [16]. This, together with its band-like energy distribution and large capture cross section, lead us to believe that the En5 is not a simple point defect, but that it may be an extended defect.

The differences in the DLTS spectra of GaAs irradiated in the reactor and in the clinical source may be explained by noting the difference in the energy distribution of the neutrons from the two sources. The clinical source yields primarily fast neutrons of which the energies extend up to 66 MeV [6], while in the reactor, on the other hand, 33% of the neutrons are thermal. The reaction capture cross section of neutrons in these energy regimes are quite different, and consequently it is to be expected that the nature of the defects formed will be different. Because it has been shown that low energy neutrons create large clusters of vacancies, we speculate that the difference in shape of the En5 for the two cases stems from the physical size of the defect volumes created by these two types of neutrons.

The introduction rates, η, of defects created in n-GaAs by irradiation in the clinical source are included in Table 1, where they are compared, for the sake of interest, with those of electrons introduced during high energy electron irradiation. As pointed out above, the reactor irradiated undoped GaAs contains too high concentrations of defects to allow for complete defect filling and therefore no quantitative calculation of η is possible in this case. Although the defect concentrations of doped GaAs which was neutron irradiated are much lower than the free carrier concentration, an accurate analysis is also not possible due to the DLTS peak saturation caused by the electric field enhanced emission.

4. Conclusions

Neutron irradiation in a reactor and a clinical source created five electron traps, En1–En5, in n-GaAs. The En3 defect is present after both types of irradiations in doped GaAs but not in undoped GaAs. This leads us to believe that the En3 is a complex of which the nature depends on the type and concentration of the dopant in GaAs (Si in the case of the doped GaAs used here). The "signatures" of the En1, En2 and En4 are similar to those of the high energy electron irradia-

Table 1
Characteristics of neutron and electron irradiation induced electron traps defects in OMVPE and MBE grown n-GaAs as detected by DLTS

Neutron irradiation defects					Electron irradiation defects					
Label	E_t [a]	σ_{na} [b] $\times 10^{-15}$	η [c]	T_p [d]	Label	E_t [a]	σ_{na} [b] $\times 10^{-15}$	η [c]	T_p [d]	Ref.
	[eV]	[cm^2]	[cm^{-1}]	[K]		[eV]	[cm^2]	[cm^{-1}]	[K]	
En1	0.041	0.6	1.0	34	E1	0.045	2.2	1.5	33	[12]
					Eβ1	0.041	0.5	2.0	34	[13]
En2	0.141	120	1.5	77	E2	0.140	120	1.5	75	[12]
					Eβ2	0.139	93	2.0	77	[13]
En3	0.34	25	1.0	184	L6	–	–	–	–	[17]
En4	0.36	3.7	1.0	208	E3	0.30	6.2 [e]	0.4	167	[12]
					Eβ3	0.38	16	0.7	208	[13]
En5	0.73	6000	10.0	305	U-band	–	–	–	< 250	[11]

[a] Effective activation energy, measured below the conduction band.
[b] Apparent majority carrier capture cross-section, determined from Arrhenius plot.
[c] Introduction rate of neutron irradiation defects created in undoped GaAs [4] using the clinical source [6], calculated from η = (defect concentration)/(radiation fluence).
[d] DLTS peak temperature, measured at a lock-in amplifier frequency of 46 Hz, that is at a decay time constant of 9.23 ms.
[e] Calculated from the E_t and σ_{na} values given in ref. [12]. The values for E3 were obtained in 10^{16} cm^{-3} doped GaAs and may therefore be affected by field assisted emission.

© University of Pretoria

UNIVERSITEIT VAN PRETORIA
UNIVERSITY OF PRETORIA
YUNIBESITHI YA PRETORIA

tion induced defects E1–E3, respectively, indicating that they are point defects. The En5 defect exhibited an extraordinary large capture cross section and its emission rate was strongly dependent on the applied electric field. Its exceptionally broad DLTS peak may not be the effect of the electric field enhanced emission alone, but could also signify that its energy position in the band gap has a band-like, instead of a discrete, nature. These properties indicate that the En5 is not a simple point defect, but that it may be associated with a defect cluster.

Defects introduced during neutron irradiation altered the properties of the epitaxial layers as well as of the SBD fabricated on them. The number of free carriers removed from the epitaxial layer as well as the increase in reverse leakage current of the SBD were found to be directly proportional to the neutron fluence. These effects are indicative of the trapping and generation–recombination nature of the neutron irradiation induced defects.

In summary, we have analyzed, by DLTS, the defects introduced in n-GaAs by neutron irradiation from a clinical source and from a reactor, and have determined, using I–V and C–V measurements, the effects of these defects on GaAs as well as on SBDs fabricated on it. The dominant defect, En5, has an emission rate which strongly depends on the applied electric field and has a very large capture cross section, leading us to believe that this defect level is not a simple point defect.

Acknowledgements

The financial assistance of the South African Foundation for Research Development (FRD) is gratefully acknowledged. We also thank Dr. Dan Jones of the National Accelerator Centre and Dr. Faanhof from the Atomic Energy Corporation for the neutron irradiations.

References

[1] M. Yamaguchi, A. Yamamoto and A. Sibukawa, Jpn J. Appl. Phys. 22 (1983) 1727.
[2] J.G. Williams, J.U. Patel, A.M. Ougouag and S.-Y. Yang, J. Appl. Phys. 70 (1991) 4931.
[3] D.V. Lang, J. Appl. Phys. 45 (1974) 3014.
[4] F.D. Auret, S.A. Goodman, G. Myburg and W.E. Meyer, J. Appl. Phys. 74 (1993) 4339.
[5] F.D. Auret and M. Nel, J. Appl. Phys. 63 (1988) 973.
[6] D.T.L. Jones, F.D. Brooks, J.E. Symons, M.R. Nchodu, M.S. Allie, T.J. Fulcher and M.J. Oliver, Med. Phys. 19 (1992) 1588.
[7] W.L. Wang, S.S. Li and D.H. Lee, J. Electrochem. Soc. 133 (1986) 196.
[8] J.W. Farmer and J.M. Meese, J. Nucl. Mater. 108/109 (1982) 700.
[9] A.F. Galashan and S.W. Bland, J. Appl. Phys. 67 (1990) 173.
[10] J. Frenkel, Phys. Rev. 54 (1938) 657.
[11] G.M. Martin, E. Esteve, P. Langlade and S. Makram-Ebeid, J. Appl. Phys. 56 (1984) 2655.
[12] D. Pons and J.C. Bourgoin, J. Phys. C 18 (1985) 3839.
[13] F.D. Auret, S.A. Goodman, G. Myburg and W.E. Meyer, Appl. Phys. A 56 (1993) 547.
[14] B. Ziebro, J.W. Hemsky and D.C. Look, J. Appl. Phys. 72 (1992) 78.
[15] T. Kawakubo, Ann. Rep. Res. Reactor Inst., Kyoto University, 23 (1990) 97.
[16] L.C. Kimerling and J.R. Patel, Appl. Phys. Lett. 34 (1979) 73.
[17] Y. Yuba, K. Gamo, K. Murakami and S. Namba, Inst. Phys. Conf. Ser. Vol. 59 (1980) Chap. 6, p 329.

© University of Pretoria

UNIVERSITEIT VAN PRETORIA
UNIVERSITY OF PRETORIA
YUNIBESITHI YA PRETORIA

Nuclear Instruments and Methods in Physics Research B67 (1992) 410–414
North-Holland

Nuclear Instruments & Methods in Physics Research
Section B

Effect of sputter voltage on the electrical characteristics of argon ion sputtered n-type GaAs

F.D. Auret, G. Myburg, S.A. Goodman, L.J. Bredell and W.O. Barnard
Physics Department, University of Pretoria, Pretoria 0001, South Africa

Epitaxially grown n-type GaAs was sputtered by bombarding it with Ar ions at voltages between 0.5 and 5 kV at a dose of 10^{13} ions/cm^2. The electrical characteristics of the sputtered GaAs were investigated by studying the sputter induced defects using deep level transient spectroscopy (DLTS). The effect of these defects on the electrical characteristics of gold (Au) Schottky barrier diodes (SBDs) was studied by current–voltage (I–V) and capacitance–voltage (C–V) measurements. It was found that the barrier height of the SBDs changed nonmonotonically with sputter voltage, and this could be correlated with the combined effect of sputter induced defects with discrete and continuous energy levels in the GaAs band gap.

1. Introduction

The processing of semiconductor surfaces with energetic particles is a widely used process in semiconductor technology, because, amongst others, it offers the capability of performing several processing steps in vacuum without exposing the semiconductor surface to the atmosphere. The nature, energy and dose of the particles are selected in accordance with the task that has to be accomplished. For example, a dose of about 10^{17} Ar/cm^2 (at 0.5 keV) may be required to remove a 500 Å thick layer of GaAs [1].

However, the use of energetic particles may also result in unwanted changes in the surface and subsurface substrate properties, e.g. structural disorder [2] or nonstoichiometry in the case of compound semiconductors [2,3]. Several studies have shown that surface and subsurface disorder in semiconductors can cause significant changes in the electrical properties of Schottky barrier diodes (SBDs) fabricated on these surfaces [4,5]. For example, after exposing the surface of GaAs to 0.5 kV Ar particles at a dose of 10^{15} Ar/cm^2, the barrier height of Au SBDs on these surfaces decreased from 0.97 to 0.48 eV [4]. From studies where the effects of energetic particle processing of semiconductors were investigated, it was found that numerous defects with energy levels in the semiconductor band gap were introduced by the energetic particles at and below the semiconductor surface [4–6]. Some of these defects had the same electrical properties (activation energy and capture cross section) as those formed during electron [7] and proton [8] bombardment of GaAs. Furthermore, it has been found that when sputtering at a fixed voltage, an increase in the dose of the bombarding particles leads to an increased amount of surface disorder, which in turn leads to an increase in the degree of change of the SBD properties [4,5].

The aim of this study was to systematically investigate the dependence of SBD properties on the pre-metallization Ar sputter voltage in the 0.5–5 kV range. This was realized by employing deep level transient spectroscopy (DLTS) [9] to characterise the sputter induced defects which strongly influence the barrier properties. Particular attention was given to the detection of defects close to the interface which have nondiscrete energy distributions.

2. Experimental procedure

Undoped (100) oriented n-type GaAs epilayers with a free carrier concentration of 4×10^{14}/cm^3, grown by metal-organic vapor phase epitaxy (MOVPE) on n$^+$ substrates (10^{18}/cm^3 doped with Si, LEC grown), were used to investigate Ar ion sputter induced defects. After wet chemical etching, Au/AuGe/Ni ohmic contacts were fabricated on the n$^+$ backsides of the wafers as outlined previously [4]. Before sputter etching and subsequent SBD metallization, the samples were once again etched utilizing the same chemical cleaning procedure as for the ohmic contact fabrication. In chronological order this comprized degreasing in TCE, rising in isopropanol, rising in water, etching in NH_3: H_2O_2: H_2O (3 : 1 : 120, 1 min), rising in H_2O, rinsing in HCl (2 min), followed by a final rinse in H_2O. Immediately thereafter the samples were inserted into a vacuum system which was evacuated to a pressure of 10^{-8} mbar, whereafter Ar was let into the system to a pressure of 3×10^{-5} mbar. The samples were sput-

0168-583X/92/$05.00 © 1992 – Elsevier Science Publishers B.V. All rights reserved

© University of Pretoria

UNIVERSITEIT VAN PRETORIA
UNIVERSITY OF PRETORIA
YUNIBESITHI YA PRETORIA

tered by accelerating Ar ions perpendicularly onto their surfaces by a PHI 04-191 ion gun at voltages of 0.5, 1, 2, 3 and 5 kV at a dose of $10^{13}/cm^2$. Immediately after sputter etching, without breaking vacuum, Au contacts, 0.73 mm in diameter and 1000 Å thick, were deposited by resistive evaporation on the sputtered surfaces through a metal contact mask. For control purposes, diodes were fabricated identically to these described above, except that the GaAs was not Ar sputtered prior to SBD metallization.

The sputter induced defects in GaAs were characterized by performing deep level transient spectroscopy (DLTS) [9] using a two-phase lock-in amplifier based system [10] between the temperatures 12 and 400 K. The influence of these defects on the diode properties was evaluated using standard current–voltage (I–V) and capacitance–voltage (C–V) measurements.

3. Results and discussion

Assuming that the dominant current transport mechanism in unsputtered SBDs is thermionic emission, it was found that the control diodes (Curves F1 and R1 in fig. 1) have ideality factors, n, between 1.01 and 1.03 and a mean barrier height, ϕ_b, of 0.93 eV, which are in good agreement with those reported elsewhere for Au on atomically clean n-GaAs [11]. The effect of pre-metallization Ar bombardment on the I–V characteristics is shown in fig. 1 for the two

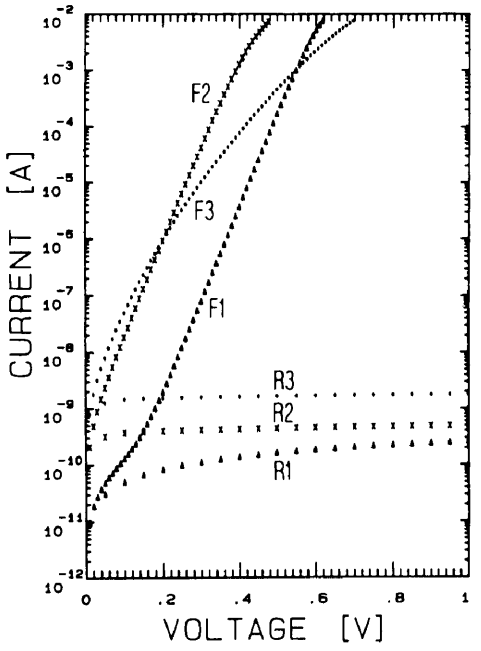

Fig. 1. Forward (F) and reverse (R) I–V characteristics of unsputtered (F1, R1) Au SBDs on n-GaAs, as well as of SBDs on GaAs sputtered at 0.5 kV (F2, R2) and 5 kV (F3, R3).

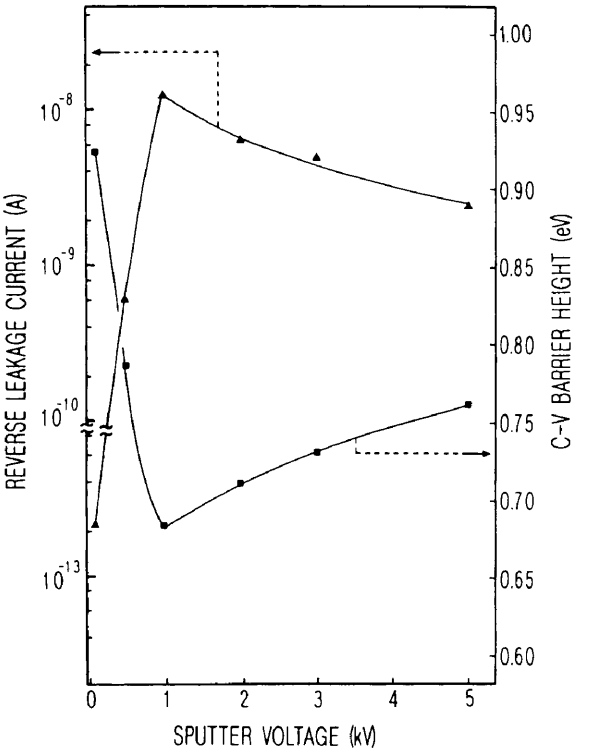

Fig. 2. Variation of I_{1V}, the reverse leakage current at 1 V (▲), as well as the C–V measured barrier height, ϕ^{cv} (■), with sputter voltage.

extreme sputter voltages of 0.5 kV (curves F2 and R2) and 5 kV (curves F3 and R3), respectively. It is clear (curve F2) that the diodes sputtered at 0.5 kV exhibited linear $\log(I)$–V characteristics in the forward direction, but a reduced barrier height. However, it was found that at sputter voltages of 1 kV and above, the diodes do not exhibit linear $\log(I)$–V characteristics and the degree of nonlinearity increases as the sputter voltage increases (curve F3 for 5 kV). It is therefore neither possible nor meaningful to compare the diode qualities via conventional parameters extractable from I–V measurements, such as the ideality factor or barrier height as defined in the thermionic emission theory. Instead, we used the leakage current, I_{1V}, at a reverse bias of 1 V as a measure of comparison. Fig. 2 illustrates the effect of the sputter voltage on I_{1V} and it shows that as the sputter voltage increases from 0 to 1 kV, I_{1V} increases from 10^{-13} to above 10^{-8} A. However, for sputter voltages larger than 1 kV, I_{1V} decreases with increasing sputter voltage to 2×10^{-9} A at 5 kV, the highest voltage investigated. On the same figure the results for the C–V measured flatband barrier height, ϕ^{cv}, are also plotted as a function of sputter voltage. If it assumed that I_{1V} is a measure of the effective barrier height (irrespective of which model is used to describe it), when the results of the I–V and

© University of Pretoria

UNIVERSITEIT VAN PRETORIA
UNIVERSITY OF PRETORIA
YUNIBESITHI YA PRETORIA

C–V measured barrier heights in fig. 2 qualitatively follow the same trend with increasing sputter voltage. The interpretation of this curve is not straightforward. One might be tempted to argue intuitively that the use of higher sputter voltages should lead to more lattice defects and that a monotonic increase of leakage current with increasing sputter voltage should therefore be expected. From fig. 2 this is obviously not the case.

In order to establish the possible origin of the barrier heights vs sputter voltage relationship, the SBDs were analyzed by energy resolved (ER-)DLTS using the following methodology: First, DLTS scans were recorded at a constant quiescent bias V_r, and filling pulse biases, V_f, that were incrementally increased by δV from one scan to the next. In order to eliminate the possible effects of slight peak shifts when scanning in different temperature directions, the *average spectra* of two DLTS recorded scans in opposite temperature directions but using the same bias conditions, were aquired. Next, the *averaged spectra* which were recorded at pulse bias differences of δV, were subtracted from each other, yielding *ER-DLTS spectra*, which provide information about defects in two regions, as indicated in fig. 3. The first region is the semiconductor adjacent to the interface where continuous level defects (CLDs), i.e. defects with continuously distributed energy levels in the energy interval $\delta E = q\,\delta V$ at

$$E = \phi_b - qV_f \tag{1}$$

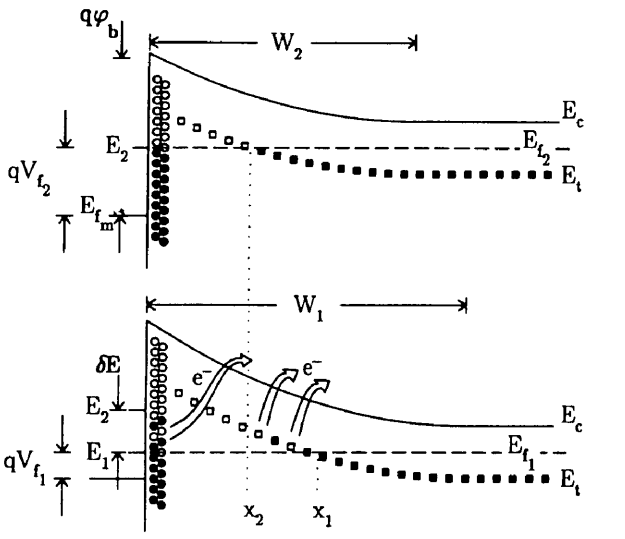

● Filled continuous levels ■ Filled discrete levels
○ Empty continuous levels □ Empty discrete levels

Fig. 3. Energy band diagram of SBD structure on n-GaAs containing defects with discrete level defects (DLDs) as well as continuous level defects (CLDs). The bands are drawn for two forward biases V_{f1} and $V_{f2} = V_{f1} + \delta V$.

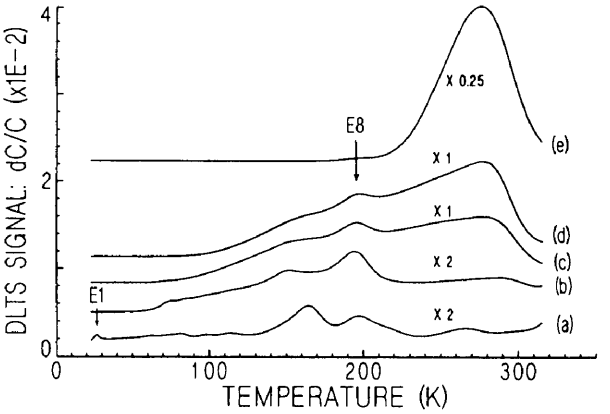

Fig. 4. Conventional DLTS spectra of SBDs sputtered with a dose of 10^{13} Ar/cm^2 before metallization. Curves (a)–(e) are for sputter voltages of 0.5, 1, 2, 3 and 5 kV, respectively. All curves were recorded at a lock-in amplifier frequency of 10 Hz, a quiescent reverse bias of $V_r = 0.5$ V and a filling pulse amplitude of $V_f = 1.5$ V.

below the conduction band, can be investigated. The underlying assumption for analyzing defects in this region is that the semiconductor Fermi level is free to move at the interface and that its position during the forward bias pulse therefore changes by the same amount as the bias across the SBD. Secondly, a region of width $\delta x = x_1 - x_2$ located at

$$x_f = [2\epsilon(V_{bi} - V_f)/qN_d]^{1/2} - [2\epsilon(E_t - E_f)/qN_d]^{1/2} \tag{2}$$

is probed. Here V_{bi} is the built-in voltage of the SBD, V_f is the voltage across the diode during the filling pulse and the other symbols have their conventional meanings. This region contains information primarily regarding the discrete level defects (DLDs), i.e. defects with discrete energy levels in the band gap, located at a depth x_f below the SBD interface. The two regions probed by investigating the DLTS difference spectra are indicated in fig. 3 for an n-type semiconductor.

Conventional and ER-DLTS spectra for Ar sputtered SBDs are presented in fig. 4 (for 0.5–5 kV) and fig. 5 (for 3 kV), respectively. Two types of features can be distinguished on the conventional spectra (fig. 4). First there are peaks of which the temperature positions do not change upon changing V_f, e.g. E1 and E8 [4]. These peaks are characteristic of DLDs. Second, the discrete spectra seem to be superimposed on skewed or partly elevated baselines of which the degree and onset of baseline skewing were found to increase with increasing sputter voltage as well as V_f. This nonuniform baseline offset is caused by the emission of carriers from CLDs in the entire region of the band gap swept by the Fermi level during the DLTS pulsing sequence.

© University of Pretoria

UNIVERSITEIT VAN PRETORIA
UNIVERSITY OF PRETORIA
YUNIBESITHI YA PRETORIA

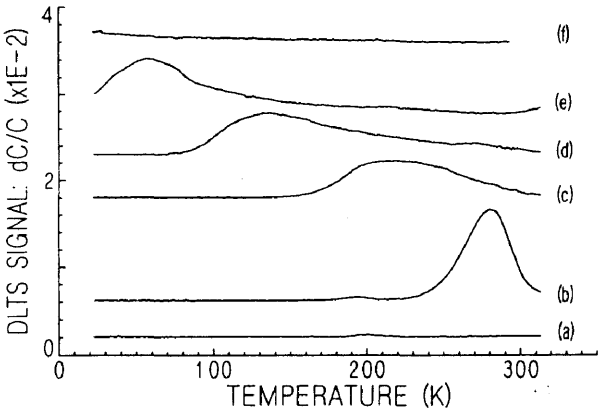

Fig. 5. Energy resolved DLTS spectra for 3 kV sputtered SBDs obtained for a quiescent reverse bias of $V_r = 0.5$ V and a lock-in amplifier frequency of 10 Hz. The forward biases during the filling pulse for curves (a)–(f) were $V_f = -0.1$, 0.1, 0.3, 0.5, 0.7 and 0.9 V, respectively, and for all curves the incremental voltage was $\delta V = 0.01$ V.

The presence of CLDs is evidenced by the ER-DLTS curves (a)–(f) in fig. 5 which were obtained for $\delta V = 0.01$ V. The main features in curves (b)–(e) are the broad peaks moving to lower temperatures as V_f is increased. To understand this phenomenon, it should be remembered that if two DLTS peaks with the same capture cross sections are observed at different temperatures, then it implies that the defects giving rise to the lower temperature peak are located closer to the conduction band. With this in mind the results depicted in fig. 5 imply that as V_f is increased, those defects located closer to the conduction band are observed. For example, by using eq. (1) in conjunction with the pulse conditions outlined in the caption of fig. 5 and an approximate barrier height of 0.74 eV as determined by C–V measurements for the 3 kV case, it is found that the peaks on curves (b)–(e) are mainly caused by emission from defects (assumed close to the interface) at approximately $E_c - 0.64$, $E_c - 0.44$, $E_c - 0.24$ and $E_c - 0.04$ eV. Since the shift of this ER-DLTS peak continued from about 300 K for $V_f = 0.1$ V (curve (b)) to apparently below 15 K for the highest V_f value namely 0.9 V (curve (f)), we conclude that the energy distribution of the defects giving rise to these ER-DLTS peaks are indeed continuous in the energy interval of approximately ($E_c < E < 0.7$ eV) which was analysed. The reason why no CLDs with energies $E > E_c - 0.7$ eV were detected, is because the barrier height is about 0.74 eV and therefore defects close to the interface located below 0.74 eV in the band gap will be in equilibrium with the Fermi level of the metal rather than with the conduction band of the semiconductor.

Next we consider the dependence of the conventional and ER-DLTS peak heights, which serve as a measure of the concentration of DLDs and CLDs, respectively, on the sputter voltage. From fig. 6 it is clear that the concentration of the E8 increases with increasing sputter voltage up to 1 kV. For larger sputter voltages its concentration decreases and it becomes almost undetectable after sputtering at 5 kV. In contrast, the concentration of the CLDs was found to increase monotonically with an increase in sputter voltage.

After having qualitatively established the effect of the sputter voltage on the formation of defects in the GaAs, we propose the following model to explain the reverse leakage current vs sputter voltage behaviour depicted in fig. 2. At low sputter voltages the main effect of sputtering is the introduction of donor-like discrete level defects at and close to the interface (curve (a) in fig. 4). For 3 kV Ar sputtering it has been found that the damaged region extends to at least 1000 Å below the interface [13], but it may extend much deeper [6]. These defects cause a considerable lowering of the effective barrier height due to tunneling and recombination via their energy levels in the band gap [12,14], which gives rise to the observed lowering of the barrier height in the 0–1 kV sputter voltage region (fig. 2). At increased sputter voltages (> 1 kV), more structural damage occurs causing the formation of a layer with a high degree of crystal disorder [13]. This in turn leads to the formation of defects with continuously distributed enegy levels and a reduction in the concentration of DLDs. Associated with defects which have a

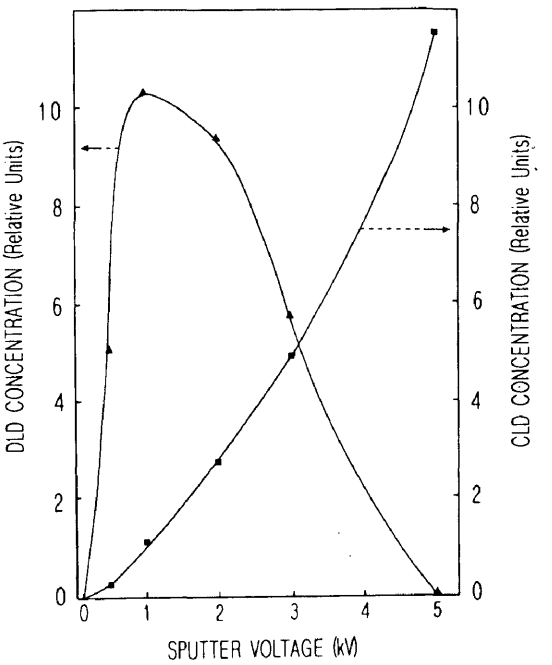

Fig. 6. Concentration of discrete level defects (DLDs) (▲) and contiuous level defects (CLDs) (■), in relative units, as a function of sputter voltage.

© University of Pretoria

UNIVERSITEIT VAN PRETORIA
UNIVERSITY OF PRETORIA
YUNIBESITHI YA PRETORIA

continuous energy distribution in the band gap is a neutral level, ϕ_0, which is normally positioned around midgap for a uniform defect distribution. It determines the Fermi level position in the semiconductor at the interface and thus the barrier height. At sputter voltages above 1 kV there seem to be two competing mechanisms for controlling the effective barrier for current transport, namely tunneling via near-surface levels and Fermi level pinning. In this sputter voltage domain it seems that there is a reduction in effect of the tunneling assisted barrier lowering and an increase in barrier height, as depicted in fig. 2. It should further be noted that a dose of 10^{14} Ar/cm^2 is considered sufficient to cause the onset of amorphization of GaAs. The dose of 10^{13} Ar/cm^2 used in this study may therefore be high enough to cause the GaAs to display some of the properties characteristic of amorphized GaAs, e.g. a widening of the band gap and the consequent increase in barrier height.

After sputtering at 5 kV, the concentration of the CLDs is so high that the Fermi level becomes strongly pinned. This is evidenced by the fact that the ER-DLTS peak of the 5 kV sputtered SBDs shows almost no shift towards lower temperatures, even for pulse voltages as high as $V_f = 1$ V. The energy of the defects resulting in the peak on the 5 kV spectrum (curve (e) in fig. 4) is $E_c - 0.74$ eV as determined from the standard Arrhenius analysis. Its capture cross section determined from the same measurements was about 10^{-11} cm^2, which seems unacceptably large. It is instructive to note that the C–V calculated barrier height for the 5 kV sputtered SBDs is about 0.76 eV, which is in good agreement with the estimated Fermi pinning position determined from the DLTS measurements.

4. Conclusions

Sputter etching GaAs with Ar ions before SBD metallization introduces discrete level defects (DLDs) as well as continuous level defects (CLDs) in the GaAs band gap. The concentration of DLDs increases with increasing sputter voltages up to 1 kV, but decreases for larger sputter voltages. In contrast, the concentration of CLDs increases monotonically with sputter voltage. These defects control the current transport in SBDs and cause current transport mechanisms other than thermionic emission. The DLTS measurements also indicated that strong Fermi level pinning occurs after sputtering with 5 kV Ar ions.

It has previously been shown [4] that the DLDs consist of point defects (which have the same DLTS "signatures" as the primary defects introduced in GaAs by electron irradiation) as well as defect complexes. Furthermore, it was also reported that as the sputter dose was increased, more defects with closely spaced energy levels were introduced in the GaAs band gap. It may well be that at the higher sputter voltages these energy levels become so close to each other that they are detected as a band of CLDs, as reported in the present study. This may also constitute the first stages of amorphization in the outermost layer of the damaged GaAs in which case the CLDs detected here may be considered to be characteristic of the first stages of this process. In order to cast more light on this subject, the present measurements should be supplemented by C–V-, optical transmission- and reflection measurements, as well as optical DLTS. This is the aim of a similar study recently initiated, where GaAs layers will be exposed to Ar, as well as other ions.

References

[1] I.L. Singher, J.S. Murday and J. Comas, J. Vac. Sci. Technol. 18 (1981) 161.
[2] I. Konomi, A. Kawano and Y. Kido, Surf. Sci. 207 (1989) 427.
[3] I.L. Singer, J.S. Murday and L.R. Cooper, Surf. Sci. 108 (1981) 7.
[4] L.J. Bredell, F.D. Auret and G. Myburg, Appl. Surf. Sci. 50 (1991) 466.
[5] S.J. Fonash, S. Ashok and R. Singh, Appl. Phys. Lett. 39 (1981) 423.
[6] S.V. Dubonos and S.V. Koveshnikov, Phys. Status Solidi A120 (1990) 77.
[7] F.D. Auret and M. Nel, Jpn. J. Appl. Phys. 30 (1991) 80.
[8] F.D. Auret, M. Nel and H.C. Snyman, Radiat. Eff. 105 (1987) 225.
[9] D.V. Lang, J. Appl. Phys. 45 (1974) 3014.
[10] F.D. Auret and M. Nel, J. Appl. Phys. 63 (1988) 973.
[11] N. Newman, Z. Liliental-Weber, E.R. Weber, E.R. Washburn and W.E. Spicer, Appl. Phys. Lett. 53 (1988) 145.
[12] D. Bauza and G. Pananakakis, J. Appl. Phys. 69 (1991) 3357.
[13] E.D. Cole, S. Sen and L.C. Burton, J. Electr. Mat. 18 (1988) 527.
[14] F.H. Mullins and A. Brunnschweiler, Solid State Electron. 19 (1976) 47.
[15] Y.X. Wang and P.H. Holloway, J. Vac. Sci. Technol. A2 (1984) 567.

© University of Pretoria

UNIVERSITEIT VAN PRETORIA
UNIVERSITY OF PRETORIA
YUNIBESITHI YA PRETORIA

Jpn. J. Appl. Phys. Vol. 33 (1994) pp. 2633-2634
Part 1, No. 5A, May 1994

Short Note

Neutron Irradiation Induced Defects in Low Free Carrier Concentration Epitaxially Grown n-GaAs

F. Danie AURET, Stewart A. GOODMAN, Albertus WILSON and Gerrit MYBURG
Physics Department, University of Pretoria, Pretoria 0002, Republic of South Africa

(Received October 29, 1993; accepted for publication February 19, 1994)

Deep level transient spectroscopy (DLTS) of low free carrier concentration n-GaAs revealed that high energy neutron irradiation introduced five electron traps, En1-En5, in molecular beam epitaxy (MBE) grown GaAs. Only four of these defects, En1, En2, En4 and En5 could be detected in irradiated GaAs grown by organo-metallic vapor phase epitaxy (OMVPE). The En1, En2 and En4 have similar DLTS "signatures" as the E1, E2 and E3 defects created during high energy electron irradiation of GaAs. The DLTS "signatures" of En5 in the MBE and OMVPE samples are different, and this difference is attributed to the presence of a near-surface defect which is more readily detectable in the MBE GaAs.

KEYWORDS: GaAs, deep level-transient spectroscopy, neutron radiation induced defects

High speed GaAs devices are frequently used in space applications where neutron irradiation can be severe[1] and it has, for example, been shown that defects introduced in semiconductors during neutron irradiation can have a pronounced influence on the characteristics of metal-semiconductor field-effect transistors (MESFETs).[2] In order to quantitatively explain the influence of radiation on device performance, it is necessary to know the *concentration and electronic properties* of the radiation induced defects, which depend on the semiconductor material, and the impurities and defects present before radiation. Deep level transient spectroscopy (DLTS)[3] has been employed to determine the electrical properties, i.e. energy level in the bandgap and capture cross section of the defects introduced during neutron irradiation. In these studies[4-6] the most prominent defect exhibited a broad DLTS band (U-band[4]), but because GaAs with a free carrier concentration above 10^{16} cm^{-3} was used, electric field enhanced emission[7] prevented an accurate determination of the electronic properties of the U-band and other neutron induced defects. Consequently our present knowledge regarding neutron irradiation induced defects in GaAs is insufficient to allow an understanding or prediction of their influence on electronic devices.

In this paper we compare the electrical properties of defects created during high energy neutron irradiation of n-GaAs grown by molecular beam epitaxy (MBE) and organo-metallic vapor phase epitaxy (OMVPE), and demonstrate that one of the neutron irradiation defects can only be observed in lightly doped MBE GaAs, but not in undoped OMVPE grown GaAs. The use of low free carrier concentration GaAs reduced the electric field enhanced emission and thus allowed an accurate determination of defect properties.

Nominally doped (with Si) n-type GaAs, grown by MBE, and undoped n-type GaAs grown by OMVPE on n^+-GaAs substrates were used for this experiment. After fabrication of Ni/AuGe/Au ohmic contacts on the n^+-backsides of the samples, 200 nm thick Pd Schottky barrier diodes (SBDs), 0.75 mm in diameter, were deposited on their epitaxial sides by resistive evaporation. Capacitance-voltage (C-V) measurements yielded free carrier concentrations of N_d-N_a=$(3.5\pm0.5)\times10^{14}$ cm^{-3} and $(1.4\pm0.2)\times10^{15}$ cm^{-3} for the unirradiated OMVPE and MBE grown wafers, respectively. After recording control DLTS spectra using a lock-in amplifier based system, the SBDs were irradiated with high energy neutrons from a p(66)/Be(40) clinical source at fluences of between 1×10^{11} and 1×10^{13} cm^{-2} as described elsewhere.[8] The energy level E_t in the band gap and apparent capture cross-section σ_{na} (DLTS "signatures") of defects were determined from conventional DLTS Arrhenius plots[3] using a quiescent reverse bias of V_r=1 V and a pulse amplitude of V_p=1.1 V. Depth profiling was performed by employing the double correlation DLTS technique (DDLTS),[9] in which spectra recorded at (V_r, V_p) are subtracted from those recorded at (V_r, $V_p+\delta V_p$). In this way information is obtained about defects in a narrow spatial region below the SBD interface, which are located well above the Fermi level.

Spectra of unirradiated GaAs SBDs (not shown) indicated that EL2 (present in all OMVPE GaAs) and EM5 are the dominant defects in the OMVPE and MBE grown wafers, respectively. Curves (b) and (d) in Fig. 1 show the DLTS spectra of OMVPE and MBE grown n-GaAs which were neutron irradiated at fluences of 3×10^{12} and 10^{13} cm^{-2}, respectively. To equalize the effect of the electric field on carrier emission from defects, the spectra were recorded at V_r biases of 8 V and 1 V for the OMVPE and MBE GaAs, respectively, which yielded equal maximum fields. Curve (b) shows that neutron irradiation of OMVPE GaAs introduced the defects En1, En2, En4 and En5, the most prominent being the En5. From curve (d) it is evident that neutron irradiation of MBE GaAs introduced all four defects observed in the OMVPE GaAs as well as an additional defect, the En3 with E_t=0.34 eV and $\sigma_{na}=2.5\times10^{-14}$ cm^{-2}. The "signatures" of the En1, En2 and En4 in MBE GaAs were found to be the same as in OMVPE GaAs measured under low field conditions.[8] However, the En5 "signature" in MBE GaAs (E_t=0.66 eV, $\sigma_{na}=6\times10^{-13}$ cm^2), determined at (V_r, V_p)=(1 V, 1.1 V), is significantly different from that of the En5 in OMVPE GaAs (E_t=0.73 eV, $\sigma_{na}=6\times10^{-12}$ cm^2) when determined at the same conditions.

© University of Pretoria

UNIVERSITEIT VAN PRETORIA
UNIVERSITY OF PRETORIA
YUNIBESITHI YA PRETORIA

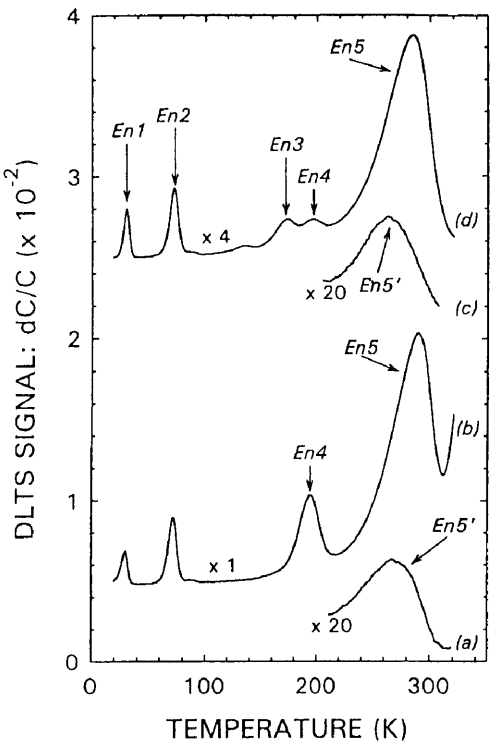

Fig. 1. DLTS spectra (curves (b) and (d)) and DDLTS spectra (curves (a) and (c)) of neutron irradiated OMVPE ($N_d-N_a=3.5\times10^{14}\,cm^{-3}$) and MBE ($N_d-N_a=1.4\times10^{15}\,cm^{-3}$) n-GaAs recorded at a lock-in amplifier frequency of 10 Hz: curve (a): OMVPE GaAs: $V_r=1$ V, $V_p=1.3$ V, $\delta V_p=0.1$ V; curve (b): OMVPE GaAs: $V_r=8$ V, $V_p=8.1$ V; curve (c): MBE GaAs: $V_r=1$ V, $V_p=1.3$ V, $\delta V_p=0.1$ V; curve (d): MBE GaAs: $V_r=1$ V, $V_p=1.1$ V; The fluences for the OMVPE and MBE layers were 3×10^{12} and $1\times10^{13}\,cm^{-2}$, respectively.

The main differences between the DLTS spectra of neutron irradiated MBE and OMVPE grown GaAs are the presence of the En3 only in the MBE GaAs and the different "signatures", peak shapes and peak positions of En5. In order to explain the presence of En3, we note that the MBE GaAs epitaxial layer differs from the OMVPE grown layer in that it is lightly doped with Si and its carrier density is about four times that of the OMVPE GaAs. The fact that the En3 is observed in MBE GaAs containing Si, but not in undoped OMVPE GaAs, suggests that it may be a radiation induced complex involving Si. A defect with similar properties as the En3 has also been observed in alpha particle irradiated Si-doped OMVPE grown GaAs, but not in irradiated undoped OMVPE GaAs.[10]

Next, consider the different "signatures" and peak shapes of the En5 in MBE and OMVPE GaAs. Despite the fact that curves (b) and (d) were recorded at equal maximum electric fields, they show that the En5 peak in MBE GaAs is shifted to lower temperatures and has a larger half-width than in the OMVPE GaAs. In order to investigate this, DDLTS depth profiling was performed. This indicated that the introduction rate of the En5 further than about 0.2 μm from the interface in both types of GaAs is $(7\pm2)\,cm^{-1}$. However, the DDLTS spectra (a) and (c) of Fig. 1 (for OMVPE and MBE GaAs, respectively) reveal that when spectra recorded at different forward bias filling pulses are subtracted from each other, a defect En5′ is observed. This defect has a peak at 20–25 K lower than the En5, indicating that its energy level is closer to the conduction band than that of En5. Further, it follows from Fig. 1 that in the MBE GaAs the ratio of its peak height to that of the En2 is 4–5 times higher than in the OMVPE GaAs.

The DLTS "signatures" of the neutron irradiation induced defects En1, En2 and En4 are very similar to those of the electron irradiation induced point defects E1, E2 and E3, respectively.[10-12] It has been proposed that E1 and E2 are two different charge states, $(-/0)$ and $(0/+)$ of the isolated arsenic vacancy, V_{As}, in GaAs,[13] while the E3 is speculated to be related to close arsenic vacancy-interstitial pairs, V_{As}–As_I.[13] The correspondence between the DLTS "signatures" of the neutron and electron irradiation induced defects indicates that En1, En2 and En4 are also point defects. The most prominent defect, En5, is the only one of the neutron irradiation induced defects observed here which is not introduced in observable concentrations during electron and alpha particle irradiation of identical GaAs layers[10] as used in the present study.

In summary, the use of low, but different, free carrier density GaAs enabled us to establish that whereas some neutron irradiation induced defects (En1, En2 and En4) are the same as the main point defects introduced during electron irradiation, the properties of others (En3, En5 and En5′) depend on the GaAs growth technique and carrier density, implying that they depend on defects or impurities in the as-grown GaAs.

The financial assistance of the South African Foundation for Research Development (FRD) is gratefully acknowledged. We also thank Dr. Dan T. L. Jones of the National Accelerator Centre for the neutron irradiation.

1) M. Yamaguchi, A. Yamamoto and A. Sibukawa: Jpn. J. Appl. Phys. **22** (1983) 1727.
2) A. F. Galashan and S. W. Bland: J. Appl. Phys. **67** (1990) 173.
3) D. V. Lang: J. Appl. Phys. **45** (1974) 3014.
4) G. M. Martin, E. Esteve, P. Langlade and S. Makram-Ebeid: J. Appl. Phys. **56** (1984) 2655.
5) J. W. Farmer and J. M. Meese: J. Nucl. Mater. **108 & 109** (1982) 700.
6) A. P. Mamontov and V. V. Peshev: Sov. Phys. Semicond. **18** (1984) 624.
7) J. Frenkel: Phys. Rev. **54** (1938) 657.
8) F. D. Auret, S. A. Goodman, G. Myburg, W. O. Barnard and D. T. L. Jones: J. Appl. Phys. **74** (1993) 4339.
9) H. Lefevre and M. Schultz: Appl. Phys. **12** (1976) 45.
10) F. D. Auret, S. A. Goodman, G. Myburg and W. E. Meyer: Appl. Phys. A **56** (1993) 547.
11) D. Pons and J. C. Bourgoin: J. Phys. C: Solid State Phys. **18** (1985) 3839.
12) F. D. Auret, L. J. Bredell and G. Myburg: Jpn. J. Appl. Phys. **30** (1991) 80.
13) B. Ziebro, J. W. Hemsky and D. C. Look: J. Appl. Phys. **72** (1992) 78.

© University of Pretoria

4.7 SUMMARY OF RESULTS (DEFECTS)

4.7.1 ELECTRONIC CHARACTERISTICS

TABLE 4.1a Electronic properties of defects detected after alpha-particle irradiation of MOVPE-grown Si-doped ($1.2 \pm 0.4 \times 10^{16}$ cm^{-3}) n-GaAs.

ALPHA-PARTICLE IRRADIATION (n-TYPE)			
DEFECT LABEL	**E_T (eV)**	**σ_{na} (cm^{-2})**	**η (cm^{-1})**
Eα1	0.026	1.5×10^{-17}	2963
Eα2	0.117	1.3×10^{-14}	9638
Eα3	0.304	2.8×10^{-15}	≈ 4560
Eα4	0.353	1.2×10^{-14}	3060
Eα5	0.635	1.6×10^{-13}	1737
Eα7	0.070	9.7×10^{-16}	—
Eα8	0.175	9.8×10^{-14}	—
Eα9	0.190	6.7×10^{-16}	—
Pα0*	0.152	1.7×10^{-15}	—
Pα1*	0.376	1.8×10^{-14}	—
Pα2*	0.600	3.8×10^{-14}	—

* Defects detected after annealing

© University of Pretoria

TABLE 4.1b Electronic properties of defects detected after alpha-particle irradiation of MOVPE-grown ($3.5 \pm 0.5 \times 10^{14}$ cm^{-3}) n-GaAs.

ALPHA-PARTICLE IRRADIATION (n-TYPE)			
DEFECT LABEL	**E_T (eV)**	**σ_{na} (cm^{-2})**	**η (cm^{-1})**
Eα1	0.041	6.8×10^{-16}	—
Eα2	0.141	1.2×10^{-13}	—
Eα3	0.337	2.5×10^{-14}	—
Eα4	0.378	1.6×10^{-14}	—

TABLE 4.1c Electronic properties of defects detected after alpha-particle irradiation of MBE-grown Be-doped ($1.8 \pm 0.2 \times 10^{16}$ cm^{-3}) p-GaAs.

ALPHA-PARTICLE IRRADIATION (p-TYPE)			
DEFECT LABEL	**E_T (eV)**	**σ_{pa} (cm^{-2})**	**η (cm^{-1})**
Hα1	0.08	2.6×10^{-15}	4705
Hα3	0.15	5.9×10^{-15}	≈ 490
Hα4	0.20	1.2×10^{-15}	1050 - 4335
Hα5	0.30	1.6×10^{-14}	2100

© University of Pretoria

TABLE 4.2a Electronic properties of defects detected after electron irradiation of MOVPE-grown Si-doped ($1.2 \pm 0.4 \times 10^{16}$ cm^{-3}) n-GaAs.

ELECTRON IRRADIATION (n-TYPE)			
DEFECT LABEL	**E_T (eV)**	**σ_{na} (cm^{-2})**	**η (cm^{-1})**
Eβ1	0.024	8.0×10^{-18}	2.0
Eβ2	0.117	1.7×10^{-14}	2.0
Eβ4	0.342	6.0×10^{-15}	0.7

TABLE 4.2b Electronic properties of defects detected after electron irradiation of MOVPE-grown ($3.5 \pm 0.5 \times 10^{14}$ cm^{-3}) n-GaAs.

ELECTRON IRRADIATION (n-TYPE)			
DEFECT LABEL	**E_T (eV)**	**σ_{na} (cm^{-2})**	**η (cm^{-1})**
Eβ1	0.041	5.4×10^{-16}	2.0
Eβ2	0.139	9.3×10^{-14}	2.0
Eβ4	0.380	1.6×10^{-14}	0.7

© University of Pretoria

TABLE 4.2c Electronic properties of defects detected after electron irradiation of MBE-grown Be-doped ($1.8 \pm 0.2 \times 10^{16}$ cm^{-3}) p-GaAs.

ELECTRON IRRADIATION (p-TYPE)			
DEFECT LABEL	**E_T (eV)**	**σ_{pa} (cm^{-2})**	**η (cm^{-1})**
Hα1	0.08	2.6×10^{-15}	4705
Hα3	0.15	5.9×10^{-15}	≈ 490
Hα4	0.20	1.2×10^{-15}	1050 - 4335
Hα5	0.30	1.6×10^{-14}	2100

TABLE 4.3 Electronic properties of defects detected 2.0 MeV proton irradiation of MOVPE-grown Si-doped ($1.2 \pm 0.4 \times 10^{16}$ cm^{-3}) n-GaAs.

PROTON IRRADIATION (n-TYPE)			
DEFECT LABEL	**E_T (eV)**	**σ_{pa} (cm^{-2})**	**η (cm^{-1})**
Ep1	0.023	9.0×10^{-18}	1056
Ep2	0.112	5.9×10^{-15}	1766
Ep3	0.301	2.1×10^{-15}	≈ 385
Ep4	0.362	1.9×10^{-14}	470
Ep5	0.636	1.2×10^{-13}	127

© University of Pretoria

TABLE 4.4 Electronic properties of defects detected after neutron irradiation of MOVPE-grown ($3.5 \pm 0.5 \times 10^{14}$ cm^{-3}) n-GaAs.

ALPHA-PARTICLE IRRADIATION (n-TYPE)			
DEFECT LABEL	**E_T (eV)**	**σ_{na} (cm^{-2})**	**η (cm^{-1})**
En1	0.041	6.0×10^{-16}	1.0
En2	0.141	1.2×10^{-13}	1.5
En3*	0.340	2.5×10^{-14}	1.0
En4	0.360	3.7×10^{-15}	208
En5	0.730	6.0×10^{-12}	10

* detected in MBE-grown Be-doped material (1.4×10^{15} cm^{-3}).

© University of Pretoria

TABLE 4.5 Electronic properties of defects detected after argon-ion sputtering of MOVPE-grown ($3.5 \pm 0.5 \times 10^{14}$ cm^{-3}) n-GaAs.

ARGON-ION SPUTTERING (n-TYPE)			
DEFECT LABEL	**E_T (eV)**	**σ_{na} (cm^{-2})**	**η (cm^{-1})**
EAr1	0.050	1.0×10^{-13}	—
EAr2	0.107	1.0×10^{-14}	—
EAr3	0.125	8.0×10^{-15}	—
EAr4	0.16	1.0×10^{-13}	—
EAr5	0.19	8.0×10^{-14}	—
EAr7	—	—	—
EAr8	0.30	8.0×10^{-15}	—
EAr9	0.40	4.0×10^{-14}	—
EAr10	0.52	7.0×10^{-14}	—
EAr11	0.70	3.0×10^{-14}	—

© University of Pretoria

4.7.2 THERMODYNAMIC CHARACTERISTICS

TABLE 4.6 Activation energy (ΔH), factor (ν) and annealing temperature (T) of the electron traps in alpha-particle irradiated MOVPE-grown Si-doped ($1.2 \pm 0.4 \times 10^{16}$ cm^{-3}) n-GaAs.

ALPHA-PARTICLE IRRADIATION (n-TYPE)			
DEFECT LABEL	**ΔH (eV)**	**ν (s^{-1})**	**T (K)**
Eα1	1.55 ± 0.10	$10^{12.0 \pm 0.5}$	500
Eα2	1.60 ± 0.10	$10^{12.0 \pm 0.5}$	500
Eα2"	1.60 ± 0.10	$10^{12.0 \pm 0.5}$	500
Eα3	1.55 ± 0.10	$10^{12.5 \pm 0.5}$	460
Eα4	1.45 ± 0.10	$10^{11.0 \pm 1.0}$	460
Eα7	0.86 ± 0.05	$10^{15.0 \pm 1.0}$	245
Eα9	0.88 ± 0.05	$10^{17.0 \pm 1.0}$	225

© University of Pretoria

TABLE 4.7.3 Electronic properties of defects detected after electron, α-particle, proton, neutron irradiation and argon sputtering in MOVPE-grown ($3.5 \pm 0.5 \times 10^{14}$ cm^{-3}) n-GaAs.

DEFECT LABEL	E_T (eV)	σ_{na} (cm^{-2})	η (cm^{-1})
Eα1 [5]	0.041	6.8×10^{-16}	—
Ep1	0.042	8.0×10^{-16}	—
En1 [15]	0.041	6.0×10^{-16}	1.0
Eβ1 [5]	0.041	5.4×10^{-16}	2.0
EAr1 [13]	0.050	1.0×10^{-13}	—
Eα2 [5]	0.141	1.2×10^{-13}	—
Ep2	0.140	1.0×10^{-13}	—
En2 [15]	0.141	1.2×10^{-13}	1.5
Eβ2 [5]	0.139	9.3×10^{-14}	2.0
EAr3 [13]	0.125	8.0×10^{-15}	—
Eα3 [5]*	0.337	2.5×10^{-14}	—
Ep3*	0.340	2.5×10^{-14}	—
En3 [15]*	0.340	2.5×10^{-14}	≈ 1
Eβ3*	—	—	—
EAr8 [13]	0.300	8.0×10^{-15}	—
Eα4 [5]	0.378	1.6×10^{-14}	—
Ep4	0.370	1.4×10^{-13}	—
En4 [15]	0.360	3.7×10^{-15}	208
Eβ4 [5]	0.380	1.6×10^{-14}	0.7
EAr9 [13]	0.400	4.0×10^{-14}	—
Eα5	—	—	—
Ep5	—	—	—
En5 [15]	0.730	6.0×10^{-12}	10
Eβ5	—	—	—
EAr11 [13]	0.700	3.0×10^{-14}	—

* Detected in MOVPE-grown n-GaAs (2×10^{15} cm^{-3}).

© University of Pretoria

4.4 ELECTRIC FIELD EFFECT

Deep level transient spectroscopy is based on an analysis of the thermal emission of electrons (or holes) by traps in the space-charge region of a rectifying semiconductor device. The presence of an electric field in the space-charge region of a metal-semiconductor system may enhance the emission of carriers from defect states to the conduction band in the case of n-type material. There are three possible mechanisms: Poole-Frenkel, phonon-assisted tunnelling and "pure" tunnelling. These emission enhancement mechanisms may adversely influence the accurate determination of the defect concentration and the DLTS "signature". This is illustrated upon examination of eqn 2.1.12, used to determine the "signature". The DLTS peak appears at lower temperatures when the emission rate is enhanced by one of the above mechanisms. Also, this peak may appear broadened towards the lower temperature side, leading to erroneous defect concentration profiles.

The relationship between the electric field strength in the space-charge region and the thermal emission rate of electron defects E1, E2 and E3 is presented. The experimental enhanced emission rates are compared to modelled results of the Poole-Frenkel potential barrier lowering mechanism and the phonon-assisted tunnelling mechanism. Defects E2 and E3 both exhibit a field dependent emission rate, and the dependence is well described by the phonon-assisted tunnelling mechanism. The Huang-Rhys factor for E2 and E3 is 4.5 ± 0.5 and 7.5 ± 0.5, respectively. Electron defect E1, on the other hand, cannot be explained by this mechanism; the field dependence of this defect may be a combination of mechanisms, or the present mechanism may have to be refined to explain the dependence.

PUBLICATION:

(11) S.A. Goodman, F.D. Auret and W.E. Meyer, "Electric Field Effect on the Emission of Electron-Irradiation-Induced Defects in n-GaAs", Jpn. J. Appl. Phys. **33**, 5 (1994) 1949.

© University of Pretoria

UNIVERSITEIT VAN PRETORIA
UNIVERSITY OF PRETORIA
YUNIBESITHI YA PRETORIA

Jpn. J. Appl. Phys. Vol. 33 (1994) pp. 1949–1953
Part 1, No. 4A, April 1994

Electric Field Effect on the Emission of Electron-Irradiation-Induced Defects in n-GaAs

Stewart A. GOODMAN, F. Danie AURET and Walter E. MEYER
Physics Department, University of Pretoria, Pretoria 0002, Republic of South Africa

(Received November 15, 1993; accepted for publication December 18, 1993)

The enhancement of the emission rate of electron-irradiation-induced defects in the presence of an electric field in n-type GaAs with carrier concentrations ranging from 1×10^{14} to 1×10^{16} cm^{-3} has been investigated using deep level transient spectroscopy (DLTS). The relationship between the electric field strength and the emission rate of the three major electron traps (E1, E2 and E3) in electron-irradiated n-type GaAs material is presented. Using the models for phonon-assisted tunnel emission of electrons from deep levels developed by Pons *et al.* and the enhancement due to Poole-Frenkel potential barrier lowering a correlation was attempted between the experimental results and those predicted by the above-mentioned two models. From these results an estimate of the Franck-Condon shift for the three defects is presented.

KEYWORDS: GaAs, enhanced emission, electric field, deep level transient spectroscopy (DLTS), electron radiation induced electron traps, phonon assisted tunnelling

1. Introduction

Deep levels in semiconductors are often studied by experimental methods based upon the thermal emission of electrons (holes) by the traps in the space charge region. The electric field dependence of the thermal emission of trapped carriers at deep level centres in semiconductors may adversely affect the accurate determination of defect concentration[1,2] as saturation of the defect peak amplitudes may occur depending on the effect of the electric field on the emission of electrons from the defect. According to Pons and Makram-Ebeid[2] the deep level transient spectroscopy (DLTS) signal of a defect that saturates quickly with an increase in filling pulse amplitude has an emission rate that depends strongly upon the electric field strength in the depletion region. The presence of an electric field in the depletion region may also adversely influence the accurate determination of the DLTS[3] "signature" (position in the band-gap (E_t) and apparent capture cross-section (σ_{na})). As is well documented[4-8] electron irradiation will produce the electron defects E1–E5 and much work has been done to identify and characterize these defects. The major defects E1–E3 have been widely studied and are generally thought to be related to vacancy-interstitial pairs in the arsenic sub-lattice, with E1 and E2 reported to be different charge states of the close arsenic vacancy-interstitial pair and E3 a separated Frenkel pair.[9]

It is well established that the thermal emission probability from deep levels is influenced by the local electric field within the space charge region of a semiconductor junction, and due to the spatial variation of this electric field, substantial deviations from the simple exponential capacitance transients have frequently been observed. The field dependent emission rate contains information about the potential well structure around defects that might provide valuable insight into the nature of the defect. There are a few mechanisms that can be responsible for the enhanced thermal emission of a trapped carrier from a defect level. The first and probably the most well known is the Poole-Frenkel mechanism,[10] emission enhancement due to this mechanism is predominantly for shallow levels when there is a low electric field in the space-charge region, and this mechanism cannot account for the strong field enhancement observed for deeper lying levels. The Poole-Frenkel effect leads to a decrease ΔE_i of the ionisation energy E_i, so that the more general expression for the thermal emission rate (e_n) becomes:[11]

$$e_n' = e_n^{\infty} \exp\left(\frac{\Delta E_i - E_i}{kT}\right) \tag{1}$$

where e_n^{∞} is the pre-exponential factor and is a property of the defect under consideration, it is assumed that it is not modified by the electric field (F). For a Coulombic well ΔE_i is represented by the following equation:[11]

$$\Delta E_i = \sqrt{\frac{qF}{\pi\varepsilon}} \tag{2}$$

where ε is the dielectric constant of the material and q the electron charge.

It is generally accepted that a tunnelling mechanism is responsible for the strong field enhancement. The two possible tunnelling mechanisms are "pure" tunnelling and phonon-assisted tunnelling, with the "pure" tunnelling mechanism being predominant in the high field regions ($>8.0\times10^7$ V·m^{-1}).[11] The phonon-assisted mechanism is very sensitive to the interaction of the deep levels with the vibronic modes of the lattice, resulting in a linear coupling mechanism between the deep levels and the lattice phonon modes. Because of this coupling the trapped electron can occupy a set of stationary quasi levels separated by $\hbar\omega$, with $\hbar\omega$ being the phonon energy. Elastic tunnelling can then occur from any of these quasi deep levels to the conduction band. The coupling constant or Huang-Rhys factor S,[12] is represented by the following equation where the phonon energy is $\hbar\omega$ and the temperature T:[13]

$$S = \frac{\Delta E}{\hbar\omega} \tag{3}$$

where ΔE refers to the vibrational energy loss. The field emission rate due to phonon assisted tunnelling

© University of Pretoria

UNIVERSITEIT VAN PRETORIA
UNIVERSITY OF PRETORIA
YUNIBESITHI YA PRETORIA

emission as derived by Pons and Makram-Ebeid,[2] is given in eq. (4)

$$e_f = \sum_p \Pi_p . \Gamma(\Delta_p) . (1 - f_{1,p}) \tag{4}$$

The $(1-f_{1,p})$ factor in the above equation is the Fermi-Dirac probability of finding an empty conduction band state. The tunnelling emission probability for an electron at a quasi level $\Gamma(\Delta)$ as found by Korol[14] for an electron trapped in a delta function potential well can be written as:

$$\Gamma(\Delta) = \gamma \frac{\Delta}{qK} e^{-K} \tag{5}$$

where Δ is the energy position of the deep level below the conduction band and K is the WKB attenuation of the wave function across the potential barrier separating the trapping site from the free conduction band states. The pre-exponential factor γ depends on the form of the short-range potential and assuming a uniform field F and a triangular barrier, K is given by:

$$K \doteq \frac{4}{3} \frac{\sqrt{2m^*}}{\hbar F} \Delta^{3/2} \tag{6}$$

The electric field strength in the space charge region is represented by the symbol F and the electron effective mass by m^*. The probability Π_p of finding an electron at a given quasi level ($E_c - \Delta_p$, where $p=0, \pm 1, \pm 2, \cdots$) may be calculated from:

$$\Pi_p (1 - e^{-\hbar\omega/kT}) \sum_{n=0}^{+\infty} e^{-n\hbar\omega/kT} J_p^2 \left(2\sqrt{S\left(n + \frac{1}{2}\right)} \right) \tag{7}$$

where J_p is a Bessel function of the first kind and n the integer number of phonons. This model is based on the assumption that the phonons have a single well-defined angular frequency (ω).

The experimental and theoretical electric field dependence of the thermal emission of trapped carriers from defect E3 has been reported in numerous works.[1,2,15-17] In this paper we shall compare the experimental and modelled data obtained for E3 in our laboratory to the modelled data presented by Pons and Makram-Ebeid.[2] We shall also present for the first time results illustrating the enhanced emission rate for the other two major electron traps E1 and E2. In order to determine the mechanism responsible for the enhancement of the emission rate of these defects the experimental data were modelled using the "exact" model proposed by Pons and Makram-Ebeid[2] and the enhancement due to the Poole-Frenkel potential lowering was also calculated and compared to the experimental data.

2. Experimental Details

The samples studied in this work were n-type GaAs films 8.0 μm thick grown by OMVPE on n^+ bulk grown GaAs substrates. The free carrier concentration determined from capacitance-voltage (C-V) measurements at 1.0 MHz of the samples ranged from 1×10^{14} for the undoped material to 1×10^{16} cm^{-3} for the silicon doped material. The back surfaces (n^+) of the wafers were coated with Ni/AuGe/Au films and alloyed to form ohmic contacts. After ohmic contact fabrication, 0.73 mm diameter palladium dots were deposited on the front surface through a metal mask to form Schottky barrier diodes. The Sr electron source used to irradiate the samples was disc shaped with a diameter of 8.4 mm and an activity of 20 mCi. ^{90}Sr radio nuclides decay first to Y with the emission of an 0.5 MeV electron (half-life 28.5 years) and then to Zr with the emission of a 2.3 MeV electron (half-life 64.1 h). The Schottky diodes were exposed to electron irradiation by placing them 1 mm away from the Sr radioactive source. Depending upon the carrier density of the material under investigation the exposure time varied. By applying the conventional criteria for accurate DLTS determination of defect states the sum of trap concentrations was never larger than 10% of the free carrier concentration.[18]

A two-phase lock-in amplifier-based (LIA) deep level transient spectroscopy (DLTS) system, comprising a Stanford Research SR530 LIA, a modified Boonton 72BD capacitance meter[19] and an Air Products cryostat with temperature controller, was employed to detect and to characterize the defects introduced during electron irradiation. The DLTS spectra of the electron irradiated material were acquired at a rate of 2.50 K·min^{-1} in both temperature directions so as to eliminate any peak temperature discrepancies due to uneven cooling or heating especially in the temperature range in which E1 and E2 are detected. The magnitude of the electric field was varied by changing the reverse bias applied to the metal-semiconductor system. The magnitude of the reverse bias chosen depended upon the carrier concentration of the material under measurement. For the low carrier density material the maximum reverse bias that could be applied was 1.50 V, before the n^+ substrate was reached, whereas for the 1×10^{16} cm^{-3} material a reverse bias of 8.0 V was applied. By increasing the forward bias in half-volt increments from 0.5 V to the value of the reverse bias applied and subtracting subsequent averaged spectra from one another, enabled us to determine the trap characteristics (energy and capture cross-section) at different field strengths in the depletion region. The electric field in these sections of the depletion region was determined by calculating the corrected depletion depth, and using this width the average electric field in the region under consideration was calculated. From the Arrhenius plots (e_n/T^2 vs $10^3/T$) the apparent trap energy and capture cross-section were determined. Although E_t and σ_{na} thus calculated are meaningless since pure thermal emission is not the only emission process, they nevertheless serve the purpose of allowing us to calculate the emission rate at any temperature which in turn allows us to compare data acquired at different electric field strengths at a specific temperature.

3. Results

The most important parameter under investigation in this study was the enhanced emission rate as a function of electric field in samples with different free carrier densities. From inspection of Fig. 1 which depicts

© University of Pretoria

UNIVERSITEIT VAN PRETORIA
UNIVERSITY OF PRETORIA
YUNIBESITHI YA PRETORIA

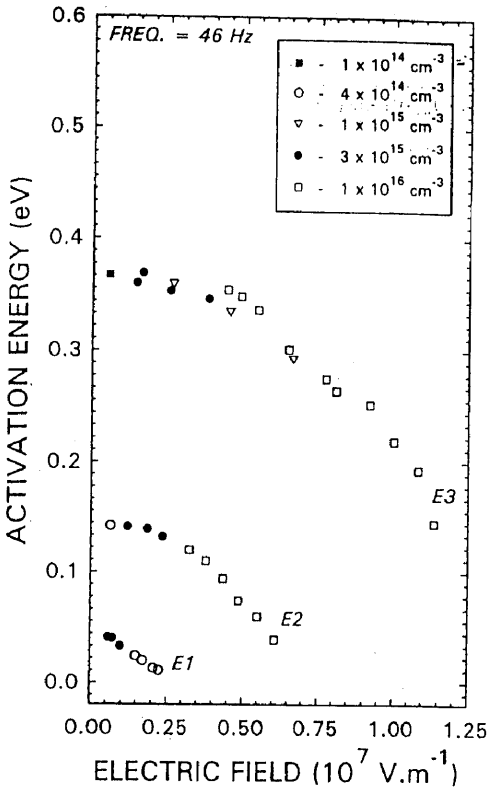

Fig. 1. The change in activation energy of defects E1–E3 in different carrier density n-GaAs as a function of electric field strength in the space charge region.

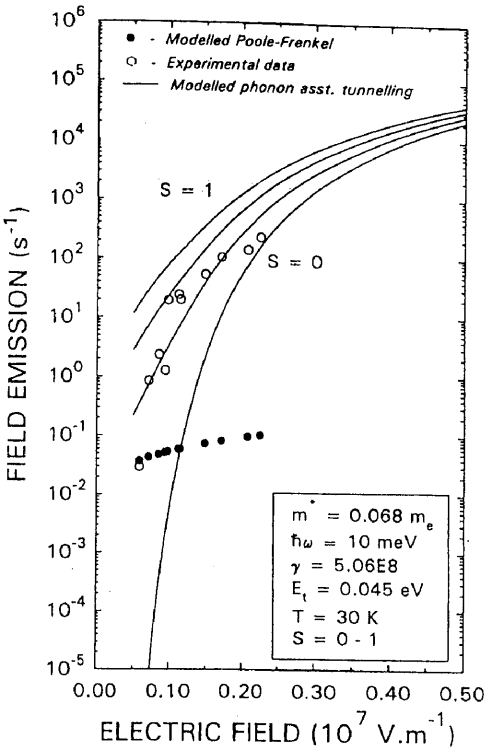

Fig. 2. Electric field dependence of the emission rate (e_n) of defect E1. The solid lines (——) represent the phonon-assisted tunnelling modelled results as a function of the Huang-Rhys factor S. The modelled Poole-Frenkel emission dependence is represented by (●), the experimental emission data are represented by (○).

the activation energy for different carrier densities as a function of electric field strength for defects E1–E3, it is clear that the activation energies are influenced by the electric field strength in the depletion region. It must be noted that these activation energies were calculated assuming a temperature-independent capture cross-section, and this assumption is not always valid. For example, the defect E3 has been reported to have a temperature-dependent capture cross-section, where the capture cross-section activation energy is approximately 0.09 eV [20] Figure 1 also illustrates how easily erroneous trap characteristics can be measured by assuming the influence of the electric field in the space charge region to be negligible. For defect E1 the position in the bandgap can vary from 0.042 to 0.012 eV for the high field region, if the influence of the electric field is ignored, the change in activation energy as a function of electric field strength varies almost linearly, whereas for the other two defects E2 and E3 the change follows a parabolic-like trend.

Figures 2–4 illustrate the experimental and modelled results for the electric field dependence of the field emission rates (emission rates due to the electric field) for electron traps E1–E3, respectively. The experimental points are the total emission rate minus the low field or thermal emission rate, resulting in the field-assisted emission rate. From inspection of Fig. 2, it is evident that neither of the two enhancement mechanisms (phonon-assisted tunnelling or Poole-Frenkel effect) fit the experimental data for defect E1. The phonon-assisted

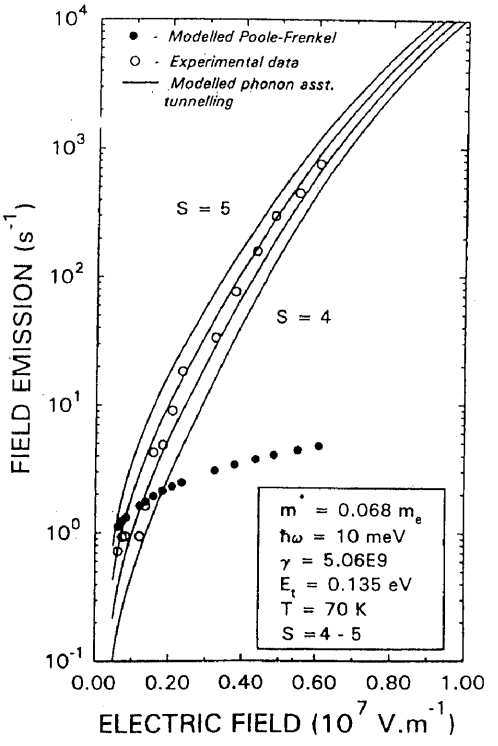

Fig. 3. Electric field dependence of the emission rate (e_n) of defect E2. The solid lines (——) represent the phonon-assisted tunnelling modelled results as a function of the Huang-Rhys factor S. The modelled Poole-Frenkel emission dependence is represented by (●), the experimental emission data are represented by (○).

© University of Pretoria

UNIVERSITEIT VAN PRETORIA
UNIVERSITY OF PRETORIA
YUNIBESITHI YA PRETORIA

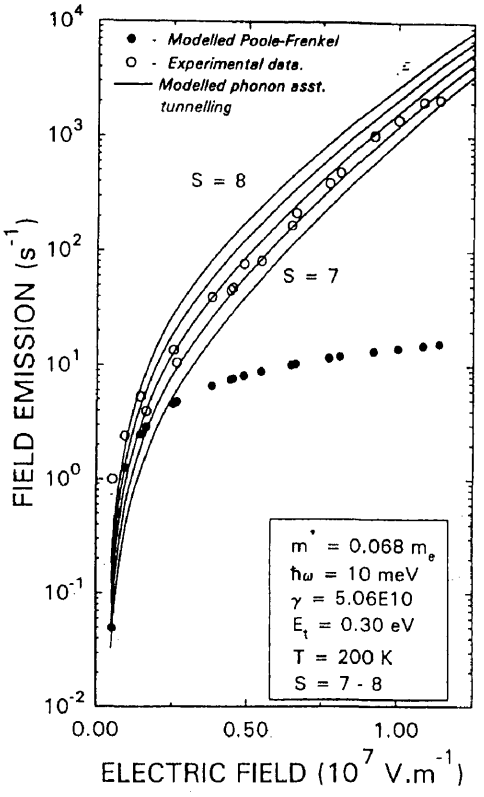

Fig. 4. Electric field dependence of the emission rate (e_n) of defect E3. The solid lines (——) represent the phonon-assisted tunnelling modelled results as a function of the Huang-Rhys factor S. The modelled Poole-Frenkel emission dependence is represented by (●), the experimental emission data are represented by (○).

tunnelling model[2] is based on the assumption that $kT > \hbar\omega$, which implies a temperature of 116 K, if the phonon energy is assumed to be 10 meV. Electron trap E1 peaks at approximately 30 K at 46 Hz, so the validity of the results in this low temperature region is in question. One would possibly expect the enhancement of the emission rate to be explained by the Poole-Frenkel potential lowering, as the defect level is shallow (0.045 eV) and the field strength in the space charge layer would favour this mechanism over the "pure" tunnelling mechanism. However, this is not the case and the field dependence of the emission rate will have to be explained using another model. Recently, Pons and Bourgoin[21] proposed a mechanism termed carrier hopping capture mechanism, this model suggesting that capture in the presence of an electric field may occur through hopping conduction. We speculate that the emission of carriers from this shallow level (E1) may occur through a similar hopping mechanism. An attempt was made to apply the model by Zhu *et al.*,[22] because their paper presents a model for the Poole-Frenkel potential lowering from a Gaussian potential; however, the results from this model did not fit our experimental data.

Figures 3 and 4 depict the modelling and experimental results for the electron defects E2 and E3. From these graphs we conclude that the enhancement of the emission rate can be explained by phonon-assisted tunnelling with $S=4.5\pm0.5$ and $S=7.5\pm0.5$ for E2 and E3, respectively. Table I lists the values of the model parameters, the values being calculated using an electron effective mass of $0.068m_0$, the model parameters for defect E3 are compared to those obtained by other authors.[2] As expected, the Franck-Condon shift for defect E3 was very similar to that obtained by Pons and Makram-Ebeid,[2] the value of the pre-factor gamma (γ) (which depends on the form of the short range potential) for this defect being $5.06\times10^{10}\,eV^{-1}s^{-1}$, ($=1\times10^{-4}\times(q/3\hbar)$). This value differs from that reported by Pons and Makram-Ebeid[2] (4.554×10^{13}), however this value really only translates the modelled curves in the y-direction. From the modelled results one can obtain an approximate value for the Franck-Condon shift ($S\hbar\omega$)[23] for E2. The electric field dependence of the emission rates of defects E1 and E2 cannot be explained by the same mechanism, even though they are regarded as the same defect, the difference in their charge state and position in the bandgap are probably the controlling factors determining the dominant enhancement mechanism.

Table I. Values of model parameters obtained using the phonon-assisted tunneling model,[2] the parameters were calculated using $m^*=0.068m_0$, and a phonon energy of 10 meV.

Defect	S	E_t(eV)	γ($eV^{-1}\cdot s^{-1}$)	$S\hbar\omega$(meV)	$S\hbar\omega$(meV)[2]	$T^{a)}_{peak}$(K)
E1	0–1	0.045	5.06×10^{8}	0–10		30
E2	4–5	0.135	5.06×10^{9}	40–50		70
E3	7–8	0.300	5.06×10^{10}	70–80	75 ± 22	200

[a)]Peak temperature at a LIA frequency of 46 Hz.

4. Conclusions

The influence of the presence of an electric field in the space charge region on the emission rate of electron defects E1–E3 has been illustrated. It has been shown that defect E2 exhibits a field-dependent emission rate, and the dependence is well described by the phonon-assisted tunnelling mechanism, from the modelling results the Franck-Condon shift was measured to be 40–50 meV. Defect E1 on the other hand, also exhibits a fairly strong field dependence, but neither the phonon-assisted tunnelling mechanism or the Poole-Frenkel potential lowering could explain this field emission, a possible mechanism could be the carrier hopping mechanism.[21] From this paper it is obvious that the field-assisted emission rates cannot clearly be explained, especially for electron trap E1, by using one of the enhancement mechanisms, but by possibly a combination of the mechanisms or even a new mechanism.

Acknowledgements

The financial assistance of the South African Foundation for Research Development (FRD) is gratefully acknowledged. We thank G. Myburg of the University of Pretoria for ohmic contact and SBD fabrication.

1) H. Lefevre and M. Schulz: J. Appl. Phys. 12 (1977) 45.
2) D. Pons and S. Makram-Ebeid: J. Phys. (Paris) 40 (1979) 1161.

© University of Pretoria

UNIVERSITEIT VAN PRETORIA
UNIVERSITY OF PRETORIA
YUNIBESITHI YA PRETORIA

3) D. V. Lang: J. Appl. Phys. **45** (1974) **3014**.
4) D. Pons and J. C. Bourgoin: J. Phys. C: Solid State Phys. **18** (1985) 3839.
5) D. Pons, P. M. Mooney and J. C. Bourgoin: J. Appl. Phys. **51** (1980) 2038.
6) J. C. Bourgoin, H. J. von Bardeleben and D. Stievenard: Phys. Status Solidi a **102** (1987) 499.
7) J. W. Farmer and D. C. Look: Phys. Rev. B **21** (1980) 3389.
8) S. Loualiche, A. Nouailhat, G. Guillot and M. Lannoo: Phys. Rev. B **30** (1984) 5822.
9) D. Stievenard, X. Boddaert, J. C. Bourgoin and H. J. von Bardeleben: Phys. Rev. B **41** (1990) 5271.
10) J. Frenkel: Phys. Rev. **54** (1938) 657.
11) G. Vincent, A. Chantre and D. Bois: J. Appl. Phys. **50** (1979) 5484.
12) K. Huang and A. Phys: Proc. Roy. Soc. London, Ser. A **204** (1950) 406.
13) S. Makram-Ebeid: Appl. Phys. Lett. **37** (1980) 464.
14) E. N. Korol: Sov. Phys. Solid State **19** (1977) 1327.
15) S. Makram-Ebeid and M. Lannoo: Phys. Rev. Lett. **48** (1982) 1281.
16) S.. Makram-Ebeid and M. Lannoo: Phys. Rev. B **25** (1982) 6406.
17) V. N. Brudnyi and V. V. Peshev: Phys Status Solidi a 118 (1990) 219.
18) W. E. Philips and J. R. Lowney: J. Appl. Phys. **45** (1983) 2786.
19) T. I. Chappel and C. M. Ransom: Rev. Sci. Instrum. **55** (1984) 200.
20) C. H. Henry and D. V. Lang: Phys. Rev. B **15** (1977) 989.
21) D. Pons and J. C. Bourgoin: Phys. Rev. B **43** (1991) 11840.
22) O. S. Zhu, K. Hiramatsu, N. Sawaki, I. Akasaki and X. N. Liu: J. Appl. Phys. **73** (1993) 771.
23) J. C. Bourgoin and M. Lannoo: *Point Defects in Semiconductors II* (Springer-Verlag, Berlin, 1983) p. 255.

© University of Pretoria

4.5 DEFECT ANNEALING

When defects have been intentionally introduced in GaAs, it is possible to reduce the concentration or even completely remove them by annealing the material at the correct temperature for a specific period. A knowledge of the thermodynamic characteristics of radiation-induced defects may also be useful in identifying these intentionally-introduced defects. The mobility of a defect may depend upon which sub-lattice the defect is positioned on; defects which form part of the Ga-sublattice are very mobile, even at room temperature, and, hence, cannot be detected under normal conditions. To enable thermodynamic and electronic characterization of these very mobile defects, the material was irradiated at 15 K.

After 15 K alpha-particle irradiation of n-type GaAs, two defects (Eα7 and Eα9) with introduction rates of 41 and 187 cm^{-1} were detected. It is speculated from their annealing kinetics that they may be complex or divacancy type defects related to the Ga-sublattice. The annealing kinetics of defects introduced at 300 K using alpha-particles are also presented. These kinetics are similar to those observed for defects detected after electron irradiation. A new defect (Pα0) situated 0.152 eV below the conduction band was observed after annealing for 105 minutes at 473 K.

PUBLICATIONS:

(12) S.A. Goodman and F.D. Auret, "DLTS Characterization of defects introduced in n-GaAs after alpha irradiation at 15 K", Jpn. J. Appl. Phys. **32** (1993) L1120.

(13) S.A. Goodman, F.D. Auret and G. Myburg, "Defect annealing of alpha-particle irradiated n-GaAs", Accepted for publication in Appl. Phys. A. (1994).

© University of Pretoria

UNIVERSITEIT VAN PRETORIA
UNIVERSITY OF PRETORIA
YUNIBESITHI YA PRETORIA

Jpn. J. Appl. Phys. Vol. 32 (1993) pp. L 1120–L 1122
Part 2, No. 8B, 15 August 1993

Deep Level Transient Spectroscopy Characterization of Defects Introduced in n-GaAs after Alpha Irradiation at 15 K

S. A. GOODMAN and F. D. AURET
Physics Department, University of Pretoria, Pretoria 0002, Republic of South Africa

(Received May 24, 1993; accepted for publication July 7, 1993)

Using conventional deep level transient spectroscopy (DLTS), we have characterised the defects introduced in OMVPE n-GaAs at 15 K by 5.4 MeV alpha particle irradiation from an americium 241 radio-nuclide. After this low temperature irradiation two new defects not yet reported for alpha irradiated GaAs before, Eα7 and Eα9, were detected 0.07 eV and 0.19 eV below the conduction band, respectively. The introduction rates of Eα7 and Eα9 are calculated to be 41 cm^{-1} and 187 cm^{-1} respectively. It was observed that both defects obeyed first order annealing kinetics, with Eα9 being removed at 225 K and Eα7 at 245 K corresponding to the well known stage I annealing region. The annealing rate of Eα7 corresponds to an activation energy of 0.86 eV, with a pre-exponential factor of 1.0×10^{15} s^{-1}; and the removal of Eα9 has an activation energy of 0.88 eV and a pre-exponential factor of 1.7×10^{17} s^{-1}.

KEYWORDS: GaAs, deep level transient spectroscopy (DLTS), alpha radiation, induced electron traps, defect annealing

1. Introduction

The effect of irradiating an electronic material and the consequent degradation in performance of devices made from such material will depend upon, amongst other factors, the type and dose of radiation. The increased speed and radiation hardness of GaAs have prompted an increase in the use of this semiconductor for applications in space and other radiation environments.[1,2] There have been studies on the effect of alpha-particle irradiation on material and device properties. Hopkins and Srour[3] reported for the first time on the measurement of alpha-particle induced charge in Schottky diodes fabricated on n-type GaAs. Umemoto *et al.*[4] reported on the influence of alpha-particle induced damage on the performance of metal semiconductor field-effect transistors (MESFETs). It has been well known that, in principle, it is possible to dope GaAs with impurities resulting from nuclear reactions based on thermal neutrons, gamma-rays and charged particles. Zakharenkov *et al.*[5] have shown that the most effective nuclear doping of GaAs is by alpha-irradiation. In a previous study we characterised the defects introduced by alpha particle irradiation at 300 K in n- and p-type GaAs.[6,7] However, as is well known from electron irradiation studies,[8] defects may be introduced which are very mobile even at room temperature (300 K) and it is necessary to irradiate at low temperatures in order to detect and characterize these very mobile defects. Sen Gupta *et al.*[9] made use of the positron annihilation technique to study the recovery of defects in n-type GaAs after α-irradiation at 300 K; their conclusion from this isochronal annealing study was that the defects revealed a smooth recovery at temperatures greater than 400 K. Hautojärvi *et al.*[10] revealed, using positron lifetime measurements that gallium vacancies (V_{Ga}) exist after 3 MeV electron irradiation and that they recover between 200–350 K. A study conducted by A. P. Mamontov and V. V. Peshev[11] investigated the annealing of defects introduced after room temperature irradiation; they concluded that the annealing of E3 was field dependent. For the first time we report on the traps introduced in n-GaAs after 15 K alpha irradiation from a radio-nuclide source.

2. Experimental Details

All samples used in this study were undoped n-type GaAs layers grown by organo-metallic vapour phase epitaxy (OMVPE) on silicon doped n^+ GaAs material. The free carrier density (N_D-N_A) of the epilayer and the barrier height of the palladium Schottky barrier diodes (SBDs) measured using capacitance-voltage (C-V) measurements at 1 MHz are $(1.1\pm0.1)\times10^{15}$ cm^{-3}, and (0.89 ± 0.01) eV, respectively. An americium 241 (^{241}Am) radio-nuclide foil with an activity of 192 $\mu Ci\cdot cm^{-2}$ was used to irradiate the samples at 15 K, with 5.4 MeV α-particles. During the decay of ^{241}Am to ^{237}Np, 85.5% of the alpha particles are emitted with a sharply defined energy peak at 5.484 MeV, while 12.3% have an energy of 5.441 MeV and 1.5% have an energy of 5.387 MeV. For this study the alphas liberated from the Am source are considered as monoenergetic. A two-phase lock-in amplifier-based (LIA) deep level transient spectroscopy (DLTS) system, comprising a Stanford Research SR530 LIA, a modified Boonton 72BD capacitance meter[12] and an Air Products cryostat with temperature controller, were employed to detect and to characterize the defects introduced during this low temperature α-irradiation. When characterizing defects and performing annealing studies it is very important to know the sample temperature as accurately as possible; this becomes particularly significant when temperature scanning measurements are made. To ensure that the sample is in thermal equilibrium with the cold finger a modified sample holder was utilised.[13] The DLTS[14] spectra of the irradiated material were acquired at a rate of 3.5 $K\cdot min^{-1}$. Prior to irradiation, control DLTS spectra were acquired for each sample to facilitate accurate trap identification. As it is assumed that the measured capacitance transient varies exponentially with time, it is important that the densities of introduced deep levels are small compared to that of shallow levels. The

© University of Pretoria

UNIVERSITEIT VAN PRETORIA
UNIVERSITY OF PRETORIA
YUNIBESITHI YA PRETORIA

trap density (N_T) should not be greater than 10% of the free carrier density ($N_D - N_A$) to ensure that the transients are exponential.[15]

3. Comparison of Results

Pons and Bourgoin[8] reported on two defects, labelled E7 and E9, which were detected after 1.0 MeV electron irradiation at 4 K. They did not determine the DLTS "signatures" of these defects, but did observe that they annealed at 250 K. Rezazadeh and Palmer[16] detected a trap 0.2 ± 0.03 eV below the conduction band after electron irradiation at 80 K which was completely annealed in the 220 K–300 K temperature region. These authors suggested that due to the broad peak this defect was a "plural" defect comprising two or more close energy levels and that the thermal annealing near 235 K was due to dissociation or internal conversion into simple defects, possibly E1 and E2. Guillot *et al.*[17] detected an electron trap 0.26 eV below the conduction band in n-GaAs after 95 K proton irradiation, which was removed after 300 K annealing. After this 300 K anneal stage there was an increase of approximately 30% in the concentration of E2 and E3.

The DLTS signatures of Eα7 and Eα9 (energy level E_T in the band gap and apparent capture cross-section σ_{na}) were determined from conventional DLTS Arrhenius plots of log (e_n/T^2) versus $1000/T$ using[18]

$$e_n = \gamma_n T^2 \sigma_{na} \, e^{-E_T/kT}. \quad (1)$$

Here e_n is the electron emission rate from the defect site at a temperature T, k is Boltzmann's constant and the γ_n is a constant equal to 2.21×10^{20} cm^{-2}·s^{-2}·K^{-2} for an electron trap,[19] if for simplicity the degeneracy is taken as one. The Arrhenius plots are presented in Fig. 1. From this graph the energy below the conduction band (E_T) and apparent capture cross-section (σ_{na}) of Eα7 are 0.07 ± 0.01 eV and 9.7×10^{-16} cm^{-2} and for Eα9 they are 0.19 ± 0.01 eV and 6.7×10^{-16} cm^{-2} respectively. The DLTS spectrum recorded after α-irradiation at 15 K is illustrated in Fig. 2. The spectrum presented here was recorded at a quiescent bias, $V_r = 1$ V and a filling pulse amplitude $V_p = 1.4$ V, thus allowing almost all defects in the depletion region to capture and emit electrons. The concentration of these defects relative to other α-irradiation induced defects (Eα1 and Eα2) is small, thus it was necessary to magnify the y-component of the spectrum which causes only a portion of Eα1 and Eα2 to be visible. It is evident from these curves that the Eα7 and Eα9 peaks are well defined so they would appear to be discrete defect levels associated with single defects. The defect labelled Eα8 in this figure is also introduced during 300 K α-irradiation.

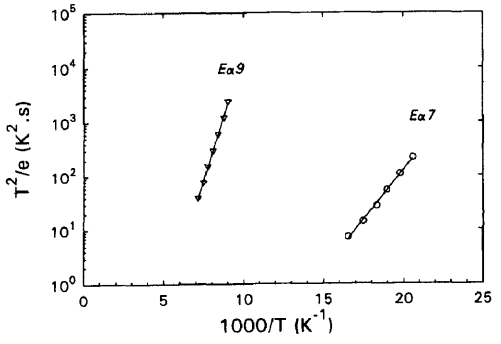

Fig. 1. Defect "signatures" of Eα7 and Eα9 on an Arrhenius plot, recorded at a quiescent bias of $V_r = 1.0$ V and a filling pulse $V_p = 1.4$ V.

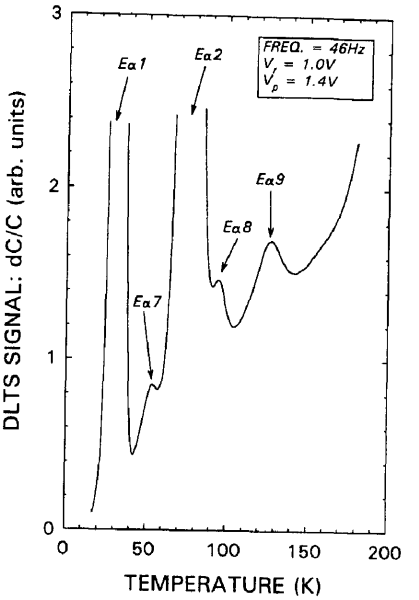

Fig. 2. DLTS spectrum of 5.4 MeV alpha (^{241}Am) irradiated samples recorded at a reverse quiescent bias of 1.0 V and a filling pulse amplitude of 1.4 V, the lock-in amplifier (LIA) frequency being 46 Hz.

As early as 1962 the annealing of n-type GaAs irradiated with electrons at room temperatures was investigated,[20] in 1970, Thommen[21] investigated the recovery of low temperature electron irradiation-induced damage in n-GaAs, identifying 3 major irreversible recovery stages (stages I, II and III). From an annealing study of low temperature α-irradiation-induced defects, it was observed that Eα9 annealed out at 225 K while Eα7 was removed at 245 K, corresponding to the stage I annealing stage. A graph of DLTS signal versus anneal time for both defects is presented in Fig. 3. From this figure it is seen that both defects undergo first order annealing kinetics. There are three possible mechanisms for first order annealing kinetics:[20] (1) close pair recombination, (2) migration directly to sinks or deep traps, and (3) trapping at certian defect sites such as impurities, followed by migration to sinks. Stievenard *et al.*[22] stated that only the short distance (correlated pairs) annealed with first order kinetics. The annealing rate (ν) of Eα7 was determined at 245 K and 255 K as 2.1×10^{-3} s^{-1} and 1.1×10^{-2} s^{-1} respectively, while the annealing rate of Eα9 at 225 K and 235 K was calculated to be 3.8×10^{-3} s^{-1} and 2.6×10^{-2} s^{-1} respectively. Using eq. (2) the activation energies[23] of Eα7 and Eα9 were calculated to be 0.86 ± 0.05 eV and 0.88 ± 0.05 eV respectively,

© University of Pretoria

UNIVERSITEIT VAN PRETORIA
UNIVERSITY OF PRETORIA
YUNIBESITHI YA PRETORIA

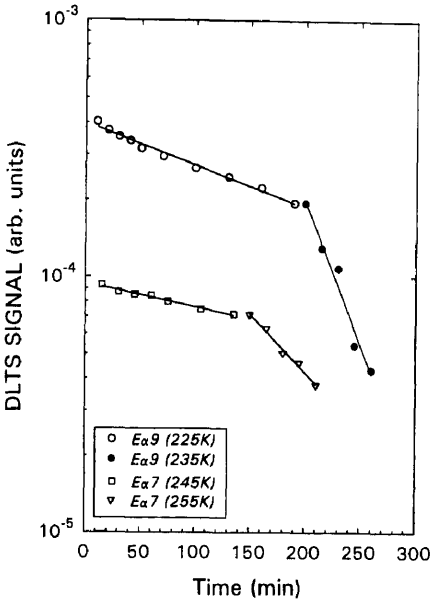

Fig. 3. DLTS signal of Eα7 (225 K and 235 K) and Eα9 (245 K and 255 K) as a function of annealing time. (DLTS signal was measured from the subtracted spectra-see text).

$$E_A = k\frac{T_1 T_2}{T_1 - T_2}\ln\left(\frac{\alpha_1}{\alpha_2}\right) \quad (2)$$

with E_A being the activation energy, α_1 the slope of the graph of defect concentration versus time at a constant temperature T_1 and α_2 the slope at a constant temperature T_2. From a knowledge of the activation energy and the annealing rate[20] the pre-exponential factors (ν_0) of Eα7 and Eα9 were calculated from equation 3 as $1\times10^{15}\ s^{-1}$ and $1.7\times10^{17}\ s^{-1}$.

$$\nu = \nu_0\, e^{-E_A/kT_i}. \quad (3)$$

Such large prefactors imply that the annealing processes in Eα7 and Eα9 involve only a small number of lattice jumps by the defects, this may be indicative of internal recombination of divacancies or complex defects into its component simpler defects. Würschum *et al.*[24] showed that a higher displacement threshold energy ($E_{th}\approx20$ eV) is required for defects that anneal out below 300 K. This higher displacement energy suggests that these defects involve divacancies or other complex defects formed by multiple displacements. It has been proposed that defects that anneal in stage I and stage II are defect complexes containing a Ga vacancy ($V_{Ga}-Ga_{As}$) which transform into a vacancy type defect on the As sublattice, (confirmed by an increase in the concentration of defects that are stable up to 500 K) which in turn anneal out at higher temperatures.[8] It has also been suggested that Thommen's stages I and II are related to the divacancy annealing which imples that divacancies are present after low temperature α-irradiation, but are unstable at room temperature.[25] From the annealing behaviour of Eα7 and Eα9 they would appear to be divacancies related to be the Ga sub-lattice which is unstable at room temperature.[26] It is generally accepted that V_{Ga} is of acceptor type[27] and can exist in negatively charged or neutral states.[28,29]

4. Conclusions

This paper has identified and characterized the electron defects introduced in $1.1\times10^{15}\ cm^{-3}$ n-type OM-VPE material with Pd SBDs during alpha irradiation from an ^{241}Am radio-nuclide at 15 K. The annealing kinetics, introduction rates and signatures of Eα7 and Eα9 have been determined and where possible correlated with traps reported after low temperature electron and proton irradiation. Eα7 and Eα9 may be complex or divacancy type defects related to the Ga sub-lattice which upon annealing, possibly recombine with a neighbouring interstitial, resulting in a single vacancy.

Acknowledgements

The financial assistance of the South African Foundation for Research Development (FRD) is gratefully acknowledged. We thank G. Myburg of the University of Pretoria for ohmic contact and SBD fabrication.

1) A. F. Galashan and S. W. Bland: J. Appl. Phys. **67** (1990) 173.
2) A. R. Knudson, A. B. Cambell, W. J. Stapor, P. Shapiro and G. P. Mueller: IEEE Trans. Nucl. Sci. **NS-32** (1985) 4388.
3) M. A. Hopkins and J. R Srour: IEEE Trans. Nucl. Sci. **NS-30** (1983) 4457.
4) Y. Umemoto, N. Masuda and K. Mitsusada: IEEE Elect. Dev. Lett. **EDL-7** (1986) No. 6.
5) L. F. Zakharenkov, V. K. Kozlovskii and B. A. Shustrov: Phys. Status Solidi (a) **117** (1990) 85.
6) S. A. Goodman and F. D. Auret: submitted to Phys. Status Solidi.
7) S. A. Goodman, F. D. Auret and W. E. Meyer: submitted to Appl. Phys. Lett.
8) D. Pons and J. C. Bourgoin: J. Phys. C **18** (1985) 3839.
9) A. Sen Gupta, S. V. Naidu and P. Sen: Appl. Phys. A **40** (1986) 95.
10) P. Hautojärvi, P. Moser, M. Stucky, C. Corbel and F. Plazaola: Appl. Phys. Lett. **48** (1986) 809.
11) A. P. Mamontov and V. V. Peshev: Sov. Phys. Semicond. **18** (1984) No. 6, 624.
12) T. I. Chappel and C. M. Ransom: Rev. Sci. Instrum. **55** (1984) 200.
13) G. Myburg, W. E. Meyer and F. D. Auret: Rev. Sci. Instrum. **63** (1992) 2101.
14) D. V. Lang: J. Appl. Phys. **45** (1974) 3014.
15) W. E. Philips and J. R. Lowney: J. Appl. Phys. **54** (1983) 2786.
16) A. A. Rezazadeh and D. W. Palmer: J. Phys. C **18** (1985) 43.
17) G. Guillot, S. Loualiche, A. Nouailhat and G. M. Martin: Inst. Phys. Ser. **59** (1981) 323.
18) P. J. Wang, T. F. Kuech, M. A. Tischler, P. M. Mooney, G. Scilla and F. Cardone: J. Appl. Phys. **64** (1988) 4975.
19) S. A. Goodman, F. D. Auret and G. Myburg: Semicond. Sci. Technol. **7** (1992) 1241.
20) L. W. Aukerman and D. D. Graft: Phys. Rev. **127** (1962) 1576.
21) K. Thommen: Radiat. Effe. **2** (1970) 201.
22) D. Stievenard, X. Boddaert, J. C. Bourgoin and H. J. von Bardeleben: Phys. Rev. B **41** (1990) 5271.
23) J. Bourgoin and M. Lannoo: *Point Defects in Semiconductors II* (Springer-Verlag, Berlin, Heidelberg, 1983) pp. 255–256.
24) R. Würschum, W. Bauer, K. Maier, A. Seeger and H. E. Schaefer: J. Phys. Condens. Matter 1 (1989) SA33–SA48.
25) D. Pons, P. M. Mooney and J. C. Bourgoin: J. Appl. Phys. **51** (1980) 2038.
26) D. Pons, A. Mircea and J. Bourgoin: J. Appl. Phys. **51** (1980) 4150.
27) G. Dlubek, O. Brümmer, F. Plazaola and P. Hautojärvi: J. Phys. C **19** (1986) 331.
28) J. Van Der Rest and P. Pecheur: Physica B **116** (1983) 121.
29) Das Sharma and A. Madhukar: Phys. Rev. B **24** (1981) 2051.

© University of Pretoria

UNIVERSITEIT VAN PRETORIA
UNIVERSITY OF PRETORIA
YUNIBESITHI YA PRETORIA

Appl. Phys. A 58, (1994)

Applied Physics A Solids and Surfaces

© Springer-Verlag 1994

Defect annealing of alpha-particle irradiated n-GaAs

S. A. Goodman, F. D. Auret, G. Myburg

Physics Department, University of Pretoria, Pretoria 0002, Rep. South Africa (Fax: +27-12/342-4143)

Received 21 December 1993/Accepted 25 April 1994

Abstract. The annealing behaviour of irradiation induces defects in n-type GaAs irradiated at 300 K with 5.4 MeV alpha-particles from an americium-241 (Am-241) radio nuclide have been investigated. The annealing kinetics are presented for the alpha-particle induced defects Eα1–Eα5 detected in Organo-Metallic Vapor Phase Epitaxially (OMVPE) grown n-GaAs doped with silicon to 1.2×10^{16} cm^{-3}, these kinetics are compared to those obtained for similar defects (E1–E5) detected after electron irradiation. While defects Pα1 and Pα2 were detected after removal of the electron defects Eα4 and Eα5, respectively, a new defect labelled Pα0, located 0.152 eV below the conduction band, was introduced by annealing. The thermal behaviour and trap characteristics of these three defects (Pα0–Pα2) are presented. In an attempt to further characterise defects Pα0 and Pα1 a preliminary study investigating the emission rate field dependence of these defects was conducted, it was observed that defect Pα0 exhibited a fairly strong field dependence while Pα1 exhibited a much weaker dependence.

PACS: 61.80.Jh, 73.20.Hb, 81.40.Ef

A knowledge of the thermodynamic and electronic characteristics of radiation-induced defects in semiconductors may be useful in the identification of these intentionally introduced defects. The effect of irradiating an electronic material and the consequent degradation in performance of devices made from such material will depend upon, amongst other factors, the type and fluence of radiation. Particle irradiation can introduce both point and extended defects into a crystal lattice. The point defects are often referred to as primary irradiation-induced defects and are introduced by electron irradiation, whereas extended defects are usually introduced when irradiating with heavier particles (alpha-particles). The increased speed and radiation hardness of GaAs have prompted an increase in the use of this semiconductor for applications in space and other radiation environments [1,2]. Studies have been performed on the effect of alpha-particle irradiation on material and device properties. Hopkins and Srour [3] reported for the first time on the measurement of alpha-particle-induced charge in Schottky diodes fabricated on n-type GaAs. Umemoto et al. [4] reported on the influence of alpha-particle-induced damage on the performance of Metal Semiconductor Field-Effect Transistors (MESFETs). It has been well known that, in principle, it is possible to dope GaAs with impurities resulting from nuclear reactions based on thermal neutrons, gamma-rays and charged particles. Zakharenkov et al. [5] have shown that the most effective nuclear doping of GaAs is by alpha-particle irradiation. As early as 1962 the annealing of n-type GaAs irradiated with electrons at room temperature was investigated [6]. In 1970, Thommen [7] investigated the recovery of low-temperature electron-irradiation-induced damage in n-GaAs, identifying three major irreversible recovery stages (stages I, II and III). In previous studies we have characterised the defects introduced by alpha-particle irradiation at 300 K in n- and p-type GaAs [8, 9, 10], we have also characterised and presented the annealing kinetics of defects introduced by alpha-particle irradiation in n-GaAs at 15 K [10, 11]. This study is a continuation of the work presented by Auret et al. [10], where the defects introduced in n-GaAs by alpha-particle and electron irradiation are studied. The defect labelled Eα8 in this work is present in the previous DLTS scans to the right of defect Eα2 [10], but was not labelled. Sen-Gupta et al. [12] made use of the positron annihilation technique to study the recovery of defects in n-type GaAs after alpha-particle irradiation at 300 K; their conclusion from this isochronal annealing study was that the defects revealed a smooth recovery at temperatures greater than 400 K. Hautojärvi et al. [13] revealed, using positron lifetime measurements, that gallium vacancies (V_{Ga}) exist after 3 MeV electron irradiation and that they recover between 200–350 K. A study conducted by Mamontov and Peshev [14] investigated the annealing of defects introduced after room temperature irradiation; they concluded that the annealing of E3 was field dependent.

© University of Pretoria

UNIVERSITEIT VAN PRETORIA
UNIVERSITY OF PRETORIA
YUNIBESITHI YA PRETORIA

Defect-enhanced annealing due to the charge state of the defect or through carrier recombination has been extensively studied [15–17].

When defects have been intentionally introduced (during alpha-particle irradiation) in GaAs it is possible to reduce the defect concentration or even completely remove these intentionally introduced defects by annealing the material at the correct temperature for a specific period. Under annealing conditions these defects become mobile and migrate through the material, eventually recombining with their counterparts (vacancies and interstitial pairs), or by forming a new type of defect which in turn may dissociate. The activation energy associated with such a thermal process is termed the defect migration enthalpy. A knowledge of the electronic and thermal properties of defects is important in understanding the operation of devices in an environment where the device may be subjected to radiation. The rate (number of defects that dissociate per unit time) at which these defects dissociate and the order of the annealing reaction may provide more detailed information about the nature of irradiation induced defects in GaAs. Consider N defects which migrate to sinks, assuming that both the defects and the sinks are randomly distributed, then the decrease in the number of defects (dN) per unit time (dt) may be written as [18]:

$$dN/dt = -KN^{\alpha}, \tag{1}$$

with α being the order of the annealing reaction and K the rate constant which is proportional to the diffusion coefficient of the defect under consideration. Assuming a second-order reaction ($\alpha = 2$) then a plot of $1/N$ versus time (t) would yield a straight line whose gradient would be the rate constant of the reaction. In the case of a first-order reaction a plot of $\ln N$ versus time (t) would yield a straight line. The activation energy or the migration enthalpy (ΔH) may be calculated by performing isochronal anneals at different temperatures and plotting a graph of annealing rate (A) versus each anneal temperature (T), the gradient of such a graph will then be equal to $\Delta H/k$, with k, being the Boltzmann constant. Equation (2) is used for this calculation [19]:

$$A = \nu \exp(-\Delta H/kT). \tag{2}$$

The value of the pre-exponential factor ν depends upon the change in entropy (ΔS) associated with the defect migration process and the number of jumps (N_j) before the defect is annihilated

$$\nu = \frac{\nu_o}{N_j} \exp\left(\frac{\Delta S}{k}\right), \tag{3}$$

where the lattice frequency represented by ν_0 may be estimated from the Debye temperature. Rewriting (2) and making use of (3) for the pre-factor yields [20]:

$$A = \frac{\nu_o}{N_j} \exp\left(\frac{\Delta S}{k}\right) \exp\left(\frac{-\Delta H}{kT}\right). \tag{4}$$

However, the annealing rate (A) can consist of two substages (A_1 and A_2), which, according to Aukerman and Graft [6], are represented by the following equations:

$$A_1 = \nu_1 \exp(-\Delta H_1/kT), \tag{5a}$$

$$A_2 = \nu_2 \exp(-\Delta H_2/kT), \tag{5b}$$

with the total annealing rate being calculated from the sum of the two sub-stage annealing rates. Both substages may exhibit first-order kinetics, as has been illustrated for the electron-irradiation-induced defect E2. A fraction exhibits a fast annealing, while the remaining fraction exhibits a slower annealing; however, both substages are characterized by the same activation energy. A possible explanation for this two-stage recovery may be that a fraction of the defect consists of uncorrelated pairs (where annealing is limited by diffusion) and the remaining fraction consists of correlated or closed pairs (where annealing is limited by a jump over a potential barrier) [21].

It is well established that the thermal emission probability from deep levels is influenced by the local electric field within the space charge region of a semiconductor junction and due to the spatial variation of this electric field, substantial deviations from simple exponential capacitance transients have frequently been observed. The field-dependent emission rate contains information about the potential well structure around defects that might provide valuable insight into the nature of the defect. There are a few mechanisms that can be responsible for the enhanced thermal emission of a trapped carrier from a defect level. The Poole-Frenkel [22] emission enhancement is predominantly for shallow levels when there is a low electric field in the space-charge region. There are two possible tunneling mechanisms, namely, pure tuneling and phonon assisted tunneling. The phonon-assisted mechanism is very sensitive to the interaction of the deep levels with the vibronic modes of the lattice, resulting in a linear coupling mechanism between the deep levels and the lattice phonon modes. The pure tunneling mechanism is predominant in the high field regions ($> 8.0 \times 10^7$ V/m^1) [23]. When reporting the DLTS "signatures" of radiation-induced defects that exhibit a field dependent emission rate, care must be taken to reduce the influence of the high electric field in the space charge region. Ways of minimising this electric field is to use semiconductor material with a low free carrier density, or to apply low reverse quiescent voltages.

Experimental details

All samples used in this study were silicon-doped n-type GaAs layers grown by Organo-Metallic Vapour Phase Epitaxy (OMVPE) on silicon doped n^+-GaAs material. The free-carrier density (N_D-N_A) of the epilayer and the barrier height of the ruthenium Schottky-Barrier Diodes (SBDs) measured using capacitance-voltage (C–V) measurements at 1 MHz were $(1.2 \pm 0.1) \times 10^{16}$ cm^{-3}, and (0.89 ± 0.01) eV, respectively. In order to ensure that degradation of the Schottky barriers due to annealing would not influence the DLTS [23], current-voltage (I–V)

© University of Pretoria

UNIVERSITEIT VAN PRETORIA
UNIVERSITY OF PRETORIA
YUNIBESITHI YA PRETORIA

and C–V measurements, high quality ruthenium SBDs were fabricated by electron beam evaporation [25]. An americium 241 (Am-241) radio nuclide foil with an activity of 192 μCi/cm² was used to irradiate the samples at room temperature [10]. For this study the alpha-particles liberated from the Am source are considered as monoenergetic. A two-phase Lock-In-Amplifier-based (LIA) Deep-Level Transient Spectroscopy (DLTS) system, as used in [10], was used in this study. When characterizing defects and performing annealing studies it is very important to know the sample temperature as accurately as possible; this becomes particularly significant when temperature-scanning measurements are made. To ensure that the sample is in thermal equilibrium with the cold finger, a modified sample holder was utilised [26]. The DLTS spectra of the irradiated material were acquired at a rate of 5.0 K/min. Prior to irradiation, control DLTS spectra were acquired for each sample to facilitate accurate trap identification. As it is assumed that the measured capacitance transient varies exponentially with time, it is important that the densities of introduced deep levels are small compared to that of shallow levels. The trap density (N_T) should not be greater than 10% of the free carrier density (N_D-N_A) to ensure that the transients are exponential [27]. The isochronal and isothermal anneals were carried out in a quartz tube mounted in a furnace, the annealing system was flushed with ultrahigh-purity argon before and during the anneal cycle to ensure that the metal-semiconductor system remained stable [28].

Comparison of results

After irradiating silicon doped n-type GaAs with 5.1×10^{10} cm^{-2}, 5.4 MeV alpha particles from an Am-241 radio nuclide, five major electron defects (Eα1–Eα5) were detected in the temperature range 15–330 K using DLTS. Defects Eα1, Eα2, Eα4 and Eα5 are identical in their DLTS signature and annealing kinetics to the electron-irradiation-induced primary defects E1, E2, E3 and E4 [8], whereas Eα3 was not detected after electron irradiation and is believed to be a metastable defect [29]. Figure 1, illustrates the DLTS spectra of the irradiated sample. After an initial 15 min anneal at 453 K, the defect labelled Eα8, located 0.177 eV below the conduction band was removed. Insert 1 of Fig. 1 depicts the increase in DLTS peak height of Eα1 and Eα2 after subtracting spectra recorded before annealing from that recorded after a 15 min anneal at 473 K and the original peak height of defect Eα8 before it was removed after the initial anneal cycle. It can be seen that the original peak height of Eα8 (E8, [30]) is approximately of the same magnitude as the increase in peak heights of defects Eα1 and Eα2, which are speculated to be different charge states (Eα1: −/o, Eα2: o/+) of the same primary defect (vacancy – interstitial pair) [30], leading us to speculate that the defect Eα8 transforms into the vacancy-interstitial pair. From inspection of insert 2 of Fig. 1 it can be seen that a new defect labelled Pα0 with a peak temperature of 102 K, at 46 Hz, was detected during the annealing of the alpha-particle-induced defects in n-GaAs. From Fig. 2 it can be seen that this defect was first detected by DLTS after the sample has been annealed at 473 K for 105 min, the concentration of this new defect increases as the anneal cycle progresses. The DLTS "signature" (energy E_t and apparent capture cross-section σ_{na}) of this defect as detected by a conventional DLTS (recorded at a quiescent reverse bias of 1.0 V and a filling pulse amplitude of 0.6 V) Arrhenius plot, was 0.152 eV and 1.7×10^{-15} cm^{-2}, respectively.

Figure 2 illustrates the annealing kinetics of defects Eα1–Eα5. Firstly, the change in defect concentration of defects Eα1 and Eα2 with temperature and time follow the same trend, confirming the previous speculations that they are indeed different charge states of the same defect. As has been observed in electron-irradiated material [19], upon removal of Eα4 (E3) and Eα5 (E4), two new defects

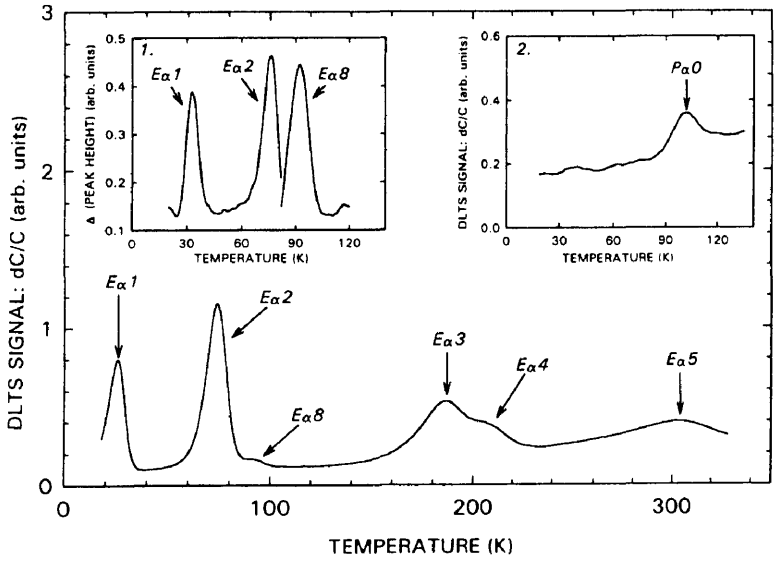

Fig. 1. DLTS spectrum of 5.4 MeV alpha-particle irradiated n-GaAs recorded at a reverse quiescent bias of 2.0 V and a filling pulse amplitude of 0.5 V, the LIA frequency being 46 Hz. Insert 1, illustrates the increase in DLTS peak height of electron defects Eα1 and Eα2 after removal of electron defect Eα8. Insert 2 illustrates the new defect Pα0, detected after the sample was annealed at 473 K for 105 min.

© University of Pretoria

UNIVERSITEIT VAN PRETORIA
UNIVERSITY OF PRETORIA
YUNIBESITHI YA PRETORIA

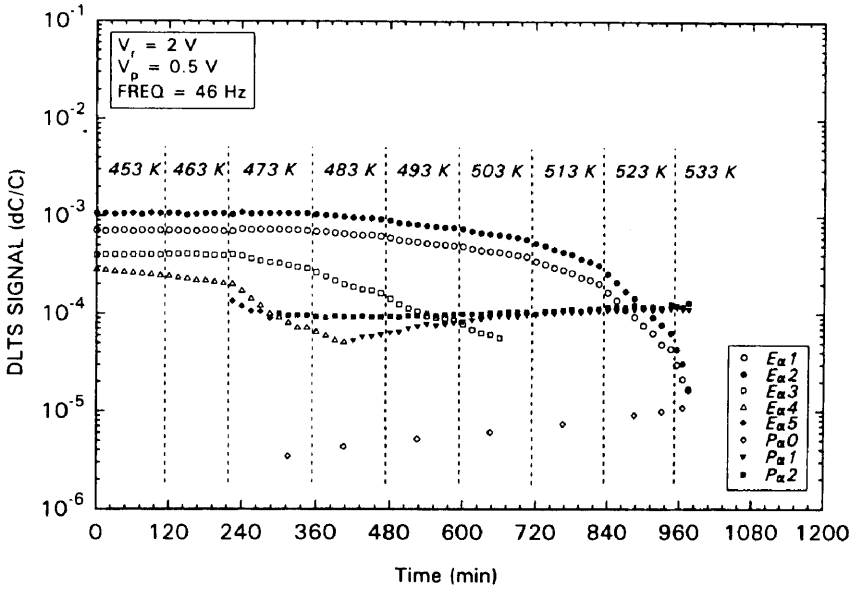

Fig. 2. Change in DLTS peak height of defects Eα1–Eα5 and Pα0–Pα2 as a function of time for temperatures ranging from 435 K to 533 K.

Pα1 and Pα2 emerge. These defects are believed to be present in the irradiated material prior to annealing but the presence of Eα4 and Eα5 prevents their detection. The DLTS "signatures" (position in the band gap and apparent capture cross-section) of Pα1 (0.376 eV, 1.8×10^{-14} cm^{-2}) and Pα2 (0.60 eV, 3.8×10^{-14} cm^{-2}) as well as their annealing behaviour confirm that they are indeed similar to P1 (0.36 eV, 6.9×10^{-15} cm^{-2}) and P2 (0.50 eV, 1.4×10^{-15} cm^{-2}) detected after annealing of electron-irradiated material [19]. In the present study it was very difficult to accurately determine the annealing kinetics of defect Eα5. A possible explanation for this is the presence of the EL2 defect in the OMVPE material which distorts the neighbouring DLTS peak of defect Eα5. Future studies using EL2 "free" MBE-grown material will be conducted to determine if this defect is indeed similar to the electron-induced defect E4. It has, however, been confirmed that this defect does anneal out during stage III. An abrupt change in the concentration of defect Eα4 from annealing temperature 463–473 K occurred, the reason for this being unclear at present. The same trend was observed using a different SBD annealed under the exact same conditions and it may possibly be due to the detection of Pα1 which is situated at approximately the same position in the bandgap as Eα4 and is masked by Eα4 up to 483 K.

For the first time the annealing kinetics of the metastable defect Eα3, detected in alpha-particle and proton-irradiated n-GaAs is presented [8, 10]. To determine the order of the annealing reaction for this defect, (1) was used with α being the order of the reaction. It was seen that a graph of ln$N$ versus time resulted in a straight line with a higher regression coefficient than a plot of $1/N$ versus time. Therefore, we conclude that the annealing reaction is primarily first order. As this defect is a metastable defect it may transform into another configuration before being completely removed, so the possibility of the annealing kinetics of this defect being a combination of different first-order processes definitely exists. However, we believe that the dominant reaction is first order and from the activation energy and pre-factor it would seem that it can be ascribed to the annihilation of a close pair.

There are three possible mechanisms for first-order annealing kinetics [6]: (i) close pair recombination, (ii) migration directly to sinks or deep traps, and (iii) trapping at certain defect sites such as impurities, followed by migration to sinks. Stievenard et al. [21] stated that only the short distance (correlated pairs) annealed with first-order kinetics. In this study the concentration of the intentionally introduced defects were approximately two orders of magnitude less than the dopant concentration, thus we assume that the Fermi level does not move very much during the course of the anneal. To confirm that there were no extensive changes in the free carrier concentration during annealing, a second sample identical to the DLTS sample was annealed simultaneously and capacitance-voltage measurements were performed to monitor the free-carrier density. Making use of (4), and assuming a typical lattice frequency $v_o = 6 \times 10^{12}$ s^{-1}, then it can be seen that only a few jumps (N_j) are necessary to annihilate the defect, thus confirming what has previously been published for annealing of electron-irradiation-induced defects, namely that the electron defects are close pairs.

The results of the annealing study are presented in Table 1, the results obtained from this study are compared to the annealing kinetics of those defects detected after electron irradiation by Pons et al. [19] and Lang et al. [31]. Obviously, a more ideal comparison would be to compare our data to electron irradiation annealing kinetics performed in our laboratory. From the table it can be seen that our data compare reasonably well with those obtained for electron irradiation, with the exception of the pre-factors (v), which are slightly smaller in our case. These factors, however, strongly depend on the annealing temperature, and so, small changes in this tem-

© University of Pretoria

UNIVERSITEIT VAN PRETORIA
UNIVERSITY OF PRETORIA
YUNIBESITHI YA PRETORIA

Table 1. Activation energy (ΔH), pre-exponential factor (ν) and annealing temperature of the major electron traps detected in alpha-particle-irradiated n-GaAs

Defect label	ΔH[eV]	ν[s^{-1}]	Anneal. temp. [K]
Pons et al.[18]			
E1	–	–	–
E2′	1.55 ± 0.15	$10^{13.5 \pm 0.5}$	500
E2″	1.60 ± 0.15	$10^{12.5 \pm 0.5}$	500
E3	1.55 ± 0.15	$10^{13.5 \pm 0.5}$	470
E4	1.50 ± 0.20	$10^{13.0 \pm 1.0}$	470
E5	1.55 ± 0.15	$10^{13.5 \pm 0.5}$	470
Lang et al.[31]			
E1	–	–	–
E2′	1.75 ± 0.17	$10^{13 \pm 1}$	500
E2″	1.75 ± 0.17	$10^{13 \pm 1}$	500
E3	1.40 ± 0.15	$10^{12 \pm 1}$	500
E4	–	–	–
E5	1.40 ± 0.15	$10^{12 \pm 1}$	500
This work			
Eα1	1.55 ± 0.10	$10^{12.0 \pm 0.5}$	500
Eα2	1.60 ± 0.10	$10^{12.0 \pm 0.5}$	500
Eα3	1.55 ± 0.10	$10^{12.5 \pm 0.5}$	460
Eα4	1.45 ± 0.10	$10^{11.0 \pm 1.0}$	460
Eα5	–	–	–
Eα8	–	–	453
Pα0	–	–	473*
Pα1	–	–	–
Pα2	–	–	–

* Formation temperature

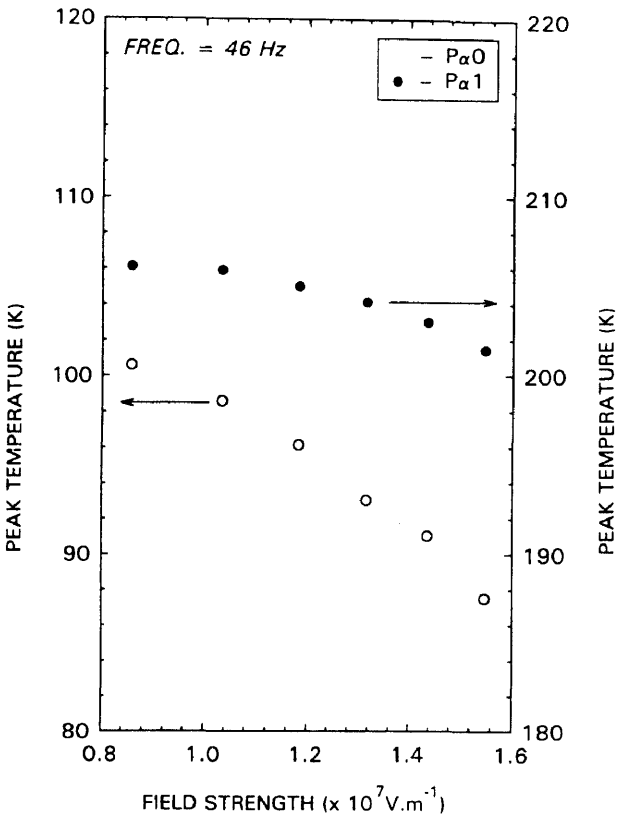

Fig. 3. DLTS peak positions of Pα0 and Pα1 recorded at a lock-in amplifier frequency of 46 Hz as a function of electric field strength in the space charge layer

perature could be responsible for this discrepancy. Unlike the electron studies [19, 31] where two first-order sub-stages with different pre-exponential factors for the electron defect E2 have been observed, only one first-order annealing stage was observed for the similar defect (Eα2) observed after alpha-particle irradiation, even when the annealing temperature was as low as 453 K. In Table 1, we have denoted Eα2 as two sub-stages (Eα2' and Eα2") with the same annealing properties, even though at present only one stage has been observed. This conclusion was confirmed by repeating the measurement in the 453–463 K annealing range using a new irradiated sample.

From a preliminary investigation into the electric field dependence of the emission rate of Pα0 and Pα1, it was observed that Pα0 exhibited a fairly strong field dependence, whereas Pα1 exhibited a weak dependence. Figures 3 illustrates the DLTS peak positions of these two defects recorded at a LIA frequency of 46 Hz as a function of electric field strength in the space charge layer. it can be seen that the peak position of Pα0 shifts from 102 K at a field strength of 8.5×10^6 V/m to 87 K when the field strength is 1.6×10^7 V/m. The peak position of defect Pα1, on the other hand, only shifts approximately 4 K for the same difference in field strengths. To determine which mechanism is responsible for the lowering of the ionisation energy of these two defects, further studies are being conducted where materials with different free carrier densities are used in order to allow one to examine the field dependence over an appreciable range of field strengths.

Conclusions

This paper has identified and characterized the electron defects introduced in silicon doped, 1.2×10^{16} cm^{-3} n-type OMVPE GaAs with Ru SBDs during alpha-particle irradiation from an Am-241 radio-nuclide at room temperature. As in electron irradiation, alpha-particle irradiation produces the primary defect pairs (Eα1, Eα2, Eα4 and Eα5). An additional metastable defect Eα3 was detected after alpha-particle irradiation. It has also been speculated using the DLTS "signatures" that the alpha-particle irradiation-induced defects (Eα1, Eα2, Eα4 and Eα5) are the same majority carrier traps observed after electron irradiation (E1, E2, E3 and E4). Apart from revealing the annealing kinetics of alpha-particle-induced electron traps, this study also confirms that the defects introduced after alpha-particle irradiation at room temperature are indeed the same defects detected after electron irradiation at the same temperature. We speculate that defect Eα8 dissociates into defects Eα1 and Eα2 after a short anneal at 453 K. The annealing kinetics

© University of Pretoria

UNIVERSITEIT VAN PRETORIA
UNIVERSITY OF PRETORIA
YUNIBESITHI YA PRETORIA

of Eα1 (E1) are also presented for the first time. A new defect (Pα0) which was detected 0.152 eV below the conduction band was detected after annealing for 105 min at 473 K. Both Pα0 and Pα1 have emission rates which depend upon the field strength in the space-charge layer.

Acknowledgements. The financial assistance of the South African Foundation for Research Development (FRD) is gratefully acknowledged.

References

1. A.F. Galashan, S.W. Bland: J. Appl. Phys. **67,** 173 (1990)
2. A.R. Knudson, A.B. Cambell, W.J. Stapor, P. Shapiro, G.P. Mueller: IEEE Trans. NS-**32,** 4388 (1985)
3. M.A. Hopkins, J.R. Srour: IEEE Trans. NS-**30,** 4457 (1983)
4. Y. Umemoto, N. Masuda, K. Mitsusada: IEEE EDL-**7,** 396 (1986)
5. L.F. Zakharenkov, V.K. Kozlovskii B.A. Shustrov: phys. stat. sol. (a) **117,** 85 (1990)
6. L.W. Aukerman, D.D. Graft: Phys. Rev. **127,** 1576 (1962)
7. K. Thommen: Radiat. Eff. **2,** 201 (1970)
8. S.A. Goodman, F.D. Auret, M. Hayes, G. Myburg, W.E. Meyer: phys. stat. sol. (a) **140,** (1993)
9. S.A. Goodman, F.D. Auret, W.E. Meyer: J. Appl. Phys. (1993) (in press)
10. F.D. Auret, S.A. Goodman, G. Myburg, W.E. Meyer: Appl. Phys. A **56,** 547 (1993)
11. S.A. Goodman, F.D. Auret: Ipn. J. Appl. Phys. Lett. **32,** 1120 (1993)
12. A. Sen-Gupta, S.V. Naidu, P. Sen: Appl. Phys. A **40,** 95 (1986)
13. P. Hautojärvi, P. Moser, M. Stucky, C. Corbel, F. Plazaola: Appl. Phys. Lett. **48,** 809 (1986)
14. A.P. Mamontov, V.V. Peshev: Sov. Phys. Semicond. **18,** 624 (1984)
15. D. Stievenard, J.C. Bourgoin: Phys. Rev. B **33,** 8410 (1986)
16. D. Pons: Inst. Phys. Conf. Ser. **59,** 269 (1981)
17. D.V. Lang, L.C. Kimerling: Phys. Rev. Lett. **35,** 22 (1975)
18. J.C. Bourgoin: *Point Defects in Semiconductors II* Springer Ser. Solid-State Sci., Vol. 35 (Springer Berlin, Heidelberg 1983) p. 252
19. D. Pons, A. Mircea, J.C. Bourgoin: J. Appl. Phys. **51,** 4150 (1980)
20. J.W. Farmer, D.C. Look: Phys. Rev. **21,** 3389 (1990)
21. D. Stievenard, X. Boddaert, J.C. Bourgoin, H.J. von Bardeleben: Phys. Rev. **B 41,** 5271 (1990)
22. J. Frenkel: Phys. Rev. **54,** 657 (1938)
23. G. Vincent, A. Chantre, D. Bois: J. Appl. Phys. **50,** 5484 (1979)
24. D.V. Lang: J. Appl. Phys. **45,** 3014 (1974)
25. G. Myburg, F.D. Auret: Appl. Phys. Lett. **60,** 604 (1992)
26. G. Myburg, W.E. Meyer, F.D. Auret: Rev. Sci. Instrum. **63,** 2101 (1992)
27. W.E. Philips, J.R. Lowney: J. Appl. Phys. **54,** 2786 (1983)
28. G. Myburg, W.O. Barnard, W.E. Meyer, F.D. Auret, H. Burger: Thin Solid Films **213,** 113 (1992)
29. F.D. Auret, R.M. Erasmus, S.A. Goodman: Appl. Phys. Lett. (1993) (submitted)
30. D. Pons, J.C. Bourgoin: J. Phys. C **18,** 3839 (1985)
31. D.V. Lang, R.A. Logan, L.C. Kimerling: Phys. Rev. B **15,** 4874 (1977)

© University of Pretoria

PUBLICATIONS:

(3) S.A. Goodman, F.D. Auret, M. Hayes, G. Myburg and W.E. Meyer, "Electrical and Defect Characterization of n-Type GaAs Irradiated with α-Particles Using a Van de Graaff Accelerator and an Am-241 Radio-Nuclide Source", Phys. Status Solidi (a), **140** (1993) 381.

(4) S.A. Goodman, F.D. Auret, M. Hayes, G. Myburg and W.E. Meyer, "Effect of RBS analysis on the quality of Schottky barrier diodes on GaAs", S. Afr. J. Phys. **16** (1993) 54.

(5) F.D. Auret, S.A. Goodman, G. Myburg and W.E. Meyer, "Electrical Characterization of Defects Introduced in n-GaAs by Alpha and Beta Irradiation from Radionuclides", Appl. Phys. A, **56** (1993) 547.

(6) S.A. Goodman, F.D. Auret and W.E. Meyer, "Hole defects in molecular beam epitaxially grown p-GaAs introduced by alpha irradiation", J. Appl. Phys. **75** (1994) 1222.

(7) S.A. Goodman, F.D. Auret and W.E. Meyer, "The effect of alpha-particle and proton irradiation on the electrical and defect properties of n-GaAs", Nucl. Instrum. & Methods B, **90** (1994) 349.

(8) F.D. Auret, S.A. Goodman, W.E. Meyer, R.M. Erasmus and G. Myburg, "Electronic Properties of Defects Introduced During Electron and Alpha Irradiation of GaAs", Mater. Sci. Forum, vols **143-147** (1994) 1559.

(9) F.D. Auret, S.A. Goodman, W.E. Meyer, R.M. Erasmus and G. Myburg, "DLTS characterization of electron irradiation induced hole traps in p-GaAs grown by MBE", Jpn. J. Appl. Phys. **32** (1993) L974.

© University of Pretoria

(10) F.D. Auret, S.A. Goodman, M. Hayes, G. Myburg, W.O. Barnard and W.E. Meyer, "Electrical characterization of particle-induced damage in n-GaAs", S. Afr. J. Phys. **16** (1993) 153.

© University of Pretoria

UNIVERSITEIT VAN PRETORIA
UNIVERSITY OF PRETORIA
YUNIBESITHI YA PRETORIA

phys. stat. sol. (a) **140**, 381 (1993)

Subject classification: 61.80; 71.55; 73.20; S7.12

Department of Physics, University of Pretoria[1])

Electrical and Defect Characterization of n-Type GaAs Irradiated with α-Particles Using a van de Graaff Accelerator and an Am-241 Radio-Nuclide Source

By

S. A. GOODMAN, F. D. AURET, M. HAYES, G. MYBURG, and W. E. MEYER

Radiation damage effects are studied in OMVPE n-GaAs for a wide range of alpha (α) particle fluences, using an americium-241 (Am-241) radio-nuclide and a linear van de Graaff accelerator as the particle sources. The samples are irradiated at 300 K, after fabricating palladium Schottky barrier diodes (SBDs) on the 1.2×10^{16} cm^{-3} Si doped epitaxial layers. The radiation induced defects are characterized using conventional deep level transient spectroscopy (DLTS). A correlation is made between the change in SBD characteristics and the quantity and type of defects introduced during α-particle irradiation. It is shown that the two parameters most susceptible to this irradiation are the reverse leakage current of the SBDs and the free carrier density of the epilayer. The introduction rate and the "signatures" of the α-particle irradiation induced defects are calculated and compared to those of similar defects introduced during electron irradiation.

Effekte von Strahlenschäden in OMVPE n-GaAs sind als Funktion der α-Teilchendosis untersucht worden, wobei das Radionuklid Americium-241 und ein van de Graaff-Beschleuniger als Strahlenquellen benutzt wurden. Die Proben sind Palladium-Schottky-Dioden, die auf 1.2×10^{16} cm^{-3} Si-dotierten epitaktischen Schichten hergestellt und bei 300 K bestrahlt werden. Zwecks Bestimmung der strahleninduzierten Defekte werden konventionelle DLTS-Messungen (deep level transient spectroscopy) durchgeführt. Die Änderung der Schottky-Parameter wird verglichen mit der Dichte und Art der durch die Strahlung erzeugten Defekte. Die beiden Parameter, die am stärksten beeinflußt werden, sind der Sperrstrom der Schottky-Diode und die freie Ladungsträgerdichte der epitaktischen Schicht. Erzeugungsrate und Eigenschaften der durch α-Teilchen erzeugten Defekte werden mit denjenigen verglichen, die nach Bestrahlung mit Elektronen beobachtet werden.

1. Introduction

Gallium arsenide is an important material in field-effect transistors, heterojunction bipolar transistors, solar cells, and integrated circuits, and since these components are becoming increasingly important in space applications [1] due to their increased speed and resistance to radiation damage [2], a knowledge of the influence of radiation damage on their performance has become an active field of research. Hopkins and Srour [3] reported for the first time on the measurement of α-particle induced charge in Schottky diodes fabricated on n-type GaAs. Umemoto et al. [4] reported the influence of α-particle induced damage on the performance of metal–semiconductor field-effect transistors (MESFETs) fabricated on semiinsulating GaAs, whereas Zardas et al. [5] investigated the dependence of the current–voltage (I–U) characteristics of GaAs MESFETs on temperature and α-particle irradiation. It has been well known for decades that, in principle, it is possible to dope gallium arsenide with impurities resulting from nuclear reactions based on thermal neutrons,

[1]) Pretoria 0002, South Africa.

© University of Pretoria

UNIVERSITEIT VAN PRETORIA
UNIVERSITY OF PRETORIA
YUNIBESITHI YA PRETORIA

γ-rays, and charged particles. Zakharenkov et al. [6] have shown that the most effective nuclear doping of GaAs is by α-irradiation. Clearly there is a need for a comprehensive study of the change in electrical properties and the nature and quantity of introduced defects due to α-particle irradiation over a wide range of fluences.

This study is divided into two sections. The first part deals with the change in current–voltage (I–U) and capacitance–voltage (C–U) characteristics of SBDs fabricated on 1.2×10^{16} cm^{-3} silicon (Si) doped OMVPE layers, with attention being paid to the change in the reverse leakage current and the free carrier density. The second part deals with the nature and quantity of defects introduced during α-particle irradiation over a wide range of fluences as measured using DLTS [7]. The two principle mechanisms, by which ions lose energy in bulk materials, are by transferring energy to the atoms in the material and to the electrons bound to the atoms. The transfer of energy to the electrons is called ionization loss, but, although it is the dominant energy loss mechanism, it is not thought to produce a significant amount of damage. The net effect of the ionization losses is some heating of the crystal. The transfer of energy to the lattice atoms creates vacancies and interstitials, but only if the magnitude of the energy transfer is greater than the displacement threshold, T_D (the minimum energy transmitted to a lattice atom, necessary to produce a displacement) which for GaAs is found to be 9 to 10 eV [8].

2. Experimental Procedure

The samples studied in this work were n-type GaAs films, 5.0 μm thick, grown using organometallic vapour phase epitaxy (OMVPE) on n^+ bulk-grown substrates. The free carrier density of the silicon-doped n-type films was 1.2×10^{16} cm^{-3}. The free carrier densities were determined by standard C–U measurements at a frequency of 1 MHz. Ohmic contacts were formed prior to SBD fabrication by the deposition of Ni–AuGe–Au on the n^+ backsides of the substrates and annealing at 450 °C for 2 min in a high-purity Ar atmosphere. After degreasing, chemical etching (in $H_2O:H_2O_2:NH_4OH$, ratio of 120:1:3), followed by oxide removal (in H_2O:HCl, ratio of 1:1) and a final rinse in de-ionized water, circular Pd contacts 0.75 mm in diameter and 300 nm thick were deposited onto the GaAs at a rate of 0.4 nm/s through a metal contact mask. Prior to exposure the SBDs were electrically characterized by I–U and C–U measurements under dark conditions using a system based around an HP4140B pA/dc source and an HP4192A LF impedance analyzer, respectively, during which currents as low as 10^{-14} A could be measured. All I–U and C–U measurements were performed in the temperature range 297.0 to 300.0 K.

A two-phase lock-in amplifier-based (LIA) DLTS system, comprising a Stanford Research SR530 LIA, a modified Boonton 72BD capacitance meter [9], and an Air Products cryostat with temperature controller was employed to detect and to characterize the defects introduced during α-particle irradiation. The DLTS spectra were acquired at a rate of 3 K min^{-1} in both temperature directions so as to eliminate any peak temperature discrepancies due to uneven cooling and heating. Prior to exposure, control DLTS spectra were acquired for each batch of samples to facilitate accurate trap concentration measurements.

The α-particle fluence rate achievable from the linear van de Graaff accelerator was 1.4×10^{11} cm^{-2} s^{-1}, with an accelerating voltage as high as 2.5 MeV. To obtain lower radiation fluences a 5.4 MeV Am-241 radio-nuclide source with an activity of 192 μCi cm^{-2} was used. Making use of this source, particle fluence rates as low as 7.1×10^6 cm^{-2} s^{-1}

© University of Pretoria

UNIVERSITEIT VAN PRETORIA
UNIVERSITY OF PRETORIA
YUNIBESITHI YA PRETORIA

could be obtained. As it is assumed that the measured capacitance transient varies exponentially with time, it is important that the densities of deep levels are small compared to that of shallow levels. The trap density (N_T) should not be greater than 10% of the free carrier density ($N_D - N_A$) to ensure that the transients are exponential [10]. For each fluence and particle type, 3 to 4 samples were irradiated, for a reasonable average.

3. Results and Discussion

3.1 I–U and C–U measurements

From a preliminary study it was found that the two most sensitive parameters to incident radiation were the reverse leakage current (I_R) of the SBDs and the free carrier density ($N_D - N_A$) of the epilayer. The variation of the parameters measured using the $I-U$ and $C-U$ techniques in the temperature range (297 to 300 K) were monitored for unirradiated, as well as α-particle irradiated material. From this investigation it was seen that only the reverse leakage current exhibited a strong temperature dependence. There was a 50% change in this value from 297 to 300 K for unirradiated material. It is important when comparing values before and after irradiation to ensure that there are no temperature dependent discrepancies. To minimize such errors, correction factors were used to normalize all current measurements to 300 K. All other parameters (e.g. barrier height, ideality factor, and built-in voltage) were temperature independent in this small temperature range. When considering the temperature dependence of current contributions only from thermionic emission and recombination–generation processes (not diffusion etc.) and comparing them to the experimental variation in reverse leakage current as a function of temperature (297 to 300 K), it is observed that the experimentally measured current values are not solely due to only these two current transport mechanisms but a weighted combination of these and other mechanisms.

For this study it was the intention to determine from $C-U$ measurements the number of free carriers removed for fluences ranging from 1.3×10^{10} to 8.5×10^{13} cm^{-2} and compare these carrier removal concentrations with the individual trap concentrations as determined from DLTS concentration profile measurements. It must be noted that the interpretation of $C-U$ profiles in the presence of deep states calls for considerable care [11]. Fig. 1 illustrates the change in free carrier density ($N_D - N_A$) after irradiation and the free carrier removal density as a function of fluence using both the linear van de Graaff accelerator and the Am-241 radio-nuclide. From these graphs, the carrier removal rate per incident α-particle can be calculated. The number of free carriers removed per incident α-particle in the dose range 2.6×10^{10} to 6.2×10^{11} cm^{-2} is 12903 cm^{-1}. This value was calculated in the range where the variation of free carrier removal as a function of fluence was linear. For fluences larger than these, nearly all of the free carriers were removed by the introduced defects, and any free carrier concentration measurement becomes highly inaccurate and therefore meaningless. The carrier removal rate value is specified per incident particle for every centimetre the incident particle travels. When making use of the van de Graaff accelerator the penetration depth of the incident α-particles can be calculated using the LSS theory [12], however, when using the Am-241 source this depth is very difficult to calculate as the incident penetration angle can vary considerably. Assuming that the incident beam enters the crystal at an incident angle of 0°, the penetration depth of the 2.0 and the 5.4 MeV beam would be 5.4 and 20.4 μm, respectively.

© University of Pretoria

UNIVERSITEIT VAN PRETORIA
UNIVERSITY OF PRETORIA
YUNIBESITHI YA PRETORIA

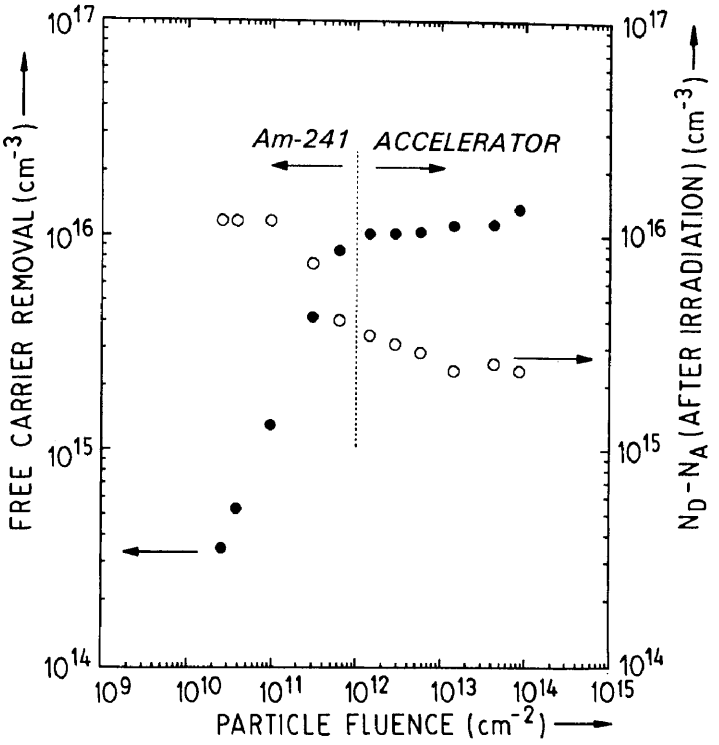

Fig. 1. Free carrier removal and free carrier density after irradiation vs. α-particle fluence. The initial free carrier density being 1.2×10^{16} cm^{-3}

From inspection of Fig. 2, where the change (reverse leakage current after irradiation minus reverse leakage current before irradiation) in reverse leakage current measured at 1.0 V (ΔI_R) is plotted as a function of incident α-particle fluence, it can be seen that there is a linear change. It must be noted that the ideality factor (n) for the irradiated samples was not larger than 1.05, hence the dominant current transport mechanism in the forward bias region (0.15 to 0.40 V) is still thermionic emission. From $I-U$ measurements it was

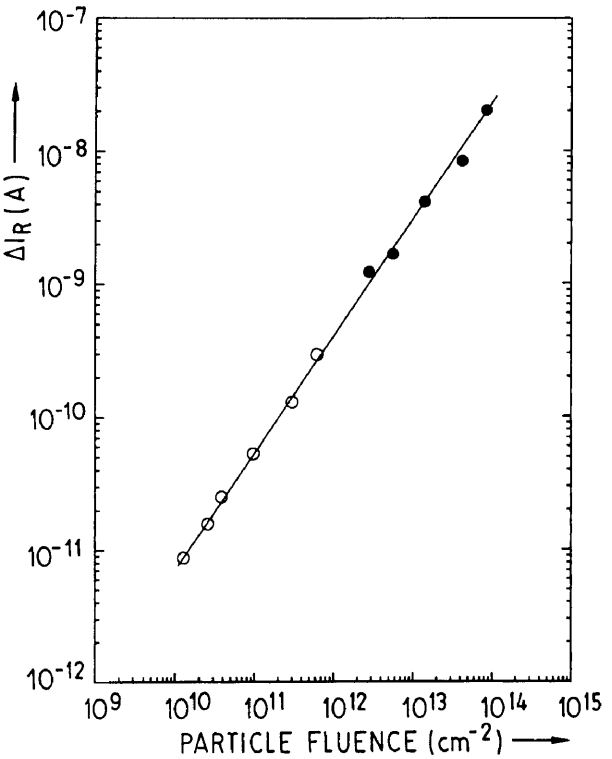

Fig. 2. The increase in reverse leakage current ($\Delta I_R = I_{R\,after} - I_{R\,before}$) measured at 1.0 V vs. incident fluence for a van de Graaff accelerator (2.0 MeV) (●) and an Am-241 radio-nuclide source (5.4 MeV) (○)

© University of Pretoria

UNIVERSITEIT VAN PRETORIA
UNIVERSITY OF PRETORIA
YUNIBESITHI YA PRETORIA

seen that there was no significant decrease in the barrier height, so any increase in this reverse leakage current cannot be accounted for by a reduction in the barrier height. The change in the reverse leakage current as a function of incident fluence for both the 5.4 MeV radio-nuclide (1.3×10^{10} to 6.2×10^{11} cm^{-2}) and the 2.0 MeV linear accelerator (2.8×10^{12} to 8.5×10^{14} cm^{-2}) follow a similar linear trend, even though their incident energies vary by a factor of 2. A possible explanation for this is that in the linear accelerator channelling of the incident particles occurs, whereas when using the radio-nuclide, the sample is placed face down on the active material and the particles can enter the semiconductor over a wide range of incident angles.

The model proposed by Donoval et al. [13] was modified by accounting for the effect of image force lowering, this model determines the barrier height of rectifying metal–semiconductor contacts avoiding the use of the so called ideality factor n, the magnitude of the series resistance, and the recombination current of a metal–semiconductor system can be calculated. The equations used in this modelling procedure are as follows:

$$I = I_s \{\exp [q(V - IR_s)/kT] - 1\} + I_g \{\exp [q(V - IR_s)/2kT] - 1\} + (V - IR_s)/R_{sh} \quad (1)$$

with the thermionic emission saturation current pre-factor (I_s) represented by the following equation:

$$I_s = AA^*T^2 \exp(-\Phi_B/kT) \quad (2)$$

with R_{sh} being the leakage resistance (important in low-voltage regions, $qV \ll kT$), R_s the series resistance, A the area of the diode, $A^*(A^* = 4.8 \times 10^4$ Am^{-2} K$^{-2})$ [14] is the experimentally obtained Richardson constant for palladium on GaAs.

From inspection of inset B of Fig. 3, where the I–U curves for an unirradiated (control) sample and irradiated samples are depicted it can be seen that after irradiation the recombination current dominates the current flow in the low forward bias region (0.01 to 0.1 V) and increases as the incident fluence increases. The forward characteristics of the irradiated samples were modelled using a modified model of Donoval et al. [13], from which the magnitude of the recombination pre-factor and the series resistance were obtained, these values are depicted in Table 1. From this table it can be seen that as the α-fluence increases from 3.0×10^{11} to 6.2×10^{11} cm^{-2} there is a corresponding increase in the recombination pre-factor and the series resistance. Inset A of Fig. 3 illustrates the change in forward current as a function of voltage (note the linear y-axis). It is seen that the control sample has the lowest series resistance, whereas the diode that received the highest particle fluence has the highest series resistance. The increase in the series resistance does not appear to be due to degradation of the Schottky contact or the ohmic contact as they did not deteriorate during irradiation, however, where the incident particles come to rest in the semiconductor material a damaged layer is caused which results in this increased series resistance. From Fig. 1 it is clearly evident that there was a carrier reduction after irradiation. The carrier reduction was due to the introduction of defect levels at various positions in the band gap, these levels trap the free carriers, this reduction in free carrier density in turn leads to an increase in the resistivity of the material, which is observed in the increased series resistance measured after irradiation. The most effective recombination centres are those centres located near the middle of the band gap whose electron and hole capture cross-sections are equal [15].

© University of Pretoria

UNIVERSITEIT VAN PRETORIA
UNIVERSITY OF PRETORIA
YUNIBESITHI YA PRETORIA

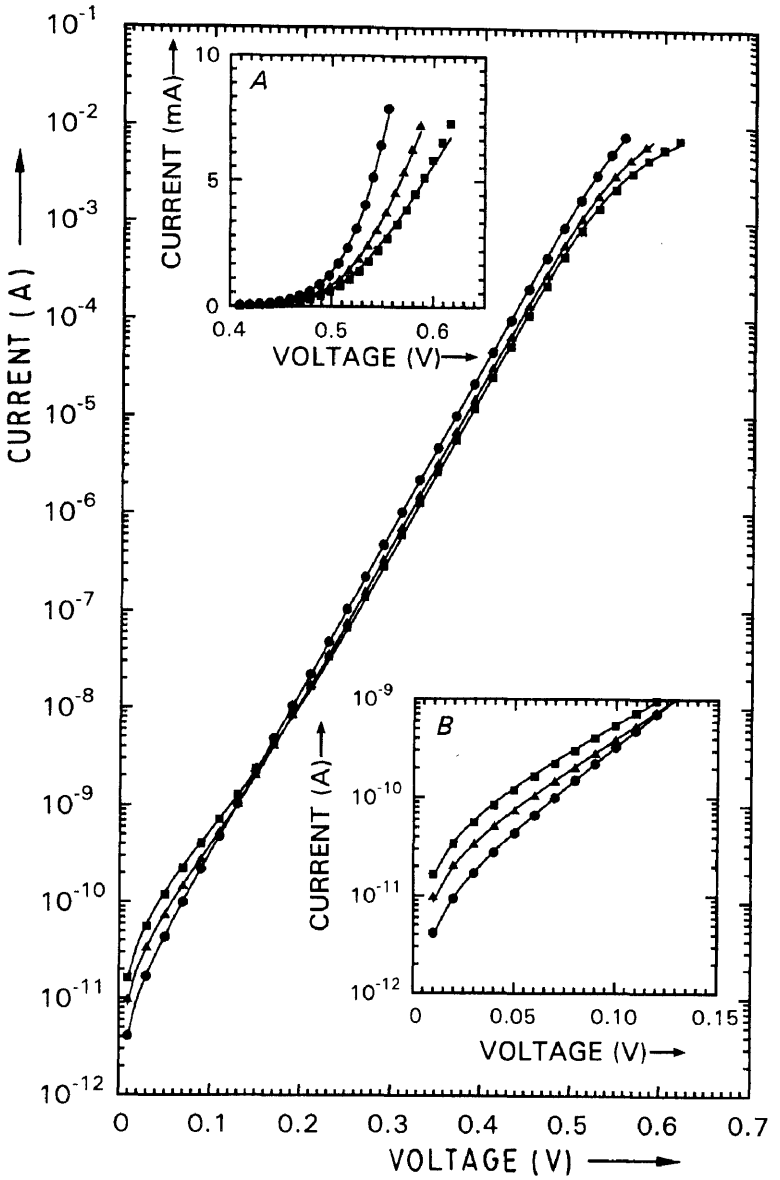

Fig. 3. The $I-U$ characteristics for a control (unirradiated) diode (●), for an incident α-particle fluence of 3×10^{11} cm^{-2} (▲), and for a fluence of 6.2×10^{11} cm^{-2} (■). The modelled (———) $I-U$ characteristics for all three curves were obtained using the modified model of Donoval et al. [13]. Inset A: illustration of the effect of an increase in series resistance on the forward current as a function of incident α-particle fluence. Inset B: illustration of the increase in the recombination current as the incident fluence increases

Table 1

Recombination current pre-factor (I_g) and the series resistance (R_s) as a function of incident alpha (α) fluence, using a modified version of the model of Donoval et al. [13]

fluence (cm^{-2})	I_g (A)	R_s (Ω)
control (unirradiated)	3.9×10^{-12}	1.6
3.0×10^{11}	2.9×10^{-11}	4.9
6.2×10^{11}	6.5×10^{-11}	8.5

© University of Pretoria

UNIVERSITEIT VAN PRETORIA
UNIVERSITY OF PRETORIA
YUNIBESITHI YA PRETORIA

The increase in the recombination current observed as a function of incident fluence in Table 1 is probably due to the presence of such centres introduced during irradiation, the concentration of which depends upon the total incident α-particle fluence.

3.2 DLTS measurements

A parameter which is often quoted when discussing radiation defects is the defect introduction rate (η), which gives a measure of the concentration (N_T) at which a particular defect will be introduced for a certain particle type and incident energy, per centimetre of penetration of the incident particle. Using the particle flux (Φ), the introduction rate (η) can be calculated:

$$\eta = \frac{\Delta N_T}{\Delta \Phi\, t}. \tag{3}$$

From Fig. 4, where the DLTS spectra of a control (curve a, unirradiated) and irradiated samples (curves b to e) are presented it is evident that, even for very low fluences (curve b, 1.2×10^{10} cm^{-2}) where little change in the electrical properties of the SBD could be detected, there are indeed traps. As the particle fluence increases the trap concentration increases, this is clearly visible in curve d, (dose = 3.8×10^{10} cm^{-2}) where the trap concentration is approximately three times that of those observed in curve b, (dose = 1.2×10^{10} cm^{-2}).

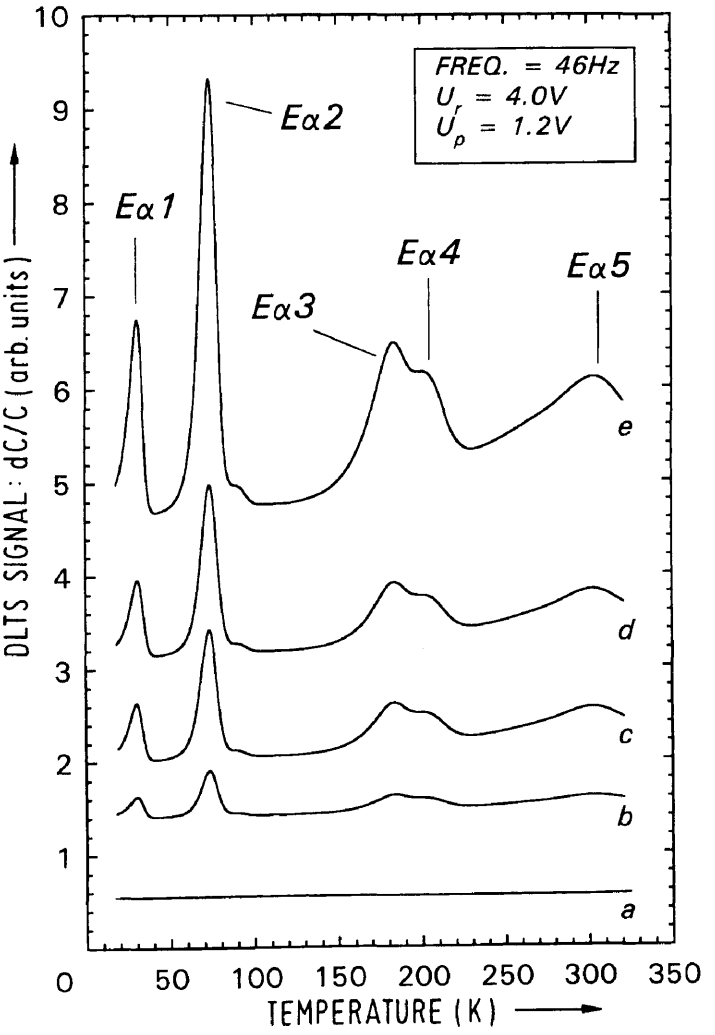

Fig. 4. DLTS spectra of 5.4 MeV α-particle (Am-241) irradiated samples at a reverse quiescent bias of 4.0 V and a filling pulse amplitude of 1.2 V, the LIA frequency being 46 Hz. (a) The control (unirradiated) spectrum, (b), (c), (d), and (e) spectra after the diodes received α-particle fluences of 1.2×10^{10}, 2.6×10^{10}, 3.8×10^{10}, and 9.6×10^{10} cm^{-2}, respectively

© University of Pretoria

UNIVERSITEIT VAN PRETORIA
UNIVERSITY OF PRETORIA
YUNIBESITHI YA PRETORIA

The DLTS signatures (energy level E_T in the band gap and apparent capture cross-section σ_{na}) of the defects detected after irradiation were determined from the conventional DLTS Arrhenius plots of $\log(e_n/T^2)$ versus $1000/T$, using [16]

$$e_n = B_n T^2 \sigma_{na} \exp(-E_T/kT). \tag{4}$$

Here e_n is the electron emission rate from the defect site at a temperature T, k is Boltzmann's constant, and B_n is a constant equal to 2.21×10^{20} cm^{-2} s^{-2} K^{-2} [17] for an electron trap, if for simplicity the degeneracy is taken as one. These defect properties are summarized in Table 2. It must be noted that these defect signatures were obtained in material with a free carrier density of approximately 1.2×10^{16} cm^{-3}, hence enhanced emission may occur due to the relatively high field present. The reason for using material with this free carrier density is twofold, firstly, many devices have an active layer with carrier densities equal to or higher than 1.2×10^{16} cm^{-3} and secondly, to investigate the changes in I–U characteristics it is necessary to use material on which high-quality Schottky contacts can be fabricated. From a comparison of defects introduced during α-particle irradiation to those detected in the same material after electron irradiation, as illustrated in Table 2, it appears that the defects are similar with the exception of Eα3 and Eα5 which were not detected during electron irradiation [18]. The defect Eα3 exhibits a metastable character, in that its magnitude and presence depends upon the bias conditions, incident particle type, and temperature. It has been proposed that E1(Eβ1) and E2(Eβ2) are two different charge states, (−/o) and (o/+) of the isolated arsenic vacancy V_{As}, in GaAs [19], while the E3(Eβ4) is speculated to be related to the close arsenic vacancy–interstitial pairs, V_{As}–As_i [8]. The correspondence between the DLTS signatures of the α-particle and electron irradiation induced defects therefore strongly suggests that Eα1, Eα2, and Eα4 also have a point defect nature. From a graph of defect concentration versus incident dose the introduction rates of the introduced defects (Eα1, Eα2, Eα3, Eα4, and Eα5) are calculated, these results are presented in Table 2. When comparing the introduction rates for the five defects detected in the α-irradiated material to defects with similar signatures introduced during electron (e^-) irradiation, it is clear that the introduction rates for α-particles are very much larger than for electrons.

Table 2

Comparison between the characteristics of α- and electron irradiation induced defects in 10^{16} cm^{-3} doped n-GaAs as detected by DLTS

α-irradiation defects				electron irradiation defects			
label	E_T[a] (eV)	σ_{na}[b] (10^{-16} cm^2)	η[c] (cm^{-1})	label	E_T[a] (eV)	σ_{na}[b] (10^{-16} cm^2)	η[c] (cm^{-1})
Eα1	0.026	0.13	2963	Eβ1	0.024	0.08	2.0
Eα2	0.117	170	9638	Eβ2	0.117	170	2.0
Eα3	0.31	58	4560	–	–	–	–
Eα4[d]	0.38	160	3060	Eβ3	0.38	160	0.7
Eα5	0.665	7100	1737	–	–	–	–

[a]) Effective activation energy, measured below the conduction band.
[b]) Apparent majority carrier capture cross-section, determined from the Arrhenius plot.
[c]) Introduction rate, calculated using (3).
[d]) The values for Eα4 and Eα3 were obtained in undoped GaAs with a free carrier density of 4×10^{14} cm^{-3} (field effect was too high in 1.5×10^{16} cm^{-3} doped material).

© University of Pretoria

UNIVERSITEIT VAN PRETORIA
UNIVERSITY OF PRETORIA
YUNIBESITHI YA PRETORIA

The two aspects which must be considered in the interpretation of these data are the difference in the incident energy and the mass of these two particles.

From calculations it is clear that the sum of the defect concentrations of all five defects is larger than the total carrier removal as measured by $C-U$ measurements for that particular dose. Siyanbola and Palmer [20] stated that it are those defects deeper than 0.2 eV below the conduction band that are responsible for carrier reduction, confirming what Bryant stated. When calculating the sum of the defect concentrations for the Eα3 and Eα4 and Eα5 defect states it is apparent that their sum is approximately equal to the carrier removal density.

4. Conclusions

It has been shown that the primary cause of performance degradation in MESFETs is the production of displacement damage causing carrier removal from the channel region, reducing the drain–source current and that a reduction in carrier mobility is a second-order effect [2]. This carrier removal will affect the active layer thickness and hence the pinch-off characteristics of a MESFET. The radiation defects created also reduce the non-equilibrium carrier lifetime in the semiconductor and, consequently result in deterioration of the main parameter of detectors, namely their energy resolution [21]. The concentrations of these defects depended upon the fluence and particle type.

α-particles cause a degradation of the $I-U$ characteristics and from experimental $I-U$ measurements and modelling results it appears that a recombination current is definitely present after irradiation, the magnitude of which is dependent upon the fluence. Whether this current is due to surface or bulk states is still under investigation and we speculate that the deeper lying defects are responsible for the increased reverse leakage current.

As the defects Eα1 and Eα2 are supposed to be different charge states of the same defect, one would expect their introduction rates to be similar as is seen in electron irradiated material [18]. However, it has been observed that their concentrations are strongly dependent upon the bias conditions chosen when acquiring the DLTS spectra of α-irradiated material. Hence, it would appear that their concentrations are strongly dependent upon the magnitude of the electrical field present during measurement. The increase in the reverse leakage current after irradiation could be due to the presence of deep states in the region near the middle of the band gap, which facilitate the tunnelling of charge from the metal to the band gap of the semiconductor and finally to the conduction band. Those shallow defect states which lie close to the conduction band cannot enhance the reverse leakage current as they cannot act as stepping sites for the moving charge.

This paper has identified and characterized the defects introduced during α-particle irradiation using two types of sources, a linear van de Graaff accelerator and an Am-241 radio-nuclide. The introduction rates and signatures of these defects have been calculated and compared to the well known electron irradiation induced defects with similar DLTS signatures. The influence of these defects on the $I-U$ and $C-U$ properties of the metal–semiconductor system were investigated and it was found that the change in the reverse leakage current as a function of fluence was linear, and from $C-U$ measurements the carrier removal rate was calculated. By applying a modified version of the model proposed by Donoval et al. [13] the recombination pre-factor and the series resistance of irradiated material were calculated.

© University of Pretoria

UNIVERSITEIT VAN PRETORIA
UNIVERSITY OF PRETORIA
YUNIBESITHI YA PRETORIA

Acknowledgement

The financial assistance of the South African Foundation for Research Development (FRD) is gratefully acknowledged.

References

[1] A. F. GALASHAN and S. W. BLAND, J. appl. Phys. **67**, 173 (1990).
[2] A. R. KNUDSON, A. B. CAMBELL, W. J. STAPOR, P. SHAPIRO, and G. P. MUELLER, IEEE Trans. Nuclear Sci. **32**, 4388 (1985).
[3] M. A. HOPKINS and J. R. SROUR, IEEE Trans. Nuclear Sci. **30**, 4457 (1983).
[4] Y. UMEMOTO, N. MASUDA, and K. MITSUSADA, IEEE Electron Devices Letters **7**, 396 (1986).
[5] G. E. ZARDAS, P. C. EUTHYMIOU, B. SZENTPALI, CH. SYMEONIDES, and K. KOURKOUTAS, phys. stat. sol. (a) **123**, K79 (1991).
[6] L. F. ZAKHARENKOV, V. V. KOZLOVSKII, and B. A. SHUSTROV, phys. stat. sol. (a) **117**, 85 (1990).
[7] D. V. LANG, J. appl. Phys. **45**, 3014 (1974).
[8] D. PONS and J. C. BOURGOIN, J. Phys. C **18**, 3839 (1985).
[9] T. I. CHAPPEL and C. M. RANSOM, Rev. Sci. Instrum. **55**, 200 (1984).
[10] W. E. PHILIPS and J. R. LOWNEY, J. appl. Phys. **54**, 2786 (1983).
[11] F. J. BRYANT, L. M. MAJID, C. G. SCOTT, and D. SHAW, Solid State Commun. **63**, 9 (1987).
[12] J. LINDHARD, M. SCHARFF, and H. E. SCHIOTT, Mat. Fys. Medd. Dan. Lid. Selsk. **33**, 14 (1963).
[13] D. DONOVAL, J. DE SOUSA PIRES, P. A. TOVE, and R. HARMAN, Solid State Electronics **32**, 11 (1989).
[14] R. M. ERASMUS, W. E. MEYER, F. D. AURET, and G. MYBURG, S. Afr. J. Phys. **16**, 58 (1993).
[15] S. M. SZE, Physics of Semiconductor Devices, 2. ed., John Wiley & Sons, New York 1981.
[16] P. J. WANG, T. F. KUECH, M. A. TISCHLER, P. M. MOONEY, G. SCILLA, and F. CARDON, J. appl. Phys. **64**, 4975 (1988).
[17] S. A. GOODMAN, F. D. AURET, and G. MYBURG, Semicond. Sci. Technol. **7**, 1241 (1992).
[18] F. D. AURET, S. A. GOODMAN, G. MYBURG, and W. E. MEYER, Appl. Phys. A **56**, 547 (1993).
[19] B. ZIEBRO, J. W. HEMSKY, and D. C. LOOK, J. appl. Phys. **72**, 78 (1992).
[20] W. O. SIYANBOLA and D. W. PALMER, Semicond. Sci. Technol. **5**, 7 (1990).
[21] E. M. VERBITSKAYA, V. K. EREMIN, A. M. IVANOV, E. S. IGNATENKO, N. B. STROKAN, U. SH. TUREBEKOV, J. VON BORANY, and B. SCHMIDT, Soviet Phys. – Semicond. **25**, 516 (1991).

(Received March 11, 1993; in revised form September 27, 1993)

© University of Pretoria

UNIVERSITEIT VAN PRETORIA
UNIVERSITY OF PRETORIA
YUNIBESITHI YA PRETORIA

S.-Afr. Tydskr. Fis. 16 nr. 1/2 (1993)

Effect of RBS analysis on the quality of Schottky barrier diodes on GaAs

S.A. Goodman, F.D. Auret, M. Hayes, G. Myburg and W.E. Meyer
Physics department, University of Pretoria, Pretoria 0002, Republic of South Africa

Presented at STEDCON '92 16–18 November 1992

When employing the Rutherford back-scattering (RBS) technique to evaluate the thickness of epilayers and metal overlayers, a certain amount of damage is introduced into these layers. This implanted damage results in an increase in the saturation current of the Schottky barrier diodes (SBDs) and a reduction in the free carrier density of the epilayer as measured by current–voltage (*I–V*) and capacitance–voltage (*C–V*) measurements respectively. A comparison is made between the degradation of the electrical quality of Schottky contacts and the introduced defects as detected by deep level transient spectroscopy (DLTS). The defects and the electrical quality of the contacts were investigated as a function of fluence and particle type. Finally the introduction rate of proton (p^+) irradiated induced defects is compared to that of defects with similar properties introduced during alpha (α) particle irradiation.

Wanneer die Rutherford-terugverstrooiingspektroskopie-metode gebruik word om die dikte van epi-lagies en metaal bo-lagies te bepaal, word 'n sekere hoeveelheid skade in hierdie lagies geïnduseer. Hierdie geïnplanteerde skade veroorsaak 'n verhoging in die versadigingstroom van die SBD's en 'n verlaging in die vrydraerdigtheid soos beaal deur *I–V*- en *C–V*-metings, onderskeidelik. Daar is ondersoek ingestel na 'n moontlike verband tussen die verswakking in die elektriese kwaliteit van die SBD's en die geïnduseerde defekte soos waargeneem deur diepvlakoorgangspektroskopie (DLTS) en wel as 'n funksie van deeltjietipe en -dosis. Sodoende kon die skeppingstempo van proton-geïnduseerde defekte met dié van alfa-geïnduseerde defekte vergelyk word.

1. Introduction

Ion implantation has received considerable attention as a technique for fabricating device structures. Proton bombardment for example, is an effective method of providing electrical and optical isolation for devices in GaAs integrated circuits and is even more important in the processing of heterojunction bipolar transistors [1]. Rutherford back-scattering (RBS) techniques can be utilised to evaluate semiconductor layer and metal overlayer thicknesses as well as the elemental composition of such layers. Unfortunately such techniques usually introduce damage in the metal–semiconductor system, this damage can lead to removal of free carriers which can be detrimental to such a contact system. An example of these detrimental aspects can be observed in the severe effects caused by ion implantation on the characteristics of light-emitting diodes, lasers and photovoltaic cells [2, 3].

A knowledge of the extent of damage and the effect of this damage on the electrical properties of the system is important in determining whether RBS analysis can be used as a relatively non-destructive characterization technique. This technique makes use of a wide range of particles with different mass numbers and charges. For this study we used alpha (α)-particle and proton (p^+) particles. Apart from the traditional uses of these particles, Gornushkina et al. [4] used high energy particles, particularly helium nuclei and protons, for the transmutational doping of silicon. The use of GaAs devices and integrated circuits in irradiation environments, such as in extra-terrestrial space, has also created a need for a better understanding of defect properties, processes and effects to enable the technology to proceed efficiently.

When irradiating n-type GaAs, deep level acceptor states are, amongst others, introduced, which reduce the free carrier density. Extensive studies have been performed on the annealing kinetics of these defects. These studies have shown that upon annealing [3, 5 – 7] the free carrier density can almost be restored to its pre-irradiation value. It is known that high energy electron-, proton- and helium-ion irradiations all introduce a set of prominent deep level electron traps (E1, E2, E3, E4 and E5), that can be observed by the deep level transient spectroscopy (DLTS) technique [8]. The introduction rate of these electron traps is independent of the concentration and nature of the impurities and of the native defects in the host material [8].

2. Experimental

The samples studied in this work were n-type GaAs films, 8.0 μm thick, grown using OMVPE on n^+ bulk-grown substrates. The free carrier density of the defect-free (detection limit $>10^{10}$ cm^{-3}) silicon-doped n-type films was between 1.0 and 1.35×10^{16} cm^{-3}. It is assumed in conventional DLTS analysis that the measured capacitance transient varies exponentially with time. However, this will not be true if the densities of deep levels are not small compared to that of shallow levels. The trap density (N_T) should not be greater than 10% of the free carrier density ($N_D - N_A$) to ensure that the transients are exponential [9]. The back surfaces (n^+) of the wafers were coated with Ni/AuGe/Au films and alloyed to form ohmic contacts. After ohmic contact fabrication, 4000 Å thick 0.75 mm diameter palladium (Pd) contacts were deposited on the front surface through a metal mask to form Schottky barrier diodes. Before irradiation each sample was characterized by current–voltage (*I–V*) and capacitance–voltage (*C–V*) measurements, and a control DLTS spectrum was obtained for each batch of samples.

© University of Pretoria

UNIVERSITEIT VAN PRETORIA
UNIVERSITY OF PRETORIA
YUNIBESITHI YA PRETORIA

A two-phase lock-in amplifier-based DLTS system was employed to detect and to characterize the defects introduced during both alpha (α)-particle and proton (p^+) irradiation. The DLTS spectra were acquired at a rate of 5 K min^{-1} in both temperature directions so as to eliminate any peak temperature discrepancies due to uneven cooling and heating. The $I-V$ and $C-V$ characteristics were obtained under dark conditions, at room temperature (297.0 – 300.0 K, depending upon the climatic conditions), using a system based around an HP4140B pA/dc source and an HP4192A LF impedance analyzer. Currents as low as 10^{-14} A could be measured, and $C-V$ measurements were performed at 1.0 MHz. Irradiation was performed in a van de Graaff accelerator, the accelerating voltage being 2.0 MeV. For each fluence and particle type, 3 – 4 samples were irradiated, for a reasonable average.

3. Results

From a preliminary study it was found that the two most sensitive parameters to incident radiation were the reverse leakage current (I_R) of the SBDs and the free carrier density ($N_D - N_A$) of the epilayer. The variation of the parameters measured using the $I-V$ and $C-V$ techniques in the temperature range (297.0 – 300.0K) were monitored for unirradiated, as well as α-particle and p^+ irradiated material. From this investigation it was seen that only the reverse leakage current exhibited a strong temperature dependence. There was a 50% change in this value from 297.0 K to 300.0 K. It is important when comparing values before and after irradiation to ensure that there are no temperature-dependant discrepancies. To minimize such errors, correction factors were used to normalize all current measurements to 300.0 K. All other parameters (eg. barrier height, ideality factor and built-in voltage) were temperature-independent in this small temperature range. When considering the temperature-dependence of current contributions only from thermionic emission and recombination–generation processes (not diffusion etc.) and comparing them to the experimental variation in reverse leakage current as a function of temperature (297.0 K – 300.0 K), it is observed that the experimentally measured current values are not due to these two current transport mechanisms only but to a weighted combination of these and other mechanisms.

For this study it was the intention to determine from $C-V$ measurements the number of free carriers removed for fluences ranging from 1.4×10^{11} cm^{-2} to 9.0×10^{13} cm^{-2} for both α-particle and p^+ irradiation, and compare these carrier removal concentrations to the individual trap concentrations as determined from DLTS profile measurements. It must be noted that the interpretation of $C-V$ profiles in the presence of deep states calls for considerable care [10]. Figure 1 illustrates the change in free carrier density ($N_D - N_A$) after irradiation and the free carrier removal density as a function of fluence for p^+ and α-particle irradiated material respectively. From these graphs, the carrier removal rates per incident proton and alpha particle can be calculated. The number of free carriers removed per incident proton in the fluence range 1.4×10^{11} to 2×10^{13} cm^{-2} is 658 cm^{-1}, and the same factor per alpha particle in the fluence range 2.8×10^{11} to 6×10^{11} cm^{-2} is 13 377 cm^{-1}. These values

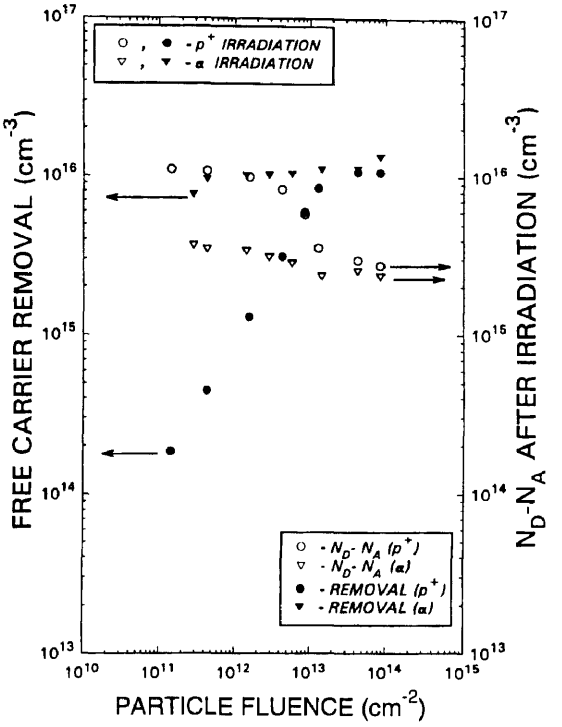

Figure 1 Free carrier removal versus alpha (α)-particle (▼) and proton (p^+) (●) fluence and free carrier density after irradiation ($N_D - N_A$) versus α-particle (▽) and p^+ (○) fluence. The initial free carrier density being $1.0 - 1.35 \times 10^{16}$ cm^{-3}.

were calculated in the range where the variation of free carrier removal as a function of fluence was linear. For fluences larger than those specified, nearly all of the free carriers are removed by the introduced defects, and any free carrier concentration measurement becomes highly inaccurate and therefore meaningless. These carrier removal rate values are specified per incident particle for every centimetre the incident particle travels. From LSS calculations [11], the penetration depths of 2.0 MeV incident α and p^+ particles is 5.43 and 32.8 μm, respectively. Thus the total number of carriers removed per incident particle in the actual penetration depth can be calculated as 7.26 for α-particles and 2.16 for p^+.

A parameter which is often quoted when discussing radiation defects is the defect introduction rate (Γ), which gives a measure of the concentration at which a particular defect (N_T) will be introduced for a certain particle type and incident energy, per centimetre of penetration of the incident particle. Using the particle flux, (Φ), which can be determined during the RBS measurements, the introduction rate, (Γ), can be calculated from

$$introduction\ rate\ (\Gamma) = \frac{\Delta trap\ density\ (\Delta N_T)}{\Delta\,(flux\,(\Phi) \times time\ (t))} \qquad (1)$$

To compare introduction rates for α-particle and p^+ irradiation-induced defects, it was necessary to use a radionuclide source (Am 241) for the α-particle irradiation;

© University of Pretoria

UNIVERSITEIT VAN PRETORIA
UNIVERSITY OF PRETORIA
YUNIBESITHI YA PRETORIA

because, when irradiating the GaAs with α-particles produced in the van de Graaff accelerator, the lowest achievable total fluence removes approximately 9×10^{15} cm^{-3} free carriers, which makes accurate DLTS profiling impossible. When comparing the introduction rates for the 5 defects detected in α-particle and p$^+$ irradiated material as illustrated in Table 1, it is clear that the introduction rates for α-particles is very much larger than for p$^+$; therefore the two aspects which must be considered in the interpretation of these data is the difference in the incident energy and the mass of these two particles. From simple calculations in which the defect concentrations as a function of fluence was obtained, it is clear that the sum of the defect concentrations of all 5 defects is much larger than the total carrier removal as measured by $C-V$ measurements for that particular fluence. Yuba et al. [12] performed 2.0 MeV proton (p$^+$) implantation at a fluence of 5×10^{13} cm^{-2} in 3×10^{16} cm^{-3} GaAs material and observed a carrier reduction of 2.15×10^{16} cm^{-3}. However, because they only calculated the defect concentration in the 100K to 400K temperature range, an accurate comparison of the free carrier density measured, using the DLTS and $C-V$ techniques, is not a straightforward procedure. Blood [10] stated that the traps responsible for carrier removal are the well known E3 and E4 irradiation-induced acceptor-like defect states. Siyanbola et al. [2] stated that it is those defects deeper than 0.2eV below the conduction band that are responsible for carrier reduction, confirming what Blood stated.

When calculating the sum of the defect concentrations for the E3 and E4 defect states it is apparent that their sum is approximately equal to the carrier removal density. From inspection of Figure 2, where the difference in the reverse leakage current measured at 1.0 volt is plotted as a function of fluence, it can be seen that at a fluence of 6×10^{12} cm^{-2} the α-particle irradiation increases this current approximately 10 times as much as the lighter p$^+$ particle. The ideality factor (n) for samples irradiated by both α-particles and p$^+$ is not larger than 1.05 even for those samples irradiated by fairly high fluences. Thus the dominant current transport mechanism in the forward bias region (0.2 – 0.6V) is still thermionic emission. However, from inspection of Figure 3 where the $I-V$ characteristics of an unirradiated sample and an irradiated sample are plotted it can be seen that there is deviation from linearity in the forward bias region of the $I-V$ curves, especially in the low voltage region, which proves that other current mechanisms contribute to the leakage

Table 1 The defect (E1, E2, EM, E3 and E4) introduction rates for 5.5 MeV alpha particle and 2.0 MeV proton (p$^+$) irradiated samples.

Defect label	5.5 MeV alpha (α) (I, cm^{-1})	2.0 MeV protons (p$^+$) (I, cm^{-1})
E1	12 888	1056.3
E2	24 722	1765.6
EM	—	384.8
E3	12 227	470.4
E4	—	126.7

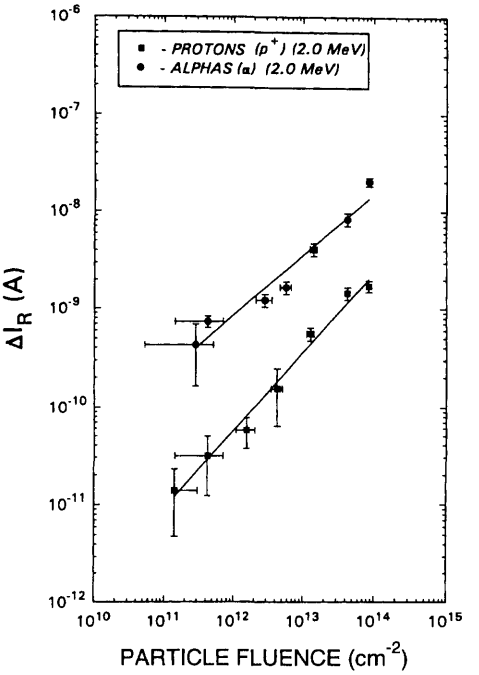

Figure 2 The difference in reverse leakage current ($\Delta I_R = I_{Rafter} - I_{Rbefore}$) measured at 1.0 volt for 2.0 MeV proton (■) and alpha particle (●) irradiation.

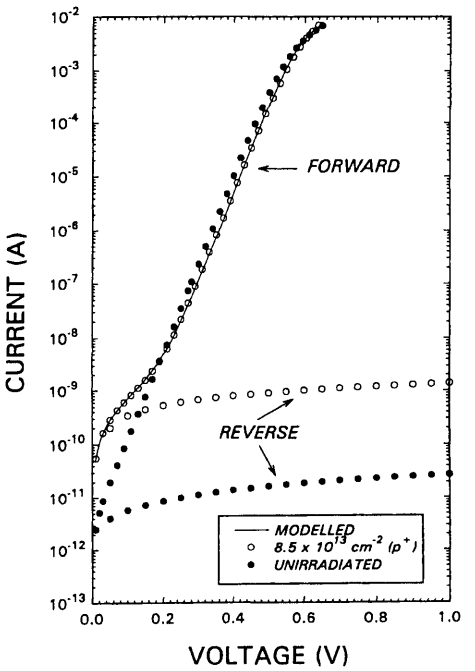

Figure 3 The experimental (●, ○) and modelled (—) $I-V$ characteristics for an unirradiated and a 2.0 MeV proton (p$^+$) irradiated (8.5×10^{13} cm^{-2}) sample.

© University of Pretoria

UNIVERSITEIT VAN PRETORIA
UNIVERSITY OF PRETORIA
YUNIBESITHI YA PRETORIA

current. Using the model proposed by Donoval et al. [13], the forward characteristics of the irradiated sample (8.5×10^{13} cm^{-2} p$^+$) were modelled, from which the magnitude of the recombination current pre-factor (4.0×10^{-11} A), and the series resistance (7.5 Ω) were obtained.

In Figure 4, the DLTS spectra of a proton-irradiated sample are presented. From these spectra it can be seen that when the fluence increases by a factor of 4.0 (4.2×10^{11} cm^{-2} to 1.6×10^{12} cm^{-2}) there is a corresponding increase in the defect concentrations. The slight discrepancy can be attributed to the error in accurately determining the fluence. This error is larger for small fluences as is evident in the spectra for the two lowest fluences (1.4×10^{11} and 4.2×10^{11} cm^{-2}). Apart from the well known E1 – E4 defects, a defect labelled EM is also detected, the origin and nature of which is unknown.

4. Conclusions

From this study it is evident that defects are created when using RBS analysis to investigate the thickness of metal–semiconductor systems. The concentrations of these defects depended upon the fluence and particle type. Proton irradiation may be a more suitable process than alpha particle irradiation for this method of characterization, as less damage is caused by the lighter particle. However, Hayes et al. [14] illustrate that alpha particles are the most suitable particles for thickness determinations. Both particle types cause a degradation of the I–V characteristics and from experimental I–V measurements and modelling results it appears that a recombination–generation current is present after irradiation, the magnitude of which is dependant upon the fluence and particle type. Whether this current is due to surface or bulk states is still under investigation and whether the defects responsible for carrier removal are also responsible for the increased reverse leakage current is debatable. As the defects E1 and E2 are supposed to be different charge states of the same defect, one would expect their introduction rates to be similar, however this is not the case in α-particle and p$^+$ irradiated samples, and it is seen that their concentrations are strongly dependent upon the incident particle type and bias conditions chosen when acquiring the DLTS spectra. Hence, it would appear that their concentrations are strongly dependent upon the magnitude of the electrical field present during measurement.

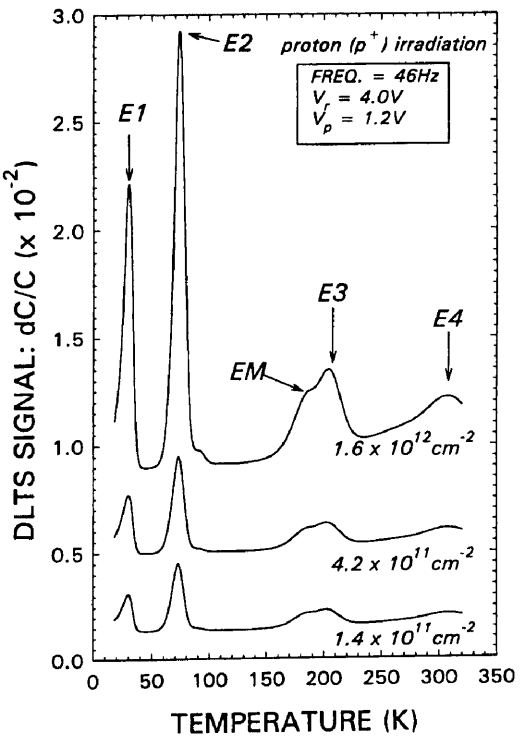

Figure 4 DLTS spectra of 2.0 MeV proton (p+) irradiated samples acquired at a reverse quiescent bias of 4.0 V and a filling pulse amplitude of 1.2 V, the LIA frequency being 46 Hz.

Acknowledgement

The financial assistance of the South African Foundation for Research Development (FRD) is gratefully acknowledged.

References

[1] G.T. Brown, S.J. Barnett, S.J. Courtney and S.S. Gill, Mater. Sci. Eng. **B2** (1989) 91
[2] W.O. Siyanbola and D.W. Palmer, Semicond. Sci. Technol. **5** (1990) 7
[3] E.M Verbitskaya, V.K. Eremin, A.M. Ivanov, E.S. Ignatenko, N.B. Strokan, U.Sh. Turebekov, J. von Borany and B. Schmidt, Sov. Phys. Semicond. **25** (1991) 516
[4] E.D. Gornushkina, V.A. Didik, V.V. Kozlovskiĭ and R.Sh. Malkovich, Sov. Phys. Semicond. **25** (1991) 1232
[5] D. Stievenard, X. Boddaert and J.C. Bourgoin, Phys. Rev. **34** (1986) 4048
[6] S. Loualiche, A. Nouailhat and G. Guillot, Solid State Commun. **44** (1982) 41
[7] Y. Yuba, K. Gamo, K. Murakami and S. Namba, Inst. Phys. Conf. Ser. **59** (1981) 330
[8] D. Pons and J.C. Bourgoin, J. Phys. C **18** (1985) 3839
[9] W.E. Phillips and J.R. Lowney, J. Appl. Phys. **54** (1983) 2786
[10] P. Blood, Inst. Phys. Conf. Ser. **56** (1981) 24
[11] J. Lindhard, M. Scharff and H.E. Schiott, Mat.-Fys. Medd. K. Dan. Vidensk. Selsk. **33** (1963) 14
[12] Y. Yuba, M. Matsuo, K. Gamo and S. Namba, Inst. Phys. Conf. Ser. **59** (1981) 329
[13] D. Donoval, J. de Sousa Pires, P.A. Tove and R. Harman, Solid-State Electron. **32** (1989) 961
[14] M. Hayes, F.D Auret, E. Friedland, S.A. Goodman, W.E. Meyer and G. Myburg, Submitted to Nucl. Instrum. Methods

© University of Pretoria

UNIVERSITEIT VAN PRETORIA
UNIVERSITY OF PRETORIA
YUNIBESITHI YA PRETORIA

Appl. Phys. A 56, 547–553 (1993)

Applied Physics A Solids and Surfaces
© Springer-Verlag 1993

Electrical Characterization of Defects Introduced in n-GaAs by Alpha and Beta Irradiation from Radionuclides

F. D. Auret, S. A. Goodman, G. Myburg, W. E. Meyer

Physics Department, University of Pretoria, Pretoria 0002, Rep. of South Africa (Fax: +27-12/342-4143)

Received 14 December 1992/Accepted 12 February 1993

Abstract. We investigated defect production in n-type GaAs with two different free-carrier densities (4×10^{14} and 1×10^{16}/cm^3) by using particles liberated from radionuclides. ^{90}Sr and ^{241}Am were employed as beta and alpha sources, respectively. The results obtained for electron irradiation showed that the same set of primary defects can be produced by beta irradiation from the Sr source as by electrons produced in an accelerator. Similarly, the defects produced by alpha irradiation from the Am source closely resemble those introduced by alpha irradiation in a Van de Graaff accelerator. It was found that the relative concentrations of the primary defects in electron-irradiated GaAs are different to those in alpha-particle irradiated GaAs. Further, for the first time, an alpha irradiation induced defect which seems to be related to the doping concentration was observed in the 10^{16}/cm^3 Si doped GaAs. It is concluded that the use of radionuclides is an inexpensive and convenient method to introduce and to study radiation induced defects in semiconductors.

PACS: 81.40.Rs; 61.80.−X

During the past few decades defect introduction by energetic particle irradiation in solids, and particularly in semiconductors, has been extensively studied, facilitating a better understanding of the nature and manifestations of particle-induced defects particularly in semiconductors [1–3]. This, in turn, resulted in novelty particle related semiconductor processing steps, e.g. device isolation by proton implantation [4] and neutron transmutation doping of silicon [5]. It is important to note that particle irradiation can produce both point and extended defects. Point defects can be controllably introduced, among others, by irradiating the semiconductor with electrons having energies above the so-called *threshold energy* (approximately 250 keV for GaAs) [1, 3]. This is the minimum energy that an incident electron should have, which must be elastically transferred to a lattice atom, in order to produce a Frenkel pair. The point defects thus introduced are often referred to as *primary radiation induced defects*. Extended defects, on the other hand, are usually introduced by irradiation with heavier particles, such as protons or alphas. During a collision some of these particles may transfer enough energy via knock-on processes to create, apart from point defects, the so-called *displacement spikes*, i.e. lattice disorder that may extend over several tens of angstroms [6]. Up to now, most of the particle irradiation induced defects studied have been generated in accelerators.

Deep level transient spectroscopy (DLTS) [7] is currently the most sensitive technique to study the electrical properties of radiation induced defects in semiconductors. It yields the energy level of a defect in the bandgap and its capture cross section (the combination of which is referred to as its DLTS *signature*), as well as its concentration. The standard way of identifying unknown defects by DLTS is to compare their "signatures" to those of defects that have already been characterized or identified. The primary radiation-induced defects in GaAs have well established DLTS "signatures" [1–3], and may therefore readily be recognized in a DLTS spectrum, even in the presence of other defects. When comparing the DLTS "signatures" of unknown defects (e.g. those cause by particle processing) to those of well known defects (e.g. radiation-induced defects), both sets of defects should ideally be characterized in the same laboratory, because non-identical temperature measurements in different laboratories may yield different "signatures" for the same defect. This becomes especially noticeable for defects observed at low temperatures, for example, the $E1$ and $Ee1$ defects introduced in GaAs by above- and subthreshold electron irradiation, respectively [8]. For a unique defect identifiction, especially at low temperatures, it is essential to compare *in the same laboratory* the characteristics of the unknown defects to those of "semiconductor laboratory standards" which contain defects of which the characteristics are known. The production of such "standards" may however be cumbersome and expensive if accelerators are required to produce the radiation damage.

In this study we investigated defect introduction in semiconductors by radiation from radionuclides. We present experimental results obtained after irradiating two different free carrier densities of n-type GaAs with alphas from an ^{241}Am

© University of Pretoria

UNIVERSITEIT VAN PRETORIA
UNIVERSITY OF PRETORIA
YUNIBESITHI YA PRETORIA

source and with betas (electrons) from a ^{90}Sr source at doses of up to 5×10^9 α/cm^2 and 10^{14} e/cm^2, respectively. It will be shown that the same defects which are produced during electron and alpha particle irradiation in accelerators are also introduced in GaAs by particle irradiation from radionuclide sources. We were also able to compare the properties of defects introduced by electrons and alphas, respectively. A defect produced by alpha irradiation which seemed to depend on the doping concentration of the GaAs was also observed for the first time. The results presented here showed that the use of radionuclides is a convenient and inexpensive method to study fundamental aspects of radiation induced defects and to prepare "laboratory standards" containing radiation induced effects.

1 Experimental Procedure

Two different carrier densities of n-type GaAs samples were used to study the defects created by particles emitted from the radionuclides. These n-type samples consisted of 8 µm thick epitaxial layers with free carrier densities of 4×10^{14}/cm^3 (*undoped*) and 1×10^{16}/cm^3 (Si-*doped*), respectively, grown by OMVPE on n^+ bulk-grown GaAs substrates having a doping density of 1×10^{18}/cm^3. The undoped sample is a section of the same OMVPE grown n-GaAs wafer used in [8] where the defects introduced by electron irradiation in a linear accelerator were studied. Ni/AuGe/Au ohmic contacts were formed on the n^+-GaAs sides of the samples before irradiation. In order to investigate the possible effects of metal atoms from the Schottky contact that can be knocked into the semiconductor during irradiation, the GaAs was irradiated both before and after Schottky barrier diode (SBD) metallization. Palladium (Pd) SBDs, 400 nm thick and 0.75 mm in diameter, were resistively deposited after chemically cleaning the GaAs substrates [9]. Standard current – voltage ($I-V$) and capacitance – voltage ($C-V$) measurements were used to evaluate the electrical properties of the SBDs before and after irradiation.

A two-phase lock-in amplifier based DLTS system [10] was employed to detect and characterize the defects introduced during irradiation by the different particle types. During temperature cycling in a closed-cycle liquid-helium cryostat the sample was mounted on a specially designed sample holder which ensured good thermal contact to the cold finger of the cryostat while electrically isolating the sample from the cryostat and thermocouple [11]. The energy level E_t of a defect level in the bandgap and its aparrent capture cross section σ_{na} were calculated from the DLTS Arrhenius plots of e_n/T^2 versus $1000/T$, using

$$e_n = \gamma_n T^2 \sigma_{na} \exp(-E_t/kT) . \quad (1)$$

Here e_n is the electron emission rate from the defect site at a temperature T, k is Boltzmann's constant and the γ_n is a constant equal to 2.21×10^{20} cm^{-2} s^{-2} K^{-2} for an electron trap, if the degeneracy is taken as one, for simplicity. The defect concentration distribution below the metal – GaAs interface was calculated using fixed-bias variable-pulse DLTS profiling in conjunction with the approach of Zohta et al. [12].

The Am alpha source used here had an activity of 0.39 µCi and was disc shaped with a diameter of 9.7 mm. During the decay of ^{241}Am to ^{237}Np, 85.5% of the alpha particles are emitted with a sharply defined energy peak at 5.484 MeV, while 12.3% have an energy of 5.441 MeV and 1.5% have an energy of 5.387 MeV. For studies pertaining to radiation induced defects the alphas liberated from the Am source can therefore be considered as monoenergetic.

The Sr electron source used here was disc shaped with a diameter of 8.4 mm and an activity of 20 mCi. ^{90}Sr radionuclides decay first to Y with the emission of an 0.5 MeV electron (halflife 28.5 yrs) and then to Zr with the emission of a 2.3 MeV electron (halflife 64.1 h). Unlike the alpha source, however, the electrons emitted from the electron source have a continuous energy distribution, as shown in Fig. 1. From this figure it is clear that approximately 70% of the total number of emitted electrons have energies above 250 keV, i.e. the threshold for producing defects by elastic collisions.

During alpha and beta irradiation the samples were placed 1 mm away from the center of the radioactive discs. The particle flux reaching a SBD in this position was assumed to be the same as that which leaves the surface of the source. For the alpha source the flux was 2×10^4 α/cm^2 s. Alpha irradiation was performed for periods of 1–10 h for the undoped GaAs and for 30–300 h for the doped GaAs. Because the Sr electron source emits electrons with energies below and above the threshold energy for defect creation in GaAs, one should distinguish between the *total* and *effective* electron doses and dose rates. The *total dose rate* of electrons emitted is simply obtained from the activity of the Sr source, remembering that each Sr decay effectively results in the emission of two electrons because the halflife of Y is much

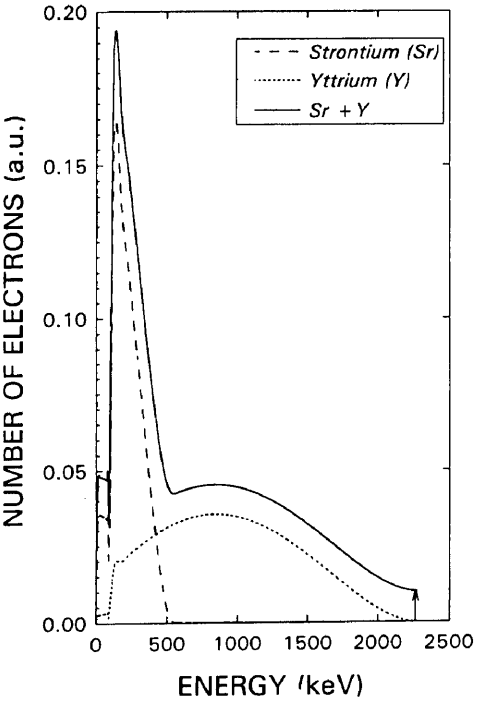

Fig. 1. Energy distribution of electrons emitted by a ^{90}Sr radionuclide. For clarity the sum of the Sr and Y contributions has been displaced by an amount indicated by the arrow

© University of Pretoria

UNIVERSITEIT VAN PRETORIA
UNIVERSITY OF PRETORIA
YUNIBESITHI YA PRETORIA

shorter than that of Sr. This total dose is represented by the total area below the curve (Sr + Y) in Fig. 1. If we assume that 250 keV is the threshold electron energy for producing point defects in GaAs, as then the *effective electron dose rate* is proportional to the area to the right of 250 keV, below the curve in Fig. 1, which amounts to $1.9 \times 10^9\, e/\mathrm{cm}^2\,\mathrm{s}$ for the 20 mCi source used here. Electron irradiation was performed for periods of 1–30 min for the undoped GaAs and for 10–100 min for the doped GaAs. For dose rates as low as these employed in this study, it can safely be assumed that the Fermi level of the semiconductor remains unperturbed and that temperature of the sample remains constant during irradiation.

2 Results

The DLTS spectra of the undoped ($4 \times 10^{14}/\mathrm{cm}^3$) GaAs samples (unirradiated as well as electron and alpha irradiated) are presented in Fig. 2, while those of the doped ($10^{16}/\mathrm{cm}^3$) GaAs are depicted in Fig. 3.

2.1 Control Samples

Curve (a) in Fig. 2 shows the DLTS spectrum of the undoped control (unirradiated) n-GaAs sample. Although only its low temperature DLTS "tail" is shown, it should be mentioned that the most prominent defect in the unirradiated n-GaAs is the well known $EL2$ defect which is present in all OMVPE grown GaAs. At the frequency (46 Hz) used here it has a DLTS peak at about 390 K. DLTS profiling indicated that the $EL2$ distribution is approximately constant and equal to $2 \times 10^{14}/\mathrm{cm}^3$. In addition, the $EO4$ defect, which has also been observed in similar GaAs [9], is detected at 207 K, but in a much lower concentration ($8–9 \times 10^{11}/\mathrm{cm}^3$). Because the low temperature "tail" of the $EL2$ peak inhibits the detection of any defects in low concentrations above 300 K, the undoped n-GaAs used in this study is therefore suitable to study radiation induced defects with concentrations as low as $10^{12}/\mathrm{cm}^3$, but only in the 10 K–300 K temperature range.

In the case of the doped GaAs (curve (a) in Fig. 3) no defects in the 10 K to 300 K range giving rise to DLTS signals $\Delta C/C$ larger than 10^{-4}, corresponding to a defect concentration of about $2 \times 10^{12}/\mathrm{cm}^3$, could be detected. The effect of the $EL2$ defect is also less pronounced enabling the recording of spectra at higher temperatures.

2.2 Defects Created by Electron Irradiation from a ^{90}Sr Electron Source

First we discuss the results obtained after irradiating the undoped GaAs with electrons from the Sr radionuclide for

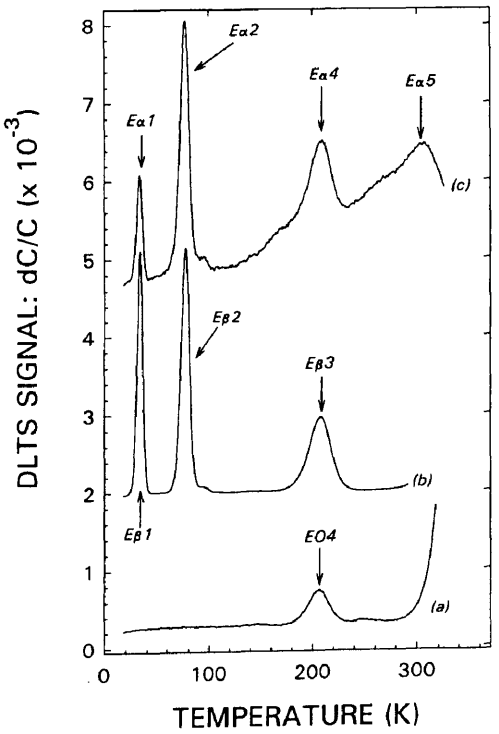

Fig. 2. DLTS spectra of OMVPE-grown n-type GaAs with a free carrier density of $4 \times 10^{14}/\mathrm{cm}^3$. *(a)* unirradiated GaAs; *(b)* electron irradiated through the SBD for 30 min ($3.4 \times 10^{12}\, e/\mathrm{cm}^2$); *(c)* alpha particle irradiated through the SBD for 10 h ($1.8 \times 10^8\, \alpha/\mathrm{cm}^2$). In curves *(b)* and *(c)* the contribution of the defects in the unirradiated control sample has been subtracted. All spectra were recorded at a lock-in amplifier frequency of 46 Hz, a quiescent reverse bias of 8 V and a filling pulse amplitude of 4 V

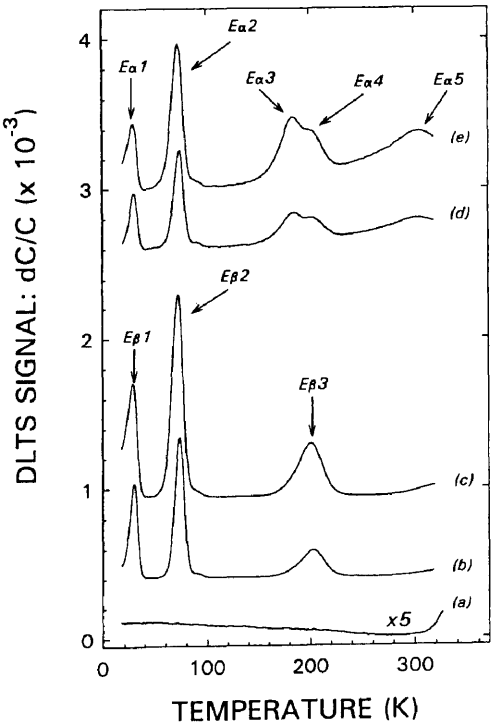

Fig. 3. DLTS spectra of OMVPE-grown n-type GaAs with a free carrier density of $1 \times 10^{16}/\mathrm{cm}^3$. *(a)* unirradiated GaAs; *(b)* and *(c)* electron irradiated through the SBD for 1000 min ($1.1 \times 10^{14}\, e/\mathrm{cm}^2$); *(d)* and *(e)* alpha particle irradiated through the SBD for 300 h ($5.4 \times 10^9\, \alpha/\mathrm{cm}^2$). All spectra were recorded at a lock-in amplifier frequency of 46 Hz and a quiescent reverse bias of 4 V. For curve *(a)* the filling pulse amplitude was $V_p = 4$ V, for curves *(c)* and *(e)* we used $V_p = 1.2$ V, while for curves *(b)* and *(d)* we used $V_p = 0.8$ V

© University of Pretoria

UNIVERSITEIT VAN PRETORIA
UNIVERSITY OF PRETORIA
YUNIBESITHI YA PRETORIA

periods of up to 30 min, i.e. a dose of 3.4×10^{12} e/cm^2. $I-V$ measurements indicated that the ideality factor, barrier height and reverse leakage current remained unaltered, even after the longest irradiation period of 30 min. In order to eliminate any possible effects of the $EO4$ defect on the $E\beta3$ peak as well as the effect of the low temperature $EL2$ tail, the control spectrum (containing the $EO4$) was numerically subtracted from the spectra recorded after irradiation. Curve (b) in Fig. 2 was recorded after irradiating the GaAs through the SBD with electrons from the Sr electron source for 30 min. It shows that three prominent electron traps, the $E\beta1$, $E\beta2$ and $E\beta3$, with peaks in the 10 K–300 K temperature range, were introduced during beta (electron) irradiation. In the nomenclature used here, "E" implies electron traps while "β" indicates that the defects were introduced by beta (electron) irradiation. The spectrum thus obtained [curve (b)] therefore contains only the defects caused by irradiation. In order to allow depth profiling to a reasonable depth, all curves in Fig. 2 were recorded at a quiescent reverse bias of $V_r = 8$ V. In exploratory DLTS scans it was observed that saturation of the DLTS signal of the $E\beta1$ signal commences when V_p is increased to above 4 V. This possibly occurs because of electric field enhanced electron emission from the defect potential wells. The choice of $V_p = 4$ V for the spectra in Fig. 2 is a trade-off between obtaining a strong, yet reasonably undistorted, DLTS signal.

The DLTS "signatures" of the electron irradiation-induced defects were measured only in the undoped material, and by using small quiescent bias (1 V) and filling pulse amplitude (1 V), to avoid inaccuracies due to the electric field-enhanced emission rate. In Table 1 the defect energies E_t and aparent capture cross section σ_{na} thus obtained are compared to those previously reported for defects introduced in n-GaAs by electron irradiation in accelerators [1, 8]. From this comparison it is evident that the "signatures" of the $E\beta1$–$E\beta3$ are almost identical to those of the $EE1$–$EE3$ of [8] and the $E1$–$E3$ of [1]. This implies that the most prominent defects introduced by electron irradiation from the Sr radionuclide are the same as those introduced by electron irradiation in accelerators, namely the so-called *primary electron irradiation induced defects*. The $E1$ and $E2$ are strongly suspected to be two different charge states, $(-/0)$ and $(0/+)$, of the isolated arsenic vacancy V_{As} in GaAs [13], while the $E3$ is speculated to be related to close arsenic vacancy – interstitial pairs V_{As}–As_I [1, 2].

DLTS depth profiles were obtained using the fixed-bias variable-pulse method in conjunction with the approach of Zohta et al. [12]. For the electron-irradiated undoped GaAs a reverse bias $V_r = 8$ V was used and the filling pulse amplitude V_p was varied between 1 and 8 V. To circumvent the problems associated with field assisted emission, spectra recorded by increasing V_p in steps of 1 V were subtracted from each other so that information of only a narrow spatial region, instead of that corresponding to the full pulse height, is analyzed. This method is similar to the DDLTS method [14]. The depth profiles thus obtained, for all electron irradiation doses, indicated that the concentrations of the $E\beta1$–$E\beta3$ are approximately constant in the region profiled, i.e. the first five microns below the SBD interface. During a 30 min irradiation the dose of 3.4×10^{12} e/cm^2 introduced both the $E\beta1$ and $E\beta2$ in concentration of $7–8 \times 10^{12}$/cm^3 and the $E\beta3$ in a concentration of about $2–3 \times 10^{12}$/cm^3. For all other doses investigated it was observed that $E\beta1$ and $E\beta2$ are present in about equal concentrations, and that their concentration is about three times that of the $E\beta3$.

The introduction rates η for the $E\beta1$, $E\beta2$ and $E\beta3$ were calculated from

$$\eta = N_t/(\varphi t)\,, \tag{2}$$

where φ is the irradiation-dose rate. The dose φt used for these calculations was the *effective dose* of electrons with energies above 250 keV, i.e. 3.4×10^{12} e/cm^2. When using this dose, the introduction rate calculated here should be considered to be an *average introduction rate* for electrons having energies in the 250 keV–2.3 MeV energy range. The average introduction rates of the $E\beta1$ and $E\beta2$ were both found to be 2.0 cm^{-1}, while that of the $E\beta3$ was 0.7 cm^{-1}. It is interesting to note that the ratio of the introduction rate of

Table 1. Characteristics of electron- and alpha-particle irradiation-induced defects detected by DLTS in OMVPE-grown n-GaAs

Defects detected here				Similar defects				
Label	E_t [a]	σ_{na} [b]	T_{peak} [c]	Label	E [a]	σ_{na} [b]	T_{peak} [c]	Ref.
$E\alpha1$	0.041	$6.8E-16$	34	$EE1$	0.043	$1.1E-15$	35	[8]
$E\beta1$	0.041	$5.4E-16$	34	$E1$	0.045	$2.2E-15$	33[d]	[1]
				$PE7$	0.046	$4E-14$	30	[17]
$E\alpha2$	0.141	$1.2E-13$	77	$EE2$	0.142	$1.2E-13$	78	[8]
$E\beta2$	0.139	$9.3E-14$	78	$E2$	0.140	$1.2E-13$	75[d]	[1]
				$PE6$	0.140	$1.0E-13$	79	[17]
$E\alpha3$	0.337	$2.5E-14$	184	$L-6$	–	–	180	[18]
				$PE4$	0.310	$4E-14$	173	[17]
$E\alpha4$	0.378	$1.6E-14$	208	$EE3$	0.375	$1.3E-14$	209	[8]
$E\beta3$	0.378	$1.6E-14$	208	$E3$	0.30	$6.2E-15$	167[d]	[1]
				$PE3$	0.390	$6.0E-14$	209	[17]

[a] Effective activation energy, measured below the conduction band
[b] Apparent majority carrier capture cross section
[c] Measured at a lock-in amplifier frequency of 46 hz, i.e. at a decay time constant of 0.23 ms
[d] Calculated from E_t and σ_{na} values given in [1]. The values for $E3$ were obtained in 10^{16} cm^3 doped GaAs and may therefore be affected by field-assisted emission

© University of Pretoria

UNIVERSITEIT VAN PRETORIA
UNIVERSITY OF PRETORIA
YUNIBESITHI YA PRETORIA

the $E\beta1$ to that of the $E\beta3$ is about three, almost the same as that observed for defect production by electron irradiation in accelerators. The values of the average introduction rates measured here are in good agreement with those obtained after irradiating GaAs in accelerators with electrons in the same energy range [1].

An additional factor that should be borne in mind is that the introduction rates of electron irradiation-induced defects have been found to depend on the orientation of the GaAs crystal with respect to that of the electron beam [15]. In our experiment, however, the direction of the electrons are random. Although the Sr source was placed in front of the (100) face of the GaAs, electrons may enter the crystal in directions other than the [100] direction, which may also influence the values of the average introduction rates.

Next, we discuss the DLTS results obtained by irradiating the $10^{16}/cm^3$ doped GaAs with electrons for periods of up to 1000 min (i.e. a dose of $1.1 \times 10^{14}\, e/cm^2$). Electron irradiation had no influence on $I-V$ characteristics of the SBDs, not even for the longest time of 1000 min. For this carrier density it should be borne in mind that when applying a quiescent bias of a few volts, the electric field in the depletion region is high enough to cause an observable enhancement of the emission rate. This gives rise to broad DLTS peaks which are also displaced to lower temperatures. Because the electric field increases from zero at the edge of the depletion region to a maximum at the interface, the field effect can be reduced by monitoring only defects near the edge of the depletion region. To illustrate this we show curves (b) and (c) in Fig. 3 which were recorded at a reverse bias of $V_r = 4\,V$, and filling pulses of $V_p = 0.8\,V$ and 1.2 V, respectively. It is clear that curve (b), which represents defects closer to the edge of the depletion region, is not as distorted as curve (c) which also includes defects further away from the edge of the depletion region (i.e. in a higher-field region). From these curves it should be clear that if spectra of defects in the doped GaAs are to be meaningfully compared to those of defects in the undoped GaAs, then curve (b) in Fig. 3 should be used. When therefore comparing curve (b) in Fig. 3 to curve (b) in Fig. 2 for the undoped GaAs, it is evident that electron irradiation introduced the same set of defects in both carrier density GaAs samples.

DLTS depth profiling of electron irradiated doped GaAs was performed using a quiescent bias of $V_r = 4\,V$. Because the effect of the electric field on the emission rate of the $E\beta1$ is rather severe, only the $E\beta2$ and $E\beta3$ could be profiled. Furthermore, in order to minimize the effect of the electric field, the filling pulse amplitudes were limited to below 2 V and DLTS peaks were subtracted from each other to obtain differential peak heights. The results thus obtained showed that, for all the doses investigated, the concentration of the $E\beta2$ was the same in the doped and undoped GaAs. The same was true for the $E\beta3$ concentration. This confirms previous observations [1] that the defects introduced by electrons are point defects and do not involve dopant atoms.

Finally, we investigated the effect of electron irradiating the GaAs directly versus irradiating it through the Schottky metal. Pons et al. [1] have reported the presence of a defect $E6$ which could only be observed *after irradiating* GaAs *through a gold* SBD. However, we could not observe any difference between spectra from GaAs using Pd SBDs which were deposited before and after irradiation. Further, the baseline of the spectrum remained flat upon recording spectra at different filling pulse amplitudes, even when the voltage during the pulse extended up to the flat band voltage. This indicates that if interface or near-surface states (which communicate with the GaAs conduction band) are introduced by irradiating the GaAs through the metal contact, then their concentrations are below the DLTS detection limit. These observations are in correspondence with our $I-V$ results which indicate that the barrier properties remained unaltered after electron irradiation.

2.3 Defects Created by Alpha Irradiation from a ^{241}Am Source

First, consider irradiation of the undoped n-GaAs. $I-V$ measurements indicated that alpha irradiation at the longest time of 10 h (i.e. with a dose of $1.8 \times 10^8\, \alpha/cm^2$) has no influence on the barrier properties. Curve (c) of Fig. 2 depicts the DLTS spectrum of this material which was irradiated *through a* Pd SBD with this dose. It shows the presence of three well defined defect peaks labelled $E\alpha1$, $E\alpha2$ and $E\alpha4$, as well as two other less pronounced defect peaks which seem to be superimposed onto a skewed baseline. No capacitance DLTS data of alpha irradiated GaAs could be found in the literature. When comparing the spectrum of alpha irradiated GaAs (curve (c) in Fig. 2) to that of electron irradiated GaAs (curve (b) in Fig. 2), it seems that the $E\alpha1$, $E\alpha2$ and $E\alpha4$ are similar to the $E\beta1$, $E\beta2$ and $E\beta3$, respectively. To verify this, their DLTS "signatures" (obtained under identical pulse and bias conditions) are compared in Table 1. From this comparison it is clear that these two sets of defects indeed have the same "signatures", implying that their electronic structures are the same. We therefore conclude that the three most prominent alpha irradiation induced defects in the undoped GaAs are the same as those introduced during electron irradiation of the same material. Because the $E\alpha5$ is not well resolved, its electronic properties could not be derived at this stage.

It is further interesting to note that whereas the $E\beta1$ and $E\beta2$ in electron irradiated GaAs occur in about the same concentration, the $E\alpha1$ concentration is significantly lower than that of the $E\alpha3$. This was observed for all irradiation doses of the undoped GaAs, which raises the following problem: We have shown that the $E\alpha1$ and $E\alpha2$ have identical electronic properties as the $E1$ and $E2$, respectively, which in turn have been proposed to be two different charge states of the same defect. If this is true, and the defect concentration is much lower than the free carrier density (as is the case here), then the two different charge states should have the same concentrations and should be equally populated. However, as observed here, this is not the case. We speculate that the charge state occupation giving rise to the $E\alpha1$ is suppressed for some reason, perhaps by a local disturbance like the closeness of other (extended) defects.

An additional feature of the spectrum of alpha-irradiated GaAs that deserves attention is the skewing of the baseline. To test whether this was possibly due to interface states resulting from irradiation-induced interface state mixing, we

© University of Pretoria

UNIVERSITEIT VAN PRETORIA
UNIVERSITY OF PRETORIA
YUNIBESITHI YA PRETORIA

recorded spectra at a fixed quiescent reverse bias, but at filling pulses of different magnitudes. The results indicated that the degree of baseline skewing increases as the pulse amplitude increases, but that it occurs irrespective of whether or not the filling pulse extends into forward bias. This is an indication, but not conclusive evidence, that the baseline skewing is not caused by interface states [16]. To further investigate the possibility of radiation induced interface mixing, we compared the DLTS spectra of GaAs irradiated with alphas *before* and *after* SBD metallization. The results showed that baseline skewing occurs irrespective of whether irradiation is done before or after metallization. It is therefore evident that the skewed baselines are not caused by interface mixing during irradiation.

Next, consider the results obtained after irradiating the $10^{16}/\text{cm}^3$ doped n-GaAs with alphas. As was the case for the low doped sample, $I-V$ measurements showed that, even at the longest time of 300 h (i.e. a dose of $5.4 \times 10^9\ \alpha/\text{cm}^2$) alpha irradiation left the Schottky barrier properties unaltered. The DLTS spectra, curves (d) and (e) in Fig. 3, show that the $E\alpha 1$ and $E\alpha 2$ again seem to be the same as the $E\beta 1$ and $E\beta 2$ introduced during electron irradiation of the same material. This spectrum further shows that, in the doped GaAs, the $E\alpha 3$ occurs and has a higher concentration than the $E\alpha 4$. The main difference between the two types of GaAs used here is that the free-carrier concentration of the doped GaAs is about 25 times higher than that of the undoped GaAs. This indicates that the $E\alpha 3$ is a defect caused either by the higher electric field in the higher doped GaAs, or by the dopant atoms themselves (i.e. a complex involving the radiation induced defects and the dopant atoms). If the $E\alpha 3$ is a simple complex between Si and a vacancy or interstitial, then it should also have been observed in electron irradiated doped GaAs where vacancies and interstitials are the most abundant irradiation products. This was, however, not the case and therefore we rule out this possibility. It is instructive to note that a defect similar in nature to the $E\alpha 3$ has been observed before in proton irradiated GaAs [17, 18]. In the case of [17] its presence seemed to be enhanced by the application of a large forward bias filling pulse.

3 Conclusions

The results obtained in this study indicate that the defects introduced in n-type GaAs by alpha and beta irradiation from radionuclides are identical in nature to those introduced by particle irradiation in Van de Graaff and linear accelerators. The main defects in beta-(electron-)-irradiated n-GaAs are the $E\beta 1$, $E\beta 2$ and $E\beta 3$, the same as the $E1$, $E2$ and $E3$ observed after electron irradiation of GaAs in an accelerator. Electron irradiation of the $1 \times 10^{16}/\text{cm}^3$ doped GaAs showed that the same set of defects were introduced at the same introduction rates as in the $4 \times 10^{14}/\text{cm}^3$ (undoped) GaAs. This confirms previous observations that the electron traps introduced during electron irradiation of n-GaAs are point defects which do not depend on impurities such as dopant atoms. Considering that the betas emitted from the radionuclide are not monoenergetic, the introduction rates obtained here are in good agreement with the average rates in the same energy range of defects introduced in electron accelerators. Because the introduction rates are constant for the dose range investigated, these radionuclides are ideal for producing samples containing radiation induced defects in specific concentrations, which can be used as "laboratory standards" for defect identification or for temperature calibration purposes.

The most prominent defects introduced by alpha irradiation of undoped n-GaAs are the $E\alpha 1$, $E\alpha 2$ and $E\alpha 4$, which have the same properties as the $E\beta 1$, $E\beta 2$, and $E\beta 3$, i.e. the $E1$, $E2$ and $E3$. In the case of doped GaAs, alpha irradiation introduced the $E\alpha 3$, and in a higher concentration than the $E\alpha 4$. It is significant to note that we did not observe the $E\alpha 3$ in any electron-irradiated GaAs or in the alpha-irradiated undoped GaAs. We speculate that the $E\alpha 3$ is related to the presence of the higher amount of dopant atoms in the doped GaAs. However, to confirm this more extensive studied comprising GaAs doped with different dopants to various levels extending well into the $10^{16}/\text{cm}^3$ range should be undertaken.

Our DLTS measurements indicated that identical spectra were obtained whether irradiating before or after (i.e. through the) SBD metallization. This observation was supplemented by $I-V$ measurements which showed that the barrier properties of the SBDs were unchanged after irradiating through them, even after the highest doses ($1.1 \times 10^{14}\ e/\text{cm}^2$ and $5.4 \times 10^9\ \alpha/\text{cm}^2$).

Because particles from radionuclides introduce the same defects as particles from accelerators, we conclude that during many experiments radionuclides are suitable for studying radiation induced defects. The exceptions are when the direction of the particle beam has to be accurately known or when high dose rates are required. The main advantages of using radionuclides, rather than accelerators, for defect production is that the radionuclides are inexpensive and simple to handle compared to accelerators. Radionuclides are therefore also in some cases suitable to irradiate electronic devices for radiation-hardness testing.

In summary, by using commercially available electron and alpha sources in the form of radionuclides, primary and extended radiation induced defects were introduced in OMVPE-grown n-GaAs. We have demonstrated that the use of radionuclides is a convenient and powerful, yet inexpensive, method to introduce and study radiation-induced defects in semiconductors. The introduction rates of these defects were found to be in good agreement with those of the same defects introduced by irradiation in accelerators. In addition, we reported the presence of an alpha irradiation-induced electron trap in Si doped GaAs which seems to be related to the presence of the dopant.

Acknowledgements. The financial assistance of the Foundation for Research Development (FRD) is gratefully acknowledged. Thanks are also due Miss R. Gerber for technical assistance with the radionuclide irradiations.

References

1. D. Pons, J.C. Bourgoin: J. Phys. C. Solid State Phys. **18**, 3839 (1985)
2. D. Stievenard, X. Boddaert, J.C. Bourgoin, H.J. von Bardeleben: Phys. Rev. B **41**, 5271 (1990)

© University of Pretoria

UNIVERSITEIT VAN PRETORIA
UNIVERSITY OF PRETORIA
YUNIBESITHI YA PRETORIA

3. D. Stievenard, X. Boddaert, J.C. Bourgoin: Phys. Rev. B **34**, 4048 (1986)
4. G.T. Brown, S.J. Barnett, S.J. Courtney, S.S. Gill: Mater. Sci. Eng. B **2**, 91 (1989)
5. W. Cleland, K. Lark-Horovitz, C. Pigg: Phys. Rev. **78**, 814 (1950)
6. J.H. Crawford, L.M. Slifkin (eds.): *Point Defects in Solids*, (Plenum, New York 1975) p. 45
7. D.V. Lang: J. Appl. Phys. **45**, 3014 (1974)
8. F.D. Auret, L.J. Bredell, G. Myburg, W.O. Barnard: Jpn. J. Appl. Phys. **30**, 80 (1991)
9. G. Myburg, F.D. Auret: J. Appl. Phys. **71**, 6172 (1992)
10. F.D. Auret, M. Nel: J. Appl. Phys. **63**, 973 (1988)
11. G. Myburg, W.E. Meyer, F.D. Auret: Rev. Sci. Instrum. **63**, 2101 (1992)
12. Y. Zohta, M.O. Watanabe: J. Appl. Phys. **53**, 1809 (1982)
13. B. Ziebro, J.W. Hemsky, D.C. Look: J. Appl. Phys. **72**, 78 (1992)
14. H. Lefevre, M. Schulz: Appl. Phys. **12**, 45 (1977)
15. D. Pons, J.C. Bourgoin: Phys. Rev. Lett. **47**, 1293 (1981)
16. F.D. Auret, G. Myburg, L.J. Bredell, W.O. Barnard, H.W. Kunert: J. Mater. Sci. Forum **83–87**, 1499 (1992)
17. F.D. Auret, M. Nel, H.C. Snyman: Radiat. Effects **105**, 225 (1988)
18. Y. Yuba, K. Gamo, K. Murakami, S. Namba: Inst. Phys. Conf. Ser. No. 59, Chap. 6, 329 (1980)

© University of Pretoria

UNIVERSITEIT VAN PRETORIA
UNIVERSITY OF PRETORIA
YUNIBESITHI YA PRETORIA

Hole defects in molecular beam epitaxially grown *p*-GaAs introduced by alpha irradiation

S. A. Goodman, F. D. Auret, and W. E. Meyer
Physics Department, University of Pretoria, Pretoria 0002, South Africa

(Received 9 April 1993; accepted for publication 21 September 1993)

Epitaxial aluminum Schottky barrier diodes on molecular beam epitaxially grown *p*-GaAs with a free carrier density of 2×10^{16} cm^{-3} were irradiated with alpha particles at room temperature using an americium-241 (Am-241) radio nuclide. For the first time, the radiation induced hole defects are characterized using conventional deep level transient spectroscopy (DLTS). The introduction rates and DLTS "signatures" of three prominent radiation induced defects $H\alpha1$, $H\alpha4$, and $H\alpha5$, situated 0.08, 0.20, and 0.30 eV above the valence band, respectively, are calculated and compared to those of similar defects introduced during electron irradiation.

Gallium arsenide is an important material in field-effect transistors, heterojunction bipolar transistors, solar cells, and integrated circuits and, since these components are becoming increasingly important in space applications,[1] due to their increased speed and resistance to radiation damage,[2] a knowledge of the influence of radiation damage on their performance has become an active field of research. Hopkins and Srour[3] reported for the first time on the measurement of an alpha particle induced charge in Schottky diodes fabricated on *n*-type GaAs. Umemoto *et al.*[4] reported on the influence of alpha particle induced damage on the performance of metal-semiconductor field-effect transistors (MESFETs) fabricated on semi-insulating GaAs with a buried *p* layer. It has been well-known for decades that, in principle, it is possible to dope gallium arsenide with impurities resulting from nuclear reactions based on thermal neutrons, gamma rays, and charged particles. Zakharenkov *et al.*[5] have shown that the most effective nuclear doping of GaAs is by alpha irradiation. There have been many extensive studies on the defects produced by electron irradiation in *n*-type GaAs[6–10] but fewer on the hole defects introduced during this type of irradiation.[6,11,12] However the same cannot be said for alpha irradiation induced defects, where there has been very little work done on the traps introduced in *n*-type GaAs[13,14] and, until now, there have been no reports on the traps detected in *p*-type GaAs.

All layers used in this study were grown by molecular beam epitaxy in a VG V90H system using solid sources; the samples studied in this work were *p*-type GaAs films, 0.5–1.0 μm thick on p^+ bulk-grown substrates.[15] From capacitance-voltage (C-V) measurements at a frequency of 1 MHz, the free carrier density (N_A-N_D) and the built-in voltage (V_{bi}) of the beryllium (Be)-doped *p*-type layer at 300 K were measured as $(1.8\pm0.2)\times10^{16}$ cm^{-3} and 0.5 ± 0.03 eV, respectively. The free carrier density and the built-in voltage were also determined at the defect peak temperatures by variable temperature (C-V) measurements. Single-crystal 0.2-μm-thick aluminum Schottky diodes were grown on the Be-doped material in the molecular beam epitaxy (MBE) system without breaking vacuum, thereby ensuring relatively oxide free Schottky diodes.[15]

A two-phase lock-in amplifier-based (LIA) deep level transient spectroscopy (DLTS) system, comprised of a Stanford Research SR530 LIA, a modified Boonton 72BD capacitance meter,[16] and an Air Products cryostat with temperature controller, was employed to detect and characterize defects introduced during alpha(α) irradiation. The DLTS[17] spectra were acquired at a rate of 4 K min^{-1} in both temperature directions to eliminate any peak temperature discrepancies due to uneven cooling or heating. Prior to irradiation, control DLTS spectra were acquired for each sample to facilitate accurate trap concentration measurements.

An americium 241 (Am-241) radio nuclide with an activity of 192 μCi cm^{-2} was used to irradiate the samples with 5.4 MeV α particles at a fluence rate of 7.1×10^6 cm^{-2} s^{-1}. As it is assumed that the measured capacitance transient varies exponentially with time, it is important that the densities of introduced deep levels are small compared to those of shallow levels. The trap density (N_T) should not be greater than 10% of the free carrier density (N_A-N_D) to ensure that the transients are exponential.[18]

The DLTS spectra, all recorded under the same DLTS conditions in the temperature range 15–300 K, are presented in Fig. 1. The DLTS spectrum of the control (unirradiated) sample is shown in curve (a); no defects (with concentrations lower than 2×10^{12} cm^{-3}) could be detected by DLTS. After alpha irradiation at least six defects labeled $H\alpha1$–$H\alpha6$ were introduced, as illustrated in curve (c) and were recorded afterward at a fluence of 8.9×10^{10} cm^{-2} alpha particles. If there is a decrease in the particle fluence, there is a corresponding decrease in the trap concentrations, as is illustrated in curve (b), recorded after a fluence of 5.1×10^{10} cm^{-2}. The broad peak, $H\alpha6$, shows an increase in peak height with an increase in incident fluence. This broad peak is possibly due to the presence of a band of defects in the band gap that may also be responsible for the nonuniform baseline offset.[19] The three most prominent defects after alpha irradiation are $H\alpha1$, $H\alpha4$, and $H\alpha5$. Their DLTS signatures (energy level E_T in the band gap and apparent capture cross section σ_{pa}) were determined from conventional DLTS Arrhenius plots of $\log(e_p/T^2)$ vs $1000/T$ using [20]

 0021-8979/94/75(2)/1222/3/$6.00 © 1994 American Institute of Physics

© University of Pretoria

UNIVERSITEIT VAN PRETORIA
UNIVERSITY OF PRETORIA
YUNIBESITHI YA PRETORIA

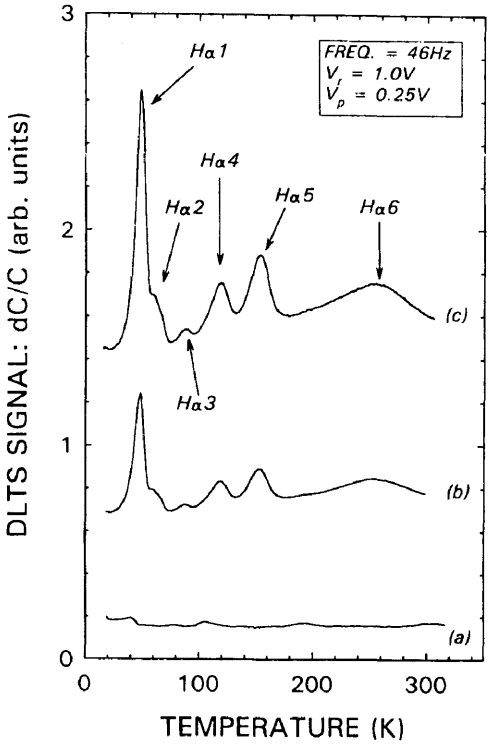

FIG. 1. DLTS spectra of 5.4 MeV alpha (Am-241) irradiated samples recorded at a reverse quiescent bias of 1.0 V and a filling pulse amplitude of 0.25 V, the lock-in amplifier frequency of 46 Hz. Curve (a) is the control (unirradiated) spectrum, while curves (b) and (c) are the spectra after the diodes received fluences of 5.1×10^{10} cm^{-2} and 8.9×10^{10} cm^{-2} alpha particles, respectively.

TABLE I. Comparison between the characteristics of alpha and electron irradiation induced defects in MBE grown 10^{16} cm^{-3} Be-doped p-GaAs and similar defects detected by others after electron irradiation. (VPE stands for vapor phase epitaxy.)

Label	E_T[a] (eV)	σ_{pa}[b] $\times10^{-16}$ (cm^2)	η[c] (cm^{-1})	References
MBE[d]				
$H\alpha1$[e]	0.08	26	4705	This work
$H\alpha3$	0.15	59	≈490	This work
$H\alpha4$	0.20	12	1050–4335	This work
$H\alpha5$	0.30	160	2100	This work
(VPE)				
$H0$ ($H\alpha1$)	0.06	1.6	0.8	24
$H0$ ($H\alpha1$)	0.06	–	–	11
−($H\alpha1$)	0.06	0.07	0.8	12
$H1$ ($H\alpha5$)	0.25	14.0	0.09	11
$H1$ ($H\alpha5$)	0.25	83.0	0.25	12
$H2$ ($H\alpha5$)	0.29	590	0.7	25
$H1$ ($H\alpha5$)	0.29	20.0	0.1–0.7	6
MBE[d]				
$H\beta1$[e]	0.08	28	1.5	23
$H\beta3$	0.16	170	0.03	23
$H\beta4$	0.20	12	0.05–0.20	23
$H\beta5$	0.30	120	0.2	23

[a]Effective activation energy, measured above the valence band.
[b]Apparent majority carrier capture cross section, determined from an Arrhenius plot.
[c]Average introduction rate η with the trap density calculated in voltage ranges of V_r=2.0 V and V_p=0.2–1.0 V, and V_r=1.0 V and V_p=0.2–0.6 V.
[d]MBE material obtained from the same wafer and electron irradiated and measured in the same laboratory. DLTS signatures for this material are at near zero-field conditions.
[e]DLTS scanning rate was 2.0 K min^{-1}.

$$e_P=\Upsilon_P T^2\sigma_{pa}\exp(-E_T/kT). \quad (1)$$

Here e_P is the hole emission rate from the defect site at a temperature T, k is the Boltzmann's constant, and the Υ_P is a constant equal to 1.62×10^{21} cm^{-2} s^{-2} K^{-2} for a hole trap[21] if, for simplicity, the degeneracy is taken as one. The introduction rates and signatures specified in Table I were determined by using fixed-bias variable-pulse difference DLTS depth profiling in conjunction with the approach of Zohta *et al.*.[22] This entails subtracting DLTS spectra that were recorded at the same quiescent reverse bias V_r, but at different pulse amplitudes, V_p and $V_p+\delta V_p$. To minimize any possible electric field enhancement of the emission rates, small pulse amplitudes were used. A comprehensive comparison of the defect signatures and introduction rates is displayed in Table I, where we compare the alpha irradiation induced defects to defects detected in the same material after 2.0 MeV electron irradiation[23] and to those defects detected by other workers after electron irradiation.[24,25] It appears that the defects labeled $H\alpha1$ and $H\alpha5$ detected in this study are the same defects labeled $H0$ and $H1$ found by Stievenard *et al.*[11] in electron irradiated p-GaAs. These workers concluded that these two defects are related to the arsenic vacancy-interstitial pair. Loualiche *et al.*[12] stated that $H1$ ($H\alpha5$), because of its annealing kinetics, is a single primary defect. Pons[23] stated that these two defects are due to the displacement of the same type of atom, namely, arsenic, and that the difference in their introduction rates is possibly due to the antisite defect formation through the replacement of one Ga lattice atom by one interstitial As atom in one of these defects. The correspondence between the DLTS signatures of the alpha and electron irradiation induced defects strongly suggests that $H\alpha1$ and $H\alpha5$ also have a point defect nature, with $H\alpha1$ being associated with the isolated As vacancy (V_{As}) and $H\alpha5$ a combination of isolated and correlated V_{As}-As$_i$ pairs. The defect $H\alpha4$, not previously reported, was detected in alpha and electron[23] irradiated Be-doped p-GaAs using both Al and Mg Schottky barrier diodes (SBDs). The defect concentration profiles showed that the concentrations of $H\alpha1$ and $H\alpha5$ were constant in the region profiled (0.15–0.35 μm below the SBD interface). In contrast, however, the detectable concentration of $H\alpha4$, when profiling at a constant reverse bias (V_r) and varying the pulse height (V_p), decreased sharply away from the interface. Stievenard *et al.*[26] stated that in p-type GaAs the mobility of the As$_i$ is high enough to allow for the creation of defect complexes. We speculate that $H\alpha4$ is a more complex type of defect that forms between uniformly distributed radiation induced point defects and an impurity or structural defect in which the concentration depends strongly upon the applied electric field in the depletion region. Due to this field dependent defect concentration,

© University of Pretoria

UNIVERSITEIT VAN PRETORIA
UNIVERSITY OF PRETORIA
YUNIBESITHI YA PRETORIA

the introduction rate given in Table I is presented as a range. However, the peak position of this trap is independent of the applied electric field. The complex defect labeled $H2$ detected by Stievenard *et al.*,[11] and related to the interaction of an arsenic interstitial and a copper atom, is not detected in this study since this impurity is not present in the material prior to irradiation.

This communication has identified and characterized the hole defects introduced into 2×10^{16} cm^{-3} p-type MBE material with epitaxial Al SBDs during alpha irradiation from an Am-241 radio nuclide. The introduction rates and signatures of $H\alpha1$ and $H\alpha5$ have been correlated to the well-known electron irradiation induced defects with similar DLTS signatures. The signature and possible origin of a third defect, $H\alpha4$, not previously reported even for electron irradiation, is presented.

The financial assistance of the South African Foundation for Research Development (FRD) is gratefully acknowledged. We thank Dr. M. Missous and Professor A. R. Peaker of University of Manchester Institute of Science and Technology, UK, for supplying the MBE material, and Dr. C. Schutte for the photolithography.

[1] A. F. Galashan and S. W. Bland, J. Appl. Phys. **67**, 173 (1990).
[2] A. R. Knudson, A. B. Cambell, W. J. Stapor, P. Shapiro, and G. P. Mueller, IEEE Trans. Nucl. Sci. **NS-32**, 4388 (1985).
[3] M. A. Hopkins and J. R. Srour, IEEE Trans. Nucl. Sci. **NS-30**, 4457 (1983).
[4] Y. Umemoto, N. Masuda, and K. Mitsusada, IEEE Electron. Dev. Lett. **EDL-7**, 396 (1986).
[5] L. F. Zakharenkov, V. K. Kozlovskii, and B. A. Shustrov, Phys. Status Solidi A **117**, 85 (1990).
[6] D. Pons and J. C. Bourgoin, J. Phys. C **18**, 3839 (1985).
[7] J. C. Bourgoin, H. J. von Bardeleben, and D. Stievenard, Phys. Status Solidi A **102**, 499 (1987).
[8] J. W. Farmer and D. C. Look, Phys. Rev. B **21**, 3389 (1980).
[9] D. Stievenard, J. C. Bourgoin, and D. Pons, Physica B **116**, 394 (1982).
[10] D. V. Lang, Inst. Phys. Conf. Ser. **31**, 70 (1977).
[11] D. Stievenard, X. Boddaert, and J. C. Bourgoin, Phys. Rev. B **34**, 4048 (1986).
[12] S. Loualiche, A. Nouailhat, G. Guillot, M. Gavand, A. Langier, and J. C. Bourgoin, J. Appl. Phys. **53**, 8691 (1982).
[13] A. P. Mamontov and V. V. Peshev, Sov. Phys. Semicond. **18**, 624 (1984).
[14] A. Sen Gupta, S. V. Naidu, and P. Sen, Appl. Phys. A **40** (1986).
[15] M. Missous, E. H. Rhoderick, K. E. Singer, and W. S. Truscott, J. Cryst. Growth **111**, 1116 (1991).
[16] T. I. Chappel and C. M. Ransom, Rev. Sci. Instrum. **55**, 200 (1984).
[17] D. V. Lang, J. Appl. Phys. **45**, 3014 (1974).
[18] W. E. Philips and J. R. Lowney, J. Appl. Phys. **54**, 2786 (1983).
[19] F. D. Auret, G. Myburg, S. A. Goodman, L. J. Bredell, and W. O. Barnard, Nucl. Instrum. Meth. B **67**, 410 (1992).
[20] P. J. Wang, T. F. Kuech, M. A. Tischler, P. M. Mooney, G. Scilla, and F. Cardone, J. Appl. Phys. **64**, 4975 (1988).
[21] S. A. Goodman, F. D. Auret, and G. Myburg, Semicond. Sci. Technol. **7**, 1241 (1992).
[22] Y. Zohta and M. O. Watanabe, J. Appl. Phys. **53**, 1809 (1982).
[23] F. D. Auret, S. A. Goodman, G. Myburg, W. E. Meyer, R. M. Erasmus, A. Wilson, and A. R. Peaker, Jpn. J. Appl. Phys. Lett. **32** (7B), 974 (1993).
[24] D. Pons, Physica B **116**, 388 (1983).
[25] M. Yamaguchi and C. Uemura, J. Appl. Phys. **57**, 604 (1985).
[26] D. Stievenard, X. Boddaert, J. C. Bourgoin, and H. J. von Bardeleben, Phys. Rev. B **41**, 5271 (1990).

© University of Pretoria

UNIVERSITEIT VAN PRETORIA
UNIVERSITY OF PRETORIA
YUNIBESITHI YA PRETORIA

Nuclear Instruments and Methods in Physics Research B 90 (1994) 349–353
North-Holland

NIM B
Beam Interactions with Materials & Atoms

The effect of alpha-particle and proton irradiation on the electrical and defect properties of n-GaAs

S.A. Goodman, F.D. Auret * and W.E. Meyer
Physics department, University of Pretoria, Pretoria 0002, South Africa

Radiation damage effects were studied in n-GaAs grown by organo-metallic vapour phase epitaxy (OMVPE) for a wide range of alpha-particle (2.0 MeV and 5.4 MeV) and proton (2.0 MeV) particle fluences, using an americium-241 (Am-241) radio-nuclide and a linear Van de Graaff accelerator as the particle sources. The samples were irradiated at 300 K, after fabricating palladium Schottky barrier diodes (SBDs) on the 1.2×10^{16} cm^3 Si-doped epitaxial layers. The irradiation-induced defects are characterized using conventional deep level transient spectroscopy (DLTS). A correlation is made between the change in SBD characteristics and the quantity and type of defects introduced during irradiation. It is shown that the two parameters most susceptible to this irradiation are the reverse leakage current of the SBDs and the free carrier density of the epilayer. The introduction rate and the "signatures" of the alpha-particle and proton irradiation-induced defects are calculated and compared to those of similar defects introduced during electron irradiation.

1. Introduction

A number of GaAs semiconductor devices manufactured today must ultimately function in an environment fraught with radiation hazards. The main applications of Schottky barrier diodes (SBDs) include rectifiers, microwave switches and mixer circuits as well as level shifting and electrostatic discharge protection circuits [1]. Some applications require optimum performance in forward bias, whereas others require optimum performance in reverse bias. Selection of a diode for an application requires evaluation of, amongst others, the reverse saturation current and capacitance variation with voltage. Hopkins and Srour [2] reported for the first time on the measurement of alpha (α)-particle induced charge in Schottky diodes fabricated on n-type GaAs. Umemoto et al. [3] reported the influence of α-particle induced damage on the performance of metal–semiconductor field-effect transistors (MESFETs) fabricated on semi-insulating GaAs, whereas Zardas et al. [4] investigated the dependence of the current–voltage (I–V) characteristics of GaAs MESFETs on temperature and α-particle irradiation. Yamaguchi et al. [5] evaluated the minority carrier diffusion length in proton (H^+) irradiated GaAs single crystals using the photo-voltaic effect of solar cells. Proton (H^+) beams have been extensively used in Rutherford backscattering–channelling (RBS-C) studies and it has been shown that low energy proton irradiation causes more displacements of Ga atoms than As atoms [6], contrary to the results for electron (e^-) irradiation. Certainly, a knowledge of radiation effects on device performance of components which must be successfully deployed in outer space, in nuclear reactors, or in proximity to detonations from nuclear weapons is required. In this study we investigate the change in electrical properties of SBDs and the nature and quantity of introduced defects in the epitaxial layer due to α-particle and H^+-irradiation over a wide range of fluences.

2. Experimental procedure

Silicon-doped 5.0 μm thick n-type GaAs films with a free carrier density of 1.2×10^{16} cm^{-3} were exposed to α-particle and H^+-irradiation. Ohmic contacts and SBDs were fabricated as described previously [7]. Prior to exposure, the SBDs were electrically characterized by I–V and capacitance–voltage (C–V) measurements under dark conditions. All I–V and C–V measurements were performed in the temperature range 297.0–300.0 K. A two-phase lock-in amplifier-based (LIA) DLTS [8] system, comprising a Stanford Research SR530 LIA, a modified Boonton 72BD capacitance meter [9] and an Air Products cryostat with temperature controller was employed to detect and to characterize the defects introduced during α-particle and H^+-irradiation. The minimum proton and alpha

* Corresponding author, tel. +27 12 4202684, fax +27 12 3424143, e-mail fauret@scinet.up.ac.za.

0168-583X/94/$07.00 © 1994 – Elsevier Science B.V. All rights reserved
SSDI 0168-583X(93)E0660-9

© University of Pretoria

UNIVERSITEIT VAN PRETORIA
UNIVERSITY OF PRETORIA
YUNIBESITHI YA PRETORIA

fluence rate achievable from the linear Van de Graaff accelerator was 1.4×10^{11} cm^{-2} s^{-1}, with an accelerating voltage as high as 2.5 MeV. To obtain lower α-irradiation fluences, a 5.4 MeV Am-241 radio nuclide source with an activity of 192 μCi cm^{-2} was used. Making use of this source, α-particle fluence rates as low as 7.1×10^{6} cm^{-2} s^{-1} could be obtained. For each dose and particle type, 3–4 samples were irradiated, to obtain a reasonable average.

3. Results and discussion

The two most sensitive parameters to incident radiation are the reverse leakage current (I_R) of the SBDs and the free carrier density ($N_D - N_A$) of the epilayer. The variation of these parameters in the temperature range (297.0–300.0 K) were monitored for unirradiated, α-particle and H^+-irradiated material. From this investigation it was seen that only the reverse leakage current exhibited a strong temperature dependence. To minimize such errors, correction factors were used to normalize all current measurements to 300.0 K. For this study it was the intention to determine from C–V measurements the number of free carriers removed and compare these carrier removal concentrations to the individual trap concentrations as determined from DLTS concentration profile measurements. It must be noted that the interpretation of C–V profiles in the presence of deep states calls for considerable care [10].

Fig. 1 illustrates the free carrier removal density as a function of fluence after α-particle irradiation using both the linear Van de Graaff accelerator and the Am-241 radio-nuclide and also as a function of H^+-irradiation using only the linear Van de Graaff accelerator. From these graphs, the carrier removal rate per incident particle can be calculated. The number of free carriers removed per incident α-particle in the fluence range 2.6×10^{10} to 6.2×10^{11} cm^{-2} is $(1.37 \pm 0.05) \times 10^{4}$ cm^{-1}, whereas the carrier removal for 2.0 MeV incident protons in the fluence range 1.4×10^{11} to 2×10^{13} cm^{-2} is $(7.1 \pm 0.2) \times 10^{2}$ cm^{-1}. Fig. 1 also illustrates the increase in reverse leakage current (ΔI_R) measured at 1.0 V as a function of incident particle fluence for both particle types. It can be seen that when plotting this graph using linear scales there is a linear change for both particles. It must be noted that the ideality factor (n) for the irradiated samples was not larger than 1.05, hence the dominant current transport mechanism in the forward bias region (0.15–0.40 V) is still thermionic emission. From I–V measurements it was seen that there was no significant decrease in the barrier height, so any increase in this reverse leakage current cannot be accounted for by a reduction in the barrier height. As has been well documented [11], the primary irradiation-induced defects in

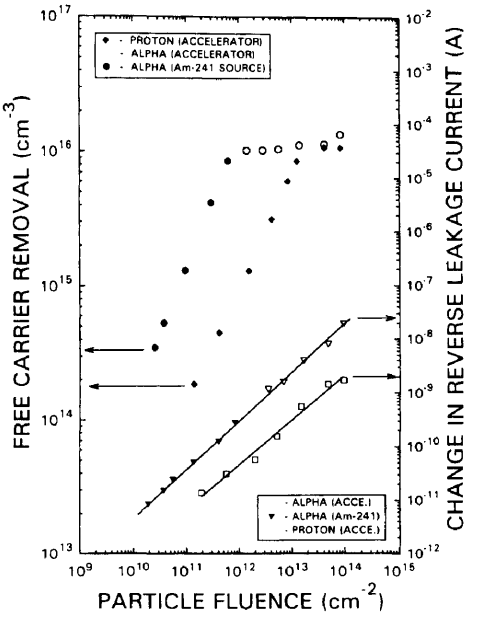

Fig. 1. Free carrier removal ($N_D - N_A$) and increase in reverse leakage current ($\Delta I_R = I_{Rafter} - I_{Rbefore}$) measured at a 1.0 V reverse bias versus alpha-particle (α) and proton (H^+) irradiation fluence.

GaAs are primary defects and since their concentration depends linearly upon the incident fluence, we speculate that the irradiation-induced defects are responsible for the increase in the reverse leakage current.

To determine the magnitude of the series resistance and the recombination current after irradiation, a modified version of the model proposed by Donoval et al. [12] was used. This model yields the barrier height of rectifying metal–semiconductor contacts by fitting the forward characteristics, avoiding the use of the so called ideality factor n.

$$I = I_S\left\{\exp\left(\frac{[q(V - IR_S)]}{kT}\right) - 1\right\} + I_G\left\{\exp\left(\frac{[q(V - IR_S)]}{2kT}\right) - 1\right\} + \frac{(V - IR_S)}{R_{sh}}, \quad (1)$$

with the thermionic emission saturation current prefactor (I_S) represented by the following equation:

$$I_S = AA^*T^2 \exp\left(\frac{-\Phi_{Bi}}{kT}\right), \quad (2)$$

with R_{sh} being the leakage resistance (important in low voltage regions, $qV \ll kT$), R_s the series resistance, A the area of the diode, A^* the Richardson constant (experimentally determined value) equal to 4.8×10^{4} A m^{-2} K^{-2} [13], I_G the generation–recombination

© University of Pretoria

UNIVERSITEIT VAN PRETORIA
UNIVERSITY OF PRETORIA
YUNIBESITHI YA PRETORIA

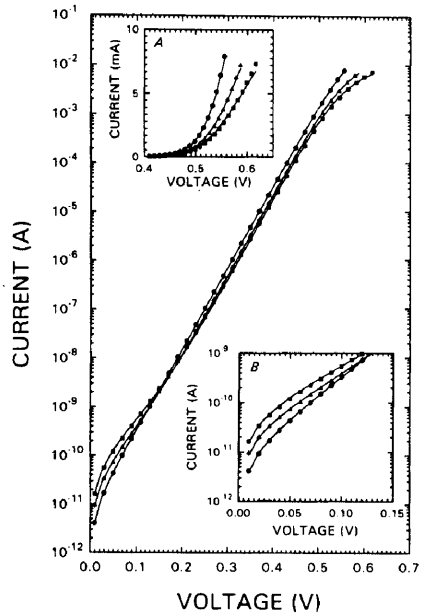

Fig. 2. The I–V characteristics for a control (unirradiated) diode (●), for an incident alpha particle fluence of 3×10^{11} cm^{-2} (▲) and for a fluence of 6.2×10^{11} cm^{-2} (■). The modelled (—) I–V characteristics for all three curves were obtained using the modified model of Donoval et al. [12]. Inset A illustrates the effect of an increase in series resistance on the forward current as a function of incident alpha particle fluence. Inset B illustrates the increase in the recombination current as the incident fluence increases.

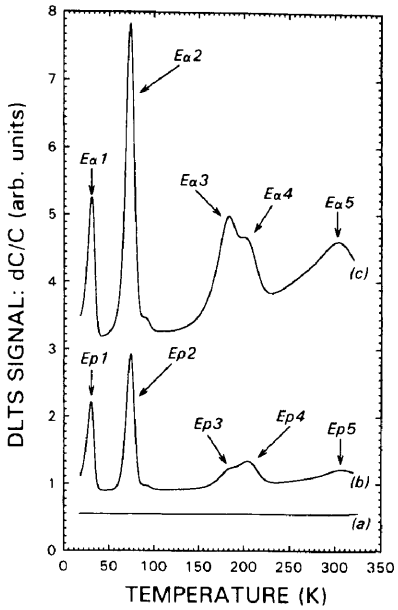

Fig. 3. DLTS spectra of unirradiated (control), 5.4 MeV alpha-particle (α) and 2.0 MeV proton (H^+) irradiated samples at a quiescent reverse bias of 4.0 V and a filling pulse amplitude of 1.2 V, the LIA frequency being 46 Hz. Curve (a) is the spectrum for the control (unirradiated) diode, curve (b) after H^+-irradiation (fluence = 1.6×10^{12} cm^{-2}) and curve (c) after α-particle irradiation (fluence = 9.6×10^{10} cm^{-2}).

pre-factor and Φ_{Bi} the barrier height with image force lowering taken into account. The results of this modelling for α-particle irradiation is depicted in Fig. 2. From inspection of inset B of Fig. 2, where the I–V curves for an unirradiated (control) sample and irradiated samples are depicted, it can be seen that after irradiation the recombination current dominates the current flow in the low forward bias region (0.01–0.1 V) and increases as the incident fluence increases. As the α-particle and H^+-fluence increases from 3.0×10^{11} to 6.2×10^{11} cm^{-2}, there is a corresponding increase in the recombination pre-factor and the series resistance. Inset A of Fig. 2 illustrates the change in forward current as a function of voltage (note the linear current-axis). It is seen that the control sample has the lowest series resistance, whereas the diode that received the highest particle fluence has the highest series resistance. The increase in the series resistance does not appear to be due to degradation of the Schottky contact or the ohmic contact as they did not deteriorate during irradiation. However, where the incident particles come to rest in the semiconductor material, a damaged layer is produced, which could result in this increased series resistance. From Fig. 1 it is clearly evident that there was a carrier reduction after irradiation. The carrier reduction was due to the introduction of defect levels at various positions in the band-gap. These levels trap the free carriers, reducing the free carrier density which in turn leads to an increase in the resistivity of the material, which is observed in the increased series resistance measured after irradiation. The most effective recombination centres are those centres located near the middle of the band-gap whose electron and hole capture cross-sections are approximately equal [14]. The increase in the recombination current is probably due to the presence of such centres introduced during irradiation, the concentration of which depends upon the total incident particle fluence.

The DLTS spectra of the control (unirradiated), H^+- and α-particle irradiated samples are illustrated in curves a, b and c of Fig. 3, respectively. The DLTS signatures (energy level E_T in the band gap and apparent capture cross-section σ_{na}) of the defects detected after irradiation were determined from conventional DLTS Arrhenius plots of $\log(e_n/T^2)$ versus $1000/T$, using ref. [15]

$$e_n = \gamma_n T^2 \sigma_{na}\, e\left(\frac{-E_T}{kT}\right). \tag{3}$$

Here e_n is the electron emission rate from the defect site at a temperature T, k is Boltzmann's constant and the γ_n is a constant equal to 2.21×10^{20} cm^{-2}s^{-2}K^{-2} [16] for an electron trap, if for simplicity the degener-

© University of Pretoria

UNIVERSITEIT VAN PRETORIA
UNIVERSITY OF PRETORIA
YUNIBESITHI YA PRETORIA

Table 1
Comparison between the characteristics of alpha-particle (α) and proton (H^+) irradiation induced defects in OMVPE grown 10^{16} cm^{-3} Si doped n-GaAs and similar defects detected after electron (e^-) irradiation

Label	E_T [a] [eV]	σ_{na} [b] $\times 10^{-16}$ [cm^2]	η [c] [cm^{-1}]
Alpha particle			
Eα1 [d]	0.026	0.15	2963
Eα2	0.117	130	9638
Eα3 [e]	0.304	28	≈ 4560
Eα4	0.353	120	3060
Eα5	0.635	1600	1737
Proton			
Ep1 [d]	0.023	0.09	1056
Ep2	0.112	59	1766
Ep3 [e]	0.301	21	≈ 385
Ep4	0.362	190	470
Ep5	0.636	1200	127
Electron			
(Eβ1) [d]	0.024	0.08	2.0
(Eβ2)	0.117	170	2.0
(Eβ3)	0.380	160	0.7

[a] Effective activation energy, measured below the conduction band.
[b] Apparent majority carrier capture cross-section, determined from an Arrhenius plot.
[c] Average introduction rate (η), with the trap density calculated in the voltage ranges: $V_r = 2.0$ V, $V_p = 0.2$–1.0 V and $V_r = 1.0$ V, $V_p = 0.2$–0.6 V.
[d] DLTS scanning rate was 3.0 K min^{-1}.
[e] Approximate introduction rate (metastable defect).

acy is taken as one. These defect properties are summarised in Table 1. From a comparison of defects introduced during α-particle and H^+-irradiation to those detected in the same material after e^--irradiation, it appears that the defects are similar with the exception of Eα3 and Eα5 in the α-particle irradiated material and Ep3 and Ep5 in the H^+-irradiated material which were not detected after electron irradiation [17]. Defects Eα3 and Ep3 which appear to be similar defects both exhibit a metastable character, in that their concentration and presence depend upon the bias conditions and incident particle type. It has been proposed that E1(Eβ1) and E2(Eβ2) are two different charge states, (−/0) and (0/+) of the isolated arsenic vacancy V_{AS}, in GaAs [18], while E3(Eβ4) is speculated to be related to the close arsenic vacancy–interstitial pairs, $V_{AS} - As_i$ [14]. The correspondence between the DLTS "signatures" of the α-particle and H^+-irradiated material and the electron irradiation-induced defects therefore strongly suggests that Eα1, Ep1, Eα2, Ep2, Eα4 and Ep4 also have a point defect nature. From a graph of defect concentration versus incident fluence the introduction rates of the introduced defects (Eα1 − Eα5 and Ep1 − Ep5) are calculated; these results are presented in Table 1. When comparing the introduction rates for the defects detected in the α-, H^+- and e^--irradiated material it is clear that the introduction rates for α-particles is very much larger than for H^+, which in turn are very much greater than for electrons. The two aspects which must be considered in the interpretation of this data is the difference in the incident energy and the mass of the respective particles.

From defect concentration calculations it is clear that the sum of the defect concentrations of all 5 defects is larger than the total carrier removal as measured by C–V measurements for that particular dose. Blood [10] stated that the traps responsible for carrier removal are the well known E3 and E4 irradiation-induced acceptor-like defect states. Siyanbola and Palmer [19] stated that it are those defects deeper than 0.2 eV below the conduction band that are responsible for carrier reduction, confirming Blood's hypothesis. When calculating the sum of the defect concentrations for the Eα3, Eα4 and Eα5 defect states, it is apparent that their sum is approximately equal to the carrier removal density. The same argument is valid for H^+-irradiated material where Ep3, Ep4 and Ep5 are responsible for the carrier reduction.

4. Conclusions

From this study we have seen that there is removal of free carriers in the epilayer after irradiation with α-particle and H^+-particles. This free carrier removal can cause severe performance degradation in devices. If for example we consider a MESFET: upon removal of carriers from the region below the SBD (gate) the active layer thickness will be modified, resulting in a reduction in the drain–source current and a change in the pinch-off characteristics of the device. Hopkins and Srour [2] have shown that a reduction in carrier mobility due to irradiation is a second order effect. The radiation defects created also reduce the non-equilibrium carrier lifetime in the semiconductor and consequently result in deterioration of the energy resolution of detectors [20]. We have shown that α-particle irradiation causes a more severe reduction in free carrier density and a larger increase in the reverse leakage current than H^+-irradiation. From experimental and modelled results it appears that the increase in the reverse leakage current is due to the presence of defects near mid-bandgap (Eα3–Eα5 and Ep3–Ep5) that act as generation–recombination centers.

It appears that defects Eα1 and Eα2, and Ep1 and Ep2, when measured under the same high electrical field conditions are similar to Eβ1 and Eβ2, which are supposed to be different charge states of the same defect [11]. Contrary to electron-irradiated material

© University of Pretoria

UNIVERSITEIT VAN PRETORIA
UNIVERSITY OF PRETORIA
YUNIBESITHI YA PRETORIA

[17], these defects do not have the same introduction rates in α- and H^+-irradiated material. Defects Eα1 and Ep1 are introduced in lower concentrations than Eα2 and Ep2, respectively. The reason for this discrepancy is not yet clear, we still believe them to be the same type of defect, but when using heavier incident particles (α and H^+), the formation of Eα2 and Ep2 occurs in preference to Eα1 and Ep1. The defect levels that are responsible for device degradation after α-irradiation appear to be Eα3, Eα4 and Eα5, whereas after H^+-irradiation Ep3, Ep4 and Ep5 are the detrimental defects.

Acknowledgements

The financial assistance of the South African Foundation for Research Development (FRD) is gratefully acknowledged. We thank Mr. M. Hayes for operation of the Van de Graaff accelerator.

References

[1] R. Goyal (ed.), Monolithic Microwave Integrated Circuits, technology and design, (Artech House, London, 1989) p. 316.
[2] M.A. Hopkins and J.R. Srour, IEEE Trans. Nucl. Sci. NS-30, (1983) 4457.
[3] Y. Umemoto, N. Masuda and K. Mitsusada, IEEE Electron. Device. Lett. EDL-7 (1986) 396.
[4] G.E Zardas, P.C. Euthymiou, B. Szentpali, CH. Symeonides and K. Kourkoutas, Phys. Status Solidi A 123 (1991) K79.
[5] M. Yamaguchi, A. Yamamoto and A. Shibukawa, Jpn. J. Appl. Phys. 22 (1983) 1727.
[6] R.S. Bhattacharya, J. Appl. Phys. 54 (1983) 5039.
[7] S.A. Goodman and F.D. Auret, Jpn. J. Appl. Phys. Lett. 32 (1993) L1120.
[8] D.V. Lang, J. Appl. Phys. 45 (1974) 3014.
[9] T.I. Chappel and C.M. Ransom, Rev. Sci. Instr. 55 (1984) 200.
[10] P. Blood, Inst. Phys. Conf. Ser. 56 (1981) 68.
[11] D. Pons and J.C. Bourgoin, J. Phys. C 18 (1985) 3839.
[12] D. Donoval, J. de Sousa Pires, P.A. Tove and R. Harman, Solid State Electron 32 (1989) 11.
[13] R.M. Erasmus, W.E. Meyer, F.D. Auret and G. Myburg, S. Afr. J. of Phys. 16 (1993) 58.
[14] S.M. Sze, Physics of Semiconductor Devices, 2nd ed., (Wiley, New York, 1981) p. 37.
[15] P.J. Wang, T.F. Kuech, M.A. Tischler, P.M. Mooney, G. Scilla and F. Cardone, J. Appl Phys 64 (1988) 4975.
[16] S.A. Goodman, F.D. Auret and G. Myburg, Semicond. Sci. Technol. 7 (1992) 1241.
[17] F.D. Auret, S.A. Goodman, G. Myburg and W.E. Meyer, Appl. Phys. A 56 (1993) 547.
[18] B. Ziebro, J.W. Hemsky and D.C. Look, J. Appl. Phys. 72 (1992) 78.
[19] W.O. Siyanbola and D.W. Palmer, Semicond. Sci. Technol. 5 (1990) 7.
[20] E.M. Verbitskaya, V.K. Eremin, A.M. Ivanov, E.S. Ignatenko, N.B. Strokan, U.Sh. Turebekov, J. von Borany and B. Schmidt, Sov. Phys. Semicond. 25 (1991) 516.

© University of Pretoria

UNIVERSITEIT VAN PRETORIA
UNIVERSITY OF PRETORIA
YUNIBESITHI YA PRETORIA

Materials Science Forum vols. 143-147 (1994) pp. 1559-1564
© Trans Tech Publications, Switzerland

ELECTRONIC PROPERTIES OF DEFECTS INTRODUCED DURING ELECTRON AND ALPHA IRRADIATION OF GaAs

F. D. AURET, S. A. GOODMAN, W. E. MEYER, R. M. ERASMUS and G. MYBURG

Physics Department, University of Pretoria, Pretoria 0002, South Africa.

Keywords: irradiation induced defects, GaAs, DLTS, electron and alpha irradiation

ABSTRACT

Irradiation induced defects in n– and p–GaAs were studied after irradiation with electrons and alphas from radio–nuclides. In alpha irradiated n–GaAs a defect (with an energy level of 0.34 eV below the conduction band) exhibiting a metastable character was observed, which transformed reversibly depending upon the experimental conditions. This defect could not be observed after electron irradiation of the same material. Further, we found that both electron and alpha irradiation introduced a hole defect (with an energy level at 0.20 eV above the valence band) in MBE grown p–GaAs epilayers which could not be observed in identically irradiated OMVPE grown p–GaAs with the same free carrier density. Finally, it was found that the emission of holes from some radiation induced hole traps, e.g. the previously detected H1, exhibits a strong field dependence.

1. INTRODUCTION

Most studies undertaken to establish the electronic properties of primary radiation induced defects in GaAs have been performed utilizing high energy electrons. The defects introduced comprise the electron traps E1 – E9 [1,2] and hole traps H0 – H5 [1,3,4]. It has been shown, using deep level transient spectroscopy (DLTS), that the most prominent of these electron traps, E1 – E5, are caused by radiation induced structural disorder, and do not involve impurities [2,5]. For example, it has been found that E1 and E2 are two charge states of the isolated arsenic vacancy V_{As} and that E3 is related to close arsenic vacancy – arsenic interstitial (V_{As}–As_I) pairs [2]. In the case of hole traps, only the H0 and H1 are believed to be purely structural point defects or point defect pairs [4]. On the other hand, several radiation induced hole traps were shown to be impurity related, for example, H2 and H3 are believed to involve Cu and Fe [3,4].

Much less detail is available regarding defects created during irradiation of GaAs with heavier particles, such as protons, neutrons and alphas. Despite the similarities recently observed between defects introduced during electron and alpha particle irradiation [6], there are several uncertainties regarding the identification of some alpha induced defects. These uncertainties are partly due to attempts to identify defects by comparing their DLTS properties to those of defects reported in the literature where experiments were neither conducted under identical conditions nor by using identical GaAs.

© University of Pretoria

UNIVERSITEIT VAN PRETORIA
UNIVERSITY OF PRETORIA
YUNIBESITHI YA PRETORIA

An aspect of fundamental interest during defect studies is the effect of an electric field on the emission of carriers from energy levels in the band gap. Although this has been dealt with in great detail for some electron irradiation induced electron traps in n–GaAs [7,8], no detailed studies have yet been reported for hole traps, apparently because they are thought not to be influenced significantly by an electric field [10].

In this paper we report the introduction of a metastable electron trap introduced during alpha irradiation of n–GaAs. We also present results which show that the emission from some irradiation induced hole traps in p–GaAs, in particular the trap previously labeled H1 [1–4], strongly depends on the electric field.

2. EXPERIMENTAL PROCEDURE

N– and p–type GaAs epitaxial layers, grown by organo–metallic vapor phase epitaxy (OMVPE) and molecular beam epitaxy (MBE) on highly doped n– and p–type bulk grown GaAs substrates, respectively, were used for this experiment. Undoped and doped (to 10^{16} cm^{-3} with Si) n–layers and doped (to $1.7x10^{16}$ cm^{-3} with Be) p–layers, were irradiated and characterized. After fabricating ohmic contacts on the heavily doped substrate sides of the samples, Pd and Al were resistively deposited to form Schottky barrier diodes (SBDs) on the n– and p–epilayers, respectively. DLTS analyses of spectra recorded from control and irradiated SBDs were performed using a two–phase lock–in amplifier based system. The DLTS "signatures" (energy level in band gap and apparent capture cross section) of defects were determined from conventional DLTS Arrhenius plots. Particle irradiation was carried out utilizing electrons and alphas from ^{90}Sr and ^{241}Am radio–nuclides at fluence rates of $1.9x10^{9}$ α $cm^{-2}s^{-1}$ and $7.1x10^{6}$ e^{-} $cm^{-2}s^{-1}$ $cm^{-2}s^{-1}$, respectively [6]. The maximum fluence to which a SBD was subjected was chosen so that it did not introduce defects in concentrations of more than 10% of the free carrier density.

3. RESULTS AND DISCUSSION

3.1 Irradiation of n–GaAs

In Fig. 1 we compare the DLTS spectra of defects introduced during electron and alpha irradiation of identically doped n–GaAs. As indicated in curve (a), the main defects introduced during electron irradiation of OMVPE grown GaAs are labeled Eβ1, Eβ2 and Eβ3. The DLTS "signatures" of these defects (which were determined in undoped n–GaAs to minimize the field effect) showed that their energy levels are located at 0.04, 0.14 and 0.38 eV below the conduction band, with apparent capture cross sections of $5x10^{-16}$, $1.2x10^{-13}$ and $1.6x10^{-14}$ cm^{2}. These defects have DLTS "signatures" similar to the familiar E1, E2 and E3 defects, respectively. Curve (b) shows that alpha irradiation produced the Eα1 – Eα5. The Eα1, Eα2 and Eα4 also have the same "signatures" as the E1, E2 and E3, respectively. Because the E1 and E2 have previously been identified as two charge states of the isolated As vacancy, V_{As}, and E3 was shown to be related to the close V_{As}–As_{I} pair [1,2,5], the present results indicate that electron as well as alpha irradiation produce V_{As} and V_{As}–As_{I} defects.

© University of Pretoria

UNIVERSITEIT VAN PRETORIA
UNIVERSITY OF PRETORIA
YUNIBESITHI YA PRETORIA

No defects with DLTS peaks similar to Eα3 and Eα5 could be observed after electron irradiation (Fig. 1, curve (a)). The most interesting feature of the spectra in Fig. 1 is the Eα3 peak which could only be observed in alpha irradiated, but not in electron irradiated n–GaAs. The magnitude of this defect depends on the direction of the DLTS temperature scan. For scans from 250 K down in temperature (curve (b)) the Eα3 peak is always a maximum. However, for scans up in temperature (curve (c)) its magnitude depends on the filling pulse height and width. From a DLTS Arrhenius analysis its energy and apparent capture cross section were determined as 0.34 eV and $2.5\text{x}10^{-14}$ cm^{-2}, respectively. The Eα3 appearance and disappearance are completely reversible and depend on pulse, bias and temperature conditions, indicating its metastability. Because alphas are capable of transferring a much larger portion of their energy during a collision than electrons, and can therefore create physically larger and more complex defects, the introduction of Eα3 by alpha but not by electron irradiation therefore suggests that it has a more complex structure than a simple point defect.

3.2 Irradiation of p–GaAs

Curves (a) and (b) in Fig. 2 are the low– and high–field DLTS spectra of alpha irradiated MBE grown p–GaAs, while curves (c) and (d) are the corresponding curves for electron irradiated identical GaAs. From these curves several important observations can be made. Firstly, the spectra indicate that electron and alpha irradiation introduced the same main defects, but in different relative concentrations. For electron irradiation the most prominent defects are the Hβ1, Hβ4 and Hβ5, located at 0.08, 0.20 and 0.30 eV above the valence band. An Arrhenius comparison showed that the main alpha induced defects, Hα1, Hα4 and Hα5 have the same "signatures" as the Hβ1, Hβ4 and Hβ5, respectively. The Hα1 (Hβ1) and Hα5 (Hβ5) have, within the experimental limit, the same DLTS "signatures" as the previously studied H0 and H1, respectively, indicating that they are As vacancy related [3,4].

The Hα4 and Hβ4 could only be observed in electron and alpha irradiated MBE grown p–GaAs, but not in OMVPE grown p–GaAs with similar or lower doping densities which had been irradiated with similar fluences. Furthermore, their concentrations decrease sharply away from the SBD interface into the substrate, unlike the concentration of the other defects which are constant in the depletion region of the SBD. This indicates that the Hα4 and Hβ4 defects may be the product of radiation with a defect or impurity in MBE GaAs which is not present in OMVPE GaAs. The capture cross section of Hβ4 (and Hα4 (as determined by direct pulse width measurement) was 10^{-21}–10^{-20} cm^2, i.e. much smaller than the other radiation induced defects. The large difference observed between the direct capture cross section measurement and that found from a DLTS Arrhenius plot (extrapolated to 1/T=0) indicates that the capture cross section is temperature activated, a property of a defect which captures carriers by multiphonon emission [7,8].

Finally, the dependence of the Hβ4 (Hα4) and Hβ5 (Hα5) emission rates on the electric field were determined by recording DLTS scans at a 3 V reverse bias for filling pulse

© University of Pretoria

UNIVERSITEIT VAN PRETORIA
UNIVERSITY OF PRETORIA
YUNIBESITHI YA PRETORIA

amplitudes of between 0.2 and 2 V. Subtraction of scans recorded at incremental filling pulse amplitudes facilitated a calculation of the increase in emission rate as a function of distance from the SBD interface, i.e. as function of the electric field. For decreasing fields the emission rates of Hβ5 (at 140 K) and of Hβ4 (at 112 K) converged to values of about 8.5 s^{-1} and 31 s^{-1} (low field values), respectively. From the curves in Fig. 3 we see that whereas the Hβ4

Figure 1

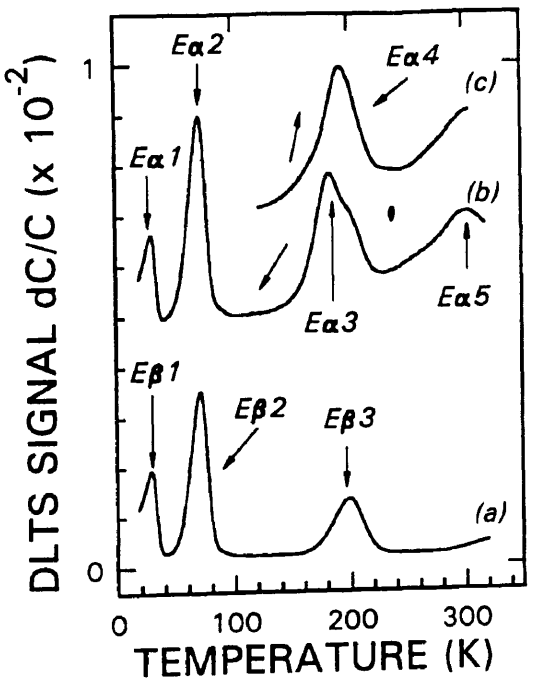

Figure 2

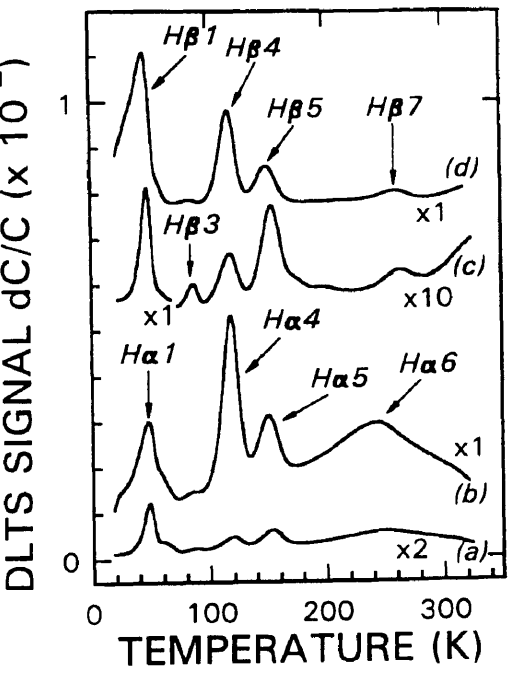

Figure 3

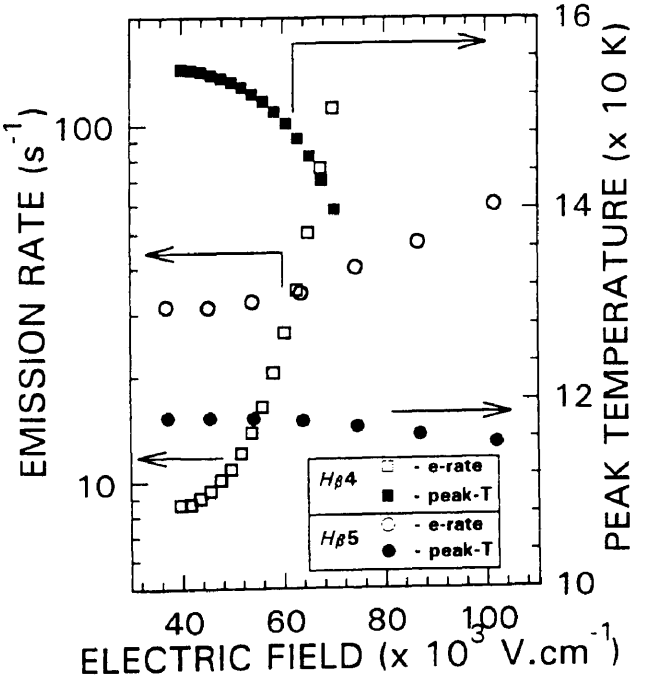

Figure 1. DLTS spectra, recorded at 46 Hz and a reverse bias of 4 V, of electron irradiation (curve (a)) and alpha irradiated (curves (b) and (c)) induced electron traps in 10^{16} doped n-GaAs. The filling pulse for curves (a) - (c) were 1.2 V, 1.2 V and 4.8 V respectively.

Figure 2. DLTS spectra, recorded at 46 Hz and a reverse bias of 2 V, of electron and alpha irradiation induced electron traps in n-GaAs. The filling pulse amplitudes of curves (a) and (c) were 0.2 V and for (b) and (d) they were 2.0 V.

Figure 3. Variation of emission rate of Hβ4 (at 112 K) and Hβ5 (at 140 K) with electric field. Also shown is the variation of DLTS peak temperature (at 46 Hz) with electric field for both defects.

© University of Pretoria

UNIVERSITEIT VAN PRETORIA
UNIVERSITY OF PRETORIA
YUNIBESITHI YA PRETORIA

emission rate only increases by a factor of 1.5 in the field region of 4–7x10^4 Vcm^{-4}, the Hβ5 emission rate increases by a factor of 12 in the same field region. The emission rate enhancement of Hβ5 is comparable in magnitude to that reported for some electron traps in n–GaAs which was explained in terms of phonon assisted tunneling [7,8], but is much larger than predicted for the Poole Frenkel effect for emission from a charged defect center [10].

4. CONCLUSIONS

We have shown that the main electron irradiation induced traps in GaAs are also observed after alpha irradiation of the same material. These defects have previously shown to be related to isolated vacancies and vacancy – interstitial pairs in the As sub–lattice. In addition, alpha irradiation introduces a metastable electron trap, Eα3, in n–GaAs which has a DLTS peak a few degrees lower than the E3 defect. At normal DLTS scanning temperatures (15 – 350 K) the Eα3 concentration is larger than that of the E3 and it can only be removed (transformed) by applying a filling pulse which allows current to flow in the depletion region.

In Be–doped (1.6x10^{15} cm^{-3}) MBE grown p–GaAs we have detected a radiation induced hole trap, labeled Hβ4 and Hα4 for electron and alpha irradiation respectively, at 0.2 eV above the valence band which has not been reported before. This defect could not be observed after irradiation of OMVPE grown p–GaAs which was doped with Zn to the same level. Perhaps most important, we have also demonstrated that the effect of an electric field on the emission rate from radiation induced hole traps is significant and much more than can be explained by the Poole – Frenkel barrier lowering [9]. Mechanisms to explain this, including phonon assisted tunneling, are presently being investigated.

The financial assistance of the South African Foundation for Research Development is gratefully acknowledged. We also thank Dr. M. Missous and Prof. A. R. Peaker of UMIST for the MBE grown p–GaAs used during this investigation.

REFERENCES

1) Lang, D.V. and Kimerling, L.C.: Phys. Rev. Lett. 1974, **33**, 489
2) Pons, D. and Bourgoin, J.C.: J. Phys. C: Solid State Phys. 1985, **18**, 3839
3) Stievenard, D., Boddaert, X. and Bourgoin, J.C.: Phys. Rev. B, 1986, **34**, 4048
4) Stievenard, D., Boddaert, X., Bourgoin, J.C. and von Bardeleben, H.J.: Phys. Rev. B, 1990, **41**, 5271
5) B. Ziebro, J. W. Hemsky, and D. C. Look, J. Appl. Phys. **72**, 78 (1992)
6) Auret, F.D., Goodman, S.A., Myburg, G. and Meyer, W.E.: Applied Physics **A**, 1992, **54**, 547
7) Pons, D. and Makram–Ebeid, S.: J. Phys. (Paris), 1979, **40**, 1161
8) Makram–Ebeid, S. and Lannoo, M.: Phys. Rev. Lett., 1982, **48**, 1281
9) Lang, D.V., Kimerling, L.C. and Leung, S.Y.: J. Appl. Phys., 1976, **47**, 3587
10) J. Frenkel, Phys. Rev. **54**, 657 (1938)

© University of Pretoria

UNIVERSITEIT VAN PRETORIA
UNIVERSITY OF PRETORIA
YUNIBESITHI YA PRETORIA

Jpn. J. Appl. Phys. Vol. 32 (1993) pp. L 974–L 977
Part 2, No. 7B, 15 July 1993

Deep Level Transient Spectroscopy Characterization of Electron Irradiation Induced Hole Traps in p-GaAs Grown by Molecular Beam Epitaxy

F. D. AURET, S. A. GOODMAN, W. E. MEYER, R. M. ERASMUS and G. MYBURG
Physics Department, University of Pretoria, Pretoria 0002, Republic of South Africa

(Received April 5, 1993; accepted for publication June 11, 1993)

Schottky barrier diodes on Be-doped p-type GaAs grown by molecular beam epitaxy (MBE) were irradiated with electrons (beta particles) from a Sr-90 radio-nuclide. Using deep level transient spectroscopy (DLTS), the radiation induced hole traps, labelled Hβ1–Hβ7, were characterized. The three most prominent defects, Hβ1, Hβ4 and Hβ5, have energy levels at 0.08, 0.20 and 0.30 eV, respectively, above the valence band. The introduction rate of Hβ1 is close to those of the electron irradiation induced electron traps E1 and E2 in n-GaAs, which have been identified as two charge states of the isolated As vacancy, V_{As}. Defect Hβ4, whose concentration decreases with depth below the metal-GaAs interface, has not yet been reported for electron irradiated GaAs.

KEYWORDS: GaAs, deep level transient spectroscopy (DLTS), radiation induced defects, hole traps, electron irradiation

1. Introduction

Detailed studies have shown that radiation of electronic devices, such as metal-semiconductor field effect transistors (MESFETs),[1] heterojunction bipolar transistors (HBTs)[2] and infra-red detectors,[3] introduces electrically active defects which can have a pronounced effect on the device characteristics. Therefore, when designing electronic systems for operation in a radiation environment, it is imperative to know the effect of radiation on the properties of electronic components and materials comprising these systems. This, in turn, requires a knowledge of the type, energy and quantity of particles present in the radiation environment, as well as the introduction rates and electronic properties of the defects introduced by each particle type in electronic materials, and in particular in semiconductors which form an integral part of most electronic devices.

Deep level transient spectroscopy (DLTS)[4] has been used successfully to study, among others, radiation induced defects in semiconductors. In the case of GaAs most of these studies concentrated on electron traps created by electron irradiation and made use of Schottky barrier diodes (SBDs) on n-GaAs or p^+-n junctions. The results indicated that electron irradiation of GaAs introduces a set of electron traps, E1–E9[5–7] and hole traps, H0–H5.[8,9] The main electron traps, E1–E3, have well established "signatures" and a point defect nature which does not depend on impurities in the GaAs.[6,7] Considerably less attention has been paid to hole traps, which were mostly studied using n^+-p junctions. The main hole traps, H0 and H1, were shown to be related to isolated point defects or point defect pairs.[8–10] Some radiation induced hole traps are complexes involving impurities, like Cu and Fe, in p-GaAs.[9,10] However, these impurities themselves act as hole traps with DLTS signals that can mask the signals of pure (non-complex) radiation induced defects. Clearly, there is a need to study radiation induced defects in high purity p-GaAs.

We report here, for the first time, the electrical properties, as determined by DLTS using SBDs, of hole traps created during electron irradiation of p-GaAs grown by molecular beam epitaxy (MBE) and having an as-grown deep level concentration below 2×10^{12} cm^{-3}. It will be shown that several hole traps are introduced and that one of the main traps, which has an energy level at 0.20 eV above the valence band, has not previously been observed.

2. Experimental Procedure

The structure used for this study consisted of a p^+-GaAs substrate (doped to $2–5\times10^{19}$ cm^{-3} with Zn) on which a 0.5 μm thick p^+-GaAs buffer layer, followed by a 1 μm thick p-type GaAs layer doped to $1.5–2\times10^{16}$ cm^{-3} with Be, were grown by MBE. Finally, a 200 nm thick epitaxial Al film was grown on top of the p-GaAs without breaking vacuum.[11] Photolithography and chemical etching were used to define 0.5 mm diameter Al Schottky contacts. Owing to the low contact resistivity of unannealed Au/Ru contact system on p-GaAs,[12] this was deposited on the p^+-GaAs substrate, after SBD processing, to form an ohmic contact. In order to check any possible influence of the SBD metal on the radiation induced defects, Mg SBDs were also resistively evaporated on a section of the Be-doped p-GaAs epitaxial layer after the Al film was removed.

DLTS using a lock-in amplifier based system[13] was employed to analyze defects in the p-GaAs. The maximum quiescent bias used for recording spectra was 2 V. In order to minimize electric field effects during emission rate measurements, spectra were recorded using small filling pulse amplitudes. Difference-DLTS measurements, obtained by subtracting DLTS spectra recorded using the same quiescent bias, V_r, but slightly different pulse amplitudes, V_p and $V_p+\delta V_p$, were employed to determine defect concentrations. After recording control spectra, the GaAs was irradiated through the Schottky contacts with electrons at a flux of 1.9×10^9 cm^{-2} s^{-1} from a strontium-90 (Sr-90) radionuclide at doses up to 10^{15} cm^{-2}. Electrons emitted from the Sr source have a continuous energy distribution[14] and approximately 70% of these have energies above 250 keV, the threshold value for producing defects in GaAs by elastic collisions.

The DLTS "signatures" (energy level E_t and apparent capture cross section σ_{pa}) of defects were determined from DLTS Arrhenius plots of $\log(e_p/T^2)$

© University of Pretoria

UNIVERSITEIT VAN PRETORIA
UNIVERSITY OF PRETORIA
YUNIBESITHI YA PRETORIA

versus $1000/T$, using

$$e_p = \gamma_p T^2 \sigma_{pa} \exp(-E_t/kT). \quad (1)$$

Here e_p is the hole emission rate from the defect site at a temperature T, k is Boltzmann's constant and the γ_p is a constant equal to $1.62\times10^{21}\,cm^{-2}\cdot s^{-2}\cdot K^{-2}$ for a hole trap, if for simplicity the degeneracy is taken as one.

3. Results and Discussion

The barrier heights of the Al and Mg SBDs were determined at room temperature by current-voltage (I-V) measurements as (0.66 ± 0.02) eV and (0.70 ± 0.04) eV, respectively. Room temperature capacitance-voltage (C-V) measurements yielded the free carrier concentration, N_a-N_d, as $(1.9\pm0.2)\times10^{16}\,cm^{-3}$ for the Be-doped GaAs. To facilitate the determination of defect concentrations from DLTS measurements, N_a-N_d was also measured at all other temperatures where DLTS peaks were observed.

DLTS spectra of unirradiated (control) SBDs showed that the GaAs epilayer below the Al and Mg contacts contained several hole traps in concentrations of up to $2\times10^{12}\,cm^{-3}$. Curves (a) and (b) in Fig. 1 depict DLTS spectra of MBE p-GaAs irradiated with electrons at a dose of $7\times10^{14}\,cm^{-2}$, which was chosen to introduce defects in concentrations well above the background defect concentration. The spectra presented here, recorded at the same quiescent bias ($V_r=2$ V) but different filling pulse amplitudes, show that electron irradiation of Be-doped p-GaAs introduced the hole defects labeled Hβ1–Hβ7, the most prominent being Hβ1, Hβ4 and Hβ5. In the nomenclature used here, "H" refers to hole trap and "β" signifies that the trap is introduced by beta (electron) irradiation form the Sr-90 radio-nuclide. The same set of defects were observed using either Al or Mg SBDs.

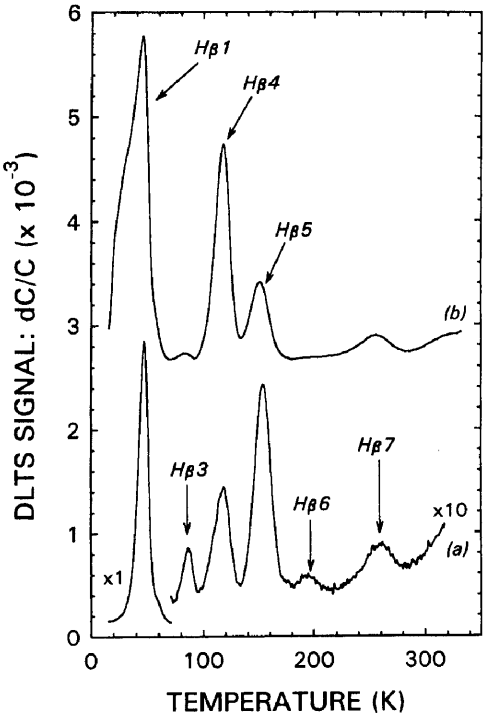

Fig. 1. DLTS spectra of MBE grown Be-doped ($1.9\times10^{16}\,cm^{-3}$) p-GaAs irradiated with electrons from a Sr-90 source at a dose of $7\times10^{14}\,cm^{-2}$. Both spectra were recorded at a lock-in frequency of 46 Hz and a quiescent reverse bias of 2 V. The pulse conditions used were: curve (a): $V_p=0.40$ V, curve (b): $V_p=2.4$ V.

Curve (a) is a DLTS spectrum obtained using a small filling pulse amplitude, $V_p=0.40$ V, thus yielding information pertaining to defects in a narrow spatial region close to the edge of the depletion region where the average electric field is low. Curve (b) was recorded at $V_p=2.4$ V, i.e. conditions that allow almost all defects in the depletion region to capture and emit holes. It is evident from these curves that especially the low temperature Hβ1 peak in curve (b) shows significant broadening due to the large electric field variation in the depletion region. Although not clearly visible in Fig. 1, it should be mentioned that whereas the Hβ5 emission rate showed a moderate electric field dependence, the emission rate of the Hβ4 seemed to be independent of the electric field. These curves therefore indicate that, in order to obtain accurate defect characteristics in $1.9\times10^{16}\,cm^{-3}$ doped p-GaAs, small pulse (low field) rather than conventional large-pulse (high field) DLTS spectra should be used.

The DLTS "signatures" of the electron irradiation induced hole traps were calculated from conventional DLTS Arrhenius plots using eq. (1), where e_p and T were determined from DLTS spectra for which $V_r=1$ V. Because Fig. 1 has shown that the Hβ1 emission rate is the most sensitive to electric field, a filling pulse amplitude of $V_p=0.12$ V (the smallest pulse at which the Hβ1 could still be clearly detected) was used to determine its "signature". For the other defects V_p values of between 0.5 and 0.75 V were used. The "signatures" obtained are tabulated in Table I where they are compared to those previously reported for electron

Table I. Characteristics of electron irradiation induced hole traps in MBE grown p-GaAs as detected by DLTS using SBDs.

Defects from this study					Defects detected elsewhere				
Label	E_t[(a)] (eV)	σ_{pa}[(b)] $\times10^{-15}$ (cm^2)	η[(c)] (cm^{-1})	T_p[(d)] (K)	Label	E_t[(a)] (eV)	σ_{pa}[(b)] $\times10^{-15}$ (cm^2)	η[(c)] (cm^{-1})	Ref.
Hβ1	0.08	1.5	1.4	49	H0	0.06	0.007	0.8	8)
					H0	0.06	0.16	0.8	15)
Hβ3	0.16	17	0.03	87	—				
Hβ4	0.20	1.2	0.05–0.2	118	—				
Hβ5	0.30	12	0.17	154	H1	0.25	8.3	0.25	8)
					H1	0.29	2.0	0.1–0.7	6)
					H1	0.25	1.4	0.09	9)
Hβ7	0.55	74	0.04	256	—				

(a) Effective activation energy, measured above the valence band.
(b) Apparent majority carrier capture cross-section, determined from Arrhenius plot.
(c) Introduction rate, calculated from η=(defect concentration)/(radiation dose).[14]
(d) DLTS peak temperature, measured at a lock-in amplifier frequency of 46 Hz, that is at a decay time constant of 9.23 ms.

© University of Pretoria

UNIVERSITEIT VAN PRETORIA
UNIVERSITY OF PRETORIA
YUNIBESITHI YA PRETORIA

irradiation induced hole traps in p-GaAs.[8,9,15]

From a comparison of the "signatures" we conclude that two of the main defects detected here can be correlated with defects reported before, while at least one of the main defects, the Hβ4, has to our knowledge not been observed before in n- or p-GaAs. It is fair to point out that Loualiche *et al.*[8] reported a defect with the same activation energy (0.2 eV) as the Hβ4, but its capture cross section was not reported. Since this defect was detected only in LPE grown GaAs, after irradiating at a dose of above 5×10^{15} cm^{-2}, it is doubtful whether it is the same as the Hβ4 observed here. The Hβ4 will be discussed in more detail after considering the defect concentration distributions. Based on the similarities of their "signatures" (within the experimental error), we conclude that Hβ1 and Hβ5 are the same as the H0 and H1 defects, respectively, previously speculated to be radiation induced point defects in the As sublattice of GaAs,[8-10] more specifically, correlated arsenic vacancy-interstitial pairs, V_{As}–As_I. The H2 and H3 reported before[8-10] were not detected in our study. Since these defects are linked to the presence of Cu and Fe in the GaAs, and the MBE GaAs used here did not contain electrically active Cu and Fe in detectable concentrations (above 10^{12} cm^{-3}), our result is not unexpected.

Fixed-bias variable-pulse DLTS concentration profiling, employing the formulation of Zohta *et al.*,[16] was used to determine the concentration of radiation induced defects. For this purpose difference-DLTS spectra were acquired using a quiescent reverse bias of 1 V and filling pulses with amplitudes incremented from 0.12 to 0.50 V in steps, δV_p, of 0.02 V. The profiles obtained for the main defects showed that the concentrations of the Hβ1 and Hβ5 are constant in the region profiled (0.2–0.3 μm below the metal-GaAs interface). In contrast, the concentration of the Hβ4 decreases away from the interface. In previous studies where n-GaAs was irradiated by high energy electrons using the same Sr-90 radio-nuclide, no electron traps with such a concentration distribution could be observed.[14] The calculated introduction rates are included in Table I. Note that the variation of the Hβ4 introduction rate is a consequence of its non-unifirmity in the depletion region. Table I shows that the Hβ1 is introduced in the highest concentration at a rate of 1.5 cm^{-1}. This is about twice as high as the 0.8 cm^{-1} reported by Pons *et al.*[6] For the H0 in 3×10^{16} cm^{-3} doped p-GaAs, speculated to be related to the correlated V_{As}–As_I pair.[9,10] Apart from not using electrons with the same energy distribution as during the study of Pons,[6] another reason why different introduction rates may be found is that if δV_p is not small enough during a difference-DLTS concentration determination, and the defect is strongly field dependent as the Hβ1 or H0, then its concentration will be underestimated due to the electric field induced dispersion in its emission rate. However, it is interesting to note that the Hβ1 introduction rate is in good agreement with the 1.1 and 1.5 cm^{-1} that we have determined for the Eβ1 and Eβ2, respectively, in 1×10^{16} cm^{-3} doped n-GaAs irradiated with electrons from the same Sr-90 radio-nuclide. The "signatures" of the Eβ1 and Eβ2[14] are the same as those of the E1 and E2,[6] believed to be two charge states of the isolated V_{As}.[17]

Finally, we discuss possible reasons why the Hβ4 has not previously been observed and speculate about its origin. The most significant differences between the present and previous investigations are the use of SBDs and Be-doped p-GaAs in this study, whereas p-n junctions and Zn-doped GaAs were previously used. Because the Hβ4 was detected in the Be-doped, but not in the Zn-doped p-GaAs, it is tempting to argue that Hβ4 is a radiation induced complex related to the presence of Be. However, its spatial distribution and the regions analyzed in this and previous studies also deserve consideration. The SBDs on Be-doped GaAs used here yield information about defects in the first 0.4 μm from the metal-GaAs interface, while p-n junctions are used to detect defects in their depletion regions which are usually a few microns below the irradiated metal GaAs interface. This allows the possibility of Hβ4 being a complex between a radiation induced point defect, with a uniform concentration, and a defect or impurity which diffuses into the SBD depletion region during or after irradiation, whose concentration decreases away from the metal-GaAs interface. Such a model would explain why the Hβ4 was detected here using SBDs, but not before by using p-n junctions. A defect with an identical "signature" and depth distribution has also recently been observed after alpha particle irradiation of the same p-GaAs.[18]

4. Conclusions

It has previously been shown that electrons (beta particles) from a Sr-90 radio-nuclide can be used to create the same set of electron traps in n-GaAs as is observed after high energy electron irradiation in accelerators. In the present study we irradiated Be-doped p-GaAs with electrons from the same electron source to introduce hole trap defects Hβ1–Hβ7, of which Hβ1, Hβ4 and Hβ5 are the most prominent. Whereas p-n junctions were used in most previous studies to detect hole traps in p-GaAs, we have successfully employed Al and Mg Schottky barrier diodes (SBDs) fabricated on p-GaAs.

From a comparison of defect "signatures" determined using small filling pulse amplitudes to minimize the influence of the electric field, we conclude that the electric properties of the Hβ1 and Hβ5 are in good agreement with those of the H0 and H1 previously observed for electron irradiated GaAs using p-n junctions, which were correlated with V_{As}–As_I pairs. It is interesting to note, however, that the introduction rate measured here for Hβ1 is roughly in agreement with those of the Eβ1 and Eβ2 introduced in 10^{16} cm^{-3} doped n-GaAs by electrons from the same Sr-90 source. The Eβ1 and Eβ2 are the same as the E1 and E2, respectively, believed to be different charge states of V_{As}.[6,17]

Apparently the Hβ4, with an energy level at 0.20 eV above the valence band and a concentration that

© University of Pretoria

UNIVERSITEIT VAN PRETORIA
UNIVERSITY OF PRETORIA
YUNIBESITHI YA PRETORIA

decreases away from the metal-GaAs interface, has not been detected before. We attribute this to the fact that Hβ4 is formed close to the metal-GaAs interface, possibly due to the interaction between uniformly distributed radiation induced point defects and a non-uniformly distributed defect or impurity in the p-GaAs.

In summary, DLTS utilizing Schottky barrier diodes has been successfully used to study radiation induced hole traps created in Be-doped (1.9×10^{16} cm^{-3}) p-type MBE grown GaAs by high energy electrons from a Sr-90 radio-nuclide source. In addition to the previously reported hole traps, a new hole trap Hβ4 with an energy level 0.20 eV above the valence band and a concentration that decreases into the metal-GaAs, was also detected.

Acknowledgements

The financial assistance of the South African Foundation for Research Development (FRD) is gratefully acknowledged. We also thank Dr. M. Missous and Prof. A. R. Peaker of UMIST for the p-GaAs material used during this investigation, as well as Dr. C. Schutte for the photolithography.

1) A. F. Galashan and S. W. Bland: J. Appl. Phys. **67** (1990) 173.
2) J. J. Liou: Phys. Status Solidi **119** (1990) 337.
3) C. M. Buttar, F. H. Combley, I. Dawson, M. Dogru, M. Harrison, G. Hill, Y. Hou and P. Houston: Nucl. Instrum. & Method A **310** (1991) 208.
4) D. V. Lang: J. Appl. Phys. **45** (1974) 3014.
5) D. V. Lang and L. C. Kimerling: Phys. Rev. Lett. **33** (1974) 489.
6) D. Pons and J. C. Bourgoin: J. Phys. C **18** (1985) 3839.
7) D. Pons and J. C. Bourgoin: Phys. Rev. Lett. **55** (1985) 1327.
8) S. Loualiche, A. Nouilhat, G. Guillot, M. Gavard, A. Laugier and J. C. Bourgoin: J. Appl. Phys. **53** (1982) 8691.
9) D. Stievenard, X. Boddaert and J. C. Bourgoin: Phys. Rev. B **34** (1986) 4048.
10) D. Stievenard, X. Boddaert, J. C. Boirgoin and H. J. von Bardeleben: Phys. Rev. **41** (1990) 5271.
11) M. Missous, E. H. Rhoderick, K. E. Singer and W. S. Truscott: J. Crys. Growth **111** (1991) 1116.
12) G. Myburg, W. O. Barnard, W. E. Meyer, C. W. Louw, N. G. van den Berg, M. Hayes, F. D. Auret and S. A. Goodman: to be published in Appl. Surf. Sci. (1993).
13) F. D. Auret and M. Nel: J. Appl. Phys. **63** (1988) 973.
14) F. D. Auret, S. A. Goodman, G. Myburg and W. E. Meyer: to be published in Appl. Phys. A (1993).
15) D. Pons: Physica **116B** (1983) 228.
16) Y. Zohta and M. O. Watanabe: J. Appl. Phys. **53** (1982) 1809.
17) S. Loualiche, A. Nouaillhat, G. Guillot and M. Lannoo: Phys. Rev. B **30** (1984) 5822.
18) S. A. Goodman, F. D. Auret and W. E. Meyer: submitted to Appl. Phys. Lett. (1993).

© University of Pretoria

UNIVERSITEIT VAN PRETORIA
UNIVERSITY OF PRETORIA
YUNIBESITHI YA PRETORIA

S. Afr. J. Phys. 16 No. 1/2 (1993)

Electrical characterization of particle-induced damage in n-GaAs

F.D. Auret, S.A. Goodman, M. Hayes, G. Myburg, W.O. Barnard and W.E. Meyer
Department of Physics, University of Pretoria, Pretoria 0002, Republic of South Africa

Presented at STEDCON '92 16–18 November 1992

The defects introduced in n-GaAs during high energy electron-, proton-, alpha particle- and neutron-irradiation were electrically characterized by deep level transient spectroscopy (DLTS). Irradiation by all of the above-mentioned particle types caused the introduction, in different relative concentrations, of the E1 and E2 defects, which have been correlated with isolated vacancies in the arsenic (As) sublattice, and the E3 defect which is related to close As vacancy–interstitial pairs. In addition, protons, alphas and neutrons also introduced other, presumably complex, defects. One of these, observed at about 180 K, has a metastable character. The main defect introduced by neutron-irradiation has a very large capture cross-section and an energy centered around 0.66 eV below the conduction band.

Defekte wat in GaAs as gevolg van bestraling met elektrone, protone, alfa-deeltjies en neutrone veroorsaak word, is elektries gekarakteriseer met behulp van diepvlak oorgangspektroskopie (DLTS). Bestralings deur genoemde deeltjies het die E1-, E2- en E3-defekte, in verskillende relatiewe konsentrasies, tot gevolg gehad. Die E1 en E2 hou verband met geïsoleerde leemtes in die arseen- (As-) subtralie, terwyl die E3 verband hou met naby As-leemte–tussenruimtelike pare. Daarbenewens het protone, alfas en neutrone ook ander, waarskynlik komplekse defekte, tot gevolg gehad. Een van hierdie defekte (met 'n DLTS-piekposisie by 180 K) vertoon 'n metastabiele karakter. Die dominante defek wat deur neutronbestraling veroorsaak is, het 'n baie groot vangswaarskynlikheid en 'n energieposisie van ongeveer 0.66 eV onder die geleiband.

1. Introduction

Particle irradiation plays a significant role in various sectors of semiconductor technology. It is utilized to controllably modify the properties of electronic materials, such as during the transmutational doping of semiconductors by neutron irradiation and device isolation by proton implantation. Often, however, particle irradiation may occur inadvertently during semiconductor processing, such as metallization by sputter deposition and electron beam evaporation. Several analytical techniques, such as transmission and scanning electron microscopy, Auger electron spectroscopy (AES), Rutherford back scattering and ion channelling, expose the sample under investigation to energetic particles. Although some of these analytical techniques are traditionally thought of as being non-destructive, the mere fact that they utilize energetic particles, implies that they have the potential of introducing damage. If these radiation-induced defects are present in high enough concentrations, they may influence the phenomena being investigated by these techniques. Further, some electronic devices have to function in radiation environments, in which case it is essential to know the effect of radiation on the device characteristics. Therefore, as part of their qualification procedure, such devices are subjected to stringent testing in the presence of particle irradiation of a specified nature.

To evaluate the influence of radiation-induced defects on materials and devices, and to optimally utilize their beneficial effects in defect engineering, the characteristics of radiation-induced defects in different materials should be known. In the case of GaAs it has been reported that the properties of radiation-induced defects depend on the particle type [1], the energy, fluence, fluence rate and direction of incidence of the particles [2, 3], substrate impurities [3] and the temperature during irradiation [4]. It is, however, not always clear whether the reported differences in defect properties are real or whether they result from DLTS measurements in different laboratories using GaAs with different carrier densities. In this regard there are two issues that require clarification, namely, the dependence of the properties of radiation-induced defects on dopant and other impurities, and a comparison of the defects introduced when irradiating with different particle types.

In the present investigation we have addressed, in part, these issues by employing deep level transient spectroscopy (DLTS) [5] to compare the defects introduced in n-type GaAs with two different free carrier concentrations by electron-, proton-, alpha particle- and neutron-irradiation. The results showed that, apart from point defects introduced in different concentrations during irradiation by all particle types, extended defects were presumably also introduced during proton-, alpha- and neutron-irradiation.

2. Experimental procedure

Epitaxially grown n-type GaAs layers with carrier densities of 4×10^{14} /cm^3 and 1×10^{16} /cm^3, grown by OMVPE on 10^{18} /cm^3 doped n$^+$-GaAs substrates, were used to study the irradiation-induced defects. For brevity we shall further refer to the 4×10^{14} /cm^3 and 1×10^{16} /cm^3 GaAs as *un-doped* and *doped* GaAs, respectively. Ni/AuGe/Au ohmic contacts were formed on the n$^+$ sides of the samples. Circular Pd Schottky barrier diodes (SBDs), 400 nm thick and 0.75 mm in diameter, were resistively deposited on the epitaxial layers before irradiation. Irradiation of the GaAs was performed at room temperature using the following particles: electrons from a Sr-90 radio-nuclide at 1.87×10^9 / cm^2/s, 2 MeV protons from a Van de Graaff accelerator at 1.4×10^{11} /cm^2/s, 5.5 MeV alphas from an Am-241 radio-nuclide at 5×10^3 /cm^2/s and neutrons (with a maximum

© University of Pretoria

UNIVERSITEIT VAN PRETORIA
UNIVERSITY OF PRETORIA
YUNIBESITHI YA PRETORIA

energy of 64 MeV) at 3.28×10^8 /cm^2/s from a p(66)/Be(40) clinical source. A lock-in amplifier based DLTS system [6] was used to detect and characterize the radiation-induced defects. The energy level, E_t, and apparent capture cross section, σ_a, of a defect (the combination which is known as its "DLTS signature"), were calculated from standard DLTS Arrhenius plots of e_n/T^2 vs $1000/T$, where e_n is the carrier emission rate at temperature T. To avoid inaccuracies due to the electric field enhancement of the emission rate, DLTS "signatures" of the defects were measured in the undoped GaAs (unless stated otherwise) using a small quiescent bias (1 V) and filling pulse amplitude (1.2 V). Defect concentrations were calculated by fixed-bias variable-pulse DLTS profiling.

3. Results and discussion

We first discuss the native defects in the control (unirradiated) samples and then present the results obtained after analyzing the radiation-induced defects in GaAs.

3.1 Control (unirradiated) samples

The main defect in doped and undoped GaAs used here is the well-known EL2 [7] which is present in all OMVPE grown GaAs. Because its concentration in the unirradiated undoped GaAs is of the same order of magnitude ($1–2 \times 10^{14}$ /cm^3) as that of the shallow donors, it results in a large DLTS signal which prohibits the detection of defects in low concentrations with DLTS peaks above 300 K. The undoped GaAs also contained the EO4 defect [8] in an approximate concentration of 8×10^{11} /cm^3 with a DLTS peak at 207 K. In the undoped GaAs the difficulty of detecting irradiation-induced defects with peaks close to those of the native defects was reduced by subtracting the DLTS spectra of unirradiated samples from those of irradiated samples.

3.2 Defects created by electron irradiation

Curves (a) in Figures 1 and 2 were recorded after irradiating the undoped and doped GaAs with electrons from the Sr electron source for 30 and 1000 minutes, i.e. fluences of 3.4×10^{12} e/cm^2 and 1.1×10^{14} e/cm^2, respectively. Both spectra show that in the 10 – 310 K range three prominent electron traps, Eβ1, Eβ2 and Eβ4, were introduced during electron irradiation. In the nomenclature used here, "E" implies an electron trap while "β" indicates that the defect was introduced by electron (beta) irradiation. Note that in the doped GaAs the DLTS peaks are slightly broader and shifted to lower temperatures due to field assisted emission. The fact that no additional defects were detected in the 10^{16} / cm^3 GaAs indicates that the electron irradiation-induced electron traps do not depend on the dopant and are therefore simple point defects.

The "signatures" determined for the Eβ1, Eβ2 and Eβ4 defects (Table 1) are, within normal experimental error limits, the same as those of the E1 – E3 of Ref. [8] and the EE1 – EE3 of Ref. [9] for electron irradiation in accelerators [8, 9]. Therefore we conclude that the same defects are introduced during irradiation by electrons from a Sr radionuclide and by electrons in accelerators, namely the primary electron irradiation-induced defects. The E1 and E2 are strongly suspected to be two different charge states, (–/0) and (0/+), of the isolated arsenic vacancy, V_{As}, in GaAs [10], while the E3 is speculated to be related to close arsenic vacancy–interstitial pairs, $V_{As} – As_I$ [2, 3].

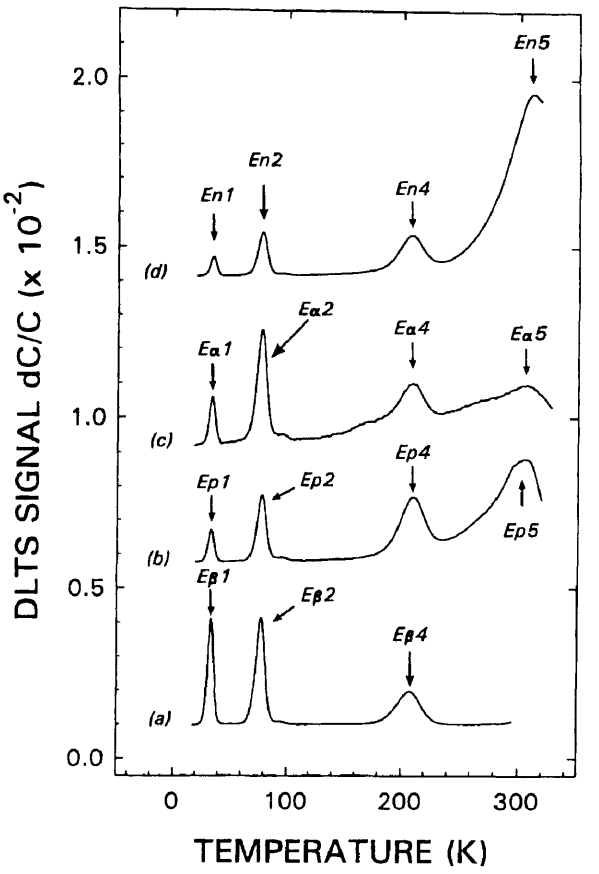

Figure 1 DLTS spectra of n-type GaAs with a free carrier density of 4×10^{14} /cm^3 irradiated with electrons [curve (a)], protons [curve (b)], alphas [curve (c)] and neutrons [curve (d)]. All spectra were recorded at a lock-in amplifier frequency of 46 Hz, a quiescent reverse bias of 8 V and a filling pulse amplitude of 4 V.

Table 1 DLTS defect "signatures" of particle irradiation induced defects in n-GaAs.

Defect label	E_t[(a)]	σ_t[(a)]	T_{peak}[(b)]	Similar defects
Eβ1, Eα1, Ep1, En1	0.042	8×10^{-16}	33	E1 [8], EE1 [6]
Eβ2, Eα2, Ep2, En2	0.14	1×10^{-13}	77	E2 [8], EE2 [6]
Eα3, Ep3, En3	0.34	2.5×10^{-14}	184	L-6 [16]
Eβ4, Eα4, Ep4, En4	0.37	1.4×10^{-13}	205	E3 [8], EE3 [6]
En5	0.66	6×10^{-13}	299	U-band? [17]

[(a)] E_t and σ_t were calculated from the slope and intercept, respectively, of the standard DLTS Arrhenius plots.

[(b)] At a lock-in amplifier frequency of 46 Hz, i.e. a decay time constant of 9.23 ms.

The concentrations of the Eβ1 and Eβ2 defects were found to be roughly equal, and about three times that of the Eβ4 defect, i.e. the same as observed for electron irradiation in accelerators. The average introduction rates, η, for Eβ1,

© University of Pretoria

UNIVERSITEIT VAN PRETORIA
UNIVERSITY OF PRETORIA
YUNIBESITHI YA PRETORIA

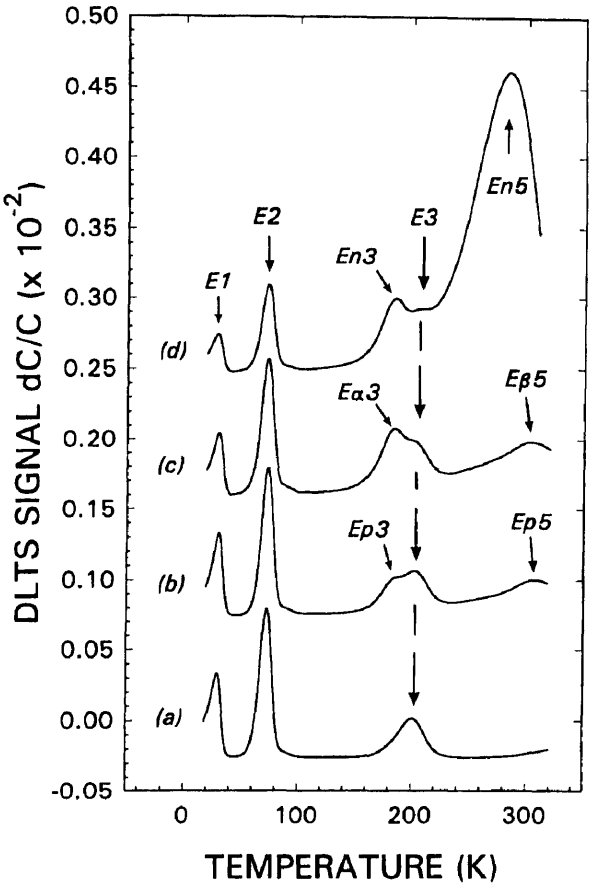

Figure 2 DLTS spectra of n-type GaAs with a free carrier density of 1×10^{16} /cm^3 irradiated with electrons [curve (a)], protons [curve (b)], alphas [curve (c)] and neutrons [curve (d)]. All spectra were recorded at a lock-in amplifier frequency of 46 Hz, a quiescent reverse bias of 4 V and a filling pulse amplitude of 1.2 V.

Table 2 Introduction rates (/cm) of particle irradiation induced defects in n-GaAs.

Defect	Electrons (SR-90)	Protons (2 MeV)	Alphas (Am-241)	Neutrons [p(66)/Be(40)]
E1	2	1×10^3	1.3×10^4	1.3
E2	2	1.8×10^3	2.4×10^4	1.9
E3	0.7	4.7×10^2	1.3×10^4	1.5
EM	—	4.7×10^2	1.1×10^4	1.7
En5	—	—	—	10.7

Eβ2 and Eβ3 were calculated using $\eta = N_t/(\varphi t)$, where N_t is the defect concentration introduced in a time t and φ is the effective radiation fluence rate (1.87×10^9 /cm^2/s), i.e. the flux of particles having energies above 250 keV (the threshold for producing point defects in GaAs). The calculated average introduction rates of Eβ1 and Eβ2 (Table 2) were about three times that of Eβ4. Considering that η is a function of the irradiation energy, the values of the introduction rates measured here are in good agreement with those obtained after irradiating GaAs in accelerators with electrons of similar energies [2].

3.3 Defects created by proton irradiation

The lowest proton fluence which could be reliably reproduced in the accelerator used in this study is 1.4×10^{11} /cm^2, which results in a free carrier reduction of about 2×10^{14} / cm^3 [11]. This means that when irradiating undoped GaAs, complete filling of the defects does not occur and hence the emission is not purely exponential. Consequently curve (b) of Figure 1 serves only as an illustration of which defects are induced by proton irradiation in low doped GaAs, but cannot be used to obtain quantitative information. A comparison of curves (b) in Figures 1 and 2 shows that, apart from Ep1, Ep2, Ep4 and Ep5 in the undoped GaAs, proton irradiation also induced the Ep3 defect in the doped GaAs, which could not be observed at all in the undoped GaAs. Because the compensation in the undoped GaAs is so high, only the introduction rates of Ep1 – Ep4 in doped GaAs were calculated and are listed in Table 2. It was further observed that the magnitude of the Ep3 signal depended on whether the DLTS scan was recorded up or down in temperature, which indicates that the Ep3 defect has a metastable nature [12]. A defect with a bistable nature which occurs roughly in the same temperature region has recently been reported by Leitch et al. [13] after hydrogen passivation of GaAs. In their case this defect was attributed to the presence of hydrogen. In our experiments, however, we also observed the metastable defect after alpha and neutron irradiation (as discussed below), which rules out the possibility of the Ep3 being hydrogen related.

When comparing the spectra of proton irradiated GaAs [curve (b) in Figures 1 and 2] to those of electron irradiated GaAs [curve (a) in Figures 1 and 2], it is evident that the Ep1, Ep2 and Ep4 peaks appear at the same temperatures as the Eβ1, Eβ2 and Eβ4 peaks, respectively. An Arrhenius comparison of their "signatures" showed that their respective electronic properties are also identical (Table 1). The "signature" of the Ep3 in Table 1 was determined under low field conditions in the doped GaAs. It should be noted that the Ep3 and Ep5 were not observed in electron irradiated doped GaAs. Because these defects are not observed after electron irradiation, which introduces mainly point defects in GaAs, it means that Ep3 and Ep5 are most likely defect complexes. Despite the correlation between the electronic properties of defects in electron and proton irradiated GaAs, the calculated introduction rates (Table 2), show that the relative concentrations (e.g. Eβ1:Eβ2:Eβ4) of the defects introduced by the two types of radiation are different.

3.4 Defects created by alpha irradiation

Curve (c) in Figures 1 and Figure 2 depict the DLTS spectra of the undoped and doped GaAs samples which were irradiated with alpha particles for 10 and 300 hours, i.e. fluences of 1.8×10^8 /cm^2 and 5.4×10^9 /cm^2, respectively. These spectra show the presence of defect peaks, Eα1 – Eα5, superimposed on a skewed baseline. From Figures 1 and 2 it is clear that the spectra of the proton and alpha irradiated undoped and doped GaAs are quite similar. An Arrhenius comparison confirmed that Eα1 – Eα5 have the same DLTS "signatures" as Ep1 – Ep5 (Table 1), from which we deduce

© University of Pretoria

UNIVERSITEIT VAN PRETORIA
UNIVERSITY OF PRETORIA
YUNIBESITHI YA PRETORIA

that they have the same electronic structure. This in turn implies that the Eα1, Eα2 and Eα4 defects have the same electronic properties as the well-known point defects E1, E2 and E3, respectively. From Figure 1 and 2 it is further clear that, as for proton irradiation, the Eα3 is observed in the doped, but not in the undoped GaAs. This, together with its metastable behaviour may indicate that the defect configuration giving rise to the Eα3 peak depends on the magnitude of the electric field.

From the introduction rates listed in Table 2 it is further evident that whereas the Eβ1 and Eβ2 defects in electron irradiated GaAs are introduced in about the same concentrations, the Eα1 concentration is about one half that that of the Eα2. Because we have shown that the Eα1 and Eα2 have the same properties as the E1 and E2, which in turn represent two charge states of the same defect, they may be expected to be observed in the same concentrations. Since this is not the case in proton and alpha irradiated GaAs, we speculate that the charge state occupation giving rise to the Eα1 is suppressed for some reason, perhaps by a local disturbance, e.g. the strain field of nearby complex defects.

An additional feature of importance in the spectrum of alpha irradiated GaAs is the skewed baseline. To test whether this was possibly due to radiation-induced interface states, we compared the DLTS spectra of GaAs irradiated with alphas before and after SBD metallization. The results showed that baseline skewing occurs irrespective of whether irradiation is done before or after metallization, thereby ruling out the possibility of it being caused by interface mixing during irradiation.

3.5 Neutron irradiation-induced defects

The DLTS spectra [curve (d) in Figure 1 and Figure 2] of undoped and doped GaAs irradiated with a fluence of 10^{12} n/cm^2 and 10^{13} n/cm^2, respectively, show the presence of defects En1 – En5, whose introduction rates are listed in Table 2. An Arrhenius analysis showed that the "signatures" of En1 – En4 (Table 1) are the same as those of Ep1 – Ep4 and Eα1 – Eα4, implying therefore that the En1, En2 and En4 are point defects with the same electronic properties as E1, E2 and E3, respectively. However, the most prominent of these defects is En5 with a broad DLTS peak at about 300 K. Its activation energy and capture cross-section are 0.66 eV and 6×10^{-13} cm^2, respectively. The large difference in its peak positions in doped and undoped GaAs can be attributed to an extremely strong field assisted emission [14]. This, together with its giant capture cross section, points to the possible capture of electrons by a double positively charged centre, which in turn suggests that it may have "negative U" properties [15].

The main difference between defects caused by neutron irradiation and charged particle irradiation, is that in the case of neutron irradiation the defect with the deepest energy level, En5, is present in a much larger concentration than the defects with shallower energy levels, En1 – En4. We speculate that this difference is caused by the different scattering mechanisms that operate during the interaction of the uncharged (neutrons) and charged projectile particles (electrons, protons and alphas) with atoms of the GaAs crystal lattice. Because neutron irradiation can introduce large clusters of defects, En5 may be related to such a complex or cluster of defects. In neutron irradiated GaAs, therefore, defect complexes or clusters seem to be present in much higher concentrations than point defects.

4. Conclusions

The main defects in electron irradiated n-GaAs are the Eβ1 (E1), Eβ2 (E2) and Eβ4 (E3), which have been shown before to have a point defect nature. This is in accordance with energy transfer considerations which indicate that at electron energies of a few MeV only sufficient energy can be transferred to create vacancies and interstitials. During proton and alpha irradiation at approximately the same energies, much more energy is transferred to atoms of the crystal, which means that not only point defects, but also defects consisting of clusters of atoms displaced from their normal lattice sites (as in a displacement spike), can be formed. The presence of defects such as Ep3 and Ep5 (for proton irradiation), and Eα3 and Eα5 (for alpha irradiation), which are not observed after electron irradiation, may therefore be related to such extended defects. Because neutrons can create defects even when they are thermalised and no coulombic interactions are possible, it is to be expected that the defects created by them may be different from those created by charged particles such as electrons and protons. This is evidenced by the presence of the En5 defect which dominates the spectrum of neutron irradiated GaAs.

The observation of defects such as the Ep3, Eα3 and En3 in proton- alpha- and neutron- irradiated 10^{16} /cm^3 doped GaAs, which could not be observed in identically irradiated 4×10^{14} /cm^3 GaAs, indicates that these defects are either related to a complex involving the dopant (Si), or that they are formed due to the higher electric field present in the doped GaAs. Their metastable behaviour supports the latter of the two possibilities.

Because different sets of defects (type and relative concentrations) are introduced during irradiation by different particle types, their effect on electronic devices may be quite different. Therefore, for device specification purposes the effect of each particle type has to be separately evaluated. Research pertaining to this aspect is presently in progress.

In summary, we have used DLTS to investigate defects with peaks in the 10 – 310 K temperature range introduced in GaAs of two carrier densities during irradiation with electrons, protons, alphas and neutrons. The results indicate that whereas electron irradiation introduces primarily point defects, proton-, alpha- and neutron-irradiation create also other defects, presumably complexes or clusters of distorted atoms.

Acknowledgements

We thank Dr. Dan Jones Mr. N. Schreuder at the National Accelerator Center for the neutron irradiation; and the Foundation for Research Development for financial support.

References

[1] P. Blood, Inst. Phys. Conf. Ser. No. 56, (1981) ch.5 p.251
[2] D. Pons and J.C. Bourgoin, J. Phys. C **18** (1985) 3839
[3] D. Stievenard, X. Boddaert, J.C. Bourgoin and H.J. von Bardeleben, Phys. Rev. B **41** (1990) 5271

© University of Pretoria

UNIVERSITEIT VAN PRETORIA
UNIVERSITY OF PRETORIA
YUNIBESITHI YA PRETORIA

[4] V.V. Kozlovski, T. I. Kol'chenko and V. M. Lomako, Sov. Phys. Semicond. **25** (1991) 707
[5] D.V. Lang, J. Appl. Phys. **45** (1974) 3014
[6] F.D. Auret and M. Nel, J. Appl. Phys. **63** (1988) 973
[7] G.M. Martin, A. Mitonneau and A. Mircea, Electron. Lett. **13** (1977) 191
[8] F.D. Auret, G. Myburg, H.W. Kunert and W.O. Barnard, J. Vac. Sci. Technol. B **10** (1992) 591
[9] F.D. Auret, L.J. Bredell, G. Myburg and W.O. Barnard, Jpn. J. Appl. Phys. **30** (1991) 80
[10] B. Ziebro, J.W. Hemsky and D.C. Look, J. Appl. Phys. **72** (1992) 78
[11] S.A. Goodman, F.D. Auret, M. Hayes and G. Myburg, S. Afr. J. Phys. **16** (1993) 54
[12] F.D. Auret, S.A. Goodman, G. Myburg and W.E. Meyer, unpublished
[13] A.W.R. Leitch, Th. Prescha and J. Weber, Phys. Rev. B **45** (1992) 14400
[14] J. Frenkel, Phys. Rev. **54** (1938) 657
[15] U. Kaufmann, E. Klausmann and J. Schneider, Phys. Rev. B **43** (1991) 12106
[16] Y. Yuba, K. Gamo, K. Murakami and S. Namba, Inst. Phys. Conf. Ser. No. 59 (1980) ch.6 p.329
[17] G.M. Martin, E.Esteve, P. Langlade and S. Makram-Ebeid, J. Appl. Phys. **56** (1984) 2655

© University of Pretoria